GEOLOGY AND GEOCHEMISTRY OF MOLYBDENUM MINERALIZATION OF THE DRAMMEN GRANITE, PERMIAN OSLO RIFT, NORWAY.

BY

INGAR F. WALDER

SUBMITTED IN PARTIAL FULLFILLMENT OF
THE REQUIREMENTS FOR THE DEGREE OF
DOCTOR OF PHILOSOPHY

NEW MEXICO INSTITUTE OF MINING AND TECHNOLOGY

SOCORRO, NEW MEXICO

DECEMBER 1992

ABSTRACT

An important source for Cu, Mo, W, Sn, Au is porphyry-type mineral deposits. These depositional systems are chemically complex, and are difficult to interpret with respect to geochemical analyses. This study focuses on molybdenite mineralization associated with rift-related granites using the Drammen granite, Oslo Rift, Norway, as a case study.

The objectives of the study were: 1.) to establish the geochemical characteristics of granite-associated fluids carrying molybdenum and sulfur and depositing molybdenite, 2.) and to use the data to test ore genesis models. Approximately 80 samples were collected for the study. The fluid geochemistry has been studied by indirect methods of stable isotope analyses of vein minerals and extraction of inclusion fluids.

The Drammen biotite granite of the Permian Oslo Rift contains numerous MoS_2-bearing hydrothermal occurrences. The granite batholith is a multiple intrusion with two major plutonic complexes having different chemical composition and petrographic features. Molybdenum-bearing veins are associated with the late intrusive phases of the batholith.

The batholith is classified as an A-type granite, showing negative correlation between silica and other major element oxides. Trace elements (Rb, Sr, Ba, Zr, Nb), whole-rock Sr isotopes, and whole-rock oxygen-isotopes, indicate that the

early phases of the granite evolved through assimilation of mainly sedimentary rocks which occurred contemporaneously with crystal fractionation. The late phases of the batholith evolved through fractional crystallization, and was followed by hydrothermal disturbance that partially reset the Rb-Sr systematics.

Comparison of Sr isotope analyses of inclusion fluids with $\delta^{18}O_{SMOW}$ of vein quartz and $\delta^{34}S_{CDT}$ of molybdenite indicates that the aqueous solutions which carried molybdenum were primary magmatic solutions; at sites of molybdenite and vein-quartz precipitation, the mild to strongly saline solution cooled by mixing with crustal equilibrated water.

Fluid inclusion gas analyses indicate that gaseous components constitute 0.2 to 9 mole % of the inclusion fluids. CO_2 is the major species: other gas species detected are H_2, CO, N_2, CH_4, SO_2, H_2S, He, Ar, and hydrocarbon compounds (from C_2 and above) mostly consisting of propane or ethane. Inclusion fluids from quartz-molybdenite veins contain both SO_2 and H_2; only SO_2 was detected in inclusions within miarolitic and rock-forming quartz.

The element concentrations in the inclusion liquids have been calculated based the amount of fluid and the amount of salts extracted per gram quartz for each sample. The mean concentration of Mo and W in vein quartz inclusion fluids are 80 ppm and 20 ppm, respectively, whereas miarolitic and rock-forming quartz inclusion fluids average 10 ppm and 1 ppm, respectively.

Discriminant analyses indicates that there are definite differences between vein quartz fluid inclusions and fluids trapped in miarolitic and rock-forming quartz. These differences can be explained by an early to late stage fluid exsolution of a fluid from a common source. Miarolitic and rock-forming quartz inclusion fluids from three late-stage granites show the same gas composition.

Oxygen fugacity calculations from the gas composition indicate that the oxidation state of the hydrothermal fluids was controlled by a mineral assemblage near the QFM buffer.

Factor analyses of the 33 elements analyzed by INAA in fluids extracted from quartz of Mo vein and miarolitic cavities suggests that the element concentration is controlled by: (1) Cl, (2) F, and (3) source geochemistry/exsolution-timing/leaching. The alkali and earth-alkali elements together with Zn and Fe correlate with the first factor whereas most of the REE's correlate with second factor. Mo, Br, Sm, Eu, and W correlate with the third factor, which is inferred to be the most important factor for producing Mo ore-forming solution.

Lack of significant MoS_2 mineralization in the Drammen granite is attributed to both low levels and the oxidized nature of sulfur in hydrothermal solutions. Total sulfur and H_2S/SO_2 ratios of fluid inclusion analyses are suggested to be an effective guide to Mo mineralization.

This study supports the genesis model of Candela and Holland (1984, 1986) for porphyry molybdenum mineralization,

in which the chemistry and evolution of the magma greatly influence the mineralization.

TABLE OF CONTENTS

LIST OF FIGURES

LIST OF TABLES

ACKNOWLEDGEMENT

I wish to thank Tom Victor Segalstad at Mineralogisk-Geologisk Museum, Oslo, Norway, and Dr. Arne Björlykke at University of Oslo, Norway, for initializing this research project and for many fruitful discussions during my research years (1985-1988) at Mineralogisk Geologisk Museum. Thanks must also go to Dr. David Norman my advisor during the last years at New Mexico Tech. He has provided me with a lot of input during these years. The other members of my Ph.D. committee, DrS. Andrew Campbell, Philip Kyle, William X. Chavez, Jr., and George Austin has been very helpful in reviewing the dissertation and providing me with help in performing neutron activation analysis and stable isotope Analysis.

A special thanks goes to Dr. William X. Chavez, Jr. whom always has the time for technical discussions and being a good inspirator. Thanks also go to fellow students for many interesting discussions.

Funding for this project came from research grants from Norwegian Council for Scientific and Technical Research (1985-1988), Charles Park Award (1990-1991) and State Mining and Mineral Resource Research Institute (1991-1992).

INTRODUCTION

BACKGROUND

Porphyry Cu, Mo, and Sn deposits are associated with granitic intrusions. The type of deposit formed depends, in part, upon the tectonic setting and the geochemistry of the intrusive body. Melts ascending through the crust will commonly contain varying contents of volatile components which depends mainly upon silica content, pressure, and the composition of the source. The volatile content of the melt increases during crystallization, until the magma becomes saturated in volatiles and a fluid phase will form. In granitic systems water is considered to be the dominant volatile specie (Burnham and Ohmoto, 1980). When the magma cools and starts to crystallize, incompatible elements (i.e., Mo, Rb, Sn, Ba, Pb, and Sb) will increase in concentration in the melt, whereas the compatible elements (i.e., Sr, Fe, Na, Eu, and Cu) will be concentrated in specific mineral phases and thus their concentration will decrease in the melt (Carmichael et al., 1974). The elements will partition into the three different phases (solid, melt, or fluid) depending on their distribution coefficients (K_D). Chloride and volatile compounds like CO_2, SO_2, and H_2S will all tend to be enriched in the fluid phase (Kilinc and Burnham, 1972; Glyuk et al., 1980; Henley et al., 1984), whereas F tends to remain in the melt (Candela, 1989a). Because of this enrichment of

volatile compounds in the fluid phase, metals that form complexes with Cl and sulfur will also be enriched in the fluid phase.

Distribution coefficients between magma and an aqueous fluid phase are not well known. There are data published on K, Ca, Mg, Mn, Zn, Pb, Rb, Cs, Sr, Ba, Yb, Cu, Cl, F, B, and REE's (Gammon et al., 1969; Holland, 1972; Kilinc and Burnham, 1972; Flynn and Burnham, 1978; Carron and Legache, 1980; Pichavant, 1981; Dingwell and Scarfe, 1983; Candela and Holland, 1984; Urabe, 1985; Reed et al., 1991). These coefficients were experimentally derived, each based on a single rock composition that vary from experiment to experiment and are therefore difficult to apply specific systems since they depend on chemistry of both the melt and fluid phase.

This study has been undertaken in order to learn more about the processes of element partitioning in a real granite system, and to apply this knowledge to understand the processes behind the Mo mineralization of the Drammen granite batholith, Norway. The main part of the study has focused on the geochemistry of fluids associated with the emplacement of the Drammen granite.

A fluid phase formed during crystallization or pressure decrease will move upwards in the magma chamber along the cooling front due to buoyancy. Vapor-saturated high-salinity fluids (50 wt. %) will not be buoyant at temperatures above

about 550°C (Henley and McNabb, 1978). This early formed fluid phase will be concentrated at the border or top of the magma chamber causing miarolitic cavity mineralization (Candela, 1991). The fluid phase formed at a late stage of the crystallization (90-95%) will tend to form fracture paths with vein mineralization (Candela, 1991; Philip Candela, pers. com., 1991), instead of bubbles, because of the high proportion of solidified magma. The types of fractures made in the surrounding rocks and in the outer part of the granite, are related to the depth of emplacement. If a magma ascends to a depth of approximately 2 km or less, loss of volatiles may be explosive and associated with caldera formation in rhyolitic systems (Burnham and Ohmoto, 1980).

The physio-chemical conditions for a fluid phase will commonly change rapidly when ascending through the newly created fracture system (Burnham, 1981). The fluid phase which was in chemical equilibrium with the crystallizing magma is now in disequilibrium with its surroundings. This disequilibrium can alter the surroundings and as the fluid geochemistry changes, result in mineralization (Burnham, 1979; Rose and Burt, 1979). The fractures may penetrate to the surface and cause a large drop from lithostatic to hydrostatic pressure that commonly results in second boiling (Burnham, 1979) or enhance mixing of the ascending fluid phase with colder water from the surrounding rocks. All these factors will influence the solubility of ore-forming minerals, leading

to precipitation of ore-forming minerals (Burnham, 1979). The grade and size of these deposits will depend upon the metal concentration in solution, the amount of solution, and the efficiency of precipitation as well as the plumbing system.

Copper ± Au, Mo, Sn, and W ± Au will generally form intramagmatic deposits associated with a porphyritic intrusion. Copper, Pb, Zn, W, Sb, and Fe are commonly found in contact metasomatic deposits around granitic intrusions, where the surrounding rocks have reacted with the magmatic solution to precipitate these elements as sulfides and oxides (Rose and Burt, 1979).

Porphyry Mo deposits associated with granitic intrusions are found associated with anorogenic type granites (A-type; Loiselle and Wones, 1979) in areas of regional extension (Mutchler et al., 1981; Sawkins, 1990; Chappell and White, 1983), such as the Great Basin and the Permian Oslo Rift, and with igneous-type granites (I-type) in orogenic zones, such as the Rocky Mountains (Mitchell and Garson, 1981; Chappell and White, 1974). Mo deposits in both types of granites are commonly associated with high-F fluid and high oxygen fugacity: higher $f(O_2)$ than those of the porphyry tin deposits, but lower $f(O_2)$ than those of porphyry copper deposits (Whitney et al., 1989). Mo deposits in multiple intrusions are common, especially where the last intrusion is porphyritic which has the associated molybdenite mineralization (White et al., 1981; Wallace et al., 1978).

Despite our knowledge of the magmatic processes which are responsible for producing metal-rich fluids from magmas a controversy remains about the origin of the magmas. Burnham (1979, 1981) states that partial melting of a Mo- enriched sialic source is a necessary precondition to form porphyry Mo deposits, whereas Candela and Holland (1984, 1986) believe that the most important process for forming these deposits is crystal fractionation of an acid magma with low water content so that Mo will be enriched in the magma during fractionation.

Molybdate or molybdic acid are the most common complexes in hydrothermal Mo solutions (Smith, 1983; Wood et al., 1988; Kudrin, 1986). If the solution contains F, it may enhance the Mo solubility with molybdenum fluoride complexes (Smith, 1983); however, later studies indicate that changing F content will not change the Mo partitioning between fluid phase and melt (Tingle and Fenn, 1984). The Cl content of the solution does not seem to affect the solubility of molybdenite (Wood et al., 1987; Smith, 1983; Koga, 1967) or the distribution coefficient between water and melt (Candela and Holland, 1984). However, HCl in the magma may destabilize the Mo-silicate complexes in the magma and thereby enhance the distribution coefficient between fluid phase and melt (Isuk and Carman, 1981; Cao, 1989).

Data from porphyry molybdenum deposits in the USA indicate a formation temperature between 400 and 600°C. Questa

porphyry Mo, New Mexico, has main fluid inclusion homogenization temperatures from 350°C to 450°C with a pressure correction of less than 40°C.

One way of establishing the $f(O_2)$ of magma and associated fluids is to study the Fe^{3+}/Fe^{2+} ratio. Climax-type molybdenum deposits have hematite and magnetite (White et al., 1981). In the Henderson mine, pyrite is found as a primary mineral and is the major secondary iron mineral formed during late alteration (Wallace, 1978). Hematite is also found at the Henderson mine as daughter minerals in primary fluid inclusion (Kamilli, 1978). However, in the Questa mine area magnetite is associated with propylitic alteration, and found as a secondary minerals altered from pyroxene and biotite (Carpenter, 1967).

OBJECTIVES

The important source for Cu, Mo, W, and Sn, with or without Au, from the porphyry-type mineral deposits, and the lack of good genesis models for Mo mineralization are principal factors leading the writer to undertake this study. The objective of this study is to produce geological and geochemical data that may be used to constrain a model of Mo mineralization and to test some of the proposed hypotheses on genesis of Mo ore deposits.

The Drammen granite batholith, Oslo Rift, Norway, has many of the characteristics of a porphyry molybdenite system, even though the mineralization is of intramagmatic vein type (Ihlen and Vokes, 1978) with contact-metasomatic deposits surrounding the batholith (Goldschmidt, 1911). The Permian-aged batholith is composed of multiple intrusions. There were extensive geothermal activity and alteration associated with the emplacement of the batholith (Olsen and Griffin, 1985a,b; Ihlen et al., 1982), yet the intramagmatic mineralization is quite minor. This paucity of intramagmatic mineralization could very well be caused by the crystallization depth of intrusion (Burnham and Ohmoto, 1980). The batholith is deeply eroded such that the source rock that may have generated a Mo-porphyry deposit is exposed.

In this study I have tested genesis models for molybdenum mineralization associated with granitic intrusives.

PREVIOUS WORK

General geology

The Drammen granites (the Drammen granite batholith, the Glitrevann granite, and the Finnemarka granite) are situated in the central part of the Permian Oslo rift (Fig. 1.1). The Drammen batholith consists of biotite granite rocks of eight petrographically different types (Table 1.1; Ihlen et al., 1982; Norman and Mearns, unpub. data). Hydrothermal quartz-molybdenite vein mineralization is associated with three of these. The batholith occupies about 700 km^2 and intrudes Precambrian gneisses and lower Paleozoic sedimentary rocks. Along the northern and the north western contact of the batholith are several contact-metasomatic ore deposits containing variable amounts of Fe, Cu, Pb, Zn, and Bi, which were mined (Ihlen and Vokes, 1978).

Orthoclase and quartz are the most abundant minerals in these granites followed by plagioclase and biotite. Muscovite occurs more rarely; sphene, iron oxides, zircon, apatite, and fluorite have also been described (El-Bouseily, 1971). Raade (1971) describes shady remnants of digested sediment inclusions many places inside the granite.

Schönwandt and Petersen (1983) suggest that the Permian granite magmas must have been doped with particular elements (like Mo) by the incorporation of Precambrian rocks into the magma. They base their interpretation on the fact that the

Fig. 1.1.

Geology of the Permian Oslo rift and location of the Drammen, Glitrevann, and Finnemarka granites based on maps from Oftedahl (1960) and Ihlen and Vokes (1978).

Fig. 1.1

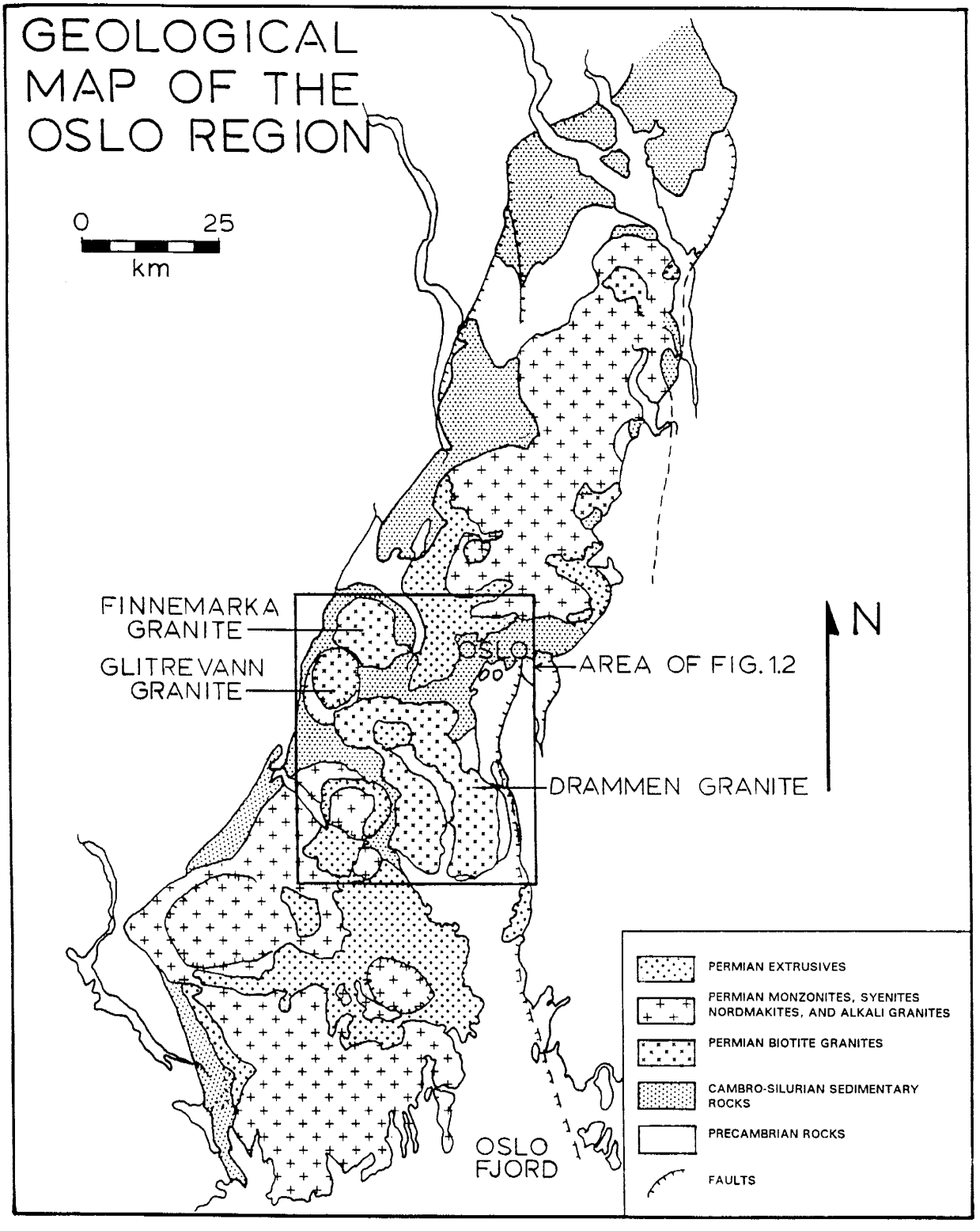
GEOLOGICAL MAP OF THE OSLO REGION
0
25
km
FINNEMARKA GRANITE
GLITREVANN GRANITE
OSLO
AREA OF FIG. 1.2
DRAMMEN GRANITE
N
OSLO FJORD
PERMIAN EXTRUSIVES
PERMIAN MONZONITES, SYENITES NORDMAKITES, AND ALKALI GRANITES
PERMIAN BIOTITE GRANITES
CAMBRO-SILURIAN SEDIMENTARY ROCKS
PRECAMBRIAN ROCKS
FAULTS

Table 1.1. Classification of the Drammen granite intrusive bodies g1 to g8 (Ihlen et al, 1982; Norman and Mearns, unpub. data).

g1	Coarse grained equigranular granite
g2	Rapakivi granite
g3	Medium to coarse grained granite
g4	Transition between g3 and g5
g5	Coarse grained, porphyritic granite
g6	Fine grained porphyritic granite
g7	Quartz-feldspar porphyry
g8	Coarse grained two mica granite

surrounding Precambrian gneisses contain many Precambrian Mo deposits (Bugge, 1963). Based on the distribution of K, Th, and U in the Drammen granite rocks and in the surrounding Precambrian rocks (Raade, 1973). Killeen and Heier (1975) suggest that the Drammen granite has assimilated Precambrian rocks on the basis of U, Th, and K distribution in the Precambrian rocks and the Drammen granite.

Extensive late- to post-magmatic hydrothermal alteration is most prominent in the central parts of the batholith. Albitization, argillic alteration, and quartz-sericite alteration are the most common types, but K-feldspar and sericite-chlorite-epidote alteration also occurs (Ihlen et al., 1982). Albitization is the only widespread alteration type and it is not related to faults nor fractures. Locally secondary K-feldspar occurs in place of albite alteration in the central part of the Drammen granite. Argillic alteration is commonly associated with fractures (Ihlen et al., 1982) indicating a low alkali/acid ratio in the hydrothermal fluid in respect fluid temperature.

Mineralization is vein type that are comprised of almost pure molybdenite or quartz and molybdenite, where the latter is most abundant (Bugge, 1963). Numerous minor occurrences of MoS_2 occurs as multiple veinlets in zones up to 2 m wide in the g6-g8 intrusions (Fig. 1.2). Grades range from 0.2 to 1.6 wt.% MoS_2. Sörumsåsen mine which is the largest deposit (situated in g7), produced 140,000 tons of ore with a grade of

0.2 wt.% MoS_2 (Bugge, 1963).

The Glitrevann granite is situated north of the Drammen granite in a double cauldron bordered north-east by the Finnemarka granite (Fig. 1.2). The Glitrevann intrusive is a medium- to coarse-grained biotite granite (Schönwandt, 1986; Jensen, 1985). Molybdenum mineralization has been discovered in the central part of the granite mainly under the Glitrevann Lake (Geyti and Schönwandt, 1979). Base metal ores were produced from metasomatic deposits on the borders of the granite (Glomsrudkollen; Ihlen and Vokes, 1978). The Finnemarka granite has no known mineral deposits (Czamanske, 1965; Czamanske and Mihálik, 1972; Czamanske and Wones, 1973).

Isotopic studies

Segalstad (1982) and Segalstad and Ohmoto (1986) indicate that the Drammen granite has assimilated crustal rock was altered by magmatic fluids and/or crustal equilibrated water. $\delta^{18}O$ values for the rock-forming quartz and the hydrothermal vein quartz indicate that only a small proportion of meteoric water could have been mixed with magmatic water in the ore-forming fluids.

Heier and Compston (1969) obtained a Rb/Sr isochron age of 286 ± 59 Ma with an initial $^{87}Sr/^{86}Sr$ of 0.703 ± 0.006 (decay constant lambda=$1.42*10^{-11}a^{-1}$) for samples from g1 and g2. Sundvoll (1978a) recalculated these data to give an isochron of 282 ± 13 Ma with an initial $^{87}Sr/^{86}Sr$ of 0.7033 ± 0.0002.

Fig. 1.2.

Geological map (after Ihlen et al., 1978) showing sample locations of the Drammen granite. The Drammen granite batholith is petrographically subdivided into eight bodies numbered g1 to g8. Mo-mineralization is only associated with the three late intrusive phases g6-g8.

Fig 1.2.

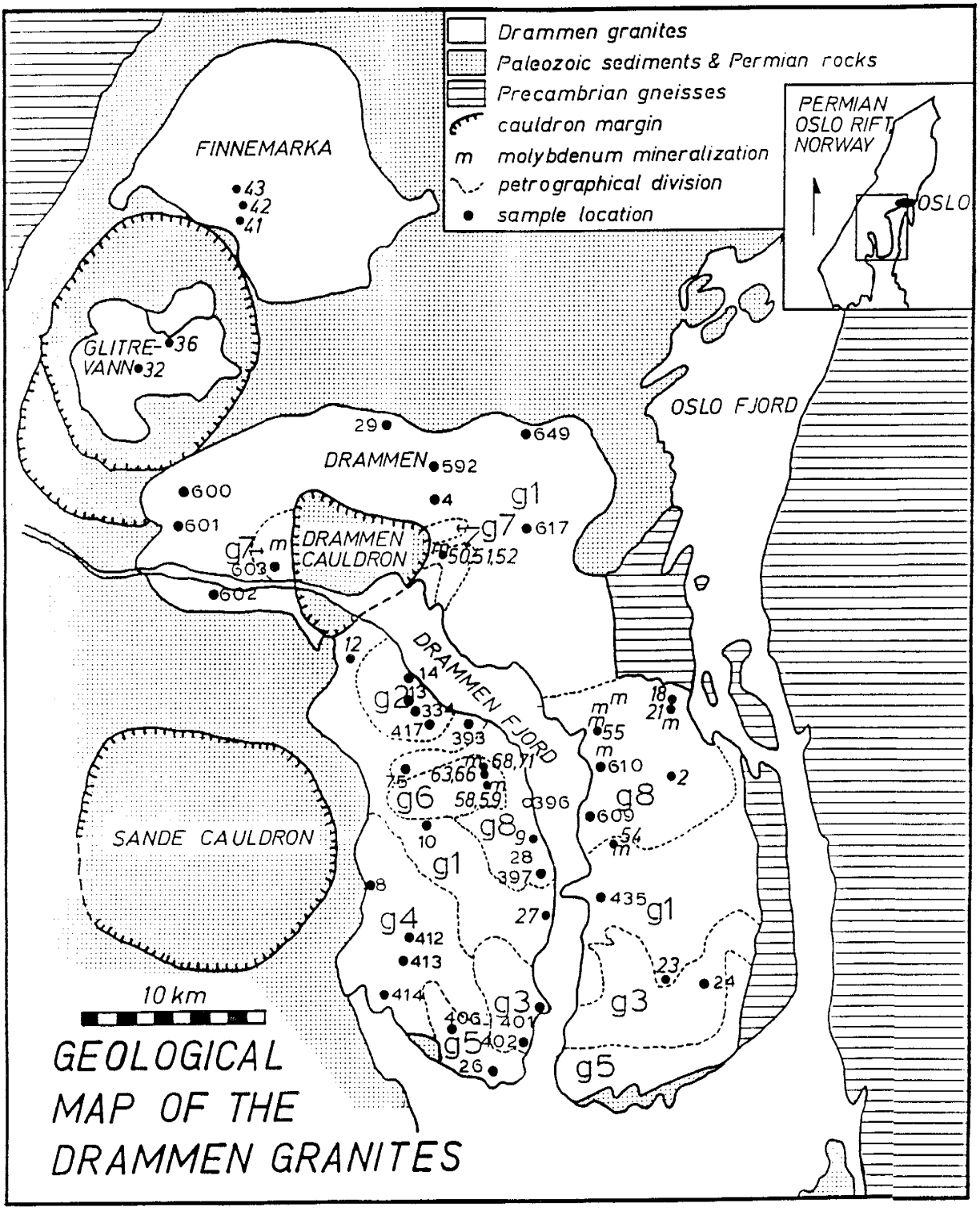
Drammen granites
Paleozoic sediments & Permian rocks
Precambrian gneisses
cauldron margin
m molybdenum mineralization
petrographical division
sample location
PERMIAN OSLO RIFT NORWAY
OSLO
FINNEMARKA
43
42
41
GLITRE-VANN
36
32
OSLO FJORD
29
649
DRAMMEN
592
600
4
g1
601
g7
617
DRAMMEN CAULDRON
603
50,51,52
602
12
DRAMMEN FJORD
14
g2
13
33
417
393
18
21
55
610
2
68,71
63,66
75
58,59
g6
396
g8
609
54
SANDE CAULDRON
10
g8
9
28
g1
397
8
435
g1
27
g4
412
413
23
24
414
g3
406
401
g3
g5
402
26
g5
10 km
GEOLOGICAL MAP OF THE DRAMMEN GRANITES

other Rb/Sr isochron ages are 268 ± 4 Ma (mineral isochron), which was obtained from g1 (Jacobsen, 1980), and for g1 274 ± 3 Ma with initial $^{87}Sr/^{86}Sr$ of 0.7051 ± 0.0005 (Norman and Mearns, unpub. data). K-Ar dates of biotite from the Drammen granite gave 259 Ma (Faul et al., 1959). Neumann (1960) cites a K-Ar date of biotite from the Drammen granite of 259 Ma and Re-Os dating of molybdenite from the Sörumsåsen mine of 235 Ma. K-Ar dating of alteration minerals associated with mineral deposits in the Oslo Rift give two peaks: 265 Ma and 235 Ma (Ineson et al., 1975). These alteration dates must be considered as minimum ages because of the fairly low blocking temperature of the K-Ar system.

Fluid inclusion work

Microscopic and microthermometric fluid inclusion studies of miarolitic cavity quartz from the Drammen granite show a fluid evolution during crystallization of the granitic magma. Olsen and Griffin (1984a) demonstrated that inclusion fluids represent an aqueous phase that separated from the magma at temperatures of 650-800°C and pressures of 1300-1500 bars. The pressure was calculated from the two melting temperature of solid inclusions. These two temperatures are interpreted to be the solidus and liquidus for a granitic rock and correspond to a P_{H2O} of 1300 to 1500 bars (Olsen and Griffin, 1984a). Later fluids trapped at about 500-600°C indicate a decrease in salt content of the fluids from 10-40 wt.% NaCl

eq. to 0-10 wt.% NaCl eq., and decrease in CO_2 content from 0-2 mole % to 0 mole % (Olsen and Griffin, 1984a). Fluid inclusions from vein-quartz associated with Mo mineralization is indicated to have been trapped at 300-350°C (Olsen, 1981).

Lower temperature fluids, richer in CO_2 close to the margin of the granite intrusion, were found to contain higher amounts of radiogenic Sr and Nd isotopes than high-temperature magmatic fluids. The excess radiogenic Sr and Nd was interpreted to be the result of transport of these constituents into the granite by crustal fluids where they mixed with magmatic fluids (Norman and Mearns, 1986; Olsen and Griffin, 1984b).

Olsen and Griffin (1984b) analyzed Drammen granite leachates from miarolitic quartz. They report measured 10 cations and 2 anions analyzed by atomic absorption and calorimetry methods. Unreasonably high values for the heavy metals (up to 24 wt.% Cu in inclusion fluids) were reported for inclusions opened by crushing. Their analyses showed much lower concentrations of metals when thermal decrepitation was used to open the fluid inclusions. The Na/K ratios of the leachates indicate a fluid in equilibrium with a one-feldspar (plagioclase) magma (Olsen and Griffin, 1984b).

WHOLE-ROCK GEOCHEMISTRY

ANALYTICAL METHODS

Thirty-six whole-rock samples were analyzed for both major and trace elements. In addition 11 samples were analyzed only for trace elements.

The whole-rock major and trace elements were determined by X-ray fluorescence spectrometry at Mineralogisk-Geologisk Museum, University of Oslo. Major elements were determined from fused pellets of rock powder mixed 1:9 with lithium tetraborate; trace elements from pressed pellets of rock powder. A Mo X-ray tube was used for Rb, Sr, and Y, and a W tube for Ba, Nb, and Zr. Sr and Rb were determined according to the method of Norrish and Chappell (1967). Interferences resulting from line overlap of $Y(K_{\alpha}1,2)$ was corrected for by use of $Rb(K_{\alpha}1,3)$ and $Zr(K_{\beta})$ with $Sr(K_{\beta}1,3)$ peaks. Appendix A shows estimated accuracy and precision derived from analysis of standards and duplicates.

The CIPW normative mineral composition was calculated assuming $Fe^{2+}/Fe^{3+}=2$. This ratio was chosen because the Drammen granite is similar to the Finnemarka granite for which the ratios measured to be 2 (Ihlen et al., 1982). El-Bouseily (1971) reported a ratio of 2 for the Drammen granite. All Fe is considered to be primary, even though the ratio of primary to secondary introduced Fe is not known, hence, some CIPW norm Fe^{2+}-bearing minerals may be calculated in excess.

Eight whole-rock samples from the Drammen batholith intrusives g1, g6, and g8 were analyzed for Sr isotopes at Mineralogisk-Geologisk Museum, University of Oslo. The elements were separated by ion exchange using a standard method (Mearns, 1986) before analysis in a VG 354 mass spectrometer. Four samples contained between 1 to 6 ppm Sr, and thus giving considerable uncertainty in the initial $^{87}Sr/^{86}Sr$.

Four whole-rock samples were analyzed for total oxygen isotope ratio at New Mexico Institute of Mining and Technology isotope lab using ClF_3 to extract O_2 after the method described by Borthwick and Harmon (1982) and Clayton and Mayeda (1963). Uncertainty of the analysis procedure is ± 0.2 per mill.

RESULTS

Petrography

A total of 30 thin sections from the Drammen granite intrusives g1 to g8 were studied. K-feldspar (mainly orthoclase) is perthitic. Some grains of K-feldspar show a cross-hatch (tartan twining) pattern together with alteration. A strong "dusting" of hematite imparts a red color and is accompanied by sericitization. Plagioclase which is partly altered to K-feldspar, show albite twinning. Quartz and feldspar occur as phenocrysts up to 0.5 cm across in g5, g6, and g7. The groundmass is fine grained in g6 and g7, fine to medium grained in g8, and coarse grained in g5.

A total of six thin sections of quartz-MoS_2 veins were studied. These quartz-MoS_2 veins may contain fluorite and feldspar. Pyrite and scheelite were observed but constitute only a volumetrically minor proportion of the ore minerals. The veins are 0.5 to 5 cm thick and occur in parallel swarms in linear zones up to 2 m wide. The veins are not zoned; MoS_2 was observed both in the center of the veins and towards the wall-rock border. Molybdenite grains have variable sizes and were seen in hand specimens with sizes up to 0.5 cm across.

Wall-rock alteration associated with the quartz-molybdenite veins is sparse. Whole-rock major and trace element analyses of the wall rock within 5 cm form the veins do not exhibit any noticeable depletion nor enrichment in any elements (Table 2.1a,b). A few of the large veins contain

Table 2.1a. Whole-rock major and trace element analyses in wt.% and ppm, respectively.

Sample #	4 DG-84	23C DG-84	27C DG-84	27E DG-84	29 DG-84	GR393 DG	GR435 DG	GR592 DG	GR600 DG	GR602 DG	GR617 DG	13 DG-84	14 DG-84	GR334 DG	GR391 DG	GR392 DG
TYPE	g1	g1	g1	g1	g1	g1	g1	g1	g1	g1	g1	g2	g2	g2	g2	g2
SiO_2	74.09	74.17	75.96	76.06	73.16	75.29	76.67	72.80	74.03	74.18	73.51	69.15	69.69	71.37	71.22	69.84
TiO_2	0.30	0.34	0.11	0.16	0.26	0.22	0.29	0.26	0.24	0.28	0.03	0.39	0.40	0.39	0.37	0.39
Al_2O_3	12.96	13.42	12.97	12.23	13.94	12.85	13.28	13.00	13.10	13.00	12.73	14.83	14.70	14.71	14.82	14.52
FeO_{tot}	1.74	1.98	0.68	1.13	1.32	1.55	1.75	1.17	1.44	1.57	1.76	2.35	2.39	2.45	2.25	2.38
MnO	0.02	0.05	0.02	0.03	0.02	0.03	0.05	0.05	0.03	0.03	0.03	0.09	0.09	0.11	0.07	0.08
MgO	0.38	0.31	0.10	0.15	0.24	0.27	0.30	0.40	0.19	0.31	0.30	0.42	0.45	0.39	0.32	0.35
CaO	0.48	0.55	0.27	0.36	0.72	0.52	0.49	0.80	0.54	0.66	0.48	0.64	0.44	0.68	0.57	0.71
Na_2O	3.33	3.76	3.71	3.41	3.63	3.41	3.67	3.53	3.39	3.33	3.41	4.55	4.24	4.36	4.31	4.30
K_2O	5.04	4.96	4.75	4.59	5.32	4.93	4.96	4.98	4.99	4.94	4.84	5.03	5.20	5.08	5.20	5.02
P_2O_5	0.06	0.06	0.02	0.03	0.05	0.05	0.05	0.05	0.05	0.05	0.05	0.09	0.10	0.08	0.07	0.08
loi	0.40	0.28	0.14	0.15	0.14	0.13	0.12	1.00	0.17	0.05	0.51	0.86	0.65	0.20	0.52	0.32
SUM	98.80	99.88	98.73	98.30	98.80	99.25	101.63	98.04	98.17	98.40	97.65	98.40	98.35	99.82	99.72	97.99
Rb	236	226	270	280	246	278	224	235	235	252	220	197	195	216	191	195
Sr	103	76	7.5	27	109	75	70	74	89	87	99	132	152	117	122	153
Y	30	70	31	40	33	39	51	25	20	24	25	29	29	31	24	31
Zr	179	268	148	148	152	151	227	165	146	157	182	286	298	304	293	292
Nb	33	66	96	48	37	50	54	32	30	35	32	67	69	70	64	70
Ba	448	323	34	94	442	211	300	408	427	411	429	461	447	388	417	431
CIPW normative mineral composition																
Ap	0.13	0.13	0.04	0.07	0.11	0.11	0.11	0.11	0.11	0.11	0.11	0.20	0.22	0.18	0.15	0.18
Il	0.57	0.65	0.21	0.30	0.49	0.42	0.55	0.50	0.45	0.53	0.06	0.75	0.76	0.75	0.70	0.75
Mt	0.84	0.96	0.33	0.55	0.64	0.75	0.84	0.57	0.69	0.75	0.86	1.14	1.16	1.20	1.09	1.15
Or	29.70	29.33	27.80	26.99	31.33	29.08	29.28	29.52	29.33	29.13	28.63	29.86	30.70	30.16	30.74	29.80
Ab	28.10	31.85	31.10	28.72	30.62	28.81	31.03	29.97	28.54	28.13	28.89	38.69	35.85	37.07	36.49	36.56
An	1.98	2.34	1.20	1.58	3.24	2.25	2.10	3.65	2.34	2.94	2.06	2.60	1.53	2.86	2.37	3.01
Hy	1.07	1.04	0.35	0.57	0.72	0.88	0.98	0.95	0.70	0.92	1.13	1.36	1.41	1.36	1.15	1.25
C	2.59	2.02	2.54	2.13	2.04	2.16	2.21	0.94	2.51	2.19	2.26	1.92	3.07	2.00	2.47	1.84
Q	33.41	31.27	35.02	37.23	29.48	34.67	34.41	30.83	33.32	33.65	33.14	21.02	23.00	24.04	24.03	23.13
Total	98.40	99.60	98.59	98.15	98.66	99.12	101.51	97.04	98.00	98.35	97.14	97.54	97.70	99.62	99.20	97.67

TYPE is granite intrusive phase from g1 to g8 (Table 1.1). Types marked with * are samples taken less than 5 cm from quartz-molybdenite veins. FeO_{tot}-total iron oxide expressed as FeO: loi-loss on ignition; Ap-apatite; Il-ilmenite; Mt-magnetite; Or-orthoclase; Ab-albite; An-anorthite; Hy-hypersten; C-corundum; Q-quartz.

Table 2.1a
Cont.

Sample #	GR417 DG	24 DG-84	GR401 DG	GR402 DG	GR412 DG	26 DG-84	60B DG-85	67 DG-85	68B DG-85	75 DG-85	52B DG-85	GR603 DG	18C DG-85	18D DG-84
TYPE	g2	g3	g3	g3	g4	g5	g6 *	g6	g6 *	g6	g7 *	g7	g8	g8
SiO_2	69.21	73.65	72.96	73.91	74.38	71.70	75.83	75.84	74.82	78.04	71.92	75.10	72.50	76.68
TiO_2	0.42	0.32	0.38	0.36	0.32	0.39	0.08	0.14	0.09	0.19	0.41	0.25	0.07	0.14
Al_2O_3	14.80	13.06	13.06	13.17	13.06	13.79	12.42	12.38	13.28	12.83	14.82	12.77	14.11	12.12
FeO_{tot}	2.79	1.93	2.07	2.02	1.60	2.23	0.90	1.11	0.97	1.23	1.52	1.40	0.89	1.08
MnO	0.16	0.04	0.06	0.03	0.03	0.07	0.01	0.04	0.03	0.02	0.01	0.03	0.01	0.02
MgO	0.39	0.33	0.23	0.22	0.10	0.33	0.09	0.13	0.09	0.07	0.31	0.13	0.08	0.10
CaO	0.28	0.47	0.45	0.38	0.18	0.64	0.55	0.42	0.36	0.01	0.10	0.10	0.68	0.30
Na_2O	4.11	3.69	3.72	3.59	3.67	3.96	3.46	3.43	3.97	3.46	4.66	2.95	4.26	3.49
K_2O	5.38	5.03	5.07	5.05	5.06	5.03	4.92	4.65	4.70	4.63	4.56	5.02	5.03	4.55
P_2O_5	0.09	0.05	0.06	0.05	0.05	0.07	0.02	0.03	0.02	0.04	0.06	0.04	0.02	
loi	0.52	0.43	0.17	0.17	0.28	0.27	0.33	0.48	0.27	0.33	0.35	0.39	0.37	0.22
SUM	98.15	99.00	98.23	98.95	98.73	98.48	98.61	98.65	98.60	100.85	98.72	98.18	98.02	98.70
Rb	221	229	223	249	244	214	334	337	521	305	198	231	374	349
Sr	112	64	63	60	46	89	2.1	18	9	19	43	56	5.1	10
Y	31	64	75	65	67	64	58	40	31	18	58	22	57	61
Zr	296	303	346	309	304	394	183	158	153	192	605	170	124	165
Nb	68	65	72	72	70	63	148	69	88	67	79	35	84	67
Ba	498	303	305	294	226	411	22	60	46	84	226	278	17	29
Ap	0.20	0.11	0.11	0.11	0.11	0.15	0.04	0.07	0.04	0.09	0.13	0.09	0.04	
Il	0.80	0.61	0.73	0.68	0.61	0.75	0.15	0.27	0.17	0.36	0.77	0.47	0.13	0.27
Mt	1.35	0.93	1.01	0.97	0.77	1.08	0.44	0.54	0.46	0.59	0.73	0.67	0.44	0.52
Or	31.72	29.81	30.05	29.77	29.70	29.84	29.08	27.36	27.63	26.92	26.55	29.14	29.73	26.79
Ab	34.70	31.32	31.58	30.31	30.86	33.65	29.29	28.91	33.43	28.81	38.86	24.53	36.06	29.43
An	0.80	2.01	1.91	1.56	0.56	2.73	2.60	1.88	1.65	-0.21	0.10	0.23	3.24	1.48
Hy	1.49	1.07	0.93	0.88	0.56	1.16	0.43	0.55	0.46	0.45	0.79	0.57	0.41	0.48
C	3.84	1.63	1.51	2.45	2.66	1.68	0.90	2.02	2.10	4.34	4.30	4.72	0.94	1.81
Q	22.74	31.08	30.22	32.04	32.62	27.16	35.34	36.58	32.39	39.19	26.14	37.38	26.65	37.71
Total	97.63	98.57	98.05	98.78	98.45	98.21	98.28	98.17	98.33	100.52	98.37	97.79	97.65	98.48

Table 2.1b. Whole-rock trace element analyses in ppm. These samples were analyzed for trace elements only.

Sample #	Type	Rb	Sr	Y	Zr	Nb	Ba
10 DG-84	g1	241	56	59	237	50	380
GR601 DG	g1	241	84	25	154	33	417
GR611 DG	g1			32	131	65	85
GR649 DG	g1	262	61	23	136	32	335
8 DG-84	g4	98	62	67	415	67	935
GR413 DG	g4	219	80	30	442	75	406
GR414 DG	g4	208	83	70	423	70	371
GR406 DG	g5	211	76	73	434	72	355
59C DG-85	g6 *	298	10	36	159	65	36
51B DG-85	g7 *	219	60	35	389	57	271
21C DG-84	g8	386	9	34	116	67	19

GR samples are samples from Raade (1973) but analyzed for this study. An asterisk (*) marks samples taken less than 5 cm from quartz-molybdenite veins.

fragments up to 3 cm long of strongly silicified wall rock.

Using Streckeisen's (1973) classification, the Drammen batholith classifies as a granite. All the Drammen granite samples are weakly peraluminous above the metaluminous field using the classification system of Shand (1947) (Fig. 2.1).

Whole-rock geochemistry

Silica content of the granites range from 69 to 78 wt. %. The Rapakivi granite (g2) has the lowest SiO_2 contents with 69 to 71 wt.% whereas g6 and g8 have 75 to 78 wt.% SiO_2. The Al_2O_3 content of the samples ranges from 12 to 14.5 wt. %. Harker diagrams of SiO_2 versus Al_2O_3, $MgO+FeO_t$, K_2O, and Na_2O are shown in Fig. 2.2. Except for K_2O, all oxides display a decrease with increasing SiO_2.

Strontium and Ba shows the same pattern as for Al_2O_3, with lowest contents for g6 and g8 and highest contents for g2 with the other granite types showing concentrations in between. Sr ranges from 2 to 150 ppm. Ba shows a range from 17 ppm to 930 ppm. Rubidium concentrations follow SiO_2 and ranges from 190 to 510 ppm. Zirconium ranges from 150 to 600 ppm where g1, g6, and g8 show the lowest contents, g2 and g3 intermediate, and g4 and g5 the highest contents. Yttrium and Nb do not show systematic patterns and range from 25 to 75 ppm and from 30 to 150 ppm, respectively.

Fig. 2.1.

Plot of molecular ratios $Al_2O_3/(K_2O+Na_2O)$ versus $Al_2O_3/(K_2O+Na_2O+CaO)$ in Shand's (1943) classification diagram for peralkaline, peraluminous, and metaluminus intrusives. The upper horizontal dotted line defines the S-type granites (above the line) and I-type granites (below the line) after Chappell and White (1974). The circles represent g1, the crosses represent g2, g3, g4, and g5, and the triangles represent g6, g7, and g8.

Fig. 2.1.

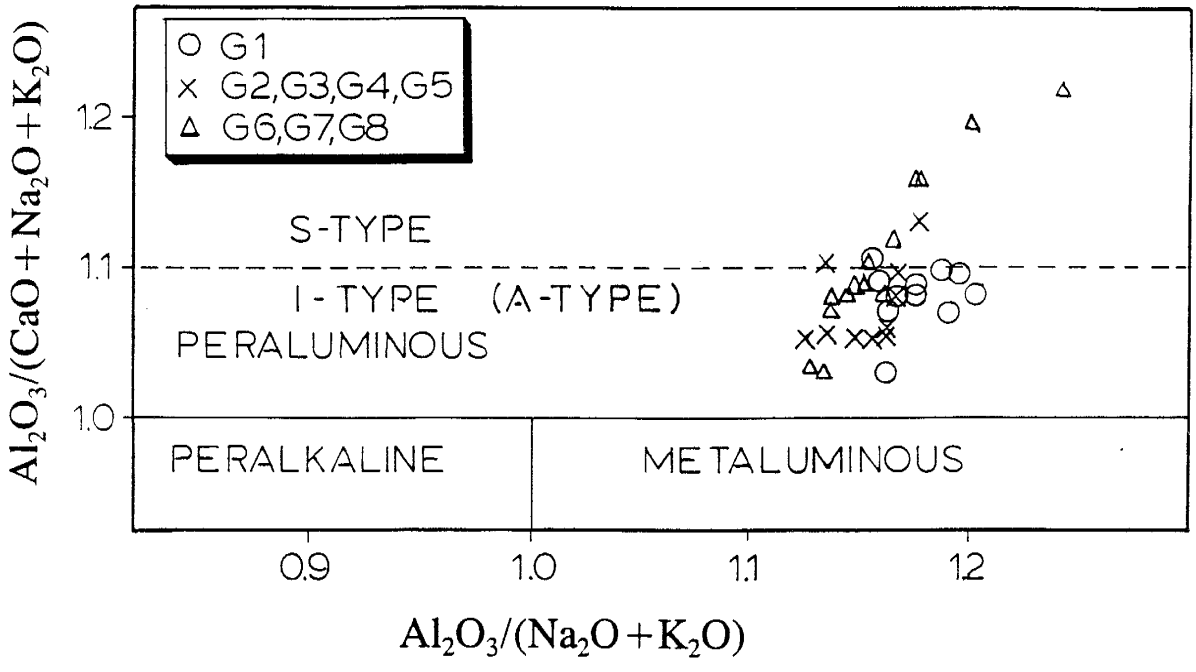
O G1
× G2,G3,G4,G5
Δ G6,G7,G8
S-TYPE
I-TYPE (A-TYPE)
PERALUMINOUS
PERALKALINE
METALUMINOUS
1.2
1.1
1.0
0.9
1.0
1.1
1.2
Al2O3/(CaO+Na2O+K2O)
Al2O3/(Na2O+K2O)

Fig. 2.2.

Oxide harker diagrams (in wt. %) with SiO_2 plotted versus Al_2O_3, FeO_t+MgO, K_2O, and Na_2O.

Fig. 2.2.

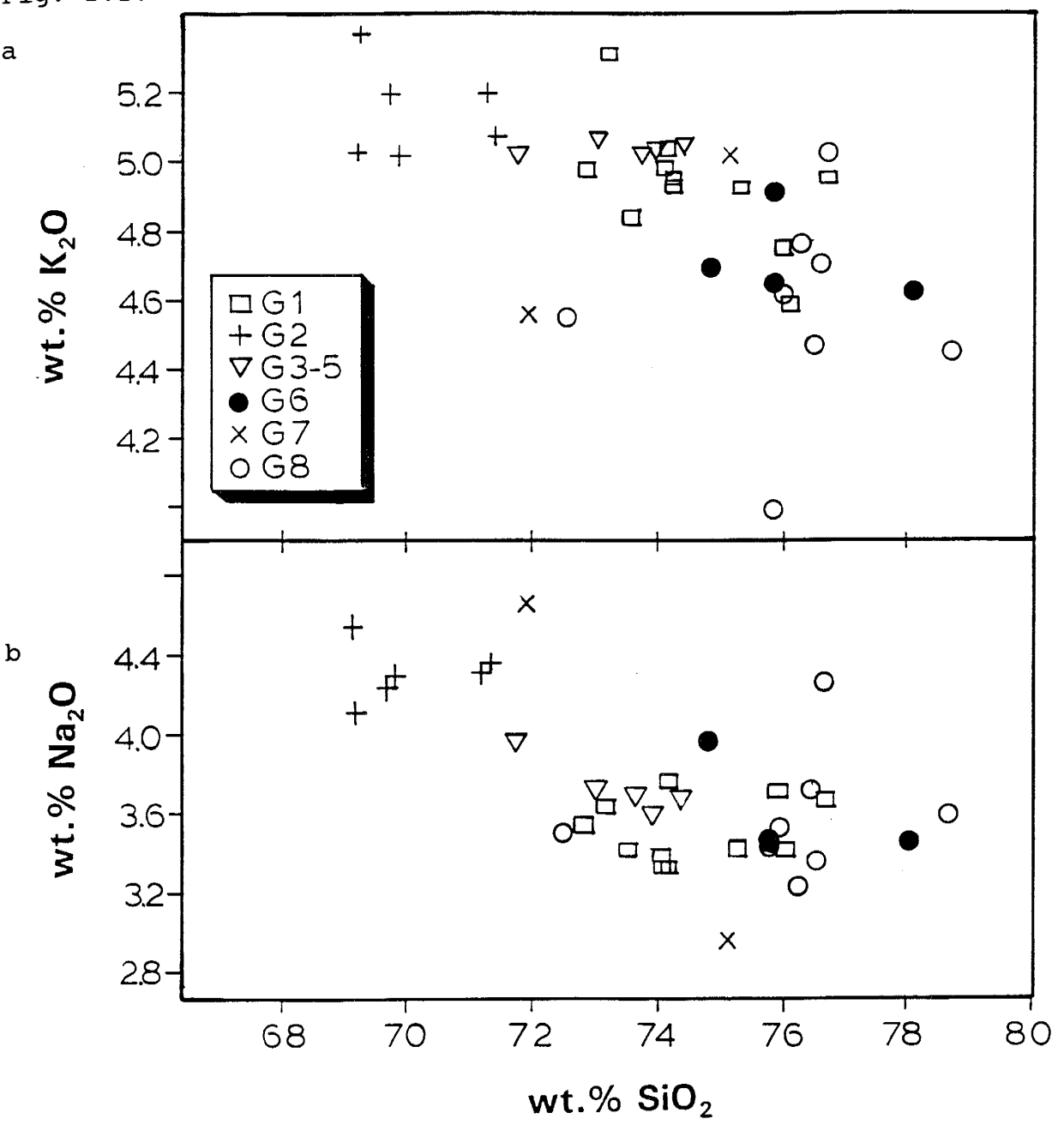
a
5.2
5.0
4.8
4.6
4.4
4.2
wt.% K_2O
G1
G2
G3-5
G6
G7
G8
b
4.4
4.0
3.6
3.2
2.8
wt.% Na_2O
68
70
72
74
76
78
80
wt.% SiO_2

Fig. 2.2 cont.

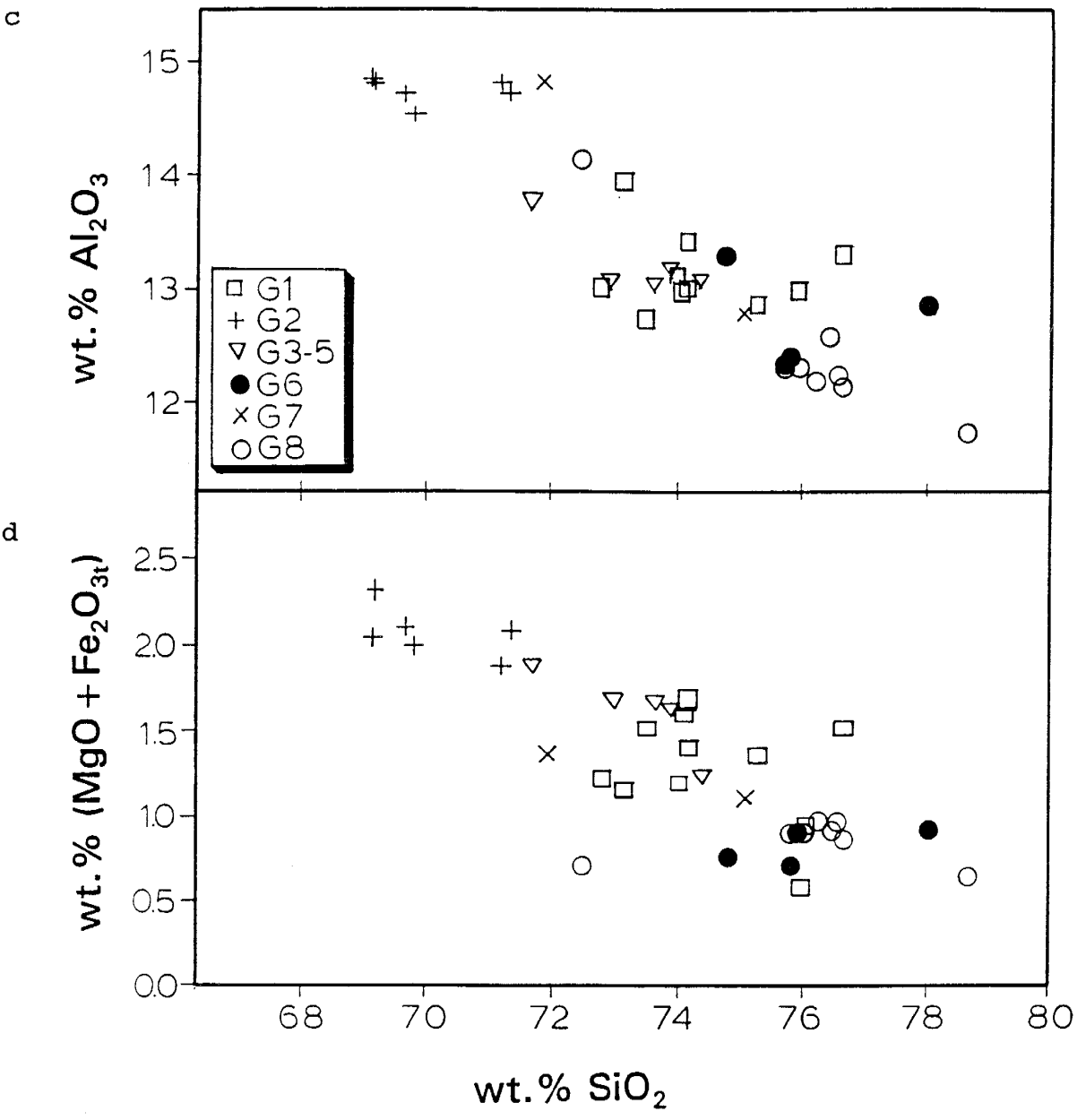
c
d
wt.% Al_2O_3
wt.% $(MgO + Fe_2O_{3t})$
wt.% SiO_2
G1
G2
G3-5
G6
G7
G8
15
14
13
12
2.5
2.0
1.5
1.0
0.5
0.0
68
70
72
74
76
78
80

Granites g6 and g8 define a group on Rb versus Sr and Ba (Fig. 2.3a,b) whereas g1 to g5 and g7 form a second group. A few g1 samples plot together with g6 and g8. Zirconium and Nb data define two geochemically different groups with linear correlation (Fig. 2.4). Intrusions g6 and g8 have Nb/Zr ratios of 0.3 - 0.5, whereas the other intrusions have Nb/Zr ratios of 0.1 - 0.2.

Initial $^{87}Sr/^{86}Sr$ ratios were calculated for the seven whole-rock Sr-isotope analyses form this study together with published data of Heier and Compston (1969), Jacobsen (1980), and Jacobsen and Wasserburg (1978) (Table 2.2). Calculated initial ratios are based on 274 Ma (Norman and Mearns, unpub. data) and 265 Ma (Ineson et al., 1975). Although the others have constructed isochrons from their data, no isochron can be obtained from the new data. Model age calculations for this studies whole-rock analyses based on initial $^{87}Sr/^{87}Sr=0.7051$ range from 237 to 295 Ma (Table 2.2).

$\delta^{18}O_{SMOW}$ (Table 2.3) shows an ^{18}O enrichment for samples taken close to the border of the granite (+8.8 and +9.5 per mill.). The samples from the central parts have somewhat lower values (+7.2 and +8.0).

Fig. 2.3

Plot of Rb versus Sr (a) and Ba (b) for whole-rock trace element analyses.

Fig. 2.3

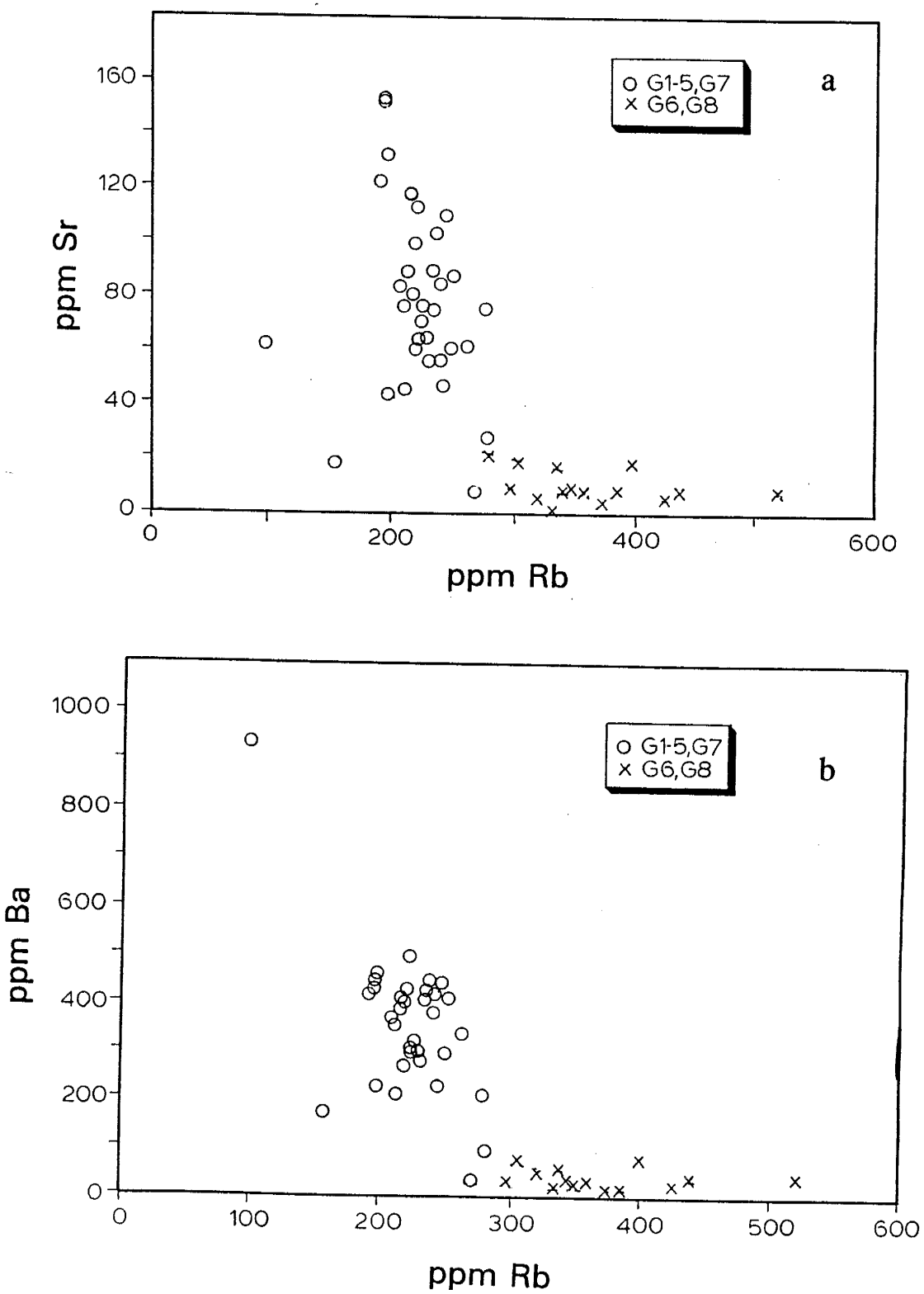
o G1-5,G7
× G6,G8
a
ppm Sr
ppm Rb
0
40
80
120
160
200
400
600
o G1-5,G7
× G6,G8
b
ppm Ba
ppm Rb
0
200
400
600
800
1000
100
300
500

Fig. 2.4.

Plot of Zr versus Nb (in ppm) for whole-rock trace element analysis. The open box represents the composition range for Paleozoic sedimentary rocks in the Oslo region (data from Björlykke, 1974). The asterisk represents the lower Paleozoic Oslo Region shale (Christie, 1975; Analytisk Sporelement Komité Norden, 1975).

Fig. 2.4

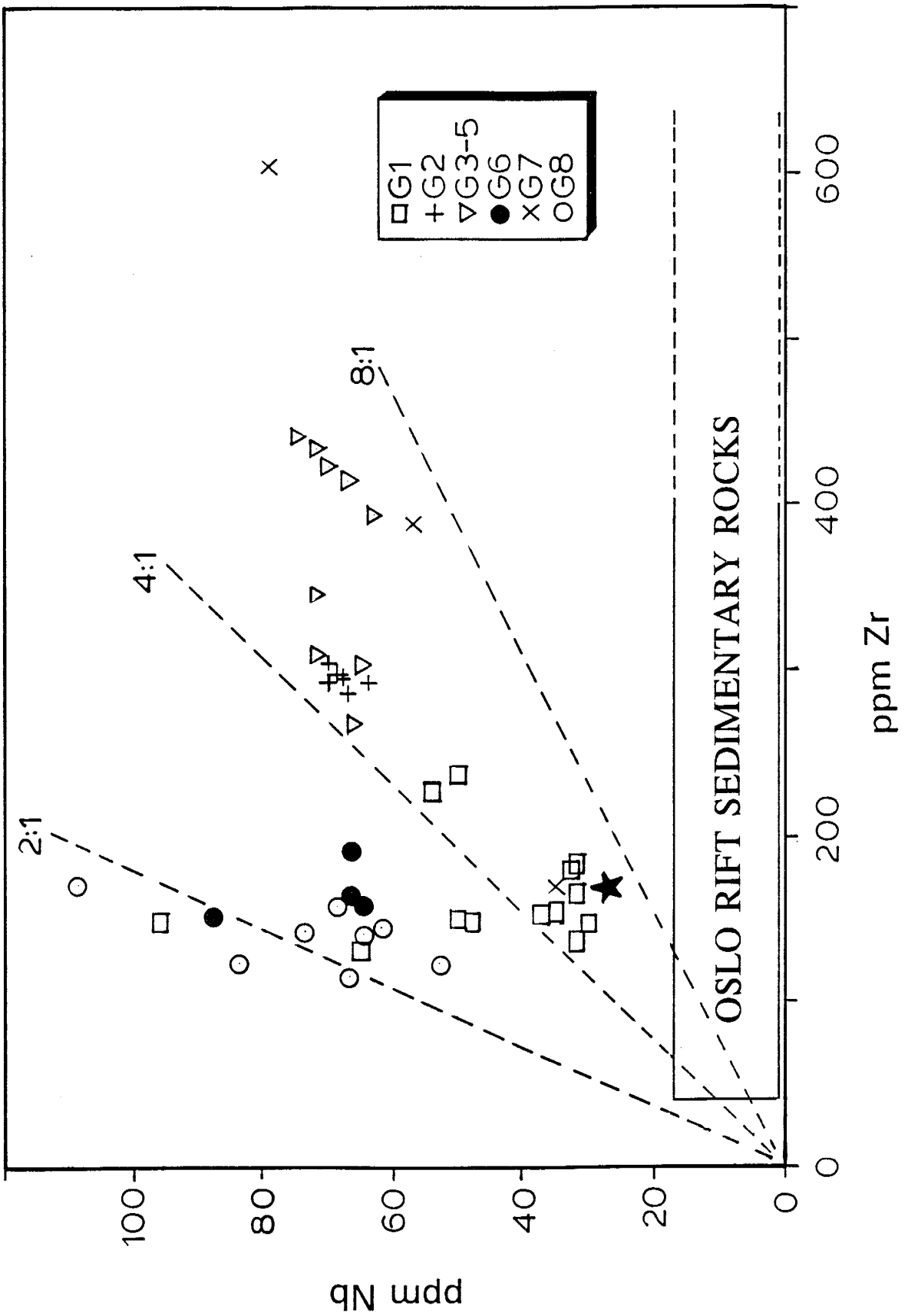
□G1
+G2
▽G3-5
●G6
×G7
○G8
2:1
4:1
8:1
OSLO RIFT SEDIMENTARY ROCKS
ppm Nb
ppm Zr
0
20
40
60
80
100
0
200
400
600

Table 2.2. Sr-isotope analyses.

Sample #	Granite type	Rb	Sr	$^{87}Rb/^{86}Sr$	$^{87}Sr/^{86}Sr$	+/- 2 sig.	Initial 274 Ma $^{87}Sr/^{86}Sr$	Initial 265Ma $^{87}Sr/^{86}Sr$	Model age 0.7051
Whole rock (this study):									
24 DG-84	3	229	64	10.38	0.74431	0.00008	0.70384	0.70517	256
26 DG-84	5	214	89	6.97	0.73445	0.00010	0.70729	0.70819	295
59C DG-85	6	298	10	88.60	1.02267	0.00010	0.67729	0.68865	252
67 DG-85	6	337	18	55.31	0.92413	0.00010	0.70850	0.71560	278
51B DG-85	7	219	60	10.60	0.74620	0.00042	0.70489	0.70625	273
GR 603 DG	7	231	56	11.96	0.75008	0.00007	0.70346	0.70500	264
28A DG-84	8	320	6.6	147.01	1.20170	0.00010	0.62858	0.64744	237
Vein fluids (this study):									
58A DG-85	6	320	161	5.75	0.73398	0.00019	0.71158	0.71231	364
59B DG-85	6	119	64	5.38	0.72584	0.00034	0.70485	0.70554	283
66A DG-85	6	391	74	15.35	0.78999	0.00030	0.73017	0.73213	393
66B DG-85	6	501	129	11.28	0.76687	0.00054	0.72292	0.72436	391
68A DG-85	6	304	104	8.48	0.76079	0.00093	0.72773	0.72882	469
59A DG-85	6	171	148	3.34	0.72061	0.00003	0.70761	0.70804	346
52A DG-85	7	666	71	27.19	0.78931	0.00037	0.68331	0.6868	220
Blank		1	4	0.59	0.58862	0.00037			
Whole rock data (Heier and Compston, 1969):									
63	1	272.4	94.3	8.36	0.736		0.70341	0.70448	268
64	2	208.8	130.7	4.62	0.7215		0.70349	0.70408	264
GA3198	1	248.7	90.2	7.98	0.735		0.70389	0.70491	272
GA3199	1	249.9	99.5	7.28	0.7329		0.70452	0.70545	277
Whole rock and separated plagioclase (Jacobsen, 1980):									
OGD-1-TR	1	249	82.6	8.72	0.73883		0.70484	0.70595	279
OGD-1-PLAG	1	50.1	309	0.463	0.7073		0.7055	0.70555	474
Fluids from cavity quartz (Olsen and Griffin, 1984b):									
36	8	20.73	221.5	2.72	0.7224		0.7118	0.71215	470
2	8	1870	16359	0.33	0.7041		0.70281	0.70286	-15
12	1	632.5	601.1	3.06	0.7256		0.71367	0.71406	491
12	1	440	1192	1.07	0.7174		0.71323	0.71337	865
9	8	537	34.2	46.31	0.8826		0.70207	0.70801	271

"g(n)" is granite type from Table 1.1. Rb and Sr concentrations are in ppm where whole rock XRF data are used. "2 sig." is 2 standard deviations. The model age is calculated with respect to initial $^{87}Sr/^{86}Sr=0.7051$.

Table 2.3. Oxygen-isotope analysis of whole rock from the Drammen granite. Two samples are from the central part of the batholith, and two samples (*) are from close to the border of the batholith. Type refers to granite type in Table 1.1.

Sample #	Type	$\delta^{18}O_{SMOW}$
8A DG-84*	g4	9.46
13 DG 84	g2	7.21
23C DG-84	g1	7.95
24 DG-84*	g3	8.78

DISCUSSION

Major element analysis

Harker diagrams indicate a decrease in alkali with SiO_2 increase (Fig. 2.2), which is the opposite trend expected for a rock series evolved through differentiation when alkali feldspar is not crystallizing. Potassium and partly Na, are commonly expected to increase during crystal fractionation since alkali feldspar will be a late crystallizing mineral phase (Bowen, 1928).

The Drammen granite shares many similarities with A-type granitoids. These alkaline granitoids are formed in rift or stable cratonic environments by differentiation from alkali basaltic source rock, typically with relatively low H_2O fugacity and high F fugacity (Loiselle and Wones, 1979). Oxygen fugacity is characteristically low to moderate for A-type granites (Loiselle and Wones, 1979), but alteration of the Drammen granite makes it difficult to calculate. Mineral geochemistry and fluid inclusion analyses indicate a relatively low $f(O_2)$ for the Drammen granite around the Ni-NiO mineral buffer (Segalstad, unpub. data; discussed under Fluid Geochemistry, this report). The Drammen batholith does not fit the definition of mantle-type granitoids (M-type; Pitcher, 1983), which show a clear relationship between mantle and/or subducted ocean crust (Whalen, 1985). The Drammen granite would classify as I-type in Fig. 2.1 (Chappell and White, 1974) based on high sodium content, low initial Sr isotope

ratio, and the linear relationship between element ratios (Fig. 2.2). However, the normative corundum is slightly too high for I-type bodies. This high normative corundum may be due to assimilation of Paleozoic sedimentary rocks (discussed later in this chapter). The Drammen granite seems to be best classified as an A-type granite.

On a ternary plot Q-Ab-Or (Fig. 2.5) the Drammen granite forms two distinct groups: one is occupied solely by Rapakivi granite (g2): and the other group may be subdivided into g6-g8 and g1-g3-g4-g5, where g7 falls outside both groups. Experimental data (Tuttle and Bowen, 1958) indicate that the Rapakivi granite crystallized under higher total pressure than other parts of the Drammen granite. The g6 and g8 may have crystallized on eutectic minima under total p_{H2O} = 500 ± 200 bars, the early intrusive phases crystallized under higher pressure (700-3000 bars). Perthitic textures of the alkali feldspar as in hypersolvus granites and the lack of a cross-hatch pattern in the non-perthitic alkali feldspar as in subsolvus granites indicate that the pressure of the Drammen granite during crystallization must have been less than 5 kbars (Martin and Bonin, 1976). Low crystallization pressures are in agreement with pressures obtained from fluid and solid inclusions in miarolitic quartz (1.5 kbars; Olsen and Griffin, 1984a).

Fig. 2.5.

Ternary plot of normative quartz (Q), albite (Ab), and orthoclase (Or). The curves are for water-saturated liquids in equilibrium with quartz and alkali feldspar at water-indicated pressures 500, 1000, 3000, and 5000 bars. Isobaric minima are labeled with a small cross, (from Tuttle and Bowen, 1959).

Fig. 2.5

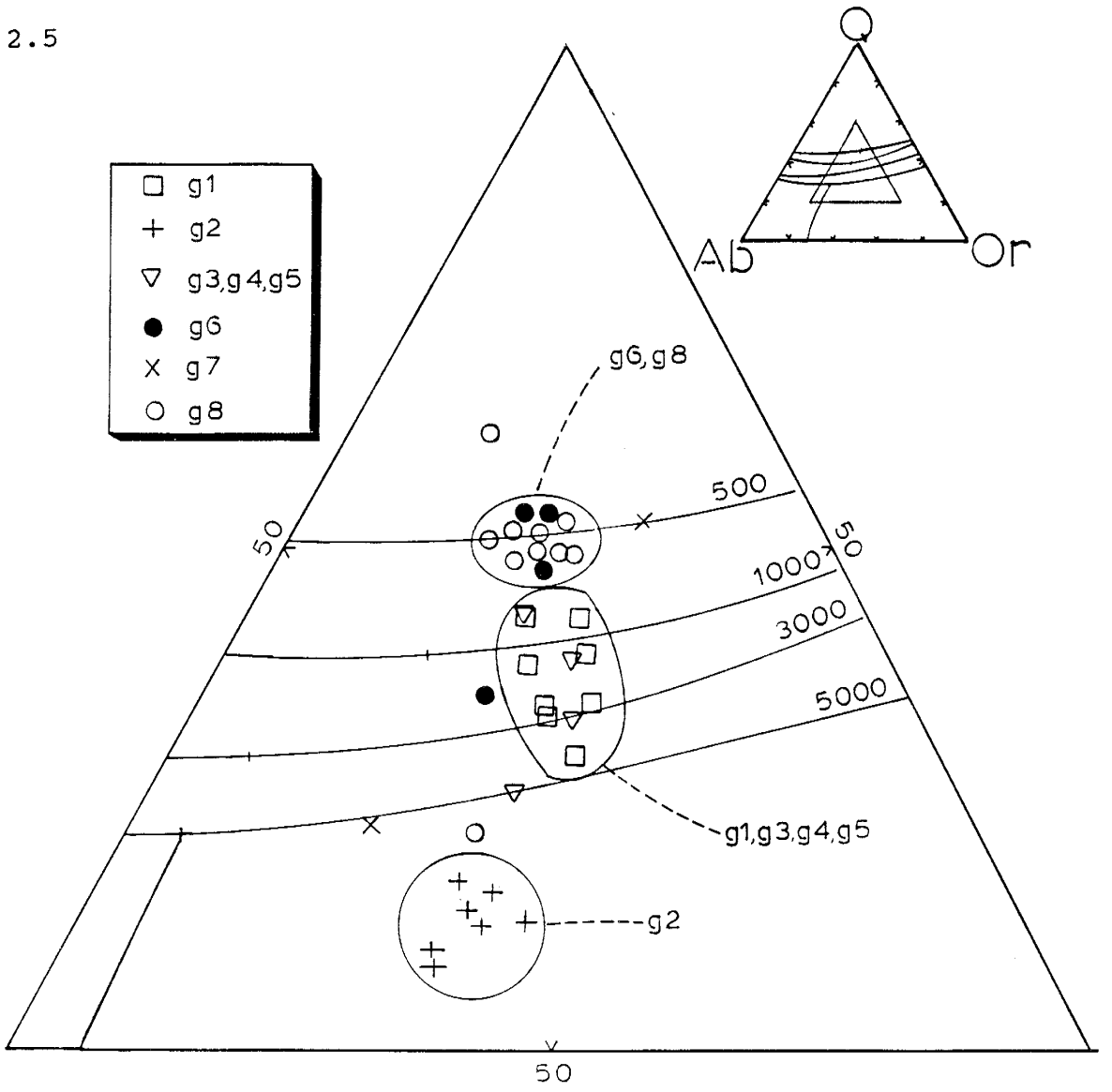
g1
g2
g3,g4,g5
g6
g7
g8
Ab
Or
g6,g8
500
1000
3000
5000
50
50
50
g1,g3,g4,g5
g2

Trace element analysis

There are three possible processes (or a combination of these) which may explain the relationship among Rb, Sr, and Ba(Fig. 2.3a,b): Crystal fractionation; partial melting; assimilation; and assimilation fractional crystallization (AFC). These processes are modelled in Fig. 2.6.

Crystal fractionation is modelled assuming melt composition with Rb, Sr, and Ba contents of 175 ppm, 40 ppm, and 220 ppm, respectively. Quartz, plagioclase, K-feldspar, and biotite were assumed to be on the liquidus. The observed Drammen granite modal composition is 30% quartz, 45% K-feldspar, 23% plagioclase, and 2% biotite (Gaut, 1981) which is used for calculating a bulk distribution coefficient (K_D crystal/melt) based on the partitioning coefficient for each mineral (McCarthy, 1976; Hanson 1978). K_D calculated is 0.23 for Rb, 1.92 for Sr, and 2.17 for Ba and the K_D's are assumed to be constant for the range of modelling. The equation for modelling crystal fractionation is from Neumann et al. (1954):

$$C_S = C_0 * K_D * (1-F)^{(KD-1)} \text{ (solid)},$$

$$C_l = C_0 * (1-F)^{(KD-1)} \text{ (liquid)},$$

where C_S and C_l are abundances of the trace element in the solid and liquid, respectively, C_0 is initial trace element abundance, and F is the weight fraction of melt. The near

horizontal line (Fig. 2.6a,b) going from the filled asterisk represents the change of melt composition during Rayleigh fractionation. Most of the samples from g6 and g8 lie in the area of 50-80% crystallization (Fig. 2.6a,b). The chemical composition of samples fromthe other intrusives cannot be readily explained by the same process if a different starting composition is assumed because data do not parallel the path calculated for fractionation.

The partial melting curve of Precambrian gneiss (larger open circle) was modelled assuming concentration of 375 ppm Rb, 30 ppm Sr, and 1000 ppm Ba (Jacobsen and Heier, 1978) in gneiss comprised of 40% K-feldspar, 59% plagioclase, and 1% biotite. Computed bulk K_D (crystal/melt) coefficients are 0.32 for Rb, 3.09 for Sr, and 2.70 for Ba. The modelling equation used is from Shaw (1970):

$$C_m=C_0(1/(F+K_D-(F*K_D)))$$

where C_m is abundance of the trace element in the melt. Trace element distribution predicted by this model poorly matches the data. Changing the gneiss composition will not improve the fit.

A granite derived from partial melting of the surrounding Precambrian gneisses or granitic melt that was contaminated with the Precambrian gneisses, would have a high initial $^{87}Sr/^{86}Sr$ ratio because these gneisses have high Sr isotope

Fig. 2.6.

Plot of Rb versus Sr (a) and Rb versus Ba (b) from whole-rock trace element analysis. The open asterisk represents the lower Paleozoic Oslo Region shale (Christie, 1975; Analytisk Sporelement Komité Norden, 1975). The lines labelled "fract. crystals" show the change in Rb, Sr, and Ba contents to crystal mush for crystallization from an initial melt containing 175 ppm Rb, 40 ppm Sr, and 220 ppm Ba. The melt crystallized 30% quartz, 45% K-feldspar, 23% plagioclase, and 2% biotite. The lines labelled "fract. melt" exhibit the melt composition relative to amount of crystallization. The lines labelled "partial melt" show the melt composition for partial melting of a rock containing 350 ppm Rb, 30 ppm Sr, and 1000 ppm Ba (open circle) made up of 40% K-feldspar, 59% plagioclase, and 1% hornblende. The lines labelled "mix" between the asterisks show mixing between a granitic magma containing 175 ppm Rb, 40 ppm Sr, and 220 ppm Ba and sedimentary rock containing 200 ppm Rb, 175 ppm Sr, and 800 ppm Ba. The lines labelled AFC represent assimilation with contemporeneous fractional crystallization.

Fig. 2.6.

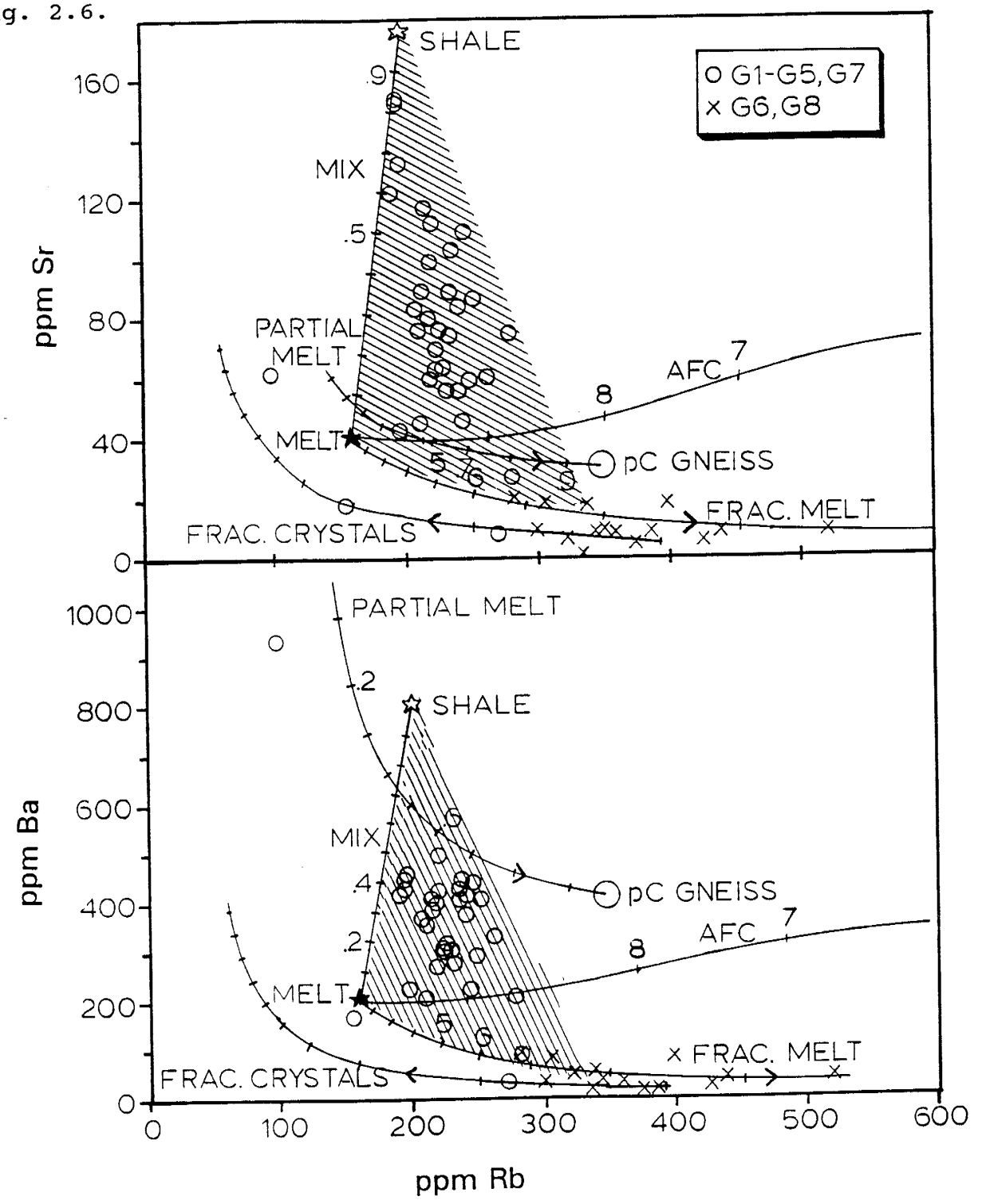
SHALE
o G1-G5, G7
× G6, G8
MIX
.9
.5
PARTIAL MELT
MELT
AFC
7
8
pC GNEISS
FRAC. MELT
FRAC. CRYSTALS
ppm Sr
160
120
80
40
0
PARTIAL MELT
.2
SHALE
MIX
.4
.2
.6
pC GNEISS
AFC
7
8
MELT
× FRAC. MELT
FRAC. CRYSTALS
ppm Ba
1000
800
600
400
200
0
0
100
200
300
400
500
600
ppm Rb

ratios of 0.79 to 1.1 today (Jacobsen and Heier, 1978). Such high ratios are not seen in the Drammen granite.

Trace element data of g1 to g5 can be explained by mixing a melt containing approximately 175 ppm Rb, 40 ppm Sr, and 220 Ba with Cambro-Silurian sedimentary rocks of the Oslo Region that have approximately 200 ppm Rb, 175 ppm Sr, and 800 ppm Ba (Björlykke, 1974). Higher concentrations of Sr and Ba are also reported (Björlykke, 1974). The mixing model is shown in Fig. 2.6a,b and is represented by the line from the open asterisk to the filled asterisk. A fan-shaped pattern between the contaminant and the fractionating magma's liquid line of descent is expected if g1 to g5 were produced through contemporaneous mixing between a crystal fractionating melt and assimilated sedimentary rocks. The mixing model indicates roughly 25 to 45 % crystallization linked with 15 to 60 % bulk mixing of sedimentary rocks. The remnants of sedimentary rocks seen in the outer part of the granite supports this sediment mixing. On the other hand, this high amount of bulk mixing/melting demands large amounts of energy.

AFC can be modelled using the following equation (DePaolo, 1981; Powell, 1984):

$$C_L = C_O * f + \frac{r}{r-1-K_D} * C'(1-f)$$

where r is the ratio of rate of assimilation to rate of

fractional crystallization and $f=F^{(r-1+KD)/(r-1)}$. By using r=0.8 and the same K_D and element concentrations as before for the initial melt and assimilating shale, the change of trace element concentration of the magma follows a line from asterisk named AFC. This line cannot explain the variation in trace elements measure in the Drammen granite. Using a lower value of r will give a poorer fit to the data. However, the modelling curve will pass through some of the g1-g5 samples with lower Sr and Ba concentration will fit the modelling curve.

Whole-rock Zr and Nb contents (Fig. 2.4; Table 2.1a,b) indicate two geochemically different suites of intrusives. Zirconium contents of g1 to g5 show a wide variation that is difficult to explain even though mixing/contamination with sedimentary rocks is possible. The g6 and g8 show a linear distribution (Fig. 2.4) but with less variation in Zr than g1 to g5. Niobium and Zr are incompatible elements for granitic melts that do not crystallize Nb- and Zr-containing minerals (Wager and Mitchell, 1951; Brooks, 1969; Watson and Harrison, 1983), hence, the linear distribution suggest a suite of rocks related by crystal fractionation. Zirconium content of the initial magma was not high enough for zircon to be saturated and thereby differentiated from the magma (Watson and Harrison, 1983). K_D (crystal/melt) for Nb and Zr are much less than one (Watson and Harrison, 1983). Therefore, crystal fractionation will result in an increase in both elements.

The fractionating magma's follow a linear trend in a Zr-Nb diagram.

Zirconium enrichment of potential selective melting of Precambrian genisses would not be feasible since the zircons are not likely to melt (Watson and Harrison, 1983). The heat content of the granite magma was not high enough to completely melt the gneiss in order to inherit Precambrian zircons in this way. Some zircons could be dissolved in the melt, but not enough zircons would be available for selective dissolution to obtain the high Zr values observed in the granite samples. Bulk assimilation of lower Paleozoic sedimentary rocks with low Nb and large variation in Zr (Christie, 1975; Analytisk Sporelement Komité Norden, 1975) could explain why some granite samples (g1 to g5) plot lower in Nb (Fig. 2.4) than the granite array (mentioned above). These sedimentary rocks would have a lower melting point than the Precambrian gneisses because of high H_2O content.

Most g1-g5 plus g7 samples plot high in Zr (227-605 ppm). The very highest values could, however, be explained by accumulation of fractionating zircons from the melt. High specific weight will reduce the possibility of accumulation in the roof zone. Another, more likely explanation is accumulation of zircons from bulk assimilation of the lower Paleozoic sedimentary rocks of the Oslo Region.

O and Sr isotope analyses

The few O-isotope analyses indicate a weak assimilation of material enriched in O-isotope along the border relative to the central part. This conclusion is also supported by Segalstad and Ohmoto's (1986) data. Because the $\delta^{18}O_{SMOW}$ for neither sedimentary rocks in the Oslo graben nor the surrounding Precambrian gneisses are known, we cannot distinguish between them with O-isotope analysis.

The widespread alteration in Drammen granite indicates action of hydrothermal fluids, which may have changed Rb-Sr systematics. Therefore, a partly resetting of the Sr-isotope ratios due to hydrothermal fluid circulation through the solidified granite is likely. This may result in variation in initial $^{87}Sr/^{86}Sr$ throughout the granite giving poor curve fitting for age dating. Resetting is also the conclusion based on a combined study of Sr and Nd isotopes in the Drammen granite by Norman and Mearns (1986). They state that "isotope systematics of the unaltered Drammen granite are only preserved in fluid inclusions in miarolitic cavities". A similar effect on Rb-Sr systematics of the Franklin Mt. granite was attributed to fluids causing a hematite alteration of feldspars (Norman et al., 1987).

The age of the Drammen granite is poorly constrained to 290 Ma to 235 Ma. The Drammen granite is younger than subsided lavas in the Drammen cauldron, but the cauldron ring faults cut the Drammen granite (Gaut, 1981). Lavas in the

Fig. 2.7.

Strontium evolution diagram from the present back to Permian time for whole-rock data. The base line is the evolution of the subcrustal lithosphere beneath the Oslo Rift (after Neumann, 1988).

Fig. 2.7

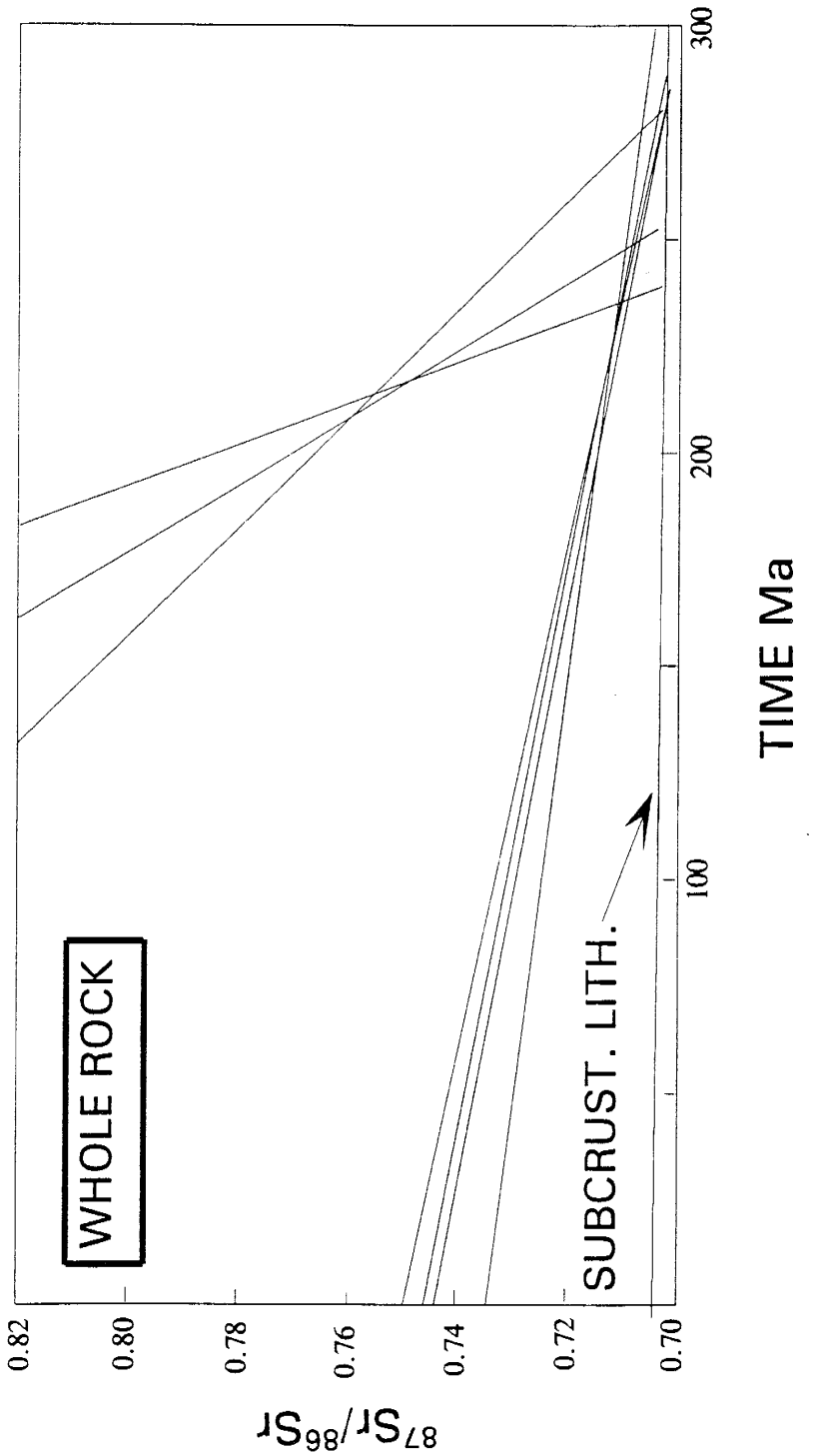
WHOLE ROCK
SUBCRUST. LITH.
0.82
0.80
0.78
0.76
0.74
0.72
0.70
87Sr/86Sr
100
200
300
TIME Ma

Oslo Rift may be close to 290 Ma old (Sundvoll, 1978b) setting an upper limit to the granite age. The lower limit would be confined by the Re-Os date of 235 Ma (Neumann, 1960). This date corresponds with K-Ar dating of alteration minerals (Ineson et al., 1975). Least altered granite samples from the early intrusive stage suggest an age of about 265 Ma.

The evolution diagram (Fig. 2.7) of whole-rock analysis shows the growth curves of the samples. The base line is subcrustal lithosphere with $^{87}Sr/^{86}Sr=0.7035$ at 300 Ma with $^{87}Rb/^{86}Sr=0.35$ (Neumann et al., 1988). This base line is based on $^{87}Sr/^{86}Sr$ data of uncontaminated early Oslo rift intrusive and extrusive rocks summarized in Neumann et al. (1988). The diagramshows intersections from 200 to 250 Ma with no uniform distribution. The late-stage granites give the largest intersection range with the base line.

Assimilation of Crustal Rocks

Lower Paleozoic sedimentary rocks of the Oslo Region have $^{87}Sr/^{86}Sr$ today at 0.71337-0.74225 with low Rb and high Sr (Segalstad and Norman, unpub. data). Assimilation of this rock at Permian times with $^{87}Sr/^{86}Sr$ of 0.7030 could yield a granite with the isotopic composition and trace element concentrations observed. If assimilating 10% of shale with Rb=200 ppm, Sr=175 ppm, and $^{87}Sr/^{87}Sr$ with a granite melt with Rb=175ppm, Sr=40 ppm, and $^{87}Sr/^{86}Sr=0.703$ the result will be a melt with Rb=178 ppm, Sr=54 ppm, and $^{87}Sr/^{86}Sr=0.709$, similar to

what is observed for g1 to g5.

Precambrian rocks enclosing the Oslo Region have high $^{87}Sr/^{86}Sr$ ratios, up to 1.19 today (Jacobsen and Heier, 1978). If partial melts of Precambrian rocks were mixed with low Sr concentration and low $^{87}Sr/^{86}Sr$ granitic melts will have high initial $^{87}Sr/^{86}Sr$ ratio. The data do not exhibit such high values. Further, the gneisses have high Rb and high Sr similar to the granite (Field and Elliott, 1974; Jacobsen and Heier, 1978; Clough and Field, 1980; Smalley and Field, 1985).

The late-stage granites g6 and g8 show more variation in strontium isotopic composition from ideal behavior than do granites g1-g5 (Table 2.2). This variation suggests a later resetting could have occurred together with hydrothermal alteration. Strontium isotope data suggest that there must have been some type of disturbance of the Rb-Sr systematics. This disturbance can be caused by a small addition of Sr to granites of low Sr content.

The late stage intrusives have a characteristic of magmatic $\delta^{18}O_{SMOW}$ value defined by Taylor (1968) with somewhat higher O-isotope ratios for the early stage granites. This O isotope data also indicates an assimilation of surrounding rock, since the early stage intrusives seems to be somewhat enriched relative to the late stage intrusives. Assimilation of sedimentary rocks is supported by rare earth element (REE) data, which is similar in pattern to average European

Paleozoic shales according to Neumann et al. (1977).

I have found no evidence for support of the speculations by Killeen and Heier (1975) and Schönwandt and Petersen (1983) that Precambrian rocks were incorporated into the magma. The lower Paleozoic black alum shale of the Oslo Region, however, constitutes a likely additional source of both Mo and radioactive elements: Mo 60 ppm; Th 14 ppm; U 22 ppm (Christie, 1975; Analytisk Sporelement Komité Norden, 1975).

The source region for the Drammen granite must be found in mantle materials. Nd isotope work on the petrogenesis of the Oslo rift igneous rocks by Jacobsen and Wasserburg (1978) and Jacobsen (1980) preclude petrogenesis through anatexis of lower crust, and rather points to petrogenesis through mixing mantle-derived melt with upper crustal materials.

CONCLUDING REMARKS ON PETROGENESIS OF THE DRAMMEN GRANITE

Based on trace element data (Rb, Sr, Ba, Zr, Nb), and Sr isotope and O isotope data, the Drammen granite batholith evolved through fractional crystallization associated with in situ bulk assimilation of mainly sedimentary rocks. The most contaminated parts of the granite occur close to the sediment contact; least contaminated granite intrusions occur in the central part of the batholith. There has been a possible later resetting and hydrothermal disturbance of the Rb-Sr systematics. These data do not support Burnham's hypothesis of porphyry Mo deposits where partial melting of sialic is a necessary precondition for forming porphyry Mo-deposits. However, Mo enrichment of the magma by assimilation of surrounding sedimentary rocks may have taken place.

FLUID GEOCHEMISTRY

ANALYTICAL METHODS

Stable isotope analysis

Fifteen MoS_2 samples were analyzed for sulfur isotope ratios at Pennsylvania State University, Pennsylvania. Sulfur dioxide was extracted by oxidizing MoS_2 with Cu_2O at about 1000°C in a vacuum system. The sulfur isotope ratios were obtained by analyzing SO_2 by mass spectrometry. Analytical error is about 0.2 per mil.

Seven quartz samples from the quartz-MoS_2 veins were analyzed for oxygen isotope ratios at Pennsylvania State University. CO_2 was extracted by reacting quartz with BrF_5 and oxidizing O_2 with graphite after method described by Clayton and Mayeda (1963). Oxygen isotope ratios were obtained by analyzing CO_2 by mass spectrometry. Analytical error is about 0.2 per mil.

Gas analyses

Twenty-eight samples were analyzed for fluid inclusion gas composition; 12 mineralized vein samples, one non-mineralized vein sample, and 15 miarolitic and rock-forming quartz samples of which 3 are from Glitrevann and 3 from the Finnemarka granite. Quartz separates were cleaned as described by Norman and Sawkins (1987) and were thermally decrepitated in a vacuum line at a temperature of 500 to

525°C. One sample (number 23C8) was heated to 800°C. The volatiles were separated by use of liquid N_2 and dry ice alcohol traps into a non-condensable (liquid N_2), condensable, and water fraction. The amounts of condensable and non-condensable fractions were determined by pressure measurement. Gaseous species and their ratios were determined by a gas mass spectrometer. The water fraction was frozen and sealed into a capillary and weighed. This method is described by Norman and Sawkins (1987) and is described in detail in Appendix C.

Salt and quartz analysis

Twenty nine samples were analyzed including 9 miarolitic quartz and 2 rock-forming quartz from the Drammen granite, 2 miarolitic quartz from the Glitrevann granite, 4 miarolitic quartz from the Finnemarka granite, and 12 vein-quartz from the Drammen granite. These samples were first coarsely crushed and quartz grains were hand picked for crushing to 60-80 mesh. Quartz was further separated by means of a Frantz magnetic separator and hand picked again. This step was especially crucial for separating rock-forming quartz from feldspar and required multi-passes through the magnetic separator. The quartz was then boiled in 50% HNO_3 for at least 24 hours, rinsed and boiled in double-distilled water for another 24-hour period, followed by cleaning in an electrolytic cell for at least a week. Fluids were extracted by thermal decrepitation and analyzed by INAA following a

method described by Norman et al. (1989). Splits of seven vein quartz samples were thermally decrepitated and salts were analyzed for Sr isotope composition. The inclusion fluids evaporated after decrepitation resulting in precipitation of salts. The salts were then dissolved in weak nitric acid solutions described by Norman et al. (1989). The salty HNO_3 solutions were evaporated to dryness, and Rb and Sr were purified by ion exchange isotope dilution method before analyzed in a VG 354 mass spectrometer. Two to 35 g of sample were used which yielded 0.3 to 16 mg of precipitates. Splits of about 75 mg of the decrepitated and leached quartz were analyzed. Duplicate and triplicate analyses were prepared by splitting a sample and separately decrepitating each split. Four blanks were made following decrepitation and leaching process as for the inclusion bearing samples. The blanks, decrepitated quarts, and salt precipitates were analyzed together subjected to the same irradiation time and counting procedures.

Salts and decrepitated and leached quartz samples were packed in ultra pure silica (supersil) vials and irradiated in the University of Missouri research reactor with flux of $2.4*10^{13}$ $n*cm^{-2}*sec^{-1}$ for 60 hours. The samples were counted three times using high purity germanium detectors: 4-6 days (for 1 hour), 7-14 days (for 2-3 hours), and 30-40 days (for 2-3 hours) after irradiation. NIST SRM 1633A (fly ash) and BCR-1 were used as standards. Data were reduced using a

Nuclear Data 6620 system and TEABAGS software (Korotev and Lindstrom, 1985).

The inclusion-fluid liquid concentration of the elements are calculated based on total dissolved solid concentration (TDS) in the fluid in Table 3.5. The TDS is calculated from amount of water thermally decrepitated from a known amount of sample and the amount of salt decrepitated from the known amount of quartz sample. Amount of element extracted per gram quartz is calculated from element concentrations in the analyzed salt multiplied with total weight of salt extracted per gram quartz assuming precipitated salts were anhydrous.

RESULTS

Fluid inclusion description and microthermometry analysis

Fifteen polished thick sections of vein, miarolitic, and rock-forming quartz were studied (Table 3.1; Appendix I). Microthermometric analysis were performed on five of these samples with a total of about 79 inclusions.

Inclusions observed in the vein quartz are all liquid dominated and no crystals were observed in the inclusions at room temperature. Inclusions observed in the miarolitic quartz are also liquid dominated where some inclusions contain halite crystals at room temperature. Most of the inclusions are small (1-5 μm). The freezing point for these small-size inclusions is difficult to determine.

A large portion of the inclusions occur along bands and planes. These bands and planes do not cross grain boundaries and the inclusions are therefore probably pseudo-secondary. Individual inclusions are also observed but these are also small and appear to be similar at room temperature to the pseudo-secondary inclusions.

Homogenization temperatures range from 130 to 350°C with the with most of the temperatures between 180 and 250°C. Calculated salt content from freezing temperatures gives a range of 2-8 wt.% NaCl eq (Appendix I). All inclusions observed homogenize to liquid upon heating.

Table 3.1. List of double polished fluid inclusion sections used for describing the fluid inclusions in the sample material.

SAMPLE #	QUARTZ TYPE	MICROSCOPY	HEATING	FREEZING
OG-2	MIAROLITIC	YES	YES	YES
OG-9	MIAROLITIC	YES	YES	YES
OG-12A	MIAROLITIC	YES	YES	YES
OG-12B	MIAROLITIC	YES	YES	YES
21B-DG	MIAROLITIC	YES	NO	NO
27A-DG	MIAROLITIC	YES	NO	NO
50-DG	VEIN	YES	NO	NO
53-DG	VEIN	YES	YES	YES
55C-DG	VEIN	YES	YES	YES
58A-DG	VEIN	YES	YES	YES
60A-DG	VEIN	YES	NO	NO
66B-DG	VEIN	YES	YES	YES
68A-DG	VEIN	YES	YES	YES
69A-DG	VEIN	YES	NO	NO
71A-DG	VEIN	YES	NO	NO

The OG samples are from Olsen and Griffin (1984a,b) where microthermometric data are presented for these four samples.

Stable isotope analysis

$\delta^{34}S_{CDT}$ for MoS_2 ranges from -0.3 to 3.2 per mill (Table 3.2). Sulfur isotopic ratios of the mineralizing solutions were calculated using fractionation equations for H_2S and SO_4^{2-} from Ohmoto and Rye (1979), assuming deposition at 300°C as reported by Olsen and Griffin (1985a). The SO_2/H_2S ratios from fluid inclusion gas analyses were used in the calculations assuming no fractionation between SO_2 and SO_4^{2-}, and that sulfate in inclusion waters yielded SO_2 when thermally decrepitated. The calculations indicate that the mineralizing solutions have somewhat heavier sulfur than assuming sulfate-free waters, but the values are still in the range where they can be considered magmatic. There is no evidence to support the idea that hydrothermal fluids contained sedimentary sulfur (Fig. 3.1). Rather, these sulfur isotope data are similar to those for porphyry-type deposits in general (Ohmoto and Rye, 1979), and those reported for porphyry molybdenum deposits (Lang et al., 1989; Ohmoto, 1985; Laughlin et al., 1969).

The $\delta^{18}O_{QTZ}$ data for the vein quartz is consistent around 9.5 per mil relative to the SMOW standard (Table 3.2). Oxygen isotope ratios calculated for 300°C solutions using the fractionation equation from Matsuhisa et al. (1979) indicate $\delta^{18}O_{W,SMOW}$ to have ranged from 2.3 to 2.7 (± 2) per mill. The uncertainty is based on analytical error, temperature uncertainty, and equation uncertainty. The possible effect of

Table 3.2.

Oxygen isotope data for quartz and sulfur isotope data for molybdenite from quartz molybdenite veins in the Drammen granite. The isotopic composition of mineralizing waters and H_2S was calculated from the data of Matsuhisa et al. (1979), and Ohmoto and Rye (1979), respectively. The fluid composition was calculated at 300°C (see temperature calculation). These calculated $\delta^{18}O$ and $\delta^{34}S$ values have a uncertainty of 2 per mil and 0.1 per mil., respectively.

SAMPLE #	$\delta^{18}O_{QTZ}$	$\delta^{18}O_{FLUID}$	$\delta^{34}S_{Mo}$	$\delta^{34}S_{FLUID}$
50	9.5	2.7	1.9	0.5
51a			0.7	5.3
52a	9.6	2.7	0.7	5.3
53			3.2	5.2
54a	9.2	2.3	-0.3	-1.7
54b			0.4	-1.0
54d			0.3	-1.1
55a	9.4	2.5	0.0	4.6
58a			1.1	5.7
59a	9.3	2.4	1.1	5.7
59b	9.5	2.6	2.3	1.0
60a			1.2	-0.2
66a	9.4	2.5	0.8	5.4
66b			1.0	-0.4
68a			8.5	1.6

Fig. 3.1.

Plot of $\delta^{18}O_{SMOW}$ for water versus $\delta^{34}S_{CDT}$. The large square represents magmatic composition (Ohmoto, 1979; Taylor, 1979). The two open boxes on the lower part of the diagram represent crustal sulfur plotted with Permian meteoric water (Segalstad, unpubl.); the box to the left represents black shale (Alum Shale) sulfur, and the box to the right, Precambrian sulfur in the rocks near the Oslo Rift (Segalstad, unpubl. data).

Fig. 3.1

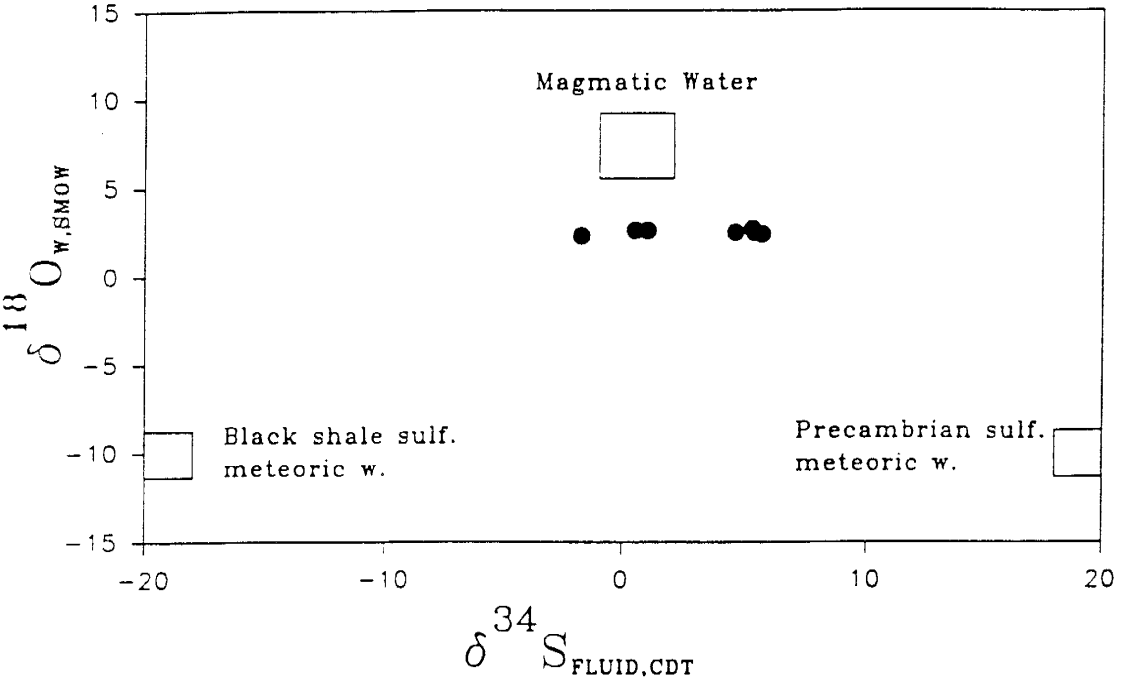
15
10
5
0
-5
-10
-15
-20
-10
0
10
20
Magmatic Water
Black shale sulf.
meteoric w.
Precambrian sulf.
meteoric w.
$\delta^{18}O_{W,SMOW}$
$\delta^{34}S_{FLUID,CDT}$

dissolved solids on oxygen isotope fractionation (Truesdell, 1974) was not considered.

Water of $\delta^{18}O_{SMOW,H2O}$=2.5 per mill. could be of magmatic origin. Assume that an aqueous fluid phase exolved from amagma at 600-700°C, then cooled to 300°C, and reequilibrated with the solidified granite the water would have $\delta^{18}O_{SMOW}$=2.2 per mill, given a granite composition with 30% quartz, 45% K-feldspar, 23% plagioclase, and 2% biotite with $\delta^{18}O_{SMOW}$=7.7 per mill for whole rock (Whole-Rock Geochemistry, this report; fractionation factors from Taylor, 1978). This calculation is based on a low water/rock ratio (i.e. a rock dominated system) where the $\delta^{18}O_{SMOW}$ for the rock stays constant.

Gas analysis

Vein samples from the Drammen granite

Table 3.3a shows the analysis of the volatile phase in inclusions of all the vein samples from the Drammen granite. Water is the dominant phase of the inclusion fluids and makes up 98 to almost 100 mole % of the volatile component. The only exception is sample 59C DG-85 for which 89 mole % of water was measured. Carbon dioxide is the second most abundant gas component and constitutes about 0.1 to 2 mole %. It is not a visible phase under the microscope in the inclusions at room temperature, or when cooled to -60°C. Light HC (hydrocarbon compounds) of methane, propane, and ethane are common among measured constituents, but comprise

Table 3.3 a.

Gas analyses in mole % of inclusion fluids normalized to 100% including H_2O for quartz from the quartz-molybdenite veins (V) from the Drammen granite, Norway. Sample 71A is from a barren vein. The table also gives the calculated gas geothermometer temperatures for the raw data, log $f(O_2)$ for the raw data for three different equations (see text), the calculated composition (B), the two gas geothermometers for the calculated composition (B), and the log f(O2) for the recalculated composition (B) for the three equations. Below log $f(O_2)$ for recalculated data are calculate log $f(S_2)$ for the three calculated log $f(O_2)$ for raw and recalculated data. At the bottom are calculated pH based on Eq. 16.

Table 3.3a. Gas analyses in mole % of inclusion fluids from vein samples. See Table 3.3b for abrivation explanations.

Sample #	50	51A	51B	52A	54D	55A	58A	59A	59B	59C	63	66A	68A	71A
Vein mineral/unmineral	V	V	V	V	V	V	V	V	V	V	V	V	V	VUM
He	nd	nd	0.00011	nd	nd	nd	nd	0.00111	0.00127	0.00036	0.00003	0.00002	0.00003	nd
H_2	0.00288	0.0294	0.00333	0.00118	0.00939	0.04272	0.3912	0.05919	nd	0.00917	0.5812	0.00512	0.00211	0.00357
PROP	nd	nd	nd	nd	0.01378	nd	nd	nd	nd	nd	0.0286	0.00116	nd	nd
BENZ	nd	nd	nd	nd	nd	nd	nd	nd	nd	nd	nd	nd	nd	nd
N_2	0.00165	0.0372	0.01228	0.0354	nd	0.5716	2.8055	0.3619	0.10727	2.1572	0.03415	0.11723	0.06741	nd
ETH	0.00241	0.00262	nd	0.00543	0.11289	0.07279	nd	0.03294	nd	2.2372	0.06509	0.01307	nd	nd
SO_2	0.01185	0.00091	0.1861	0.00044	0.00387	nd	0.00066	0.00364	0.01006	0.8886	0.06971	0.00445	0.00159	0.00025
H_2S	nd	nd	0.09264	nd	nd	nd	nd	nd	1.8997	0.01407	0.05991	nd	nd	nd
O_2	nd	nd	nd	nd	nd	nd	nd	nd	nd	nd	0.0572	nd	nd	nd
Ar	nd	0.00019	0.00004	0.00003	nd	0.00014	0.00561	0.00045	nd	0.00773	0.00004	0.00024	0.00014	0.00014
CO	0.00274	0.00336	0.0018	0.00805	nd	0.05285	0.2018	0.03679	0.09378	0.4563	0.00492	0.00281	0.0054	nd
CH_4	0.00143	0.00559	nd	0.01681	0.00661	nd	nd	0.1143	nd	0.3018	0.00352	0.00535	nd	nd
CO_2	0.0553	0.5375	0.6242	0.13314	0.2707	1.8837	0.4932	1.2326	nd	7.1067	0.935	0.1085	0.20038	0.08056
H_2O	99.9217	99.383	99.076	99.803	99.583	97.376	96.1021	98.157	98.2181	88.6614	98.25	99.7485	99.634	99.912
ETHY	nd	nd	nd	nd	nd	nd	nd	nd	nd	nd	nd	nd	nd	nd
PRPY	nd	nd	nd	nd	nd	nd	nd	nd	nd	nd	nd	nd	nd	nd
iBUT	nd	nd	nd	nd	nd	nd	nd	nd	nd	nd	nd	nd	nd	nd
BUTYL	nd	nd	nd	nd	nd	nd	nd	nd	nd	nd	nd	nd	nd	nd
PNTN	nd	nd	nd	nd	nd	nd	nd	nd	nd	nd	nd	nd	nd	nd
HC	0.00241	0.00262	0	0.00543	0.12667	0.07279	0	0.03294	0	2.2372	0.06509	0.01307	0.0286	0.00116
CO_2/HC	22.95	205.15	0.00	24.52	2.14	25.88	0.00	37.42	0.00	3.18	14.36	8.30	7.01	69.45
SUM	99.99996	99.99977	99.9965	100.0035	100.0002	99.9998	100.0001	99.99992	100.3289	101.8414	100.0004	99.99995	100.0004	100.0031
T (Eq. 1)	273	348	301	264	314	372	411	375	-	351	430	292	280	282
T (Eq. 2)	319	403	-	281	357	-	-	409	-	351	312	318	-	-
$f(O_2)$ (Eq. 5)	-35.70	-34.71	-34.64	-35.32	-35.01	-34.16	-34.75	-34.35	-	-33.59	-34.47	-35.40	-35.14	-35.53
$f(O_2)$ (Eq. 4)	-35.73	-33.32	-	-37.20	-34.68	-	-	-33.66	-	-34.94	-	-	-35.84	-35.96
$f(O_2)$ (Eq. 3)	-34.09	-33.89	-	-34.43	-34.07	-	-	-34.36	-	-34.19	-	-	-34.00	-34.29
Back calculated composition														
B H_2	-	0.0002	0.00012	-	0.00481	0.00182	0.00397	0.00226	-	0.00093	0.00281	-	-	-
B CH_4	-	0.0149	0.00185	-	0.00776	0.01023	0.09669	0.12855	-	0.30384	0.1446	-	-	-
B CO_2	-	0.5283	0.62298	-	0.26955	1.87303	0.39589	1.21828	-	7.10425	0.7904	-	-	-
Temperature and log $f(O_2)$ calculation based on back calculated composition														
B T(Eq. 1)	-	300	300	-	300	300	300	300	-	300	300	-	-	-
B T(Eq. 2)	-	325	368	-	334	317	312	301	-	282	304	-	-	-
B $f(O_2)$(Eq. 5)	-	-34.72	-34.65	-	-35.01	-34.17	-34.84	-34.35	-	-33.59	-34.54	-	-	-
B $f(O_2)$(Eq. 4)	-	-38.09	-37.31	-	-37.81	-37.51	-38.37	-38.31	-	-37.92	-38.30	-	-	-
B $f(O_2)$(Eq. 3)	-	-34.10	-33.49	-	-34.14	-33.75	-34.58	-34.39	-	-34.20	-34.51	-	-	-
Log $f(S_2)$ based on $f(O_2)$ from raw data and back calculated data.														
$f(S_2)$ $f(O_2)$ Eq.5		-	-10.01	-	-	-	-	-	-	-10.59	-10.21	-	-	-
$f(S_2)$ $f(O_2)$ Eq.4		-	-	-	-	-	-	-	-	-11.95	-	-	-	-
$f(S_2)$ $f(O_2)$ Eq.3		-	-	-	-	-	-	-	-	-11.20	-	-	-	-
$f(S_2)$ B $f(O_2)$ Eq.5		-	-10.01	-	-	-	-	-	-	-10.59	-10.29	-	-	-
$f(S_2)$ B $f(O_2)$ Eq.4		-	-12.68	-	-	-	-	-	-	-14.92	-14.05	-	-	-
$f(S_2)$ B $f(O_2)$ Eq.3		-	-8.86	-	-	-	-	-	-	-11.20	-10.26	-	-	-
pH	-9.1	-9.0	-7.8	-9.6	-8.9	-	-9.1	-8.4	-	-6.6	-7.9	-9.1	-9.2	-9.9

less than 0.1 mole % except for sample 59C DG-85. Methane generally was detected together with either propane or ethane. In a few analysis heavier HC (as propylene, iso-butyl, butylene, and pentene) with m/e units from 42 to 72 were detected. Benzene, which has a principal peak at m/e=84, was not detected. The CO_2/HC ratio varies from 2 to 70 (Table 3.3a). The system was not calibrated for all light organic species, hence the results are reported as C_nH_n (after Norman and Sawkins, 1987).

Carbon monoxide was commonly detected. It constitutes about 0.002 to 0.4 mole % of analysis fluids and is principally 1 to 2 orders of magnitude less than CO_2. In one sample (59B DG-85) CO was measured whereas CO_2 was not.

Hydrogen was measured from above the detection limit of 0.0001 to 0.6 mole %. Samples from Sörumsåsen and Oterdalen mines have the lowest values.

Argon was detected in most of the samples from the molybdenite deposits and makes up from 0.0001 to 0.007 mole % of the total fluids. For some samples the ^{36}Ar peak was detected in 2 to 4 orders of magnitude less than ^{40}Ar. Helium was detected at amounts of 0.00002 to 0.001 mole % in analyses of samples from molybdenite deposits.

The major sulfur species is SO_2, which was generally the only sulfur component detected. However, for some samples H_2S is present either about equal or at somewhat higher amounts than SO_2. Analyses of one sample from Sörumsåsen mine (51B

DG-85), two from the Vassåsen claim (59B- and 59C-DG-85), and one sample from the Oterdalen mine (63-DG-85) contain H_2S above the detection limit.

The analysis of the non-mineralized vein sample indicates that fluid inclusions constitute 99.9 mole % H_2O 0.08 mole % CO_2 and lesser amounts CO, Ar, CH_4, C_nH_n (total hydrocarbon heavier than CH_4), and He.

Miarolitic and rock-forming quartz

Drammen granite: Analyses of miarolitic- and rock-forming quartz from the Drammen granite indicate that water is the most abundant at 94 to 99.5 mole% (Tables 3.3b and 3.4). Carbon dioxide is the principal gaseous species and constitutes 0.1 to 5 mole% for most analyses. Hydrogen, N_2, and CO constitute about equal amounts, 0.01 to 0.2 mole%. Nitrogen was not detected in sample 23B, and CO was not detected in samples 18C and 21B. Methane is present in less amounts than N_2 and constitutes from 0.007 to 0.1 mole%.

Sample 23C acted differently than other samples during decrepitation. When heated to 500°C (23C5) it yielded no water, but rather CO_2 and propane at a CO_2/HC ratio of 2.0. A split of the sample was heated to 800°C (23C8). It yielded a water-dominated fluid with no HC. Argon was detected in 23C at both decrepitation temperatures. Helium was detected only during the highest temperature run.

Analyses of samples 21C and 23C8 from the Drammen granite

Table 3.3b. Same as Table 3.3a for inclusion fluids from miarolitic (M) and rock-forming (RF) quartz separates from the Drammen granite (D), Glitrevann granite (G), and Finnemarka granite (F). Fluid inclusion gas analyses in mole% with temperature and fugacity calculations.

Sample #	18A	18C	18D	21B	21B2	21C	23B	23C5	23C8	28C	32	32C	32C2	41B	41D	42
Qtz T.	M	M	RF	M	M	M	M	RF	RF	M	M	M	M	M	M	M
Granite t.	D	D	D	D	D	D	D	D	D	D	G	G	G	F	F	F
He	nd	nd	nd	nd	nd	nd	nd	nd	nd	nd	nd	nd	nd	nd	nd	nd
H_2	0.1301	0.0489	0.0484	0.0168	0.0736	0.0216	0.0789	0.4734	0.0032	0.7701	0.0356	0.3481	0.6375	0.1870	0.2026	0.1956
PROP	0.0337	nd	0.1318	nd	nd	0.1823	nd	24.729	0.1179	nd	0.0205	nd	nd	nd	nd	nd
BENZ	nd	nd	nd	nd	nd	nd	nd	nd	nd	nd	nd	0.0027	nd	nd	nd	nd
N_2	0.0594	0.1814	0.3344	0.2067	0.0658	nd	nd	23.713	0.1049	0.2803	0.0207	nd	2.0077	nd	0.5954	0.1706
ETH	nd	nd	nd	nd	nd	nd	nd	nd	nd	nd	nd	nd	0.4228	0.0006	nd	0.0009
SO_2	nd	0.062	0.1049	nd	nd	0.0014	nd	nd	0.0035	nd	0.0261	nd	0.4134	nd	nd	nd
H_2S	nd	nd	nd	nd	nd	nd	nd	nd	nd	nd	nd	nd	nd	nd	nd	nd
O_2	nd	1.4199	nd	0.0313	0.0627	nd	nd	nd	nd	nd	nd	nd	nd	nd	0.4203	nd
Ar	nd	nd	0.0011	0.0009	0.0011	nd	nd	0.0186	0.0006	nd	nd	nd	0.007	0.0013	0.0026	nd
CO	0.1376	nd	0.2746	nd	0.1351	0.0018	0.1361	1.5913	0.0074	0.5056	0.0726	0.1756	0.3148	0.4777	0.7084	nd
CH_4	0.0466	0.2225	0.1097	nd	0.0069	nd	0.0116	nd	nd	0.0921	0.0081	0.049	nd	0.2644	0.0445	0.0475
CO_2	1.5506	3.8882	2.4453	1.9484	2.1425	0.1048	0.4695	49.455	0.2371	6.0836	3.2449	2.1882	17.4611	2.1325	6.0418	3.0657
H_2O	97.9988	94.1771	96.3408	97.7959	97.4868	99.6881	99.2848	nd	0.5284	92.2409	96.281	97.1902	78.7357	96.8736	91.7242	96.4294
ETHY	nd	nd	0.0428	nd	nd	nd	nd	nd	nd	0.0275	nd	nd	nd	0.0171	nd	0.0246
PRPY	nd	nd	nd	nd	0.0254	nd	nd	nd	nd	nd	nd	0.0258	nd	0.0192	0.2601	0.0276
iBUT	nd	nd	0.0318	nd	nd	nd	nd	nd	nd	nd	nd	nd	nd	nd	nd	nd
BUTYL	0.0432	nd	0.1261	nd	nd	nd	0.0191	nd	nd	nd	0.3109	nd	nd	0.0266	nd	0.0382
PNTN	nd	nd	0.0082	nd	nd	nd	nd	nd	nd	nd	nd	nd	nd	nd	nd	nd
HC	0.0769	nd	0.3407	nd	0.0254	0.1823	0.0191	24.729	nd	0.0275	0.3109	0.049	0.4228	0.0635	0.2601	0.0913
CO_2/HC	20.16	0.00	7.18		84.35	0.57	24.58	2.00		221.22	10.44	44.66	41.30	33.58	23.23	33.58
SUM	100	100	99.999	100	99.9999		100	100	100	100.0001	99.9999	100.0001	100.000.00	99.999	100.00	
T(Eq. 1)	397	384	378	350	387	322	370	481	371	464	374	428	474	411	427	417
T(Eq. 2)	449	406	408	-	448	-	432	-	-	529	423	491	-	449	488	471
log $f(O_2)$(Eq.5)	-24.40	-24.00	-24.20	-24.30	-24.26	-25.57	-24.92	-22.89	-25.2	-23.80	-24.08	-24.25	-23.35	-24.26	-23.81	-24.10
log $f(O_2)$(Eq.4)	-22.68	-23.80	-23.71	-	-22.20	-	-23.02	-	-	-20.83	-22.72	-21.69	-	-22.98	-21.68	-22.03
log $fO_(_2)$(Eq.3)	-23.22	-23.37	-23.31	-	-22.73	-	-23.17	-	-	-23.09	-22.68	-23.16	-	-23.53	-22.94	-23.08

Qtz-quartz; t-type; Eq-equations from the text; nd- not detected; PROP-propane; BENZ-benzene; PRPY-porpylene; ETHY-ethylene; iBUT-isobutyl; PNTN-pentene; CH-sum hydrocarbons

Table 3.4.

Summary table of gas analyses with range and mean for vein samples, Drammen granite miarolitic and rock forming quartz samples, Glitrevann granite samples, and Finnemarka granite samples.

	VEIN RANGE	MEAN (14)	DRAMMEN RANGE	MEAN(9)
He	ND-0.0013	0.00021	ND-ND	ND
H_2	ND-0.58	0.081	0.017-0.77	0.15
N_2	ND-2.81	0.45	ND-0.28	0.141
SO_2	ND-0.89	0.084	ND-0.10	0.021
H_2S	ND-1.90	0.15	ND-ND	ND
Ar	ND-0.008	0.0011	ND-0.019	0.0004
CO	ND-0.46	0.062	ND-0.51	0.15
CH_4	ND-0.30	0.033	ND-0.22	0.061
CO_2	ND-7.11	0.98	0.1-6.1	2.3
HC	ND-0.45		ND-0.22	0.15
H_2O	88.7-99.9	98.1	92.2-99.7	96.9
CO_2/HC	ND-65	12	ND-66	21
L $f(O_2)$	-33.3→-35.8		-22.4→24.6	
L $f(S_2)$	-8.9→-11.2			

	GLITRE.RANGE	MEAN(3)	FINNEM. RANGE	MEAN (3)
He	ND-ND	ND	ND-ND	ND
H_2	0.04-0.64	0.34	0.19-0.20	0.20
N_2	ND-2.0	0.68	ND-0.60	0.26
SO_2	ND-0.41	0.15	ND-ND	ND
H_2S	ND-ND	ND	ND-ND	ND
Ar	ND-0.007	0.0023	ND-0.0026	0.0013
CO	0.073-0.31	0.19	ND-0.71	0.40
CH_4	0.008-0.049	0.019	0.04-0.26	0.12
CO_2	2.1-17.5	7.6	2.1-6.0	3.7
HC	0.10-0.42	0.28	0.14-0.33	0.27
H_2O	78.7-97.2	90.7	91.7-96.9	95.0
CO_2/HC	10-41	25	7-22	16
L $f(O_2)$	-21.7→24.1		-21.7→-24.3	

L-log. ND-below detection limit. Numbers in parenthesis are the amount of samples included in the mean calculation. Lf(O_2) and L f(S_2) for fluids from vein samples are calculated at 300°C and L f(O_2) are calculated at 500°C.

are very similar with respect to gas contents; about 99.5 mole% water, 0.1 to 0.2 mole% CO_2, and minor SO_2 and CO were detected. Sample 21C yielded an order of magnitudeless H_2, yet more HC than CO_2 (CO_2/HC $\approx$ 0.6), than sample 23C8. HC consists of propane.

The organic compounds of propane, ethylene, isobutane, butylene, and pentane were detected in the samples at different combinations and amounts, in addition to methane. The total organic compounds (methane included) constitute on the average 0.05 mole%, with a range from 0 to 0.15 mole% (excluding sample 59C). The CO_2/HC ratio is generally between 10 and 50 but for a few of the analyses the CO_2/CH ratio is close to one.

Sulfur dioxide was detected in four of the samples in amounts varying between 0.0006 and 0.1 mole%. The highest amounts were detected in samples from the late stage intrusions. Argon was detected in some of the samples constituting 0.001 mole% and less. Helium was detected only in sample 23C8.

Drammen granite miarolitic quartz indicate analyses indicate similar CO_2 contents as reported by Olsen and Griffin (1984a). The analyses here reported range from 0.1 to 6.1 mole and average 2.3 mole%. Olsen and Griffin (1984a) reported ranges of 2.3 to 5.7 mole% and an average of 4.1 mole % for thermal decrepitation between 600 and 1000°C and 0.7 to 6.9 mole% and an average of 3.2 mole% for crushing.

Glitrevann and Finnemarka granites: The three miarolitic quartz samples from the Glitrevann granite yielded water as a principal component ranging from 78.7 to 97.2 mole% (Tables 3.3b and 3.4), followed by CO_2 that ranges from 2.2 to 17.5%. Hydrocarbon components were detected giving CO_2/HC ratio ranging from 10 to 40. Sulfur dioxide was measured in the two samples where N_2 also was detected. No H_2S was detected. Methane, propane, benzene, propylene, H_2, CO, Ar, and O_2 were also detected.

The three miarolitic quartz samples from the Finnemarka granite yielded water as a principal component ranging from 91.7 to 96.9 mole% (Table 3.3b), followed by CO_2 ranging from 2.1 to 6.0 mole%. A small amount of SO_2 was measured (≈0.001 mole%), but no H_2S was detected. Hydrocarbon components were detected giving CO_2/HC ratio ranging from 6 to 22. The HC constitute of benzene, ethylene, propylene, butylene, and pentene. In addition, N_2, H_2, CO, and Ar were detected.

Inclusion fluid Sr-isotope analysis

Six Rb-Sr isotope analyses (Table 2.3) from fluid inclusions plot above the isochron of 274 Ma (Norman and Mearns, unpub. data) and one below. The 3 samples above show an enrichment of radiogenic Sr relative to the whole-rock isochron (Fig. 3.2). The fluids trapped at the Sörumsåsen mine are depleted in radiogenic Sr relative to the whole-rock isochron. Preferential adsorption of double charged Sr on

Fig. 3.2.

Plot of Rb-Sr isotope data of whole rock and salts (FI) extracted from thermal decrepitated vein quartz precipitated with molybdenite. The data are from four molybdenum deposits in the Drammen granite batholith. The whole-rock Rb-Sr isochron of 274 Ma for the Drammen granite is from Norman and Mearns (unpubl. data).

Fig. 3.2

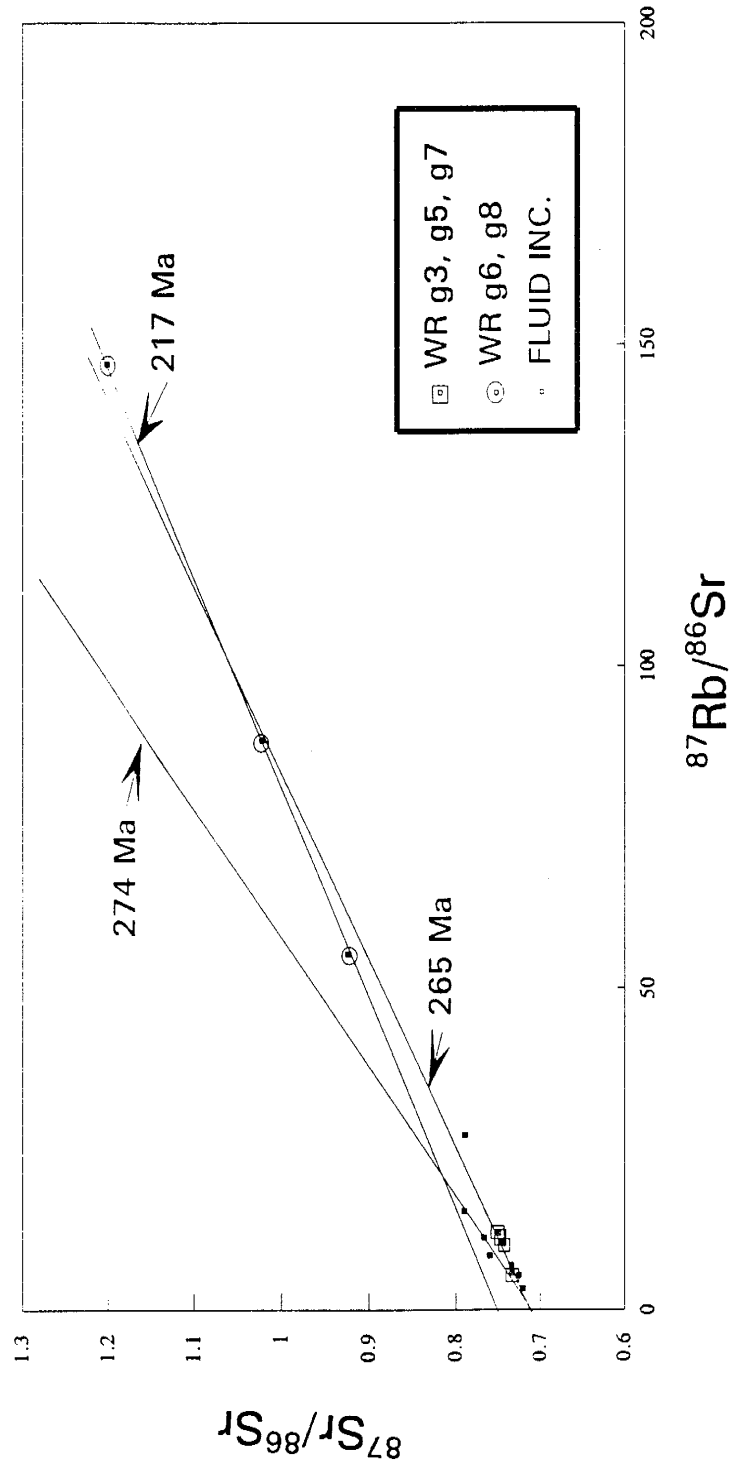
WR g3, g5, g7
WR g6, g8
FLUID INC.
217 Ma
274 Ma
265 Ma
$^{87}Sr/^{86}Sr$
$^{87}Rb/^{86}Sr$
1.3
1.2
1.1
1
0.9
0.8
0.7
0.6
0
50
100
150
200

surfaces could have affected the Rb/Sr ratios measured. Thus, the calculated $^{87}Rb/^{86}Sr$ ratio calculated maybe too high. The data fall mostly between 290 and 235 Ma isochrons, hence, probably represent fluids trapped at the time of the Drammen granite intrusion. Values for whole-rock samples for the most part fall outside this isochron. Fluid inclusion Rb-Sr systematic could reflect the irregular systematics of the granite.

Salt analysis

The salt analyses (Table 3.5) do not total to 100%. This discrepancy results because no anions except Br were measured, some principal cations such as Ca and Mg were not measured, and the dried salts likely contained some water. Some silica may also have been dissolved during the leaching process. Small fragments of quartz could have passed through the filters used. Based on the use of 40 ml of leaching fluid and solubility of quartz at 25°C in weak acid solution (Stumm and Morgan, 1981) the amount of dissolved quartz will constitute in the order of 0.001 mg.

Only Na, K, Sc, Cr, Fe, Co, Zn, As, Br, Sb, Cs, La, Ce, Nd, Sm, Eu, and Ta were detected were detected in the blanks. Not all of these elements were detected every blanks. The total amount of salts for the blanks was mostly less than 0.001 mg assuming a precipitation of 1 mg the concentrations have been calculated (Table 3.5b). All the elements measured

Table 3.5a. INAA analyses of salts in ppm from vein samples with the corresponding calculated liquid composition.

SAMPLE # 50-DG			51A-DG		52A-DG		54A-DG		54D-DG		58A-DG		59A-DG	
QTZ T.	V		V		V		V		V		V		V	V
GRANITE														
SAMP. T	S	F	S	F	S	F	S	F	S	F	S	F	S	F
Na	94735	9474	164320	14789	118325	5916	79823	8781	4867	535	5816	1745	8205	3364
K	1660	166	3238	291	4898	245	3155	347	216	24	573	172	nd	308
Sc	13.6	1.3	3.5	0.32	11.6	0.58	5.0	0.55	0.52	0.058	0.59	0.16	0.80	0.34
Cr	46	4.6	10	0.9	21	1.1	64	7.0	14	1.5	7.7	2.3	3.8	1.6
Fe	15313	1531	12981	1168	12670	634	8084	889	1065	117	762	229	933	382
Co	37	3.7	31.7	2.9	5.1	0.25	10.6	1.2	0.98	0.11	0.53	0.16	0.24	0.0984
Zn	765	77	2345	211	1905	95	1905	209	172	18.9	122	37	231	95
As	94	9.4	182	16.4	213	10.7	77	8.5	4.2	0.46	3.2	0.96	10	4.1
Br	43	4.3	64	5.8	179	9	164	18.0	3.9	0.43	2.9	0.87	1.6	0.66
Rb	118	12	99	9	100	5	415	46	18	2	88	26	nd	nd
Sr	nd	nd	470	42	490	25	nd	nd	nd	nd	44	13	nd	nd
Mo	795	80	800	72	1940	97	2370	261	51	5.6	38	11.4	180	73.8
Ag	nd	nd	nd	nd	nd	nd	7.4	0.81	0.96	0.11	nd	nd	0.26	0.11
Cd	21	2.1	nd	nd	nd	nd	nd	nd	nd	nd	nd	nd	nd	nd
Sb	nd	nd	15.4	1.4	8.3	0.42	nd	nd	0.21	0.023	0.17	0.051	0.51	0.21
Cs	47	4.6	846	76	505	25	313	34	17.7	1.9	22	6.6	42	17.0
Ba	12.9	1.3	244	22	4960	248	nd	nd	54	5.9	nd	nd	nd	nd
La	1100	110	73.3	6.6	152	7.6	370	41	49	5.3	220	66	347	143
Ce	1558	156	203	18	220	11	682	75	119	13.1	509	152	nd	nd
Nd	637	64	59	5.3	115	5.8	230	25	63	6.9	279	84	394	162
Sm	67.1	6.7	12	1.1	16.4	0.82	5305	584	15.6	1.7	71	21.2	82	34
Eu	5.4	0.54	1.3	0.12	2.1	0.10	303	33	0.6	0.066	0.68	0.20	0.79	0.32
Tb	4.0	0.40	1.6	0.14	1.8	0.091	16.7	1.8	3.5	0.38	14.7	4.4	15.1	6.2
Yb	9.1	0.91	15.2	1.37	9	0.45	163	18	30	3.3	157	47	187	77
Lu	1.9	0.19	2.8	0.25	1.8	0.091	27.5	3.0	4.9	0.54	28	8.4	33.4	13.7
Hf	nd	nd	nd	nd	nd	nd	8	0.88	0.42	0.046	0.09	0.027	0.2	0.082
Ta	nd	nd	nd	nd	3.8	0.19	nd	nd	nd	nd	0.87		2.3	1.7
W	1890	189	9	0.81	218	10.9	235	26	1.3	0.14	3.6	1.08	6.1	2.5
Ir	nd	nd	0.026	0.0023	0.015	0.0008	0.046	0.0051	nd	nd	0.0076	0.0023	0.025	0.010
Au	nd	nd	nd	nd	nd	nd	0.009	0.0009	0.008	0.0008	nd	nd	nd	nd
Hg	nd	nd	0.73	0.7							0.16		0.28	
Th	2.5	0.25	0.8	0.072	4.2	0.21	23.2	2.6	3.2	0.35	1.7	0.501	nd	nd
U	nd	nd	99	8.91	12.9	0.65	73	8.0	5.6	0.62	1.4	0.42	2	0.82
TDS wt.%	10		9		5		11		11		30		41	
SALT mg	0.34		0.98		0.204		0.13		2.78		8.73		7.64	
QTZ g	2.15		6.34		1.81		5.58		3.49		26.17		15.5	
SALT/QTZ	0.1581		0.1546		0.1127		0.0233		0.7966		0.3336		0.4929	

QTZ-quartz; T-type; V-vein; M-miarolitic; RF-rock forming; SAMP-sample; D-Drammen; S-salt; F-liquid; na-not analyzed; nd-not detected; TDS-total dissolved solids in wt%.

Table 3.5a cont. INAA analyses in ppm of salts from vein samples with corresponding calculated liquid composition.

SAMP. #	DG-59B		DG-66A		DG-66B		DG-68A		DG-71	
QTZ T.	V		V		V		V		V	
GRANITE										
SAMP. T	S	F	S	F	S	F	S	F	S	F
Na	4496	2428	57271	9736	110610	8849	82494	2475	122406	2081
K	308	166	581	99	2906	232	4483	134	4134	70
Sc	1.8	0.98	3.7	0.63	4.3	0.34	10.3	0.31	7.9	0.14
Cr	5.7	3.1	18.3	3.1	12	0.96	48	1.4	72	1.2
Fe	816	441	3957	673	8628	690	15080	452	9716	165
Co	0.23	0.12	1.9	0.32	2.7	0.22	4	0.12	7.4	0.13
Zn	146	79	1082	184	2075	166	1420	43	2510	43
As	4.1	2.2	24	4.1	51	4.1	55	1.7	73	1.2
Br	1.8	0.97	39	6.6	nd	nd	37	1.1	100	1.7
Rb	42	23	302	51	810	65	326	9.8	820	14
Sr	nd	nd	nd	nd	nd	nd	nd	nd	nd	nd
Mo	221	119	400	68	950	76	1200	36	490	8.3
Ag	nd	nd	1.8	0.31	3.6	0.29	nd	nd	nd	nd
Cd	nd	nd	nd	nd	nd	nd	nd	nd	nd	nd
Sb	0.15	0.081	1.3	0.23	2.8	0.22	8.5	0.26	6.9	0.12
Cs	18	9.7	150	26	335	27	347	10.4	426	7.2
Ba	nd	nd	nd	nd	nd	nd	510	15.3	nd	nd
La	619	334	167	28	172	13.8	125	3.8	230	3.9
Ce	1424	769	430	73	320	26	187	5.6	283	4.8
Nd	558	301	206	35	90	7.2	40	1.2	189	3.2
Sm	107	58	62	10.5	22	1.7	nd	nd	281	4.8
Eu	1	0.54	1.4	0.24	1.3	0.11	1.5	0.044	0.5	0.0085
Tb	17.9	9.7	15.9	2.7	5.9	0.47	3.7	0.11	7.4	0.13
Yb	212	114	185	31	66	5.2	57	1.7	88	1.5
Lu	39	21	34	5.7	12.0	0.96	10.8	0.32	16	0.27
Hf	1.9	1.1	2.0	0.33	11.5	0.92	22	0.66	nd	nd
Ta	1.7	0.9	2.8	0.48	5.6	0.44	18.1	0.54	1.5	0.03
W	5	2.7	13.2	2.2	16.3	1.3	39	1.2	nd	nd
Ir	0.007	0.0038	0.03	0.0051	0.035	0.0028	0.105	0.0032	0.057	0.001
Au	nd	nd	nd	nd	nd	nd	nd	nd	nd	nd
Hg	nd	nd	nd	nd	nd	nd	24.3	0.73	4.1	0.07
Th	12.9	6.9	22.2	3.8	155	12.4	77.9	2.3	36.3	0.62
U	9.3	5.0	8.9	1.5	73	5.8	285	8.55	47	0.80
TDS	54		17		8		3		1.7	
MG SALT	3.27		1.55		0.68		0.32			
G QTZ	19.01		20.67		16.19		7.11			
MG/GQTZ	0.172		0.075		0.042		0.045			

QTZ-quartz; T-type; V-vein; M-miarolitic; RF-rock forming; SAMP-sample; D-Drammen; S-salt; F-liquid; na-not analyzed; nd-not detected; TDS-total dissolved solids; MG SALT-mg salt extracted; G QTZ-g quartz used for extraction

Table 3.5b. INAA analyses in ppm of salts and calculated liquid composition.

SAMP. #	OG-2		OG-9		OG-12A		OG-12B		18A-DG		18C-DG		18D-DG		23B-DG		DG-23C	
QTZ T.	M		M		M		M		M		M		RF		M		RF	
GRANITE	D		D		D		D		D		D		D		D		D	D
SAMP. T	S	F	S	F	S	F	S	F	S	F	S	F	S	F	S	F	S	F
Na	174335.	5317.	162466.	4955.	290064.	43510.	350896.	52635.	63206.	1075.	14540.	683.	37612.	451.	79749.	2791.	65209.	9129.
K	na	na	na	na	na	na	na	na	na	na	na	na	na	na	na	na	2823.	395.
Sc	1.2	0.037	0.75	0.023	1.2	0.18	1.4	0.21	3.9	0.067	0.253	0.012	2.5	0.03	1.8	0.063	6.7	0.93
Cr	38.	1.2	97.	3.0	6.	0.9	19.	2.9	6.	0.10	0.5	0.024	50.	0.6	63	2.2	71.	9.9
Fe	5830.	178.	7929.	242.	21298.	3195.	23164.	3475.	8628.	147.	902.	42.	8628.	104.	6529.	229.	16945.	2372.
Co	28.	0.85	21.	0.64	14.	2.1	21.	3.2	0.37	0.0063	0.049	0.0023	0.5	0.006	31.9	1.1	6.6	0.92
Zn	4400.	134.	27000.	824.	4300.	645.	5600.	840.	799.	13.6	75.	3.5	376.	4.5	637.	22.3	880.	123.
As	528.	16.1	554.	16.9	665.	100.	687.	103.	254.	4.3	24.4	1.1	96.	1.2	246.	8.6	96.	13.4
Br	48.	1.5	nd	nd	41.	6.2	56.	8.4	17.8	0.30	1.1	0.05	3.3	0.04	52.	1.8	90.	12.6
Rb	1200.	37.	343.	10.	2600.	390.	3000.	450.	647.	11.	83.	4.	534.	6.	224.	8.	230.	32.
Sr	na	na	na	na	na	na	na	na	na	na	na	na	na	na	na	na	nd	nd
Mo	nd	nd	nd	nd	nd	nd	nd	nd	40.	0.68	nd	nd	125.	1.5	290.	10.2	480.	67.2
Ag	nd	nd	nd	nd	2.8	0.42	2.4	0.36	nd	nd	nd	nd	nd	nd	nd	nd	3.2	0.45
Cd	na	na	na	na	na	na	na	na	na	na	na	na	na	na	na	na	nd	nd
Sb	9.5	0.29	6.	0.18	30.5	4.6	34.	5.1	3.7	0.063	1.24	0.058	2.8	0.034	2.8	0.098	4.9	0.69
Cs	1200.	36.6	1180.	36.0	2540.	381.	3120.	468.	379.	6.4	60.8	2.9	228.	2.7	260.	9.1	145.	20.4
Ba	300.	9.2	2200.	67.1	813.	122.	1280.	192.	nd	nd	2.	0.094	301.	3.6	88.	3.1	454.	63.6
La	37.	1.1	152.	4.6	104.	15.6	183.	27.5	40.9	0.70	66.3	3.1	153.	1.8	12.8	0.45	301.	42.1
Ce	41.	1.3	175.	5.3	132.	19.8	225.	33.8	67.	1.1	174.	8.2	322.	3.9	20.	0.7	284.	39.8
Nd	12.	0.37	139.	4.2	25.	3.8	88.	13.2	23.	0.39	74.	3.5	91.	1.1	6.	0.21	221.	30.9
Sm	0.6	0.018	nd	nd	4.3	0.65	9.9	1.5	6.5	0.11	17.1	0.80	22.3	0.27	1.3	0.047	41.8	5.9
Eu	0.18	0.0055	0.2	0.0061	0.56	0.084	0.6	0.09	0.11	0.0019	0.15	0.0068	3.2	0.039	0.17	0.006	4.4	0.62
Tb	0.9	0.028	0.6	0.018	0.4	0.06	0.7	0.11	1.8	0.031	4.0	0.19	7.9	0.095	0.68	0.024	8.1	1.1
Yb	2.1	0.064	5.4	0.16	0.8	0.12	0.9	0.14	10.8	0.18	55.	2.6	52.	0.62	4.1	0.14	87.9	12.3
Lu	0.52	0.016	0.97	0.03	0.37	0.06	0.42	0.06	1.9	0.033	9.5	0.44	8.0	0.097	0.74	0.026	15.1	2.1
Hf	nd	nd	nd	nd	nd	nd	nd	nd	nd	nd	0.14	0.0066	43.9	0.53	nd	nd	30.2	4.2
Ta	116.	3.5	9.	0.28	22.	3.3	27.	4.1	0.2	0.0034	nd	nd	nd	nd	1.1	0.039	nd	nd
W	nd	nd	nd	nd	nd	nd	nd	nd	1	0.017	8.4	0.39	17.	0.20	nd	nd	19.	2.7
Ir	nd	nd	nd	nd	nd	nd	nd	nd	0.019	0.0003	0.026	0.0012	nd	nd	nd	nd	nd	nd
Au	nd	nd	nd	nd	nd	nd	nd	nd	nd	nd	nd	nd	0.006	0.000001	nd	nd	nd	nd
Hg	na	na	na	na	na	na	na	na	na	na	na	na	na	na	na	nd	nd	nd
Th	17.8	0.54	4.8	0.15	12.	1.8	18.	2.7	9.3	0.16	5.1	0.24	97.4	1.2	7.7	0.27	98.1	13.7
U	32.	0.98	656.	20.0	4.2	0.63	14.7	2.2	17.8	0.30	2.8	0.13	146.	1.8	16.9	0.59	77.	10.8
TDS	3.05		3.05		15.		15.		1.7		4.7		1.2		3.5		14	

QTZ-quartz; T-type; M-miarolitic; RF-rock forming; SAMP-sample; D-Drammen; S-salt; F-liquid; na-not analyzed; nd-not detected; TDS-total dissolved solids

Table 3.5b cont. INAA analyses (in ppm) of fluid inclusion salts and calculated liquid composition for duplicate (21B) and triplicate (27A) samples together with the blanks. See Table 3.5a for explanation of abbreviations.

SAMP. #	21B-DG1		21B-DG2		27A-DG1		27A-DG2		27A-DG3					
QTZ T.	M		M		M		M		M					
GRANITE	D		D		D		D		D					
SAMP. T	S	F	S	F	S	F	S	F	S	F	BLANK	BLANK	BLANK	BLANK
Na	77894	2259	101040	4345	42805	1306	50372	1536	58235	1776	2500	52968	11528	140
K	na	na	na	na	na	na	na	na	na	na	nd	14943	6226	nd
Sc	0.84	0.024	0.61	0.026	11.4	0.35	8.6	0.26	10.6	0.32	0.29	3.4	0.09	0.04
Cr	nd	nd	nd	nd	19	0.58	46	1.4	20	0.61	9.6	81	35	2
Fe	9095	264	9250	398	6296	192	4586	140	8084	247	520	6063	731	nd
Co	2	0.058	0.9	0.039	24	0.72	40	1.2	15	0.45	1.6	13	20	0.41
Zn	1110	32	891	38	nd	nd	160	4.9	238	7.26	97	1175	658	6
As	316	9.2	298	12.8	304	9.3	186	5.7	245	7.5	nd	nd	2.1	nd
Br	17.9	0.52	28	1.2	55	1.7	15	0.46	15	0.46	3.7	65	7.4	nd
Rb	273	8	221	10	318	10	176	5	211	6	nd	nd	nd	nd
Sr	na	na	na	na	na	na	na	na	na	na	nd	nd	nd	nd
Mo	58	1.7	47	2.0	170	5.2	240	7.3	280	8.5	nd	nd	nd	nd
Ag	1.1	0.03	nd	nd	nd	nd	nd	nd	nd	nd	nd	nd	nd	nd
Cd	na	na	na	na	na	na	na	na	na	na	nd	nd	nd	nd
Sb	4.9	0.14	5.6	0.24	5.1	0.16	3.4	0.10	4	0.12	1.2	nd	2.3	nd
Cs	377	10.9	355	15.3	439	13.4	276	8.4	457	13.9	0.88	nd	0.26	nd
Ba	nd	nd	nd	nd	996	30	624	19	798	24	nd	nd	nd	nd
La	52	1.5	37	1.6	379	11.6	271	8.3	369	11.3	2.4	1343	31	0.8
Ce	71	2.1	50	2.2	707	21	494	15.1	771	24	3.6	2251	26	nd
Nd	16	0.46	15	0.65	75	2.3	58	1.8	119	3.6	nd	920	nd	nd
Sm	0.9	0.026	0.5	0.022	nd	nd	nd	nd	nd	nd	0.14	1.6	0.11	nd
Eu	0.1	0.0029	0.1	0.0043	0.4	0.012	0.37	0.011	0.39	0.012	0.12	nd	nd	nd
Tb	0.34	0.0099	0.4	0.017	1.6	0.049	1.4	0.043	2.2	0.067	nd	nd	nd	nd
Yb	5.1	0.15	4.8	0.21	22	0.66	16.2	0.49	24	0.74	nd	nd	nd	nd
Lu	0.88	0.026	0.92	0.040	4.3	0.13	3.1	0.094	4.6	0.14	nd	nd	nd	nd
Hf	2.3	0.068	3.9	0.17	8.2	0.25	9.6	0.29	4.8	0.15	nd	nd	nd	nd
Ta	1.8	0.052	3.9	0.17	15.3	0.47	8.2	0.25	2.8	0.085	10.5	nd	nd	nd
W	7.2	0.21	6.9	0.30	17	0.52	4.6	0.14	8	0.24	nd	nd	nd	nd
Ir	0.016	0.0005	0.013	0.0006	nd	nd	0.015	0.0005	nd	nd	nd	nd	nd	nd
Au	nd	nd	nd	nd	0.004	0.0001	nd	nd	nd	nd	nd	nd	nd	nd
Hg	na	na	na	na	na	na	na	na	na	na	nd	nd	nd	nd
Th	38	1.1	38	1.6	237	7.2	183	5.6	287	8.8	nd	nd	nd	nd
U	48	1.4	45	2.0	312	9.5	234	7.1	346	10.6	nd	nd	nd	nd
TDS	2.9		4.3		3.05		3.05		3.05					

Table 3.5b cont. INAA analyses in ppm of fluid inclusion salt and calculated liquid composition for Glitrevann and Finnemarka granites.

SAMP. #	32-DG		36-DG		41B-DG		41D-DG		42-DG		43A-DG	
QTZ T.	M		M		M		RF		M		M	
GRANITE	G		G		F		F		F		F	
SAMP. T	S	F	S	F	S	F	S	F	S	F	S	F
Na	116916	3040	52226	1567	52820	12677	93622	4213	183015	23975	112984	15818
K	na	na	na	na	na	na	na	na	na	na	na	na
Sc	10.4	0.27	2.36	0.071	8.6	2.1	5.8	0.26	3.0	0.39	2.2	0.31
Cr	0		0.9	0.027	72	17.3	nd	nd	14	1.8	2	0.28
Fe	3731	97	134475	4034	11737	2817	9095	409	3887	509	2176	305
Co	0.51	0.013	15.6	0.47	0.94	0.23	nd	nd	0.1	0.013	1.1	0.16
Zn	10683	278	543	16.3	1739	417	5304	239	2446	320	3994	559
As	40.2	1.045	17.2	0.52	66	15.9	321	14.4	140	18.4	122	17.0
Br	7.4	0.19	0.6	0.02	12.2	2.9	44	2.0	2.9	0.38	34	4.8
Rb	350	9	187	6	291	70	521	23	863	113	392	55
Sr	na	na	na	na	na	na	na	na	na	na	na	na
Mo	nd	nd	134	4.0	44	10.6	55	2.5	40	5.2	nd	nd
Ag	nd	nd	nd	nd	nd	nd	1.4	0.06	2.4	0.31	3.9	0.55
Cd	na	na	na	na	na	na	na	na	na	na	na	na
Sb	4	0.10	0.39	0.012	1.5	0.36	7.2	0.32	4.4	0.58	3.8	0.53
Cs	87	2.3	22.9	0.7	127	31	288	13	456	60	255	36
Ba	nd	nd	207	6.2	156	37	304	14	89	11.7	160	22
La	268	7.0	121	3.6	124	30	110	4.9	32	4.1	39	5.4
Ce	236	6.1	280	8.4	213	51	145	6.6	42	5.4	54	7.6
Nd	62	1.6	124	3.7	80	19	70	3.2	10	1.3	31	4.3
Sm	7.7	0.20	27	0.8	14.7	3.5	12.7	0.57	3.8	0.50	4.6	0.65
Eu	1.1	0.028	1.4	0.043	1.8	0.43	2.8	0.13	0.57	0.075	0.68	0.095
Tb	0.7	0.018	4.3	0.13	2.2	0.53	3.3	0.15	1.0	0.13	0.72	0.10
Yb	8.4	0.22	10.1	0.30	29	7.1	31	1.4	10.4	1.4	3.3	0.46
Lu	1.9	0.050	1.4	0.043	5.3	1.3	5.6	0.25	2.1	0.27	0.32	0.045
Hf	0.07	0.0018	0.68	0.020	0.01	0.0024	14.8	0.67	0.37	0.049	0.14	0.020
Ta	nd	nd	nd	nd	1.5	0.36	nd	nd	nd	nd	0.2	
W	6	0.156	nd	nd	1.7	0.41	44	2.0	6.2	0.81	18	2.5
Ir	nd	nd	nd	nd	nd	nd	0.042	0.0019	0.017	0.0022	nd	nd
Au	nd	nd	nd	nd	nd	nd	nd	nd	nd	nd	nd	nd
Hg	na	na	na	na	na	na	na	na	na	na	na	na
Th	71	1.8538	24.7	0.74	69	16.7	98	4.4	73.9	9.7	5.2	0.73
U	42	1.0868	15.6	0.47	26	6.3	65	2.9	13.1	1.7	6.6	0.92
TDS	2.6		3		24		4.5		13.1		14	

in the salts except for Ir were measured in one or more of the samples of decrepitated and leached quartz.

Highly soluble elements such as As, Cs, and Br are indicated to be more enriched in the salt relative to the decrepitated and leached quartz. Fig. 3.3a,b,c, and d shows salt concentrations normalized to Na and average granite. Low-solubility elements like Hf, Ta, Sc, and Co are commonly in higher concentrations in quartz relative to the salt.

The two rock-forming quartz samples from the Drammen granite (18D and 23C) have an element concentration similar to those of the miarolitic quartz samples (Table 3.5a) and are therefore grouped together with these samples.

There are large variations in the element concentrations of the salts from sample to sample (Table 3.5 and 3.6) within the four sample groups of vein quartz and miarolitic quartz from Drammen, Glitrevann, and Finnemarka. Sodium is the main analyzed component; it is calculated as Na and ranges from 15,000 to 350,000 ppm for the Drammen granite miarolitic samples. Both the Finnemarka and Glitrevann samples fall in the same range. The vein samples indicate a somewhat lower concentration ranging form 4500 to 160,000 ppm. Fe is, the next to Na, second main component constituting close between 10 and 20% of Na. K together with Ba, Sr, Hg, and Cd was only counted in the vein samples and in sample 23C. K constitutes about 200 to 5000 ppm of these samples. Other trace elements may contain up to two orders of magnitude less concentration.

Fig. 3.3.

Spider plots of analyses of fluid inclusion dissolved solids compared with decrepitated and leached quartz of the same samples. The data are compared to average granite (Mason, 1966), by normalizing analysis to Na, then dividing by composition of average granite normalized to Na.

Fig. 3.3

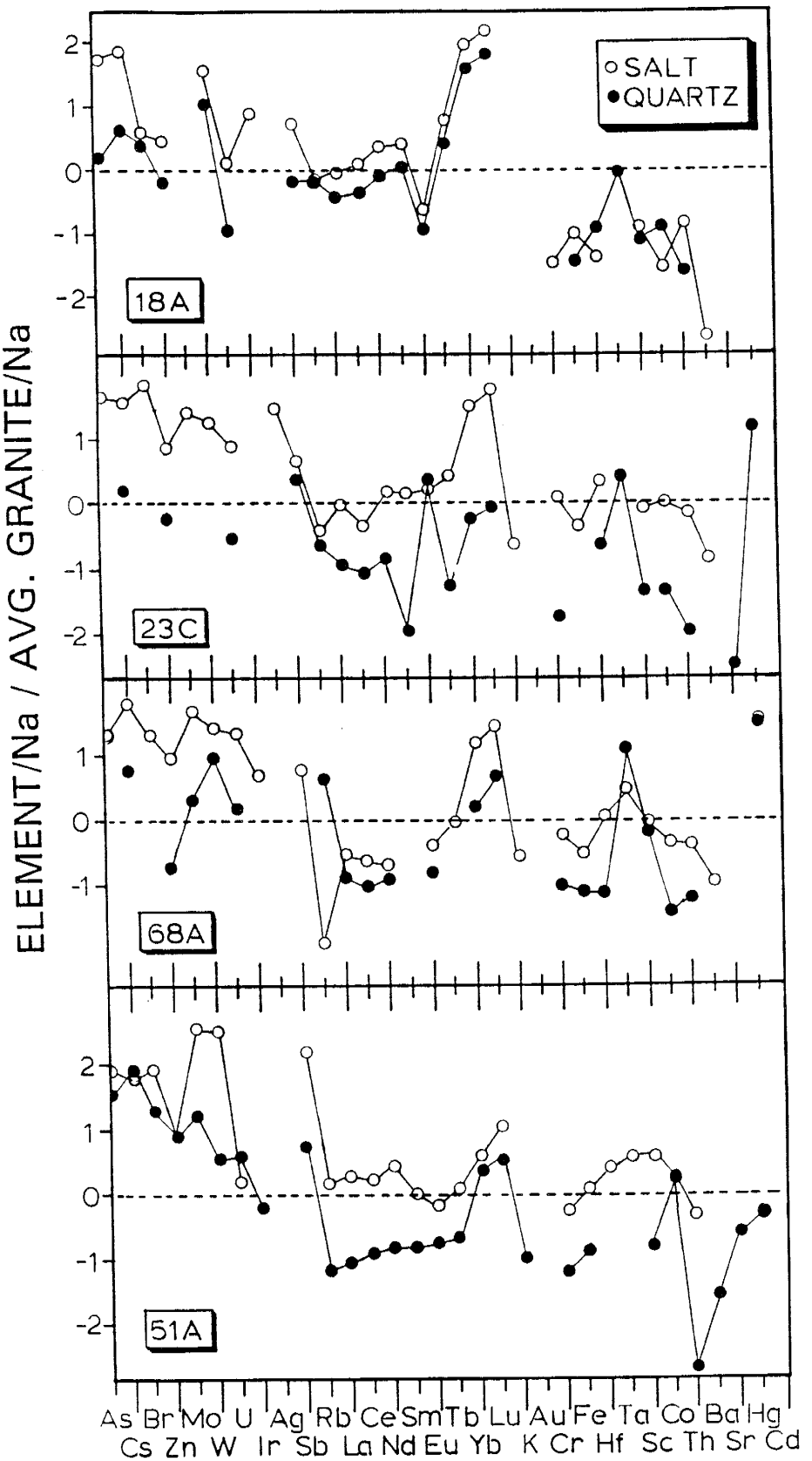
SALT
QUARTZ
18A
23C
68A
51A
ELEMENT/Na / AVG. GRANITE/Na
2
1
0
-1
-2
As Br Mo U Ag Rb Ce Sm Tb Lu Au Fe Ta Co Ba Hg
Cs Zn W Ir Sb La Nd Eu Yb K Cr Hf Sc Th Sr Cd

Table 3.6.

Range of fluid concentration from the salt analyses for vein samples, Drammen granite miarolitic and rock-forming quartz samples, Glitrevann granite samples, and Finnemarka granite samples.

Element	Vein R. N=12	Drammen R. N=14	Glitre. R. N=2	Finnemarka R. N=4
Na	486-16400	450-52600	1570-3040	4210-24000
Sc	0.05-1.4	0.01-0.67	0.07-0.3	0.3-2.1
Cr	1.0-7.2	nd-7.1	nd-0..27	nd-17
Fe	106-1500	42-3500	100-4000	300-2800
Co	0.1-3.7	0.002-3.2	0.01-0.5	nd-0.23
Zn	17.2-251	nd-840	16-280	240-560
As	0.4-18.2	1.1-103	0.5-1.0	14-17
Br	nd-16.4	nd-9	0.02-.2	0.4-4.8
Rb	nd-82	3.9-450	6-9	23-113
Mo	5.1-273	nd-48	nd-4.0	nd-11
Ag	nd-0.74	nd-0.42	nd-nd	nd-0.6
Sb	nd-1.54	0.03-5.1	0.01-0.10	0.3-0.6
Cs	1.8-84.6	2.7-468	0.7-2.3	13-60
Ba	nd-248	nd-192	nd-6	12-37
La	3.8-330	0.4-30	4-7	4-30
Ce	nd-770	0.7-33	6-8	5-51
Nd	1.2-300	0.2-22	1.6-3.7	1.3-19
Sm	nd-530	nd-4.2	nd-0.2	0.5-3.5
Eu	0.04-30	0.002-0.4	0.03-0.04	0.07-0.4
Tb	0.09-10	0.01-0.81	0.02-0.13	0.10-0.53
Yb	0.45-114	0.64-8.8	0.2-0.3	0.5-7.1
Lu	0.91-21	0.016-1.5	0.04-0.05	0.04-1.3
Hf	nd-1.0	nd-3.0	0.002-0.02	0.002-0.7
Ta	nd-0.96	nd-4.1	nd-nd	nd-0.4
W	nd-190	0-1.9	nd-0.16	0.5-2.5
Ir	0-0.010	nd-0.001	nd-nd	nd-0.002
Au	nd-nd	nd-0.0001	nd-nd	nd-nd
Th	nd-12.4	0.1-9.8	0.7-1.9	0.7-17
U	nd-9.9	0.13-20	0.5-1.1	0.9-6.3

nd-concentration below detection limit. N-number of samples used for the range.

Liquid composition

The range of the element concentrations in fluid inclusion liquid are given in Table 3.6. They show a large variation similar to that described for the salt composition. The logarithm of normalized element ratios has been plotted in a spider diagram from highest enrichment to highest depletion, keeping the REE's in order of increasing atomic number (Fig. 3.4). Samples 18A, 18C, and 18D have been used to construct element order. The graph shows the ranges for vein samples and the Drammen granite miarolitic samples. The Glitrevann and Finnemarka samples are within the limits of the latter group.

Enrichments of Ir, As, Cs, and Br are stronger for miarolitic than vein samples. These elements are siderophile and chalcophile, respectively, for the first two and lithophile for the latter two elements based on Goldschmidt's (1954) and Mason's (1966) classification. The majority of the chalcophile elements are enriched relative to average granite. Lithophile elements are equal to depleted and siderophile elements are somewhat more depleted relative to average granite. The REE's are mainly enriched for the vein samples with a tendency of being depleted for the other samples. All samples are enriched in heavy REE's relative to light REE's, where Eu is enriched in the vein sample liquids relative to the other REE's.

Fig. 3.4.

Plot of the normalized salt data (as Fig. 3.3). Values are plotted in decreasing abundance (keeping the REE' are listed in order) and using samples 18 a,b, and c as master.

Fig 3.4

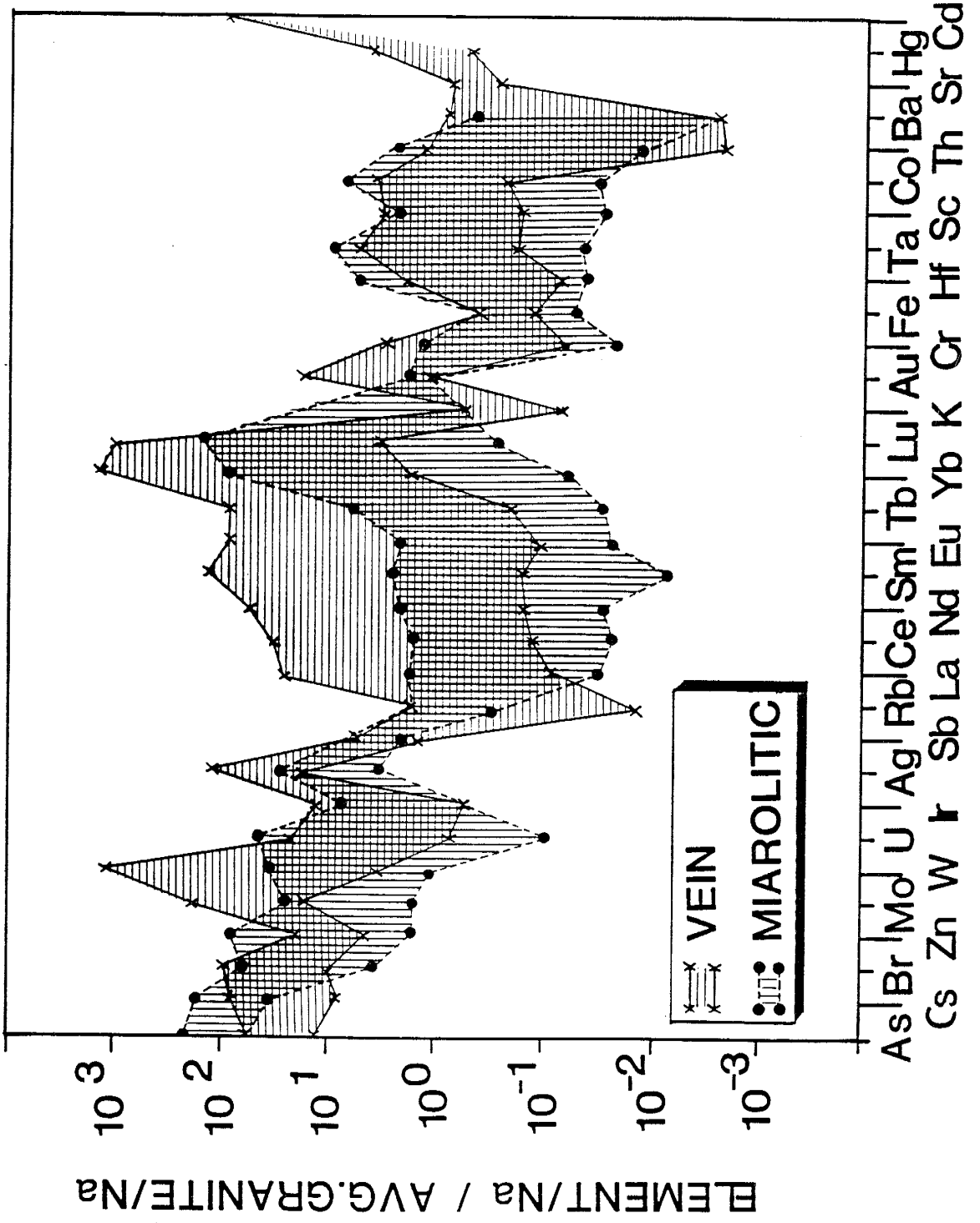
ELEMENT/Na / AVG.GRANITE/Na
10^3
10^2
10^1
10^0
10^-1
10^-2
10^-3
VEIN
MIAROLITIC
As Br Mo U Ag Rb Ce Sm Tb Lu Au Fe Ta Co Ba Hg
Cs Zn W Ir Sb La Nd Eu Yb K Cr Hf Sc Th Sr Cd

Accuracy of gas analysis

The analyses presented here (Tables 3.3 and 3.4) are bulk analyses, hence they represent the volatiles from an unknown percent of various types of inclusions present in the samples. There is predominantly one type of inclusion in the Drammen granite samples. This makes it easier to interpret than more complex fluid inclusion systems, where several types of inclusions are present in a sample. Further complications in interpreting the data arise when spurious amounts of gas species are produced during the thermal decrepitation process. This effect is only minor for inclusions decrepitated at 500°C. However, for fluids trapped at 300°C and opened at 500°C, methane and other species react with water to yield CO_2, H_2, and CO. A method for reconstructing the inclusion volatiles for this problem has been developed (Norman, 1991), and reconstructed analyses are given in Table 3.3. Note that CO is not changed by this calculation.

One of the principal problems with bulk analyses is that of excess gas. This excess can result from the analysis of a mixture of liquid-filled and vapor-filled inclusions. The latter may be trapped in greater proportion than in liquid-filled inclusions because gas bubbles tend to stick to surfaces (Roedder, 1984). A general rule of thumb is that when gaseous species are in excess of 3 mole% and no gaseous species condensed in liquid-dominated inclusions when cooled, then some analyzed components are excess gas that resided in

vapor-dominated inclusions. Therefore, an analysis may not represent the volatile content of the fluid as a whole, but rather the composition of vapor phase in equilibrium with the fluid. In general, bulk analyses give a fair representation of the average gas composition of the fluids and are compatible with stable isotope analyses, which also are bulk analyses and may represent the average values of depositing fluids over a considerable time.

Accuracy of salt analysis

Duplicate and triplicate analyses for the Drammen granite samples 21B and 27A (Table 3.5a) show similar element concentrations. The reproducibility is generally good (5-10%) for most elements, except for the indicated precision of ± 50% for Co, Ta, Hf, and W. The precision obtained in this study agrees with that found by Norman et al. (1989). The accuracy is not possible to calculate because there are no samples or standards of inclusion fluids with known concentrations. The samples are normalized to Na (in ppm) in sample, and normalized to element relative to Na in average crust from Mason (1966). This normalization is displayed in a spider diagram (Fig. 3.5a,b). It exhibits good reproducibility for most of the elements.

The analyses presented here (Tables 3.5 and 3.6) are bulk analyses of inclusion liquids, hence they represent unknown proportions of various types of fluid inclusions present in

Fig. 3.5.

Spider plot of the normalized salt (as Fig. 3.3) for the duplicate and triplicate samples 21B and 27A.

Fig. 3.5

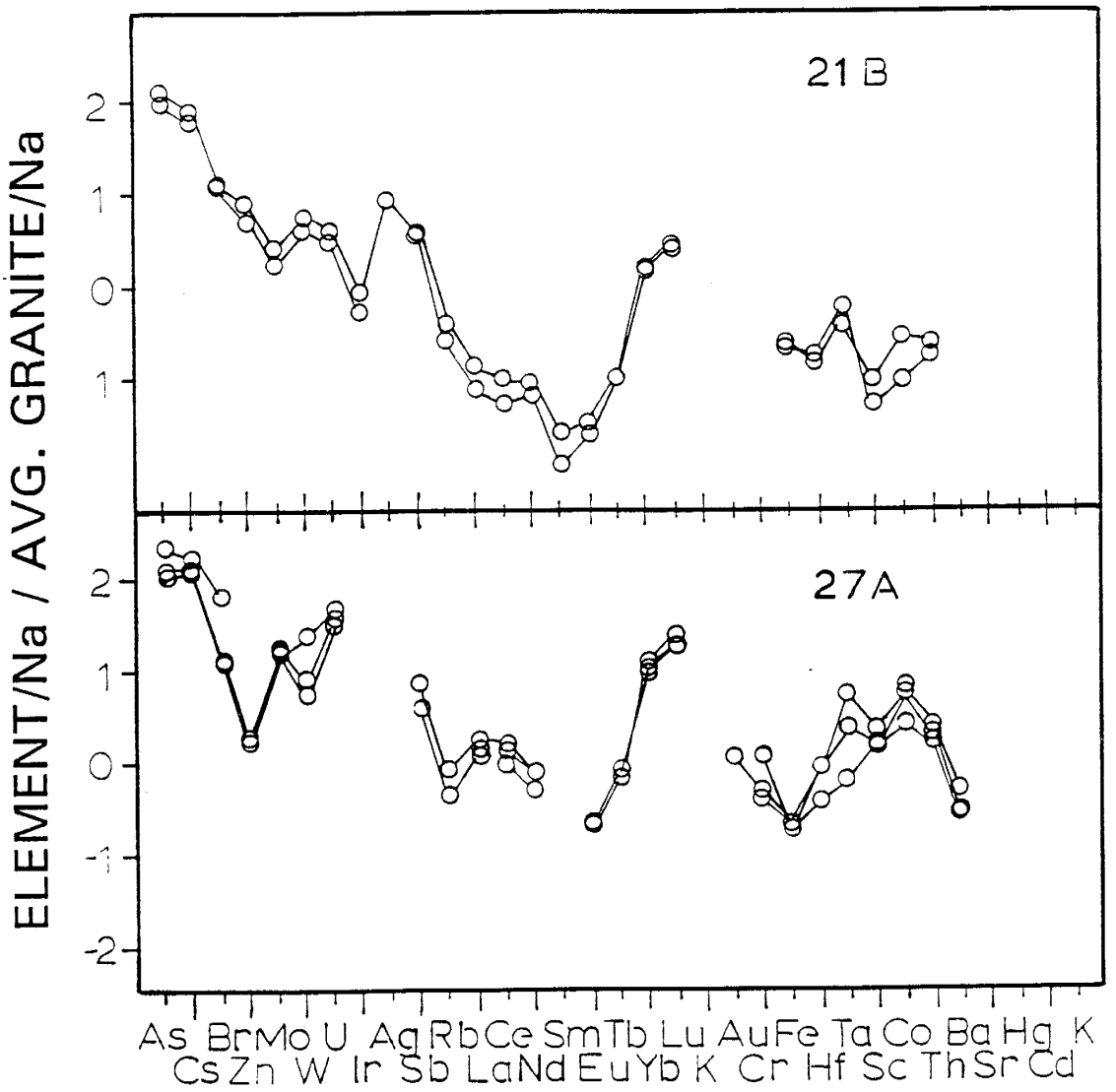
21 B
27A
ELEMENT/Na / AVG. GRANİTE/Na
2
1
0
1
2
1
0
-1
-2
As Br Mo U Ag Rb Ce Sm Tb Lu Au Fe Ta Co Ba Hg K
Cs Zn W Ir Sb La Nd Eu Yb K Cr Hf Sc Th Sr Cd

the sample. The samples have predominantly primary and pseudo secondary inclusions indicating that leachates from these fluid inclusions should give a representative composition of the inclusion liquid, a liquid which is in equilibrium with the minerals they have been trapped in. Analyses of decrepitated quartz residuals indicate that there are considerable amounts of elements left in the quartz (Table 3.7).

Leaching efficiency has been calculated from the amounts of element leached per gram of decrepitated quartz relative to the sum of element leached (per gram quartz) and amount of element left in decrepitated and leached quartz (per gram quartz). Table 3.8 gives the mean and standard deviation for the leaching efficiency for each of the measured elements based on 9 vein samples from Tables 3.4c and 3.5. This leaching efficiency represents the efficiency of leaching anything that may be in the samples: salts, impurity minerals, or interstitial elements in the quartz lattice. As, Cs, Br, Zn, Mo, U, Ag, Sb, Tb, Cr, Ba, and Sr give a leaching efficiency above 50%. Rb, Ce, Nd, Sm, Eu, Yb, Lu, Na, Fe, Co, and Th give an efficiency between 50 and 15%, while Ta, Hf, Sc, and W give a low leaching efficiency (<15%).

The elements detected in the decrepitated quartz residuals could be due to undecrepitated fluid inclusions, inclusion minerals, impurities in the matrix, and unleached elements. One scenario does not necessary preclude the other.

Table 3.7. INAA analyses in ppm of quartz after decrepitation and leaching.

SAMP. #	Q18A-DG	Q18C-DG	Q18D-DG	Q21B-DG	Q21B-DG2	Q23B-DG	Q32-DG	Q41B-DG	Q41D-DG	Q42-DG
QTZ T.	M	M	RF	M	M	M	M	M	M	M
GRANITE	D	D	D	D	D	D	G	F	F	F
Na	36	102	964	20	19	5	321	209	124	60
K	0	0	0	0	0	0	0	0	nd	0
Sc	0.012	0.011	0.022	0.004	0.011	0.009	0.104	0.034	0.042	0.096
Cr	nd	nd	nd	0.02	0.17	0.12	0.2	0.2	0.01	0.08
Fe	3.11	2.33	10.11	2.33	2.33	3.89	8.55	7.00	7.00	4.66
Co	0.026	0.014	0.02	0.02	0.022	0.03	0.022	0.029	0.03	0.019
Zn	0.6	1.2	0.38	0.3	0.3	1.8	0.24	1.65	1.2	1.4
As	0.06	0.05	0.07	0.122	0.128	nd	0.07	nd	0.108	0.077
Br	0.056	0.051	nd	0.09	0.185	0.37	0.06	0.077	0.121	0.122
Rb	5.4	7.5	74	2.4	1.57	nd	15.9	8.2	8.9	4
Sr	na	na	na	na	na	na	na	na	na	na
Mo	nd	nd	nd	nd	nd	nd	nd	nd	nd	nd
Ag	nd	nd	nd	nd	nd	nd	nd	nd	nd	nd
Cd	na	na	na	na	na	na	na	na	na	na
Sb	0.002	0.011	0.065	nd	0.019	0.025	0.019	0.014	0.014	0.023
Cs	0.245	0.267	1.038	0.223	0.243	0.068	0.212	0.115	0.153	0.235
Ba	1.8	nd	6	1	0.2	0.3	1.2	3.6	2	1.5
La	0.046	1.94	1.12	0.029	0.022	0.018	0.423	0.156	0.341	0.068
Ce	0.24	4.49	1.36	0.34	0.39	0.14	0.56	0.21	0.77	0.28
Nd	0	1.87	0.1	nd	nd	nd	0.09	nd	0.17	nd
Sm	0.002	0.486	0.021	nd	nd	nd	0.007	0.042	0.016	0.007
Eu	0.004	0.005	0.042	0.005	0.004	0.009	0.021	0.034	0.019	0.164
Tb	0.005	0.123	0.023	0.01	0.017	nd	0.006	0.014	0.005	0.018
Yb	0.006	1.63	0.112	0.006	0.032	0.001	0.059	0.187	0.073	0.334
Lu	0.001	0.277	0.016	0.011	0.016	nd	0.017	0.041	0.017	0.082
Hf	0.016	0.029	0.345	0.022	0.086	0.01	0.455	2.03	0.68	4.94
Ta	0.026	0.062	0.209	2.29	0.209	0.01	0.228	0.321	0.48	0.42
W	0.046	0.176	0.06	0.1	0.14	0.15	0.11	0.3	0.06	0.67
Ir	nd	nd	nd	nd	nd	nd	nd	nd	nd	nd
Au	nd	nd	nd	nd	nd	nd	nd	nd	nd	nd
Hg	na	na	na	na	na	na	na	na	na	na
Th	0.015	0.064	0.087	0.039	0.08	0.013	0.184	0.336	0.139	0.476
U	0.008	0.018	0.099	0.032	0.028	0.003	0.124	0.104	0.234	0.044

QTZ-quartz; T-type; M-miarolitic; RF-rockforming; V-vein; SAMP-sample; D-Drammen; G-Glitrevann; F-Finnemarka; na-not analyzed; nd-not detected.

Table 3.7 cont.

SAMP.#	Q50-DG	Q51A-DG	Q52A-DG	Q59A-DG	Q59B-DG	Q66A-DG	Q66B-DG	Q68B-DG	Q71-DG	AVG. GR
QTZ T. GRANITE	V	V	V	V	V	V	V	V	V	
Na	6	10	60	6	12	5	298	114	80	24600
K	4.1507	nd	2.4904	11.622	44.828	1.8263	23.244	nd	nd	45100
Sc	0.184	0.0569	0.0764	0.0916	0.0987	0.0222	0.0772	0.0941	0.0571	3
Cr	nd	0.055	0.107	nd	0.17	0.022	nd	0.109	0.088	22
Fe	8.08	7.38	8.94	2.05	6.45	2.67	8.47	5.36	6.14	13700
Co	0.037	0.019	0.0219	nd	0.0068	0.0058	0.008	0.0047	0.0058	2.4
Zn	2.2	1.69	2.5	4.7	1.47	1.69	1.14	0.39	0.9	45
As	1.22	0.303	0.194	0.09	nd	nd	nd	nd	nd	0.8
Br	0.17	0.18	0.106	nd	nd	0.074	nd	nd	nd	0.5
Rb	0.63	1.42	1.07	nd	5.17	0.77	3.46	46.9	11.6	220
Sr	nd	nd	nd	nd	nd	nd	nd	nd	nd	250
Mo	14.7	10.7	2.2	nd	0.91	3.75	0.79	0.68	nd	7
Ag	nd	nd	nd	nd	nd	0.25	nd	nd	nd	0.04
Cd	nd	0.09	0.11	nd	0.3	0.27	nd	nd	0.06	0.06
Sb	nd	0.276	0.19	nd	nd	0.072	nd	nd	0.038	0.4
Cs	0.23	0.371	0.211	0.126	0.146	0.108	0.136	0.433	0.274	1.5
Ba	nd	nd	nd	23	nd	nd	nd	nd	nd	1220
La	6	1.017	1.573	31.67	12.65	2.149	1.834	0.764	0.335	120
Ce	10.2	1.65	3.05	72.6	26.3	3.74	3.38	1.02	0.438	230
Nd	3.56	0.68	1.12	37	10.8	1.32	0.71	0.33	0.19	55
Sm	0.217	0.0508	0.0162	8.38	2.05	0.035	0.088	nd	0.002	11
Eu	0.0154	0.0029	0.0023	1.708	0.386	0.0057	0.0156	0.0078	0.0027	1
Tb	0.0105	0.0062	0.0029	1.708	0.386	0.0057	0.0156	nd	nd	1.1
Yb	0.022	0.0177	0.0099	20.19	4.82	0.0362	0.223	0.084	0.0166	1
Lu	0.0037	0.005	0.003	3.59	0.87	0.0101	0.0433	0.0244	0.0029	0.1
Hf	nd	0.0599	0.0559	0.016	0.065	0.0203	0.309	0.0203	0.076	5.2
Ta	nd	0.0285	0.0133	0.03	0.154	0.141	0.407	1.073	0.133	1.6
W	32.5	0.55	0.62	0.38	0.17	0.14	0.23	0.18	0.06	0.4
Ir	nd	nd	nd	nd	nd	nd	nd	nd	nd	0.006
Au	nd	nd	nd	nd	nd	0.0003	nd	nd	nd	0.002
Hg	nd	nd	nd	nd	0.07	nd	0.014	0.38	nd	0.2
Th	0.046	0.11	0.0182	0.358	0.716	0.256	0.65	0.171	0.02	52
U	nd	0.025	nd	nd	0.062	0.027	0.11	0.278	0.049	3.7

AVG.GR. is the average granite concentrations from Mason (1966) that are used for normalizing.

Table 3.8. Leaching efficiency in % for the total salt extracted and individual elements individual samples. These calculations are based on amount leached relative to amount left quartz that has been leached and decrepitated. See text for more explanations.

Sample #	Mg sampl.	Total salt mg	Total eff. %	Na2O	K2O	Sc	Cr	FeO	Co	Zn	As	Br	Rb	Sr	Mo	Ag	Cd	Sb	Cs	Ba	La	Ce	Nd	Sm	Eu	Tb	Yb	Lu	Hf	Ta	W
Q-50	64.84	1.48	9.7	78.2	49.4	15.3	100.	31.6	70.8	45.9	15.8	38.2	31.35	0.	11.7	0.	100	0.	32.5	100.	30.9	27.1	30.4	43.0	46.1	48.0	50.2	55.3	0.	0.	12.4
Q-51A	82.62	0.52	23.0	74.7	100.	10.3	25.4	24.7	75.7	72.2	52.9	39.94	11.5	100.	12.3	0.	0.	9.5	81.0	100.	11.9	18.7	14.0	30.6	45.8	31.9	61.6	51.1	0.	0.	3.0
Q-52A	94.53	1.144	9.0	19.1	70.1	15.3	19.0	14.5	21.6	47.6	56.7	66.81	10.0	100.	51.3	0.	0.	5.0	74.1	100.	10.3	7.9	10.9	54.7	51.5	42.7	52.0	41.8	0.	25.4	29.5
Q-59A	62.55	3.679	11.8	52.4	0.	6.4	100.	26.3	100.	27.8	46.8	100.	0.	0.	100.	100.	0.	100.	72.1	0.	7.9	0.	7.7	7.2	0.4	6.5	6.8	6.8	8.9	37.9	11.2
Q-59B	71.21	2.048	15.8	17.1	3.6	9.0	15.3	6.4	15.3	34.8	100.	100.	4.2	0.	56.6	0.	0.	100.	39.9	0.	20.8	22.6	21.7	21.9	1.4	20.0	19.1	19.3	13.7	5.5	13.7
Q-66A	83.62	0.330	34.2	69.1	39.6	25.5	63.1	23.4	40.0	56.8	100.	52.0	44.6	0.	18.0	1.5	0.	3.7	74.1	0.	13.8	19.1	24.3	78.4	33.9	85.2	91.3	87.3	16.5	4.0	16.2
Q-66B	70.12	6.482	1.1	3.8	11.8	5.6	100.	9.8	26.5	66.0	100.	0.	20.0	0.	56.2	100.	0.	100.	72.5	0.	9.1	9.2	11.9	20.9	8.4	28.6	23.9	22.8	3.8	1.4	7.0
Q-68B	85.33	2.506	1.6	3.4	100.	5.1	17.8	12.2	29.5	64.2	100.	100.	0.0	0.	46.5	0.	0.	100.	28.3	100	7.5	8.3	5.6	0.	8.4	100	25.0	17.9	34.8	0.1	9.6
Q-71	99.47	1.309	3.3	6.4	100.	5.9	27.0	6.7	36.4	55.8	100.	100.	3.1	0.	100.	0.	0.	7.6	41.3	0	23.7	22.6	31.0	98.451	7.7	100	70.6	71.4	0.	0.5	0.

The material was looked at after decrepitation, and there are no indications that there are undecrepitated fluid inclusions in the quartz residual. There may be some small undecrepitated fluid inclusions, but this cannot count for the relatively large amount of trace elements found in the residual quartz. The quartz was carefully hand-picked to avoid contamination from other minerals. In the cleaning process concentrated HNO_3 was used. The leaching acid is weak HNO_3. This means that this leaching fluid will not leach other material than salts exposed during decrepitation. The relatively high content of elements left in the quartz is likely due to submicroscopic mineral inclusions and elements interstitial in the quartz lattice. The high standard deviations suggest that these impurities are inhomogeneously distributed among the quartz samples.

Tungsten, U, and Sb show high correlation coefficients (Table 3.9) between elements analyzed in decrepitated and leached quartz and salt. Terbium, Yb, Lu, and Sc show intermediate but distinct correlation between element in salt and in quartz (Table 3.9), whereas the rest of the analyzed elements do not show any correlation. The very high correlation coefficient for W (0.99) is due to one sample with high content of W in both quartz and salt (1900 and 32 ppm, respectively), the rest cluster around 0. The salt analyses show large variations in Tb, but is constantly low for the quartz. This distribution gives a horizontal regression line

Table 3.9.

Correlation coefficients between elements analyzed from salt extraction and the corresponding decrepitated and leached quartz.

Elem.	Corr.C.	Elem.	Corr.C.	Elem.	Corr.C.
Na	-.15	Mo	0.37	Tb	0.54
Sc	0.56	Sb	0.72	Yb	0.59
Cr	0.10	Cs	0.18	Lu	0.58
Fe	0.16	Ba	-.11	Hf	-.12
Co	0.33	La	0.39	Ta	0.33
Zn	-.28	Ce	0.12	W	0.99
As	0.10	Nd	0.52	Th	0.29
Br	0.16	Sm	0.21	U	0.74
Rb	0.08	Eu	-.10		

with a high correlation coefficient.

If submicroscopic feldspars were exposed during decrepitation and leached, a correlation of Na, Rb, and possibly Eu between decrepitated and leached quartz and salt analyses would be expected, which is not seen (Table 3.9). Leaching minerals containing HREE's like zircon and xenotime may give rise to the correlation between salt and quartz for the HREE's. However, these minerals have very low solubility.

Therefore, the INAA of leached salts probably represent salts mainly from fluid inclusions. However, some of the elements may have a larger contribution from solid inclusions and interstitial leached elements.

DISCUSSION

The Drammen granite batholith meets most of the criteria for a Mo-granite (wt.% $SiO_2 \geq 74.0$, wt.% $NaO \leq 3.6$, and wt.% $K_2O \geq 4.5$; Mutchler et al., 1981), and the fluid inclusion data (Olsen and Griffin, 1985a,b) indicate an extensive geothermal system was once present, hence the lack of molybdenum mineralization throughout the batholith is curious. Surely, the early granites must have liberated some aqueous phase as they cooled. Three granite intrusions (g6-g8) do carry minor molybdenum deposits, and the fluid inclusion analytical data indicate that the critical difference between these bodies and the others is that the fluids moving in these bodies had some reduced sulfur.

Stable isotopes

The oxygen isotope data ($\delta^{18}O_{FLUID}$=+2.3 to +2.7 per mill from vein quartz analyses) indicate that the hydrothermal fluids could have been in isotopic equilibrium with the Drammen granite if magmatic fluids reequilibrated at about 300°C. The $\delta^{18}O_{FLUID}$ can also be explained by either meteoric waters in the process of equilibration with the granite (Fig. 3.1), or mixtures of magmatic and meteoric waters. The latter idea could well have been the case because it has been demonstrated that batholith-size granite bodies may generate magmatic fluids (Candela and Holland, 1986).

The sulfur isotope data ($\delta^{34}S_{FLUID}$ -1.7 to +5.4) are

compatible with either suggested source of fluids because sulfur could be magmatic or leached from the crystallized intrusions. If sulfur with magmatic signature was leached in a reducing fluid at high temperature (>300°C) from a rock carrying mainly sulfide minerals this fluid will also give a magmatic sulfur signature because of small fractionation factors (Ohmoto and Rye, 1979).

Inclusion fluid Sr-isotope data

The Sr isotope data of the inclusion fluids from miarolitic cavities (Olsen and Griffin, 1984b) and from quartz-molybdenite veins (Table 2.3) resemble the whole-rock data quite well supporting the idea that the fluids were dominated by magmatic water, i.e. derived from and/or in equilibrium with the granitic magma. This magmatic origin was demonstrated for the miarolitic fluids by Olsen and Griffin (1984b). Excess radiogenic Sr and Nd isotopes in inclusion fluids (from miarolitic quartz) along the granite border relative to the central part indicate fluid contamination (Olsen and Griffin, 1984b; Norman and Mearns, 1986).

The vein inclusion fluids with lowest $^{87}Rb/^{86}Sr$ plot close to the 274 Ma isochron of Norman and Mearns (1986, and unpub. data), whereas fluids with higher $^{87}Rb/^{86}Sr$ plot off the isochron (Fig. 3.2). This high $^{87}Rb/^{86}Sr$ may indicate that the solutions were subjected to crustal contamination from older rocks. Primary magmatic fluids were most likely mixed with

crustal water, which had picked up radiogenic Sr from the older crustal rocks. The low initial Sr isotope ratio measured in the inclusion fluids from the Sörumsåsen could again mean that Sr was modified by a post-magmatic hydrothermal fluid that resulted in non systematic similar to that of some whole-rock samples.

Inclusion fluid gas data

Gas composition differences between sample groups

There are few differences in gas composition between the vein quartz from the molybdenite deposits in the Drammen granite. The sulfur contents are on average higher for Sörumsåsen than for the other vein samples, but with large variation among the samples from each of the deposits. Also the measured CO_2 contents are higher for the Sörumsåsen. The total amounts of noble gases are low for Sörumsåsen and for the two deposits associated with the g_8, Rörvik and Röisåsen.

The miarolitic quartz contains only propane as HC, and the CO_2/HC ratio is much lower for the miarolitic quartz than for the vein quartz (Fig. 3.6; Tables 3.3 and 3.4). Hydrogen sulfide was detected in some of the vein samples, but not detected in any other samples from the Drammen granite. The sulfur dioxide contents are generally higher for the vein samples since many of the miarolitic quartz samples contain SO_2 below the detection limit. The Glitrevann samples had even higher sulfur dioxide contents than the vein samples.

Over all, the total gas contents are lower in vein inclusion fluids.

Discriminant analysis: A discriminant analysis program developed by Hintze (1990) has been used to determine if there is significant difference in the fluid gas composition between vein samples and miarolitic and rock-forming samples. When using this statistical analysis tool, gases not detected have been set to zero and gases not analyzed have been ignored. The program has been used to see if the classification based on the type of quartz works for the gas composition, and with what accuracy.

He, CO_2, SO_2, CH_4, N_2, H_2O, and Ar all give high F-values (ratios; described by Till, 1985), which means that all these gases add a significant amount to the classification prediction. Low probability of the F-values for N_2, H_2O, and Ar indicate that these three gases are not useful in the discriminant analysis. Calculations on both raw data and recalculated data gave same the result.

Table 3.10 gives the result of the discriminant analysis with sample numbers, the actual class (1-miarolitic and rock forming; 2- vein), predicted classification, and the probability for being in class 1 or 2. This probability calculation is based on the James (1985; p. 65) algorithm. The overall probability for correct classification based on an unknown sample is 72%. Three out of 15 miarolitic and

Table 3.10.

Classification prediction calculated using discriminant analysis program of Hintze (1990), using He, CH_4, HC, SO_2, and CO_2. Miarolitic and rock-forming quartz from Drammen, Finnemarka (1), and Glitrevann granites and vein quartz (2) extracted inclusion fluids are the two classes used. See text for more detailed explanation.

SAMPLE #	CLASS	PRE. C.	PR.1	PR.2
18A	1	1	0.72	0.28
18C	1	1	0.98	0.02
18D	1	1	0.90	0.10
21B	1	2	0.45	0.55
21B2	1	1	0.57	0.43
21C	1	2	0.41	0.59
23B	1	2	0.26	0.74
23C	1	1	1.00	0.00
28C	1	1	0.99	0.01
32	1	1	0.94	0.06
32C	1	1	0.79	0.21
32C2	1	1	0.99	0.01
41B	1	1	1.00	0.00
41D	1	1	1.00	0.00
42	1	1	0.91	0.09
50	2	2	0.12	0.88
51A	2	2	0.22	0.78
51B	2	2	0.00	1.00
52A	2	2	0.21	0.79
54D	2	2	0.35	0.65
55A	2	1	0.57	0.43
58A	2	2	0.20	0.80
59A	2	2	0.01	0.99
59B	2	2	0.11	0.89
59C	2	2	0.02	0.98
63	2	2	0.01	0.99
66A	2	2	0.13	0.87
68A	2	2	0.18	0.82
71A	2	2	0.14	0.86

Column 2 (Act.) gives the real classification, column 3 gives the predicted classification, and columns 4 and 5 give the estimated probability for individual sample to belong to either group 1 or 2, respectively.

rock-forming samples fall in the vein group, and one vein sample out of 14 falls in the other group. This grouping is shown in Fig. 3.6a,b,c, and d where SO_2 is plotted versus HC and CO_2, CH_4 versus CO_2, and CO_2 versus HC. These graphs indicate there are higher amounts of gas species in the miarolitic and rock-forming quartz inclusion in comparison to analyses of vein quartz inclusion fluids. This main difference between fluids trapped in these two different environments could be due to an evolution of the source where gas-rich salt-poor fluids escape early (strong solubility reduction of CO_2 in cooling magmas) and became trapped in rock-forming and miarolitic quartz with average total gas content of 3.1 mole% and TDS=5.5 wt.%. Olsen and Griffin data (1984a,b) indicate that early Drammen fluids were richer in salt and with lower gas content. The late escaping fluids are richer in salt and with a lower gas content became trapped in the vein quartz (total gas content of 1.9 mole% and TDS=17 wt.%).

Boiling: A plot of N_2 and H_2 from miarolitic and rock-forming quartz samples from the Drammen granite, Glitrevann granite, and Finnemarka granite, and the vein quartz samples (Fig. 3.7) indicates changes in composition that could be attributed to boiling (vapor separation) in the fluid from the early stage (inclusion fluids from miarolitic and rock-forming quartz) to the late stage (inclusion fluids from vein quartz). Partition

Fig. 3.6.

Plots of SO_2 versus HC (a); SO_2 versus CO_2 (b); CH_4 versus CO_2 (c); CO_2 versus HC (d). All data in mole % of volatiles; x's are miarolitic and rock-forming quartz, and filled circles are samples from Mo-bearing veins.

Fig. 3.6

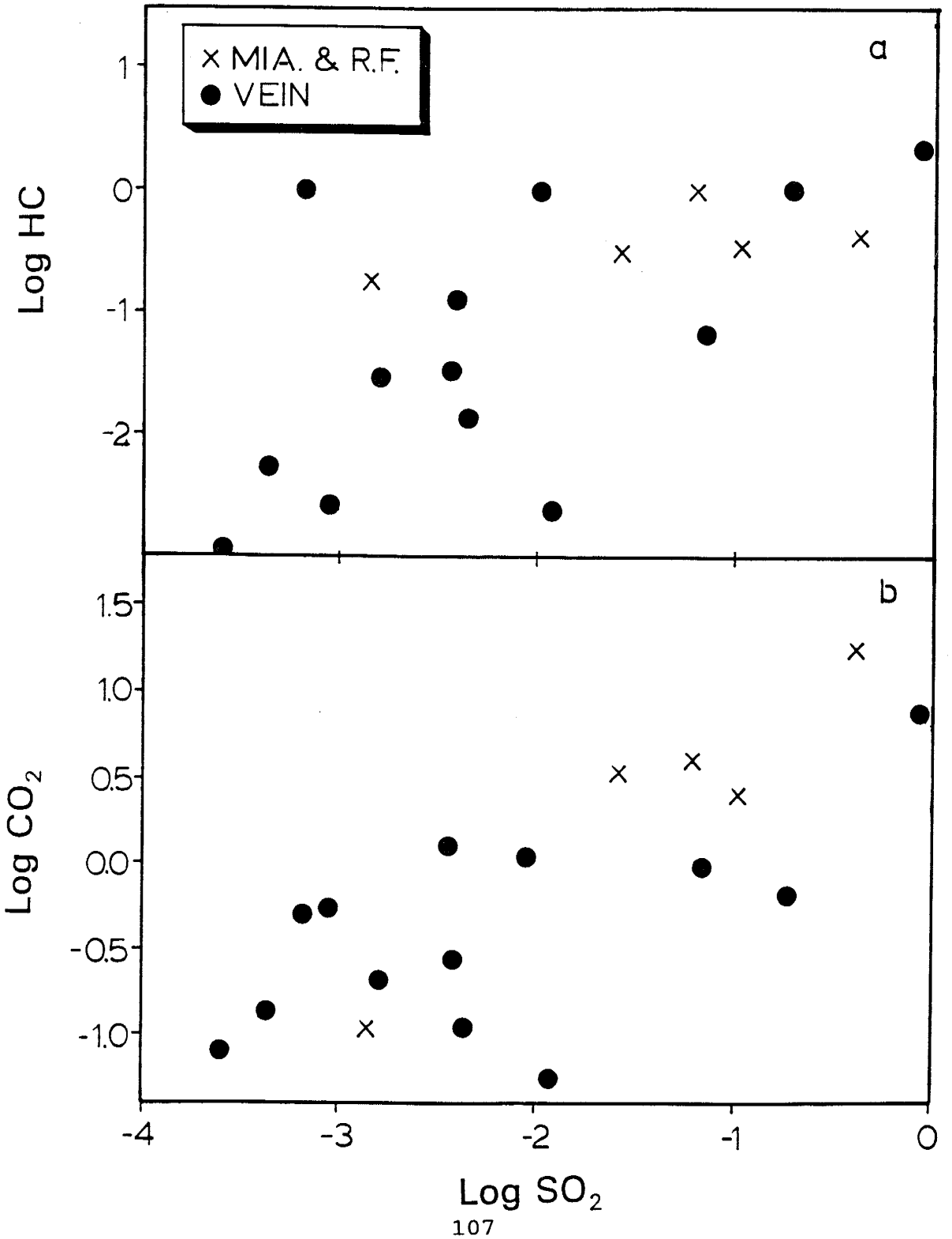

Fig. 3.6 cont.

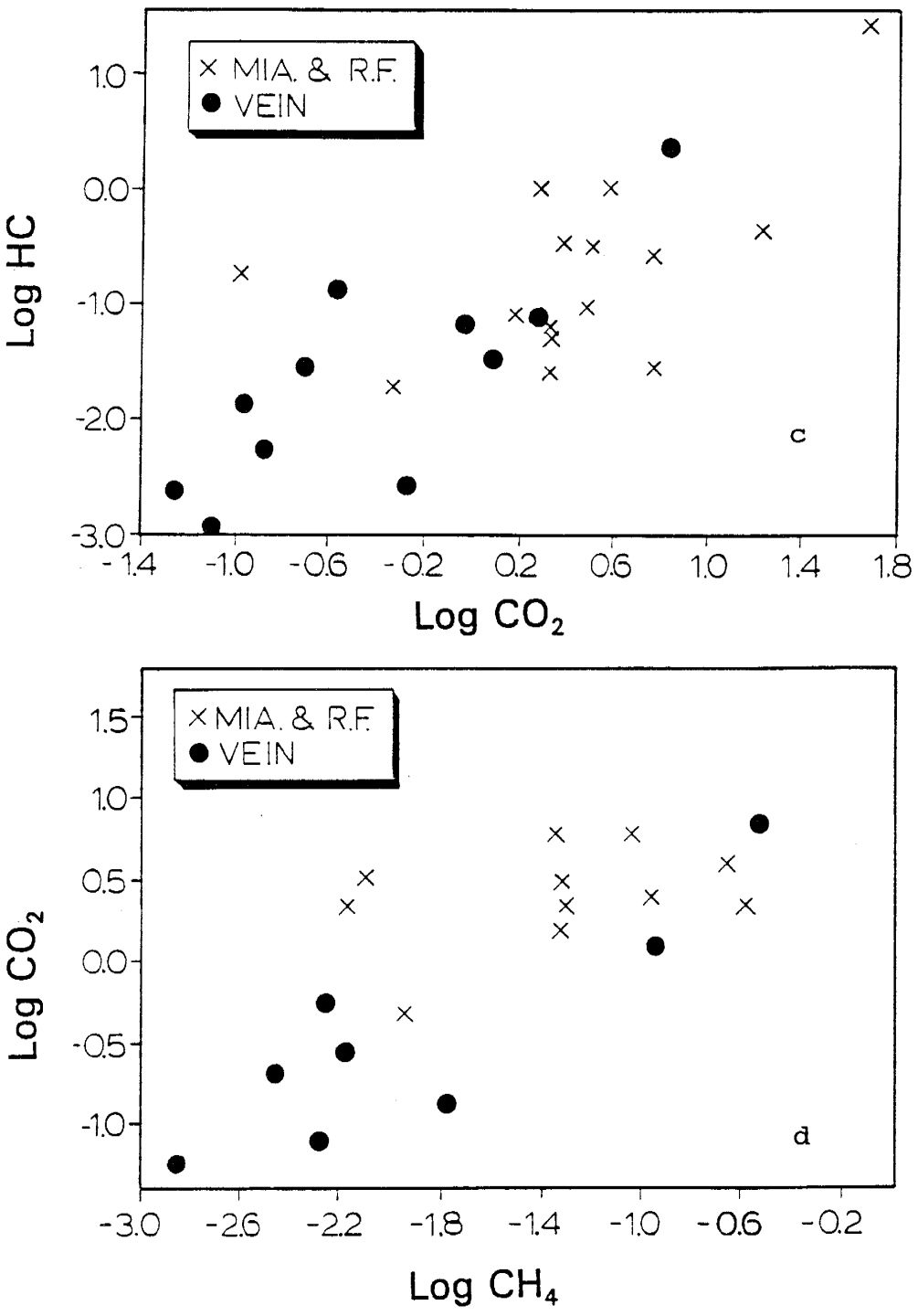
× MIA. & R.F.
● VEIN
Log HC
1.0
0.0
-1.0
-2.0
-3.0
-1.4
-1.0
-0.6
-0.2
0.2
0.6
1.0
1.4
1.8
Log CO_2
c
× MIA. & R.F.
● VEIN
Log CO_2
1.5
1.0
0.5
0.0
-0.5
-1.0
-3.0
-2.6
-2.2
-1.8
-1.4
-1.0
-0.6
-0.2
Log CH_4
d

coefficients of N_2 and H_2 from liquid to vapor phase are similar (Giggenbach, 1981). This implies that during boiling (vapor separation) the H_2/N_2 ratio in the fluid will be near constant for both closed and open boiling systems and is shown by the line (Fig. 3.7).

N_2 versus CO_2 (Fig. 3.8) indicates that boiling between early and late fluids is not a sole mechanism. Because of different gas partitioning coefficients for N_2 and CO_2 (Giggenbach, 1980; Drummond, 1981), the boiling point line is curved. During boiling the gas content of the liquid will drop drastically (Henley et al., 1984). The gas content of the inclusion fluids from both vein quartz samples (1.87 mole%) is somewhat lower than for miarolitic and rock-forming quartz samples (3.12 mole%). This indicate that there may have been some boiling or mixing. Neither this study nor Olsen and Griffin (1984a) and Olsen (1981) find any evidences for boiling from the fluid inclusion microthermometric studies.

Given the temperature 300°C (see temperature calculations) as the trapping temperature for the inclusion fluids in the vein samples, 0-10 wt.% NaCl (Olsen and Griffin, 1984b), and 1.5 mole% CO_2, boiling in a rising fluid would occur at a depth of about 2.5 to 3 km based on being under hydrostatic pressure (Haas, 1971; Takenouchi and Kennedy, 1965). Olsen and Griffin (1984a) indicates a depth of formation of 5 to 6 km (1.3-1.5 kbars lithostatic pressure). This depth would explain why boiling has not occurred during

Fig. 3.7.

Plot of N_2 versus H_2 (in mole%) for recalculated data for miarolitic and rock-forming quartz from the Drammen granite (crosses) granites, and vein quartz samples (filled circles) from the Drammen granite. The line shows a possible change of the fluid composition due to vapor saturation (boiling) from 365° to 300°C with initial composition: N_2=0.5 mole%; H_2=0.2 mole%.

Fig. 3.7

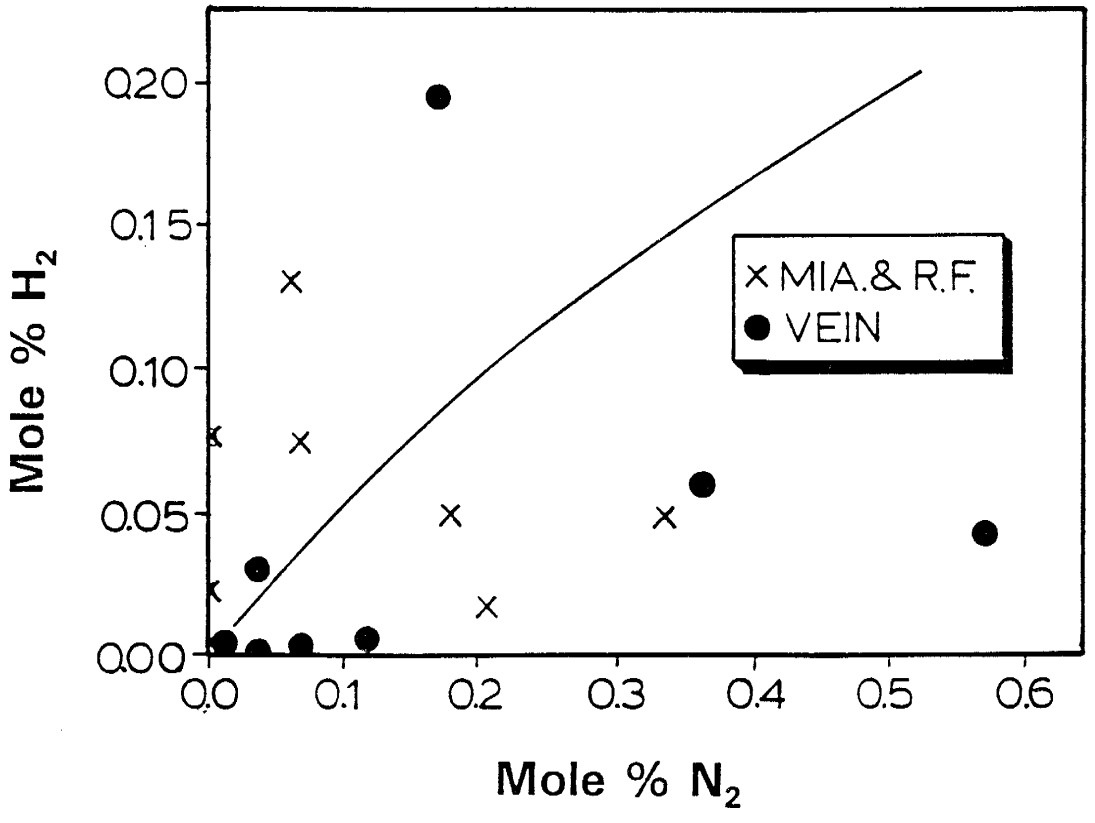
0.20
0.15
0.10
0.05
0.00
0.0
0.1
0.2
0.3
0.4
0.5
0.6
Mole % H_2
Mole % N_2
× MIA.& R.F.
● VEIN

Fig. 3.8

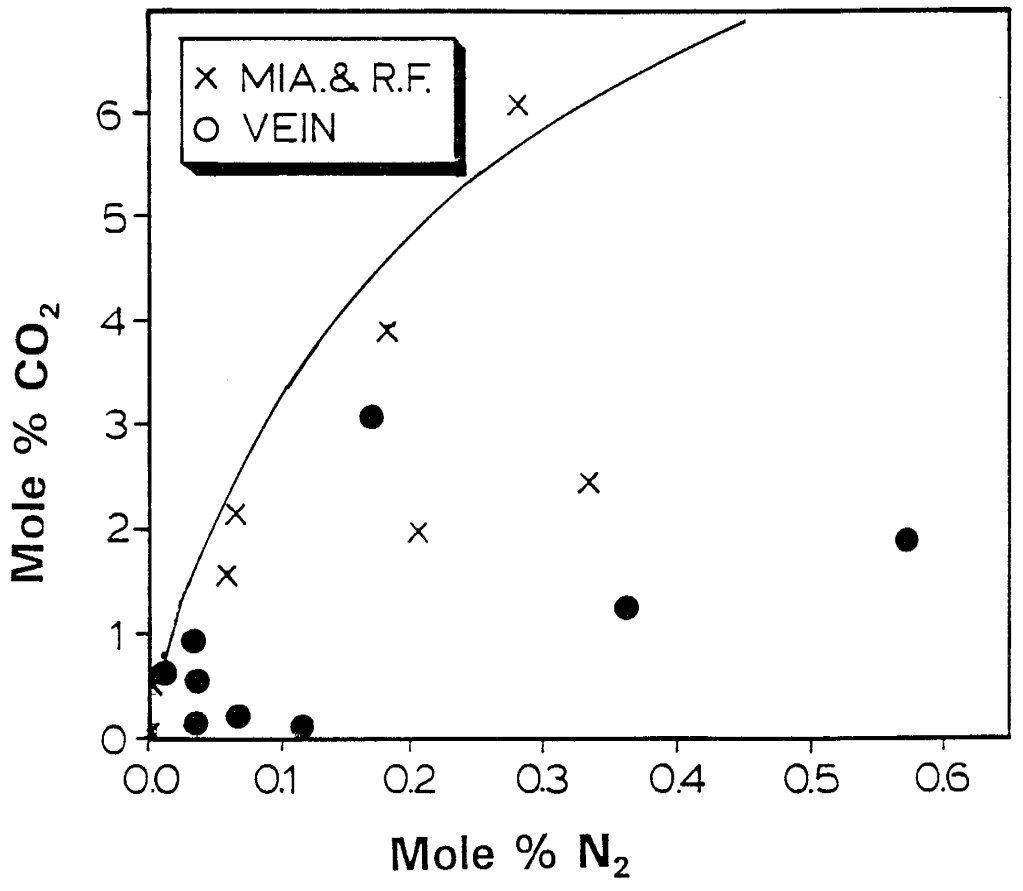

Fig. 3.8.

Plot of N_2 versus CO_2 for recalculated data, for miarolitic and rock-forming quartz (crosses) from the Drammen granite Drammen granite and from vein quartz (filled circles). The line shows a possible change of the fluid composition due to vapor saturation (boiling) from 365 to 300°C with initial composition: N_2=0.5 mole%; CO_2=7 mole%.

trapping.

Temperature calculations

Homogenization temperatures range from 130 to 350°C with the bulk of the measured temperatures between 180 and 250°C. With pressure correction based on formation at 1.3-1.5 kbars of lithostatic pressure trapping temperatures will be in the range of 300-600 °C. If this was true there would have been more than one trapping sequence with zonation of the veins. No zonation has been observed in the veins. If the inclusions were trapped in a system which varied from lithostatic to hydrostatic pressure (low homogenization temperature to high homogenization temperature) trapping temperature will be in the range of 300-350 °C. This temperature range is supported by the data of Olsen (1981).

The low K concentration relative to Na concentration indicate low fluid temperature during the vein formation (Fournier, 1981).

Equilibrium temperatures of the fluids can be calculated by using the gas geothermometers from knowledge of mole fraction of the gas species CO_2, CH_4, and H_2 (Henley et al., 1984). The CO_2-H_2-C and CH_4-H_2-CO_2 geothermometers for aqueous solutions (200 to 350°C) with minimal dissolved salts taken from Henley et al. (1984) are:

$$\log X(CO_2) + 2\log X(H_2) = -3.384 - 8982/T + 0.01377 \quad \text{(Eq. 1)}$$

$$2\log X(CO_2) + 4\log X(H_2) - \log X(CH_4) = -5.022 - 13178/T + 0.01959 \quad \text{(Eq. 2)}$$

where X is the mole fraction of the gas species and T is the temperature in Kelvin.

There is a generally good agreement between the two geothermometers (± 25°C) for the data from the vein quartz samples where methane was detected, indicating a system in equilibrium with the components in these two equations. Temperatures calculated for the inclusions in the vein samples are mostly less than 350°C, which is within the range of the geothermometers (Table 3.3a). These temperatures are within in the range where we could expect molybdenite deposits formed (Wood et al., 1987: Roedder, 1984; Smith, 1983; Westra and Keith, 1981) and as Olsen (1981) indicated with microthermometric fluid inclusion analyses. However, some of the samples indicate temperatures above expected deposition temperature for these MoS_2 mineralization (Olsen, 1981; Ihlen and Martinsen, 1986), hence the indicated temperatures may represent the average decrepitation temperature rather than the temperature of trapping. Temperatures calculated for the miarolitic and rock-forming quartz samples are higher than 350°C, hence outside the range of the geothermometers (Table 3.3b) relative to the validity of the geothermometers.

Oxygen fugacity calculations

Oxygen fugacities have been calculated from the gas analyses based on the following reactions:

$$CH_4 + 2O_2 = CO_2 + 2H_2O \qquad \text{(Eq. 3)}$$

$$CH_4 + O_2 = CO_2 + 2H_2 \qquad \text{(Eq. 4)}$$

$$C + O_2 = CO_2 \qquad \text{(Eq. 5)}$$

with the corresponding equilibrium constants (K) for the reaction (in this paper the K values are from Henley et al., 1984). Native carbon is not found in the granites studied, but does occur in the surrounding country rock. Oxygen fugacities were calculated for vein samples at 300°C with Henry's Law constants given by Henley et al. (1984, p. 58). For rock-forming and miarolitic quartz samples $f(O_2)$ calculations were made at 500°C with fugacity coefficients from Naumov et al. (1974) at 1.5 kbars total pressure.

Inclusion fluids from the mineralized and barren veins give calculated log $f(O_2)$ values between -33.3 and -35.8 at 300°C based on the raw data. Equilibrium assemblage of gases in inclusions at 300°C was calculated for samples where the gas geothermometer equations indicated a reequilibration at $T>T_{TRAPPING}$ as a result of thermal decrepitation. The samples that gave higher temperatures than 300°C (expected trapping

temperature; Olsen, 1981) were reconstructed (after algorithm described by Norman et al., 1991) to an "original" gas composition. The $f(O_2)$ calculated for this reconstructed composition indicate only small differences between log $f(O_2)$ for raw data and reconstructed values (Table 3.3a).

The log $f(O_2)$ for the fluids from rock-forming and miarolitic quartz from the Drammen granite range from -22.4 to -24.6 (total pressure equal 1.5 kbars; 1 mole% TDS; 500°C). No reconstruction of gas composition was done on these samples because the temperatures calculated by the geothermometers are commonly below or equal to expected trapping temperatures (Olsen and Griffin, 1984a), and reconstruction has shown to marginally change the calculated $f(O_2)$.

When inclusions are heated, the fluid composition may change due to chemical equilibrium reactions of fluid aqueous and gaseous species. This change in composition may also occur during cooling after the fluids were trapped in the minerals (Norman et al., 1991). If decrepitation occurs at the trapping temperature, the fluid composition obtained will be most like the one which was originally trapped, assuming reactions are reversible and kinetics permits equilibrium. However, decrepitation commonly occurs at a higher temperature than trapping the temperature. During heating of the sample, equilibrium may not be established due to slow reactions.

The reaction

$$2\ H_2O + CH_4 = 4\ H_2 + CO_2 \qquad \text{(Eq. 6)}$$

is important for the fluid composition, proceeds to the right as temperature increases. The reaction involves four of the major aqueous and gaseous species we are dealing with in this paper. Another important reaction is the one involving the breakdown of HC. This reaction can cause an increase of H_2, CH_4, and other compounds, depending upon type and amount of HC in the fluids. Eq. 6 is used for back calculations (Table 3.3a,b; Norman et al., 1991).

Piperov and Penchev (1973) discusses this problem in a study on fluid inclusion gas analysis of allanite. They did their decrepitations at temperatures between 200° and 1100°C. At decrepitation temperatures above 450-500°C considerable amounts of H_2 and CO were produced. They attributed these products to the following three reactions:

$$H^+ + Fe^{2+} = Fe^{3+} + 1/2H_2 \qquad \text{(Eq. 7)}$$

$$H_2 + CO_2 = H_2O + CO \qquad \text{(Eq. 8)}$$

$$CH_4 + H_2O = CO + 3H_2 \qquad \text{(Eq. 9)}$$

Iron oxides are not present in the samples analyzed but

dissolved iron may be in the solution. However, only very acid fluids will have enough H^+ ions to produce the quantity of H_2 detected.

Alternatively we could see the products of:

$$H_2S + 2H_2O = SO_2 + 3H_2 \quad \text{(Eq. 10)},$$

$$H_2S + CO_2 = SO_2 + H_2 + C \quad \text{(Eq. 11)},$$

$$H_2S + O_2 = SO_2 + H_2 \quad \text{(Eq. 12)},$$

$$H^+ + HSO^{4-} + = SO_2 + H_2 + O_2 \quad \text{(Eq. 13)},$$

$$4SO_4^{2-} + CH_4 + 8H^+ = 4SO_2 + CO_2 + 6H_2O \quad \text{(Eq. 14), and}$$

$$H_2S + 2CO_2 = SO_2 + 2CO + H_2 \quad \text{(Eq. 15)},$$

all which proceeds to the right with increasing temperature.

Because most equilibrium temperature calculations give values below 450°C, Eqs. 8 and 9 play only minor roles in our analysis techniques (Piperov and Penchev, 1973). Thermodynamic calculations of the amount of CO and H_2 that can be produced has been done based on detected gas composition (Appendix B and C). These calculations indicate that CO mole fractions of $1*10^{-5}$ at 300°C and $5*10^{-5}$ at 500°C could potentially have been produced via Eq. 8. Only $1*10^{-11}$ (300°C)

and $4*10^{-4}$ (500°C) of CO mole fraction could potentially have been produced through Eq. 9. However, the detected CO mole fraction could potentially have produced up to 0.9 of H_2 through Eq. 9 at 500°C at $X_{CH4} = 10^{-2}$, but very small amounts at 300°C ($2*10^{-6}$).

SO_2 is the main sulfur species but H_2S occurs in a few samples. There are no other indications (high H_2 or low CO_2) that these inclusions should have reacted differently when heated. SO_2 is not commonly measured in fluid inclusion volatiles (Norman and Sawkins, 1987). The data therefore indicate that oxidized sulfur is genuine for these samples and not generated through decrepitation heating or in the analyzer as indicated by Eqs. 10-12. These reactions require very high H_2S concentrations to produce any detectable SO_2.

The oxidized sulfur is likely occurring as sulfate in the inclusion fluids. Sulfur dioxide can only be produced according to Eq. 13 if log $f(O_2)$ is in the order of -60 at 300°C. Sulfur dioxide may be generated by oxidizing heavier HC or during heating and evaporation of inclusion fluids according to Eq. 14, but this would require a very low pH, on the order of -14, which in solution chemistry is beyond reality. If SO_2 is produced through reaction 14, this means that measured CH_4 may be too low and CO_2 somewhat too high.

Equation 15 shows an other way of producing SO_2, which is possible because all the gas species in the reaction where detected in most analyses. However, it is thermodynamically

not likely to happen during decrepitation. If this happened in the analyzer it would be during the analyzing of condensable gases where CO and H_2 are not recorded not recorded. If this reaction commonly occurred in the analyses it should be seen in all analyses of CO_2 + H_2S bearing gases, but this is not the case.

Norman and Sawkins (1987) found that H_2 and CO were produced in large amounts at high decrepitation temperatures (above 550°C). A decrepitation temperature at 500°C should avoid these generations. Problems with breakdown of HC to H_2, CH_4, and CO_2, and the reaction according to Eq. 6 cannot be avoided in general in thermal decrepitation.

Sulfur fugacity calculations

For the few samples where H_2S was detected, $f(S_2)$ can be calculated using on the equation:

$$2H_2S + O_2 = S_2(g) + H_2O \qquad \text{(Eq. 16)}$$

and using $f(O_2)$ calculated from Eqs. 3 and 4 at 300°C. This yields a range of calculated log $f(S_2)$ of -8.9 to -11.2 (Table 3.3a). Using $f(O_2)$ calculated from Eq. 5 gives somewhat lower $f(S_2)$. Because SO_2 is probably not found in the inclusion fluids any attempt to calculate $f(S_2)$ through oxidized sulfur has not been done.

pH calculations

Assuming that SO_2 detected in the vein samples is oxidized sulfate (Eq. 14) produced during heating and evaporation in the vacuum line and that the calculated $f(S_2)$ is representative for all vein samples, pH for the trapped fluid can be calculated according to the following equation:

$$SO_4^{2-} + 2H^+ = 1/2S_2 + H_2O + 3/2O_2 \qquad \text{(Eq. 17)}.$$

Thermodynamic data for the calculations are from Helgeson (1969) and Robie et al. (1979). Oxygen fugacity used for this calculation is based on Eq. 5, mean log $f(S_2)$=-10.1, and ionic potential I=1. The calculated pH gives the range 8.6 to 10.9 (Table 3.3a,b). The calculated $f(S_2)$ is the most critical number in this pH calculation since. At this pH both the C-O system and the S-O system will be in equilibrium. pH can alternatively be calculated via CO_2-carbonate system and SO_2-sulfate-H_2S-sulfide system. This calculation (Appendix G) gives pH range of 3 to 4.

The calculated pH is higher than the pH Smith (1983) found for the Questa porphyry Mo deposit, New Mexico (pH≈3-4). His estimations were based on a mineral assemblage for which sericite alteration is associated with mineralization. In the Drammen granite there are only minor sericite alteration is associated with the mineralization (Walder, 1986; Ihlen et al., 1982) indicating higher pH and/or higher K^+ for the given

conditions than for Questa. Molybdenum mineralization found associated with porphyry copper deposits are commonly associated with K-feldspar alteration indicating a pH > 5.5. The pH calculation from the combined system seems therefore to be too low.

The occurrence of SO_2 and CH_4 in analyses indicates that the sulfur system and the C-CH_4-CO_2-H_2-H_2O system is either wrong for ox/red S ratio or are not in equilibrium. If the analyzed ox/red S ratio is correct, CO_2 and/or H_2 is too high and/or CH_4 is relatively too low. Breakdown of heavy hydrocarbons will produce CH_4 and H_2 with relatively more CH_4 than H_2 because the H/C ratio is less than 4 for most heavy hydrocarbons. Breakdown of hydrocarbons could therefore produce excess amounts of these species, the result being in yield lower $f(O_2)$ than in the fluid. These reactions are as much a function of $f(O_2)$ as temperature (Helgeson, 1991; Shock, 1991). This HC breakdown may explain the calculated pH discrepancy and giving to low calculated $f(O_2)$ values.

If H_2 concentration is one order of magnitude too high, calculated $f(O_2)$ will be two orders of magnitude too high, giving a pH 1.5 too high. Smith's data (1983) also shows occurrences of SO_2 and CH_4, which is the only other published data showing non-equilibrium between the two systems described here. Apodaca (1987) detected heavy HC's but no SO_2. These analyses may well be too high in H_2 and CH_4, but since the $f(O_2)$ of the fluid is lower SO_2, is not present. Apodaca

(1987) compared thermal decrepitation with crushing and concluded that there was little to no breakdown of HC during thermal decrepitation. Levorsen (1967) concluded that breakdown will occur extensively upon heating up to 300°C, which is lower than the decrepitation temperature used in this study. However, his experiments were performed with pure HC and not HC dissolved in water.

Calculated $f(O_2)$ of inclusion fluids from the vein samples are 3.5 to 5.5 log units below the magnetite/hematite mineral equilibrium line and close to the CO_2 - CH_4 equal fugacity line for reconstructed data (Fig. 3.9). The plot indicates a reduction in oxygen fugacity from early trapped fluid to late trapped fluid relative to CO_2-CH_4 equal fugacity line and constant relative to the mineral equilibria lines. The plot also indicate that oxygen fugacity of the fluids was not the result of CH_4 being created by HC break down that should created excess CH_4. Decrease in total pressure from lithostatic pressure (1.5 kbars) to hydrostatic pressure (0.6 kbars; same depth) will change calculated $f(O_2)$ with only 0.2 log units. The $f(O_2)$ for the fluids stayed constant relative to the mineral buffers indicating that the $f(O_2)$ for the fluid is controlled by mineral buffers. This mineral buffering of the fluids explains the relatively lower CH_4 concentrations in the high temperature fluids.

Fig. 3.9.

Plot of temperature versus oxygen fugacity for the Drammen granite calculated for inclusion fluids from veins at 300°C and calculated at 500°C for the other analyses. The graph also shows the hematite-magnetite (H-M) oxygen fugacity line, the quartz-fayalite-magnetite (QFM) buffer line, and the CO_2 - CH_4 equal fugacity line.

Fig. 3.9

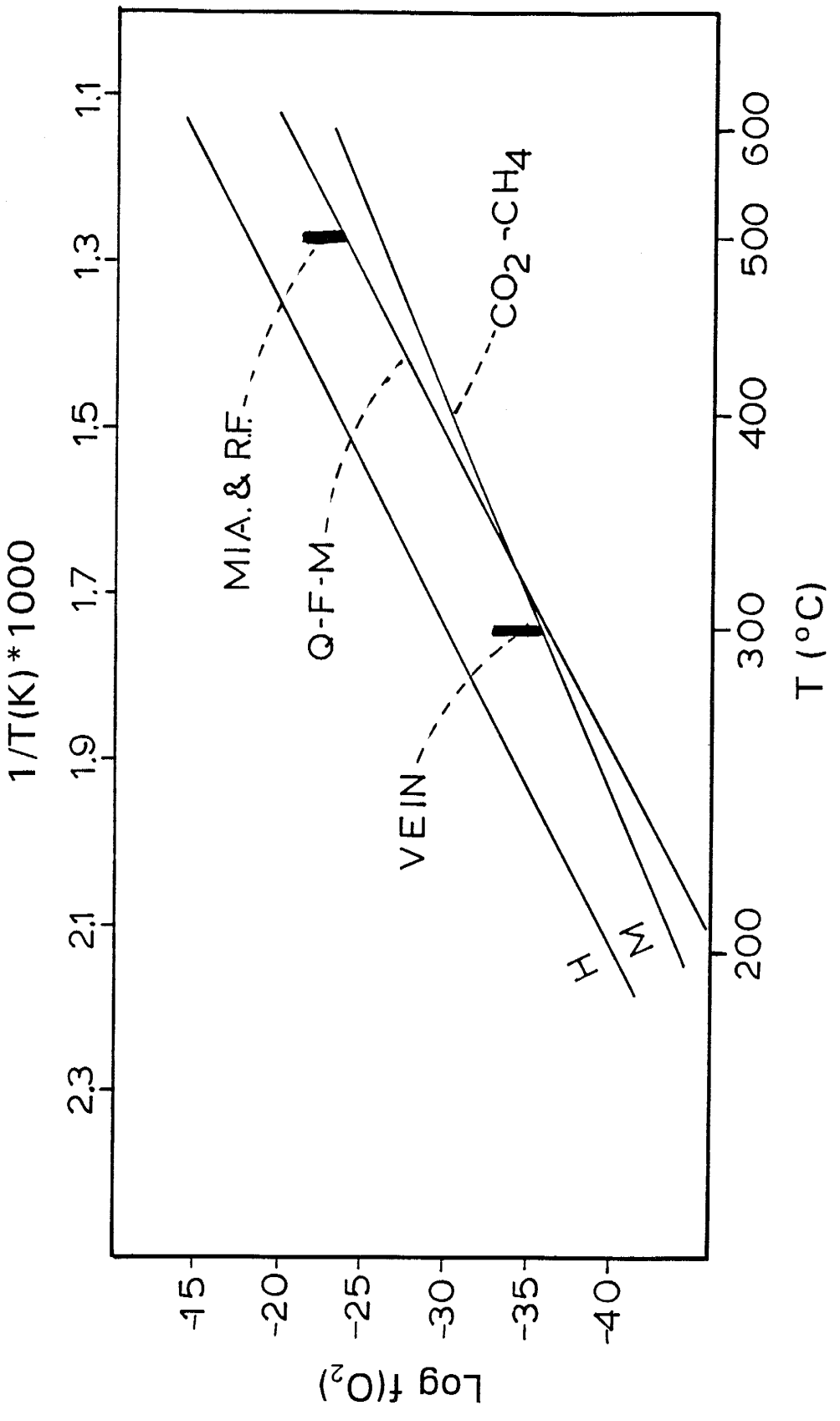
1/T(K)*1000
1.1
1.3
1.5
1.7
1.9
2.1
2.3
T (°C)
200
300
400
500
600
Log f(O2)
-15
-20
-25
-30
-35
-40
MIA. & R.F.
Q-F-M
VEIN
CO2 -CH4
H
M

Salt data

Correlation coefficients

Correlation coefficients between the concentrations of analyzed elements in the inclusion fluids have been calculated for the total amount of samples (Table 3.11). Zero was used for elements not detected and elements not analyzed were excluded from the calculation. Strong correlation may result if there are many samples with zero values and for which one sample has a much higher concentration than the other samples. Samarium and Eu correlate well, but they do not correlate with the other REE's. These REE's on the other hand correlate well. Cesium correlates well with As, Zn, Sb, Rb, Ta, and Na and As correlates well with these same elements. Molybdenum correlates with Br, Ag, and REE. Iridium correlates with the heavy REE's. Zinc correlates with Sb, Rb, and Na. Sb correlates with Rb, Na, and Ta. Silver correlates with Br and Rb with Ta and Na. Chromium correlates well with Sc.

Discriminant analysis

The fluid concentrations in ppm are used to discriminate among the sample groups Drammen (1), Glitrevann (2), Finnemarka (3), and vein (4) samples by Number Crunching Statistical Systems (Hintze, 1990). Table 3.12 gives the sample number, the group, prediction, and probability of being in the different classes. This probability calculation is based on an algorithm by James (1985; p. 65). Zero is used

Table 3.11. Matrix of correlation coefficients between the different elements calculated from the liquid composition of elements dissolved in the fluids where concentrations below detection limit have been designated to zero and elements not analyzed ignored.

	Na	Sc	Cr	Fe	Co	Zn	As	Br	Rb	Mo	Ag	Sb	Ca	Ba	La	Ce	Nd	Sm	Eu	Tb	Yb	Lu	Hf	Ta	W	Ir	Au	Th	U
Na																													
Sc	0.095																												
Cr	0.138	0.831																											
Fe	0.630	0.316	0.370																										
Co	0.579	0.189	0.110	0.489																									
Zn	0.758	0.087	0.221	0.425	0.338																								
As	0.929	-.058	0.022	0.608	0.563	0.720																							
Br	0.421	0.307	0.401	0.329	0.414	0.281	0.320																						
Rb	0.951	0.002	0.092	0.625	0.480	0.699	0.958	0.341																					
Mo	-.055	0.357	0.267	-.006	0.176	-.126	-.178	0.647	-.129																				
Ag	0.527	0.008	0.116	0.239	0.139	0.438	0.404	0.614	0.477	0.415																			
Sb	0.935	-.069	-.000	0.624	0.583	0.674	0.974	0.352	0.953	-.140	0.377																		
Cs	0.939	-.077	0.010	0.615	0.570	0.696	0.981	0.345	0.974	-.120	0.412	0.989																	
Ba	0.562	0.040	0.027	0.402	0.315	0.483	0.632	0.392	0.558	0.007	0.150	0.623	0.622																
La	-.062	0.410	0.165	-.004	0.045	-.094	-.088	-.010	-.038	0.447	-.053	-.070	-.054	-.120															
Ce	-.071	0.376	0.141	-.020	0.009	-.092	-.092	-.014	-.032	0.389	-.072	-.077	-.062	-.109	0.16														
Nd	-.111	0.333	0.124	-.058	-.054	-.121	-.134	-.056	-.079	0.416	-.073	-.105	-.092	-.148	-.915	0.101													
Sm	-.021	0.094	0.244	-.015	0.054	-.011	-.068	0.615	-.021	0.779	0.577	-.097	-.038	-.115	0.875	0.059	0.984												
Eu	-.006	0.073	0.236	0.002	0.075	0.003	-.049	0.618	-.014	0.741	0.596	-.085	-.026	-.092	0.131	-.038	0.140	0.118											
Tb	-.146	0.249	0.112	-.113	-.172	-.147	-.180	-.023	-.099	0.438	0.000	-.138	-.121	-.191	0.043	-.035	0.042	0.013	0.992										
Yb	-.149	0.244	0.108	-.121	-.191	-.146	-.181	-.042	-.103	0.422	-.014	-.138	-.123	-.191	0.802	0.049	0.911	0.964	0.189	0.083									
Lu	-.146	0.247	0.106	-.119	-.189	-.144	-.178	-.045	-.100	0.418	-.018	-.136	-.121	-.189	0.911	0.796	0.965	0.160	0.053	0.998	0.999								
Hf	-.136	0.152	0.209	0.02	-.126	-.177	-.147	0.258	-.115	0.315	0.281	-.117	-.145	-.079	0.212	0.228	0.191	0.179	0.173	0.200	0.197	0.195						
Ta	0.681	-.107	0.026	0.419	0.407	0.490	0.787	0.152	0.774	-.140	0.219	0.761	0.794	0.462	0.084	0.048	0.067	-.084	-.090	0.045	0.049	0.052	-.133						
W	0.009	0.431	0.146	0.110	0.549	-.089	0.046	0.147	-.077	0.277	-.032	-.100	-.083	-.063	0.241	0.153	0.128	0.089	0.101	-.025	-.051	-.051	-.062	-.107					
Ir	-.068	0.134	0.095	-.157	-.146	-.111	-.210	0.220	-.105	0.545	0.165	-.123	-.123	-.244	0.431	0.195	0.515	0.327	0.251	0.623	0.636	0.632	0.064	-.058	-.077				
Au	0.087	0.577	0.561	0.179	-.175	0.048	0.024	-.019	0.079	0.039	0.118	-.044	-.039	-.053	0.101	0.160	0.059	-.038	-.035	0.049	0.059	0.062	0.412	-.069	-.144	-.025			
Th	0.087	0.577	0.561	0.179	-.175	0.048	-.024	-.019	0.079	0.039	0.118	-.044	-.039	-.053	0.101	0.160	0.059	-.038	-.035	0.049	0.059	0.062	0.412	-.069	-.144	-.025	1.000		
U	-.095	0.095	0.225	-.080	0.085	0.266	0.064	0.058	-.144	0.139	-.052	-.077	-.075	0.033	-.036	0.019	-.059	0.131	0.139	-.071	-.063	-.062	0.249	-.136	-.148	-.016	0.317	0.317	

Values higher than 0.18 and lower than -0.18 gives a significant correlation using $\sqrt{n}/n$.

for elements not detected, and elements not analyzed have been excluded from the calculation. This discriminant analysis gives an insight into geochemical differences in the inclusion fluids between the sample groups and quantifies the significance with which these differences can be found. Cesium, As, Mo, Zn, Ag, U, W, Eu, Na, Fe, Hf, Cr, and Sc all give F-ratios (values; described by Till, 1985) above 1, which means that all of these elements add significant amounts to the discrimination. Fluid concentrations of these thirteen elements give an overall grouping significance of 83%, where all Drammen samples, and the two Glitrevann samples give correct group prediction. One Finnemarka and three out of twelve vein samples have inclusion fluid chemistry equal to the Drammen samples (Table 3.12).

Sodium and Mo and Zn and Mo plots (Fig. 3.10a,b) illustrate the difference between Drammen, Finnemarka, and vein samples. The vein samples show typically more variation in contents of most of the elements relative to the other samples. Plots of Na versus Mo, Cr, and Eu (Fig. 3.10a and Fig. 3.11a,b, respectively) indicate that there is no simple relationship between high Na and other elements. Commonly, on these plots analyses of two or three vein samples and one of the Finnemarka samples group together with the Drammen samples. These are the same samples the discriminant analysis showed that fit poorly into the correct group. Plots of Sc vs. Cr and As vs. Cs (Fig. 3.11a,b) illustrate that analysis

Table 3.12. Discriminant analysis and classification prediction based on salt analyses for the individual samples.

SAMPLE #	CLASS	PRED.C.	1	2	3	4
OG-2	1	1	0.886	-.050	0.089	0.076
OG-9	1	1	0.881	0.020	0.040	0.059
OG-12A	1	1	1.201	-.137	0.186	-.250
OG-12B	1	1	0.841	0.103	-.147	0.202
18A	1	1	0.634	0.133	0.036	0.197
18C	1	1	0.593	0.152	-.029	0.284
18D	1	1	0.717	0.150	-.053	0.099
21B	1	1	0.868	0.013	0.185	-.066
23B	1	1	0.877	-.159	-.039	0.321
23C	1	1	0.889	-.109	0.119	0.100
27A1	1	1	0.958	-.055	0.072	0.025
27A2	1	1	0.877	-.060	-.005	0.187
27A3	1	1	0.898	-.058	0.005	0.154
32	2	2	0.026	0.509	0.411	0.053
36	2	2	-.056	1.004	-.003	0.054
41B	3	3	0.006	0.053	0.921	0.020
41D	3	1	0.599	0.258	0.514	-.371
42	3	3	0.023	-.010	0.942	0.044
43A	3	3	-.095	0.107	0.940	0.048
50	4	4	-.003	-.004	0.005	1.002
51A	4	4	0.094	0.028	-.061	0.938
52A	4	4	-.053	-.001	0.020	1.033
54A	4	4	-.002	-.001	0.003	1.001
54D	4	1	0.643	-.006	-.136	0.500
58A	4	1	0.531	0.067	-.081	0.483
59A	4	4	0.134	-.055	-.190	1.112
59B	4	4	-.191	0.083	0.007	1.101
66A	4	4	-.202	-.027	0.173	1.056
66B	4	4	0.031	-.005	-.021	0.995
68A	4	1	0.564	0.064	-.125	0.496
71	4	4	0.028	-.035	0.148	0.859

Fig. 3.10.

Plot of Na (ppm) versus Mo (a) and Zn versus Mo (b) for fluid inclusion liquids divided into the four sample groups. These relations show the grouping between Drammen, Finnemarka, and vein samples. The inclusion fluids from vein samples show typically more spread than the other samples.

Fig. 3.10

a

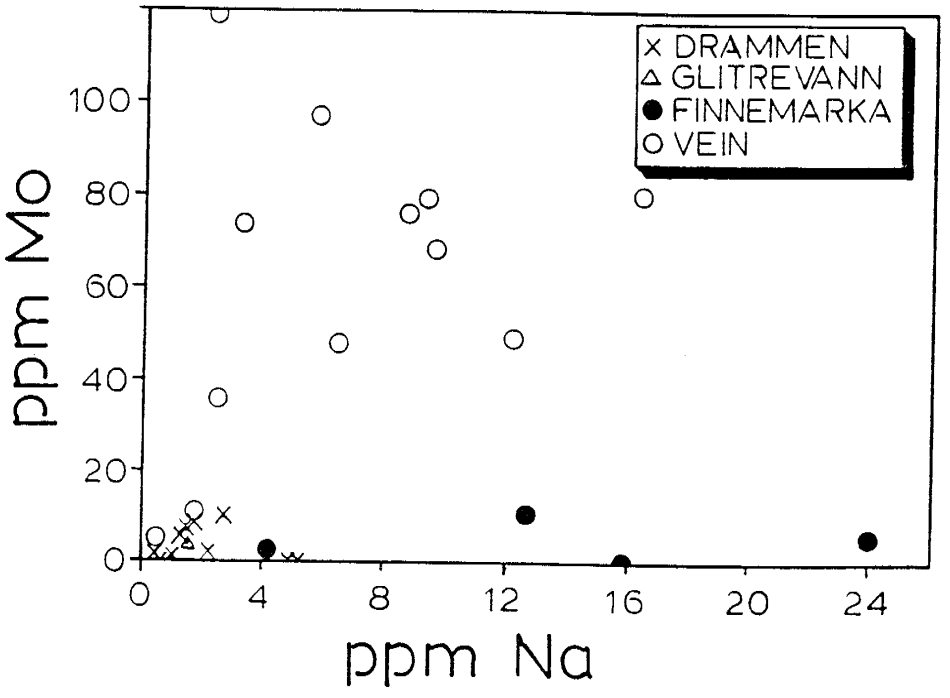
× DRAMMEN
△ GLITREVANN
● FINNEMARKA
○ VEIN
ppm Mo
0
20
40
60
80
100
0
4
8
12
16
20
24
ppm Na

b

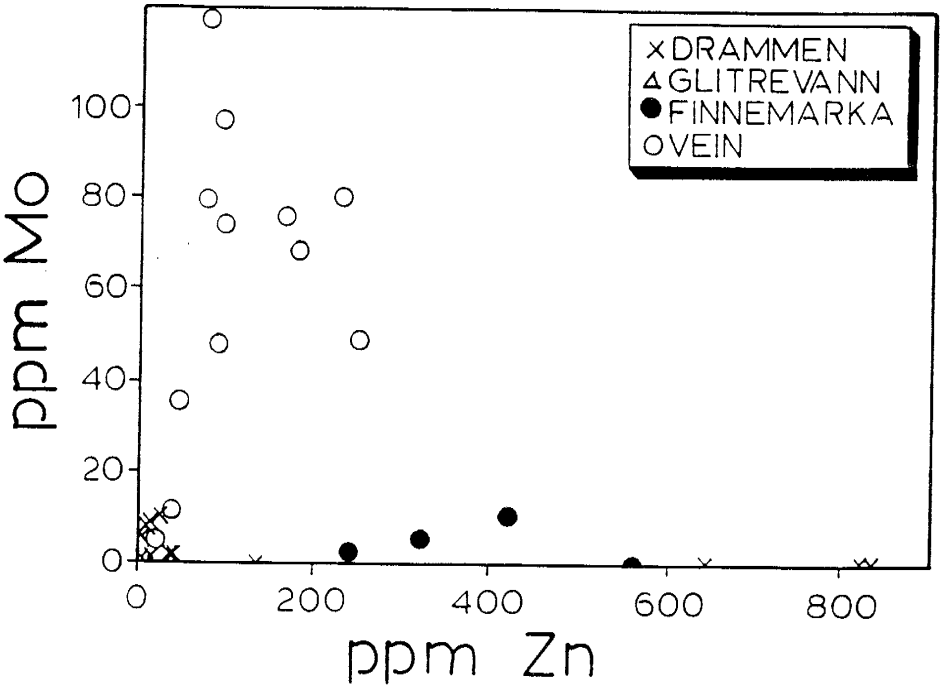
× DRAMMEN
△ GLITREVANN
● FINNEMARKA
○ VEIN
ppm Mo
0
20
40
60
80
100
0
200
400
600
800
ppm Zn

Fig. 3.11.

Plot of Sc versus Cr (a) and As versus Cs (b) for fluid inclusion liquids divided into Drammen, Glitrevann, and Finnemarka miarolitic samples and vein samples. Scandium and Cr are the two elements from Factor 4 that gives the best discrimination between fluids of vein samples and fluids of miarolitic and rock-forming quartz.

Fig. 3.11

a

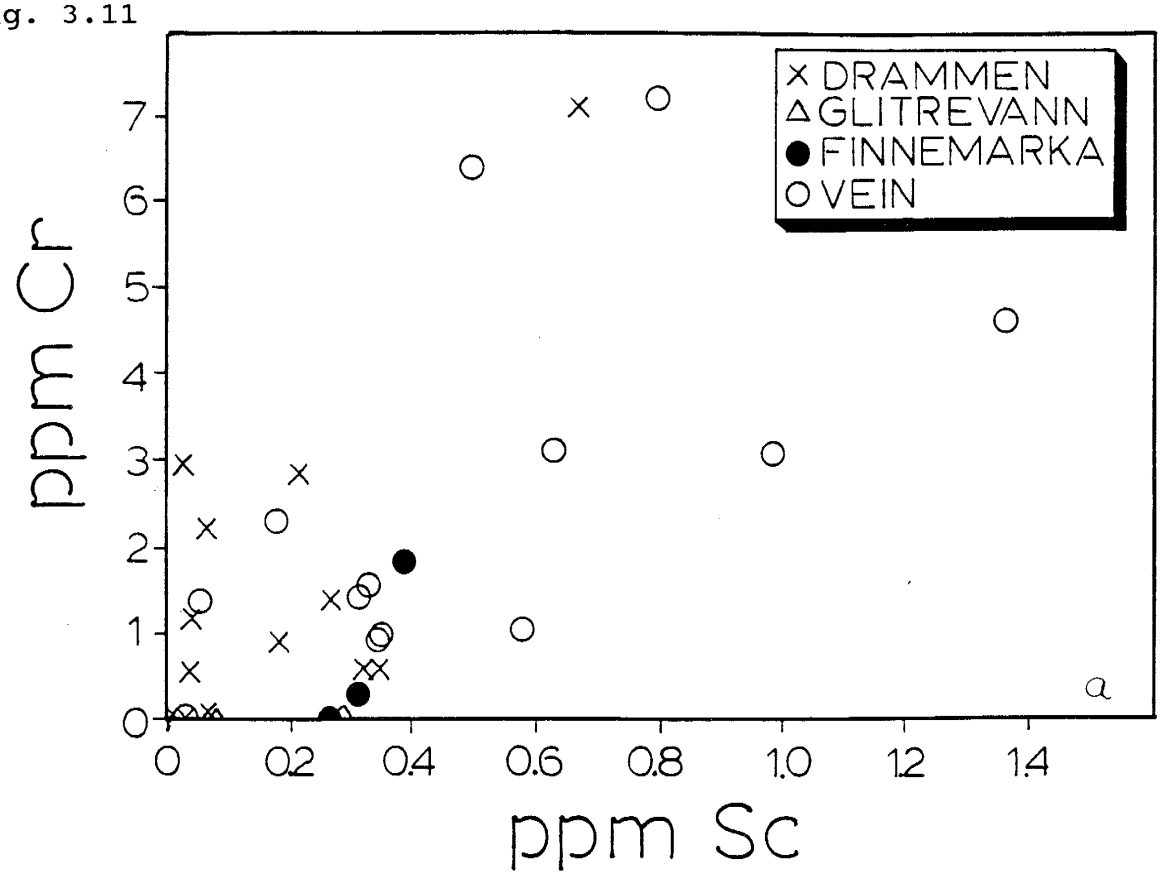
× DRAMMEN
△ GLITREVANN
● FINNEMARKA
○ VEIN
ppm Cr
ppm Sc
0
1
2
3
4
5
6
7
0
0.2
0.4
0.6
0.8
1.0
1.2
1.4
a

b

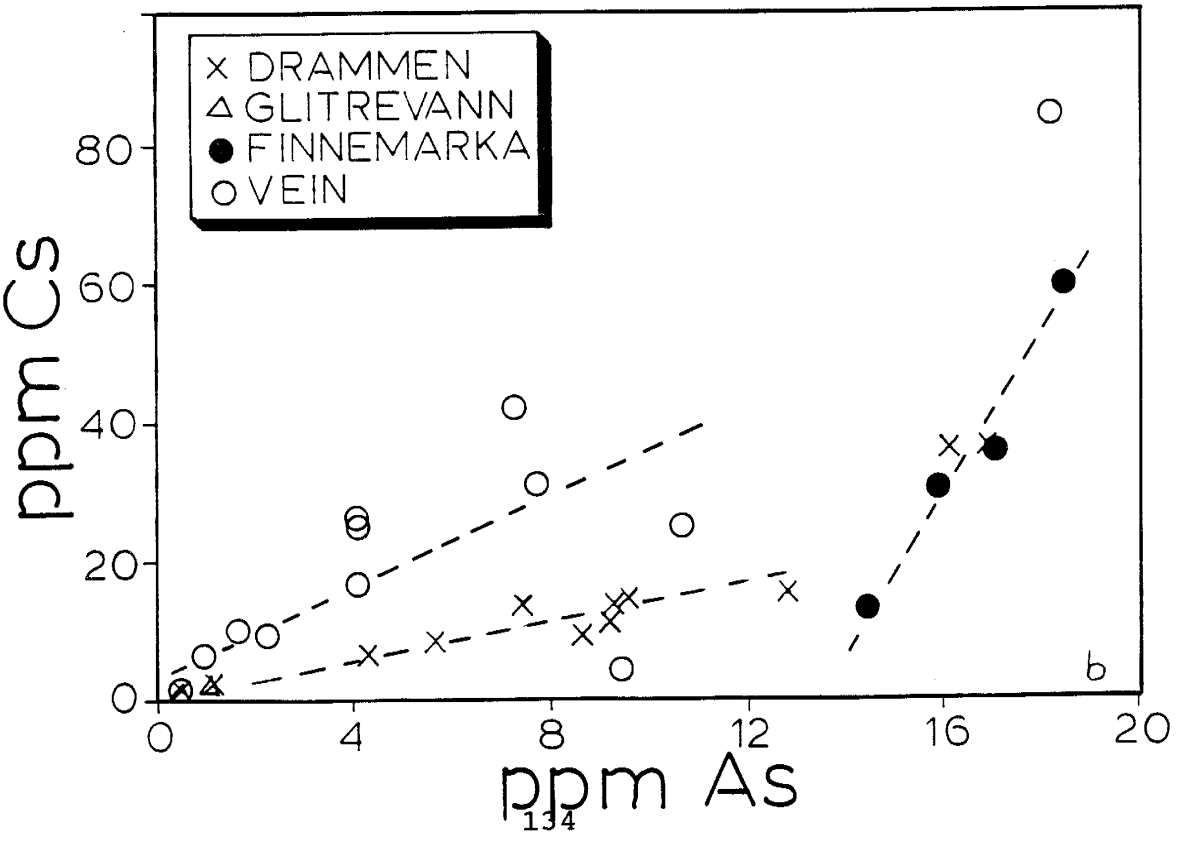
× DRAMMEN
△ GLITREVANN
● FINNEMARKA
○ VEIN
ppm Cs
ppm As
0
20
40
60
80
0
4
8
12
16
20
b

of vein inclusions exhibit linear correlation where each sample group appears to have a unique linear relationship in Fig. 3.11b.

The element concentrations of the liquid from miarolitic and rock-forming quartz shows similar variation. The element concentrations in the vein inclusion liquids are for most elements commonly higher than for the other samples. If the fluids extracted from the vein quartz and miarolitic quartz have a common fluid source this difference could be due to fluid boiling between release of fluids trapped in miarolitic and rock-forming quartz, and release/trapping in vein quartz. If this was the only process responsible for the differences between the two trapping environments, a linear relationship between most elements would be the consequence, with the vein samples in the upper part showing highest concentrations. This is not commonly seen, even though some elements correlate well (Table 3.11).

Continued crystallization of the magma with fluid release at different stages could explain the differences between vein samples and miarolitic and rock-forming quartz samples. Major exsolution of fluid will take place when the magma becomes saturated with respect to H_2O. Vapor saturation and formation of a separate vapor phase can occur either by pressure decrease or by crystallization of anhydrous phases (Candela, 1991). These aqueous bubbles which will be concentrated along the border and the top of the magma are likely to be highly

enriched in silica (Fournier and Potter, 1982). Upon cooling and/or pressure decrease silica should precipitate and form miarolitic cavity quartz, with other minerals as described by Raade (1972, 1969). The rest melt, with its dissolved water, will be strongly enriched in incompatible elements. Those elements with highest distribution coefficients, $K_{D,l\text{-}m}$ (liquid/melt) will be the most enriched in an early formed aqueous phase. Elements like Mo, W, and F have low $K_{D,l\text{-}m}$ and will therefore be enriched in the melt upon continuous crystallization, and be more enriched in a late exsolved aqueous phase (Candela and Holland, 1986).

Differing wall-rock interaction at different temperatures could also explain the variation in chemistry between fluids that formed veins and fluids that formed miarolitic and were trapped in rock-forming quartz. There is extensive alteration seen in the batholith. As and Cs are highly soluble in aqueous fluids at high temperatures (Nakagawa, 1971; Ellis, 1979). Assuming that the fluids that has been decrepitated and leached from the samples represent the fluids from which vein quartz and miarolitic quartz precipitated. If the indicated differences between miarolitic and vein samples were due to different wall-rock interaction these elements would likely be enriched in the vein samples. However, As and Cs are indicated to be lower in fluids that deposited Mo-veins that fluids that formed the miarolitic quartz suggesting that different wall-rock interaction is not the critical factor

controlling the chemistry of the fluids.

The high correlation coefficients between most of the REE's indicate that these elements behave geochemically very similar at high temperature in the melt-aqueous fluid environment as they do in low temperature aqueous environments (Brookins, 1989). Europium and Sm do not correlate very well with other REE's. Eu may not correlate because it has two valence states Eu^{2+} and Eu^{3+}. As Eu^{2+}, it may be easier trapped as a trace element in feldspar (substituting for Ca^{2+}) as the other III valence REE. Eu^{2+} is found in mantle and lower crust rocks. As Eu^{3+}, it will follow other REE's. This would explain the positive Eu anomaly in Fig. 3.12 where as the Drammen granite and the Oslo granite systems exhibit negative Eu anomalies or flat REE patterns.

Chondrite normalizing REE

Fluid inclusion composition normalized to chondrite (Fig. 3.12) is shown for vein quartz samples and miarolitic and rock-forming quartz samples. The latter group shows the variation for the Drammen granite miarolitic quartz samples and covers the variation for Glitrevann and Finnemarka samples. Both of the two sample groups cover a variation of about two orders of magnitude for most of the analyzed elements. Both groups show a strong Ce depletion and Lu enrichment. The vein samples show a Eu enrichment contrasting to the granite samples which show a flat trend. Similar Eu

Fig. 3.12.

Plot of fluid inclusion REE composition normalized to chondrite (Evensen et al., 1978) for vein quartz samples and miarolitic and rock-forming quartz samples from the Drammen granite.

Fig. 3.12

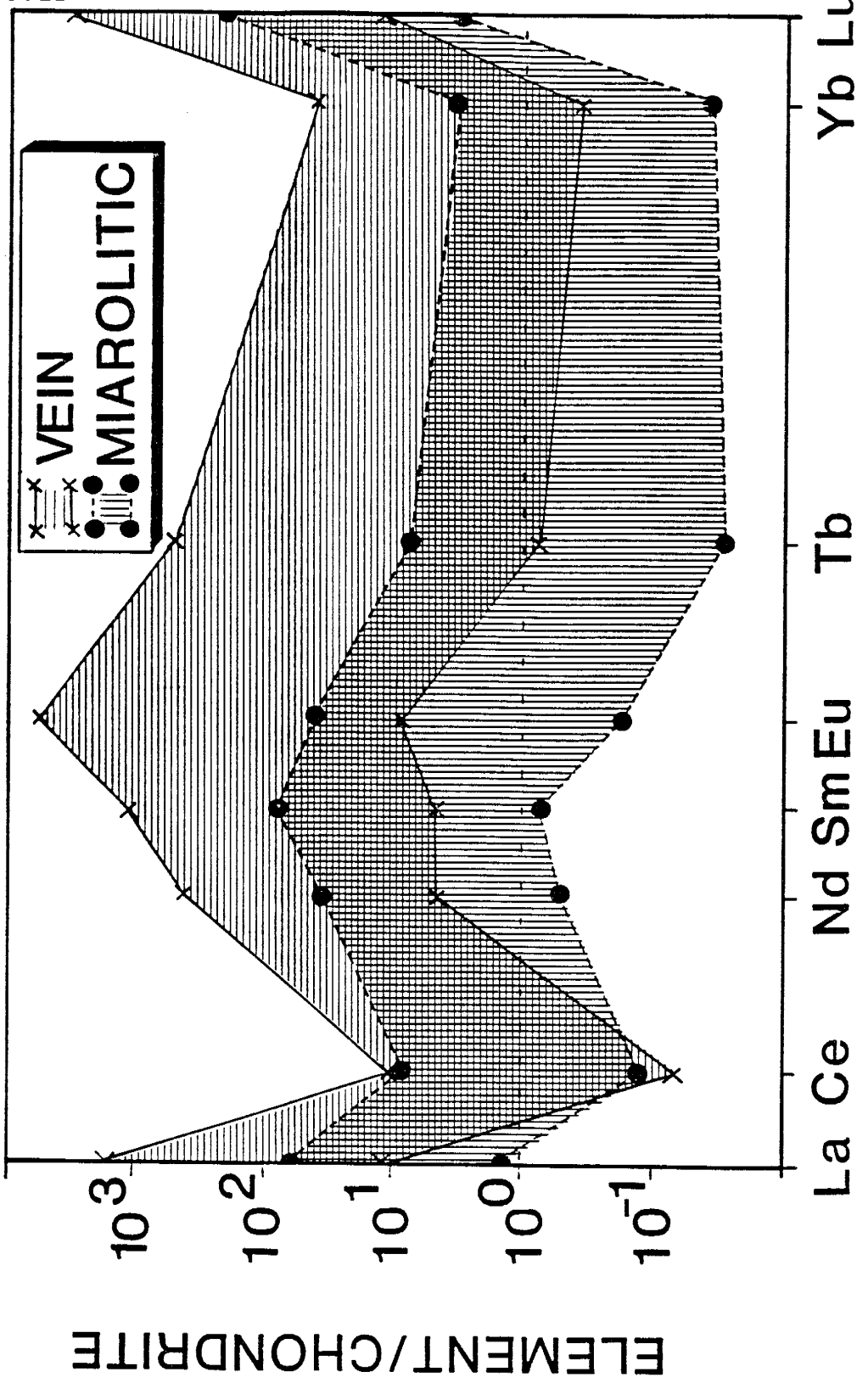
VEIN
MIAROLITIC
ELEMENT/CHONDRITE
10^{3}
10^{2}
10^{1}
10^{0}
10^{-1}
La Ce Nd Sm Eu Tb Yb Lu

enrichment is reported for oceanic hydrothermal solutions (McLennan, 1989; Michard et al., 1983) and REE partitioning experiments between an aluminum-silicate melt and an aqueous phase (Reed et al., 1991). Apatite is commonly enriched in Ce-group REE (Burt, 1989) also called Light REE (LREE) and crystallization of apatite may cause a LREE depletion in rest melt during crystal fractionation. However, apatite is commonly found in the miarolitic cavities in the Drammen granite (Raade, 1969; Raade, 1972).

Under oxidizing conditions Ce^{3+} may oxidize to Ce^{4+}. This is found to happen in marine environments (McLennan, 1989).

If there is a tendency for K-feldspar to alter at the expense of plagioclase, which is seen in the Drammen granite (Walder and Segalstad, in prep.; Ihlen et al., 1982), it may cause release of Ca^{2+} with Eu^{2+}. This alteration could again explain the Eu-enriched late-vein fluids.

Factor analysis

Factor analysis has been performed using Number Cruncher Statistical System (Hintze, 1990) to determine the main controlling factors of the element distribution. Four factors describe about 73% of the data variation, with eigen values above 2. Analyses below detection limit were given a zero value for the calculations; elements not analyzed were not included. The initial factors of totally independent

variables have been rotated using varimax rotation (Kaiser, 1958). The four factors have the highest correlation with the following elements:

Factor 1 (F1): Cs, As, Zn, Sb, Rb, Ta, Na, Ba, Fe, Co

Factor 2 (F2): Ce, La, Nd, Tb, Yb, Lu, (Ir)

Factor 3 (F3): Mo, Ag, Br, Sm, Eu, (W)

Factor 4 (F4): Th, Cr, Sc, Au, (Hf), (U).

The elements in parentheses are poorly correlated with these factors (Table 3.13). If number of factors are restricted to three, F1 and F2 will stay the same with F3 and F4 combined resulting in more poorly correlated elements. These three factors will describe only about 62% of the total data variation.

Chlorine, F, CO_2, $f(O_2)$, pH, T, P, melt composition, type of crystallizing minerals, and type of wall-rock exchange/dissolution are possible variables that could influence solubility of elements, hence, could be related to one of the factors. Sulfur content has been found to be very low in inclusion fluids and is therefore not a potential candidate.

Factor 1: Log plots of ppm Na versus Cs and Zn (Fig. 3.13a,b) show the correlation among elements belonging to F1 which constitute mainly alkali and earth-alkali elements.

Table 3.13. Correlation coefficients between elements and the four factors. The communality (COM>) of the combined factors indicate how well the data for each element are correlated with these factors as a total.

VARIABLE	FACTOR 1	FACTOR 2	FACTOR 3	FACTOR 4	COM.
Cs	0.9798	-.0337	0.0082	-.0961	0.9705
As	0.9754	-.0871	-.0246	-.0696	0.9644
Mo	-.0966	0.3871	0.8392	0.1405	0.8823
Ir	-.1368	0.5607	0.3684	-.0649	0.4731
Zn	0.7486	-.1091	0.0372	0.1076	0.5852
Sb	0.9724	-.0457	-.0252	-.0912	0.9565
Ag	0.4150	-.0632	0.6537	0.0837	0.6106
Au	0.0173	0.0332	-.1254	0.9197	0.8630
U	-.0753	-.1163	0.1008	0.4111	0.1984
Br	0.3825	-.0588	0.7901	0.1518	0.7971
W	-.0066	0.0601	0.2226	0.0317	0.0542
Ta	0.7960	0.1390	-.1064	-.1629	0.6908
Th	0.0173	0.0332	-.1254	0.9197	0.8630
Ce	-.0130	0.8561	0.0150	0.1719	0.7629
La	-.0009	0.9589	0.0578	0.1181	0.9368
Nd	-.0487	0.9882	0.0281	0.0557	0.9829
Sm	-.0684	0.0878	0.9299	0.0294	0.8779
Eu	-.0589	-.0196	0.9329	0.0361	0.8754
Tb	-.0965	0.9762	0.0905	0.0176	0.9707
Yb	-.0997	0.9765	0.0675	0.0218	0.9686
Lu	-.0964	0.9785	0.0600	0.0241	0.9710
Na	0.9594	-.0617	0.0719	0.0512	0.9321
Ba	0.6566	-.1345	-.0036	-.0150	0.4494
Fe	0.6834	-.0517	0.0374	0.2801	0.5496
Hf	-.1334	0.1490	0.2329	0.4572	0.3032
Cr	0.1182	0.0813	0.2372	0.7814	0.6874
Sc	0.0614	0.2815	0.1356	0.7642	0.6857
Co	0.6009	-.0674	0.2153	-.0473	0.4142

Fig. 3.13.

Log/log plots of Na versus Cs (a) and Zn (b) for fluid inclusion liquids. The plots exhibit good correlation between these elements of Factor 1.

Fig. 3.13

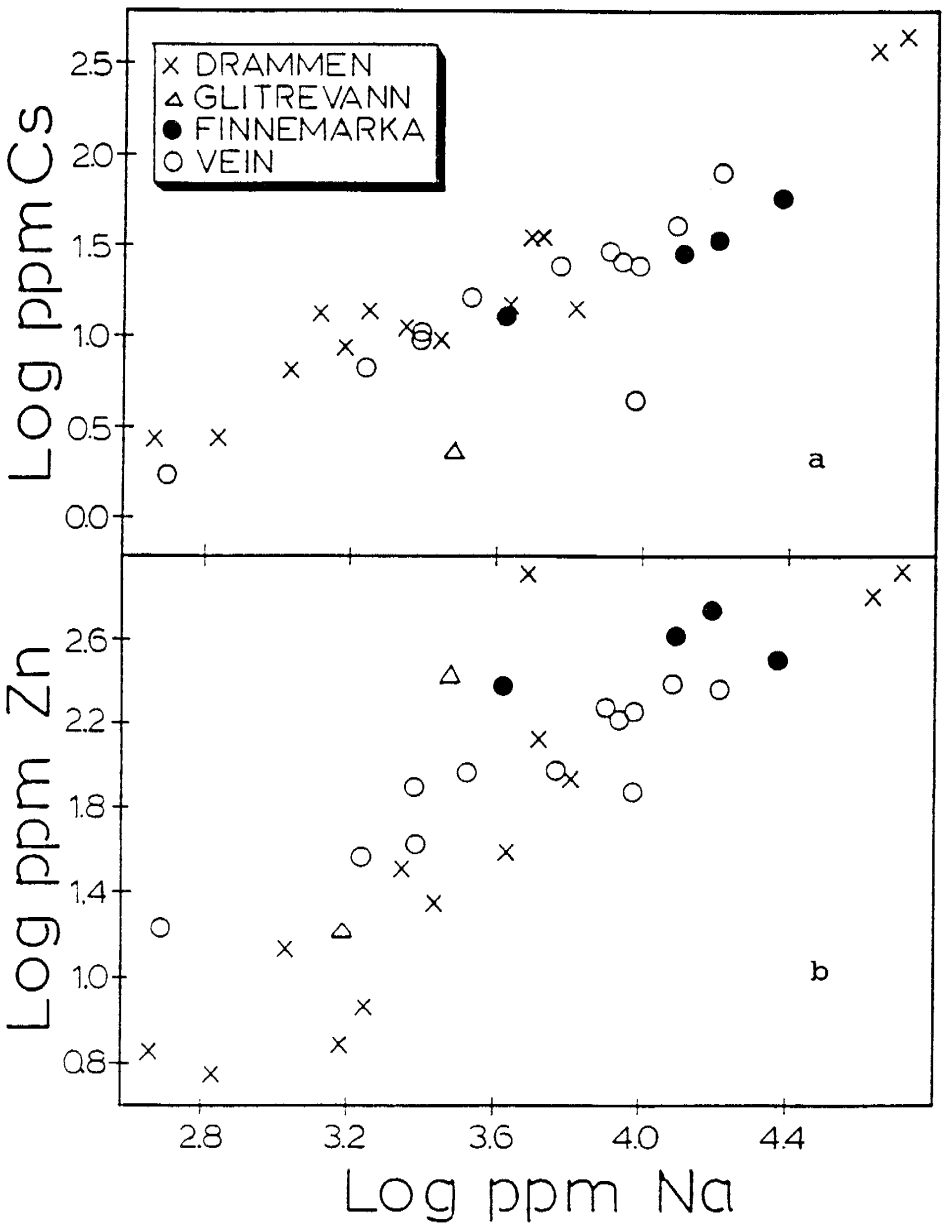
× DRAMMEN
△ GLITREVANN
● FINNEMARKA
○ VEIN
Log ppm Cs
2.5
2.0
1.5
1.0
0.5
0.0
a
Log ppm Zn
2.6
2.2
1.8
1.4
1.0
0.8
b
2.8
3.2
3.6
4.0
4.4
Log ppm Na

Partitioning of alkali and earth-alkali elements between acid melt and aqueous phase is highly controlled by Cl content of the aqueous phase (Webster et al., 1989; Holland, 1972; Malinin and Khitarov, 1984). Chloride will partition into an early formed aqueous phase because of its high D_{L-M} (Kilinc and Burnham, 1972). Hence, the evidence is strong that chloride concentration is believed to control F1. Even though, chloride may not explain why As, Sb, Ta, and Co are also well correlated with F1. Arsenic and Sb are highly soluble elements (Wood et al., 1987) either as sulfide complexes or oxide/hydroxide complexes (Heinrich and Eddington, 1986; Popova et al., 1974). Cobalt, which has chemistry similar to Fe, would also potentially be transported as chlorine complex. Tantalum behaves as lithophile element (Goldschmidt, 1954) and may be enriched in the cap of a silicic magma chamber (Webster, 1987; Webster and Holloway, 1987), but how it is partitioned into aqueous phase and transported, is not clear.

Factor 2: A good correlation exists between the elements belonging to F2 (Fig. 3.14) which constitute mainly REE. Rare-earth elements are readily transported as fluorine complexes (Kosterin, 1959). Carbonate and Cl complexing are also expected to be common complexes at least for a ground-water environment where CO_3^{2-} complexes are more stable than Cl complexes (Brookins, 1989). Carbonate complexes are expected to be stable in alkaline solutions also at high temperatures

Fig. 3.14.

Log/log plot of La versus Ce for the fluid inclusion liquids. There is a good 1:1 correlation between these REE's of Factor 2.

Fig. 3.14

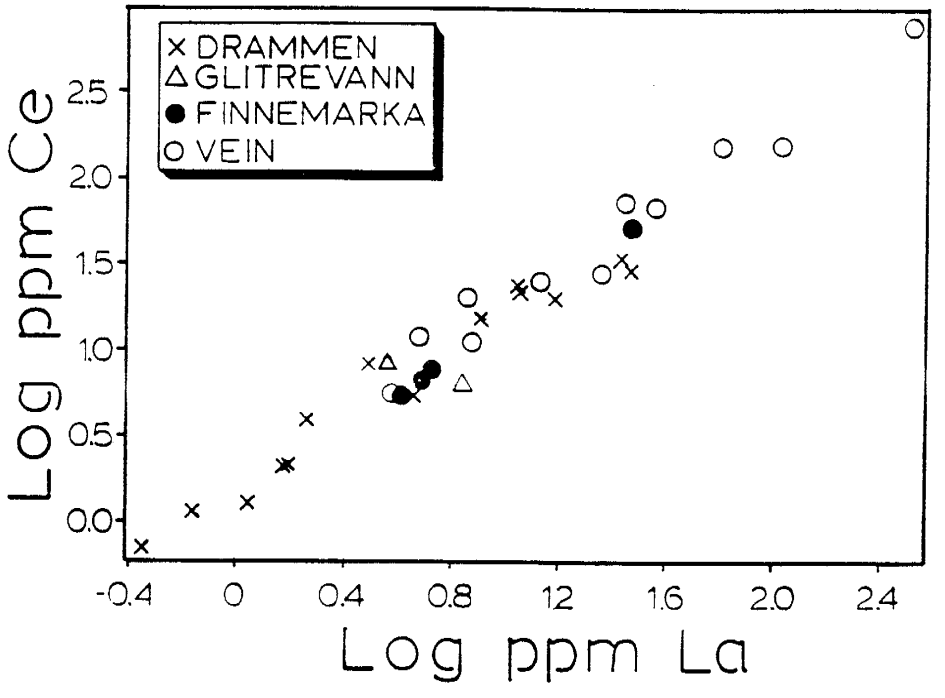
× DRAMMEN
△ GLITREVANN
● FINNEMARKA
○ VEIN
Log ppm Ce
2.5
2.0
1.5
1.0
0.5
0.0
-0.4
0
0.4
0.8
12
1.6
2.0
2.4
Log ppm La

(Kosterin, 1959; Mineyev, 1966). If chlorine was the main contributor for the REE variation it would be expected that they would correlate with the alkali and earth-alkali elements of F1. Fig. 3.15 shows no correlation between Na and Eu or Ce.

The CO_2 content of the vein fluids are lower than for the miarolitic fluids which is the opposite for REE concentrations, indicating that CO_3^{2-} complexes are of minor importance. Webster et al. (1989) found the same lack of correlation between REE and CO_2 concentration for acidic solutions, and for supercritical fluids associated with greisen alteration, F complexes will dominate over CO_3^{2-} complexes (Bandurkin, 1961). Fluoride is therefore expected to be the controlling element of F2.

Iridium is believed to be transported as F-complexes in an aqueous fluid phase and is mainly found in trivalent or quatrovalent state (Sienko and Plane, 1974). At low temperature Ir may be transported as a F or Cl complex in groundwater environment.g. California placers, and it may form Sb or As complexes in a sulfide melt (Crocket, 1978) with a strong sulfide-melt enrichment under fluid immiscibility between sulfide melt and mafic melt (Stone et al., 1990). It can be highly concentrated in minerals such as gadolinite, chromite, columbite, thortveitite, laurite, and chromespinel (Noddack and Noddack, 1931; Goldschmidt and Peters, 1932; Wright and Fleisher, 1965; Razine et al., 1965). Iridium was

Fig. 3.15.

Log/log plot of Na versus Ce and Eu for fluid inclusion liquids. The plot illustrates the lack of correlation between REE's from Factor 2 and Factor 3, respectively, and Na.

Fig. 3.15

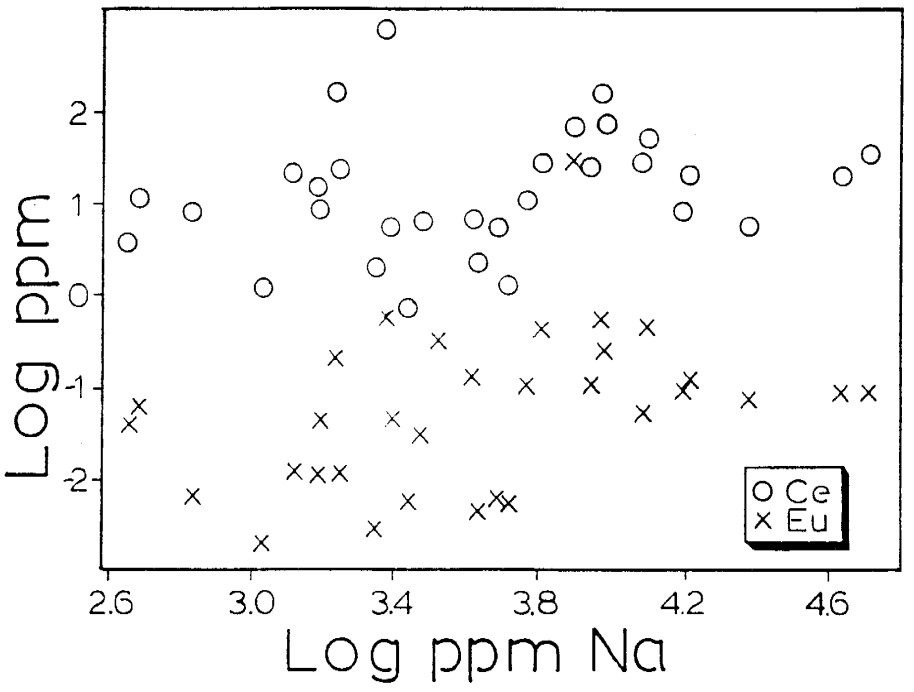

strongly enriched in the plume of Kilauea eruption in 1983, which is linked to high F content (Olmez et al., 1986; Zoller, 1983). This study suggests that Ir is transported with REE's, possibly as fluorine complex.

Factor 3: Mo, Eu, Sm, and W are elements that correlate with F3 (Table 3.13). Fig. 3.16 displays the good correlation between Eu and Mo. On the other hand, there is a poor correlation between Eu and Na (Fig. 3.15). Molybdenum, W, and Eu are shown to be affected by oxygen fugacity of magma where Mo and W may form VI/IV and Eu III/II valence states. High $f(O_2)$ favors solubility of Mo and Eu^{3+} would less likely participate in feldspar alteration.

Bromide has been shown to have several oxidizing states at low temperature. The effect this will have upon distribution coefficient between liquid and solid (D_{L-M}) for Br is unknown. Molybdenum and W, probably together with Br (and F), have fairly low D_{L-M} (Webster et al., 1989; Candela and Holland, 1984). They will therefore be enriched in the melt fraction during crystallization. They may all form oxide/hydroxide complexes, even though Br has a high electronegativity. D_{L-M} for Ag is expected to be highly controlled by Cl content in aqueous phase and $f(O_2)$ (Malinin and Kitarov, 1984). Samarium is expected to act similar to the other REE's. It is therefore hard to establish what controls this factor. The possibility that this late fluid

Fig. 3.16

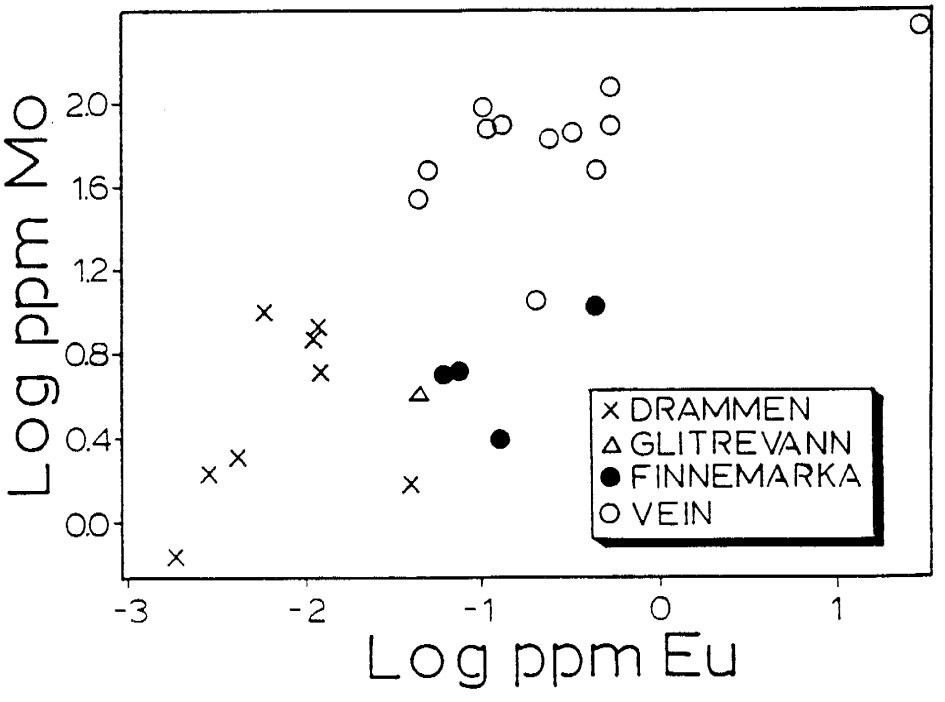
Log ppm Mo
2.0
1.6
1.2
0.8
0.4
0.0
-3
-2
-1
0
1
Log ppm Eu
× DRAMMEN
△ GLITREVANN
● FINNEMARKA
○ VEIN

Fig. 3.16.

Log/log plot of Eu versus Mo for the fluid inclusion liquids. exhibiting the correlation between these elements of Factor 3. The graph also displays the discrimination between the groups.

phase has leached element like Mo, W, Eu from the crystallized magma cannot be ruled out by any geochemical analyses performed on the granite, even though some data suggest that this is of minor importance. There may have been more than one thing happening together giving a diversified group correlated with F3. Geochemistry of the magma and timing of aqueous phase exsolution may be of importance as F3 controls perhaps together with wall-rock leaching.

Factor 4: A lack of correlation exists between Sc and Na (Fig. 3.17a) but plots of Sc and Cr (Fig. 3.17b), display the correlation between elements of F4. Thorium, U, Cr, Sc, and Hf all belong to transition elements II in the periodical system. These elements do not readily substitute into common minerals and will be highly enriched in a late phase of a granitic melt, even though chromite is stable at high temperatures and is therefore associated with ultrabasic rocks. Because these elements correlate best with F3 when constraining the factor analysis to three factors the control of F4 may be similar to F3. However, most of these elements show a low leaching efficiency (Table 3.8).

Combination of factor analysis and discriminant analysis:

Cesium and As are the elements of F1 that best discriminate between vein samples, Drammen granite, and Finnemarka granite (Fig. 3.11b). These two elements are on

Fig. 3.17.

Log/log plots of Sc versus Na (a) and Cr (b) for the fluid inclusion liquids. There is a positive correlation between Sc and Cr (b) elements of Factor 4, and lack between Sc and Na.

Fig. 3.17

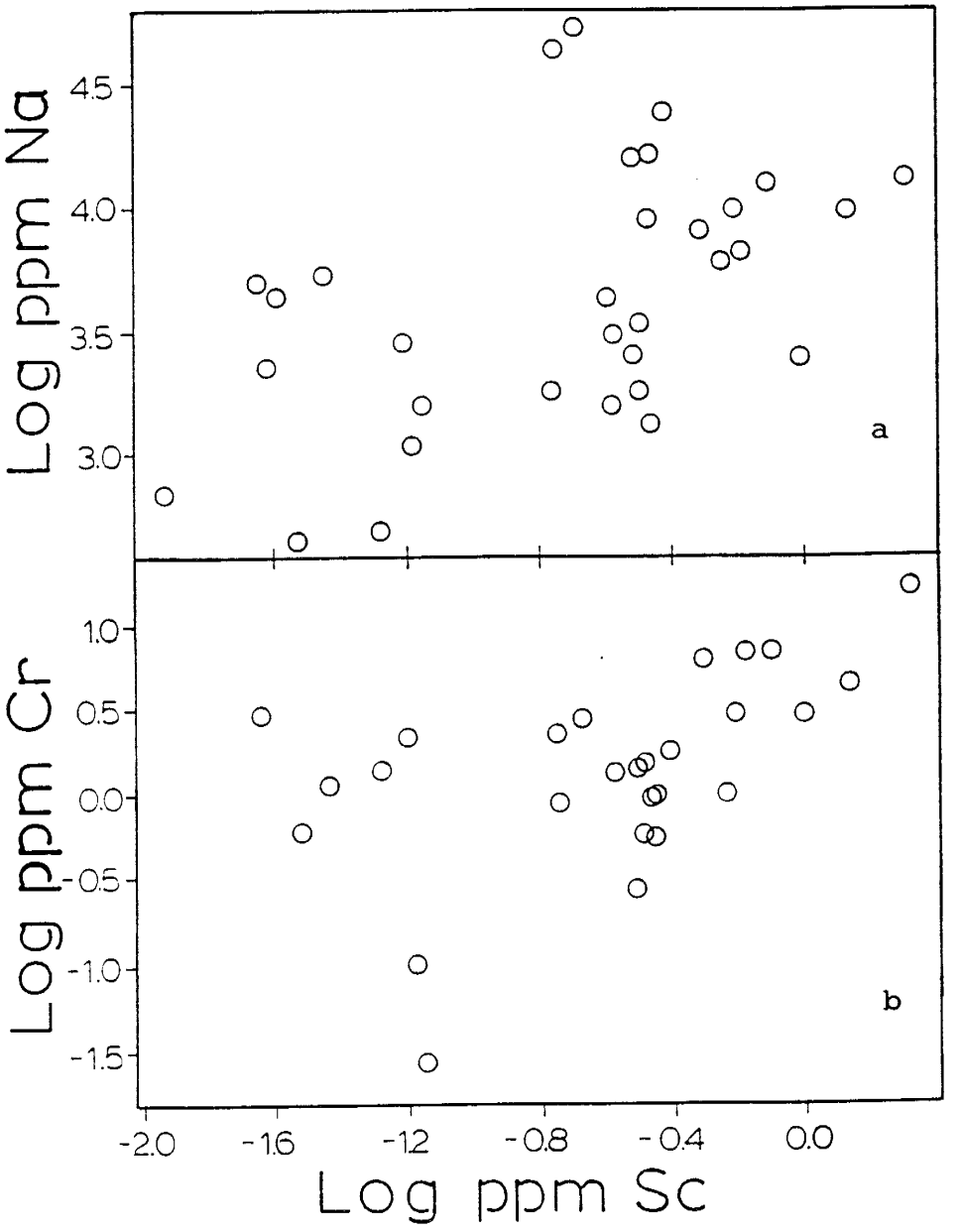
Log ppm Na
4.5
4.0
3.5
3.0
a
Log ppm Cr
1.0
0.5
0.0
-0.5
-1.0
-1.5
b
-2.0
-1.6
-1.2
-0.8
-0.4
0.0
Log ppm Sc

the same trend with Glitrevann and Finnemarka at the low and high ends of the trend, respectively. The vein samples, however, form a separate trend but within the Na concentration range for miarolitic and rock-forming quartz. If the control of F1 had been the major contributor for the discrimination between the two fluid groups forming vein and miarolitic/rock-forming quartz, the two sample groups should be along the same trend with distinct grouping (Fig. 3.11b). The fluid chemistry therefore indicates that F1 is not a major contributor for making the differences between early and late stage fluids.

None of the elements associated with F2 contribute to discrimination of the sample groups. Even though on the average there is a tendency for higher REE content in the fluids extracted from vein quartz relative to fluids from miarolitic and rock-forming quartz. It is therefore likely that the control of Factor 2 (possibly F content) varies within the same limits for the vein and miarolitic/rock-forming quartz. This lack of discriminations suggests that F2 is not a major contributor for making the differences between early and late stage fluids.

Molybdenum versus Eu plot (Fig. 3.16) indicates a good discrimination between vein samples and Drammen granite samples. The factor controlling these two elements has effectively enriched the fluid extracted from the vein samples relative to the granite samples. This good correlation

suggests that F3 is a major contributor for making the differences between early and late stage fluids.

F4 does not seem to have been very effective in dividing between these two sample groups. Scandium and Cr are the two elements that give the best discrimination. Fig. 3.17b and Fig 6a show that this discrimination is rather poor for these two elements indicating that the control of F4 has acted in a similar way for the two fluid systems.

Molybdenite solubility relative to other sulfide minerals

Calculations of MoS_2 solubility have been performed based on Smith's (1983) thermodynamic data. In addition, calculations of the transport capacity for Zn in equilibrium with sphalerite, Cu in equilibrium with bornite and chalcopyrite, Au in equilibrium with native gold, and Fe in equilibrium pyrite, chalcopyrite, and bornite with oxygen fugacity controlled by magnetite-hematite buffer in 1 mole NaCl and 0.01 mole total S solution have been performed, with distribution of H_2S (Fig. 3.18). These calculations are all based on constant total sulfur concentration, a system with fluid with Au, Cu, Pb, Zn, and sulfur, and a pure Mo(aq)-S-MoS_2 without any of the other elements or sulfide mineral present.

For pH=6 (Fig. 3.18a), pyrite and molybdenite will precipitate when the temperature drops from 350°C to 300°C. The other elements have a constant solubility over this

Fig. 3.18.

Temperature in °C versus total solubility of molybdenite in an aqueous fluid based on Smith's (1983) thermodynamic data, sphalerite, pyrite, chalcopyrite+bornite, gold, and H_2S concentration (based on solubility program by Norman (unpubl.) at steam-saturated liquid pressures at constant pH (a:pH=6; b:pH=5). Hematite-magnetite buffer is used for $f(O_2)$ control; S=0.01 m; total F=0.00001 m; Cl=1 m.

Fig. 3.18

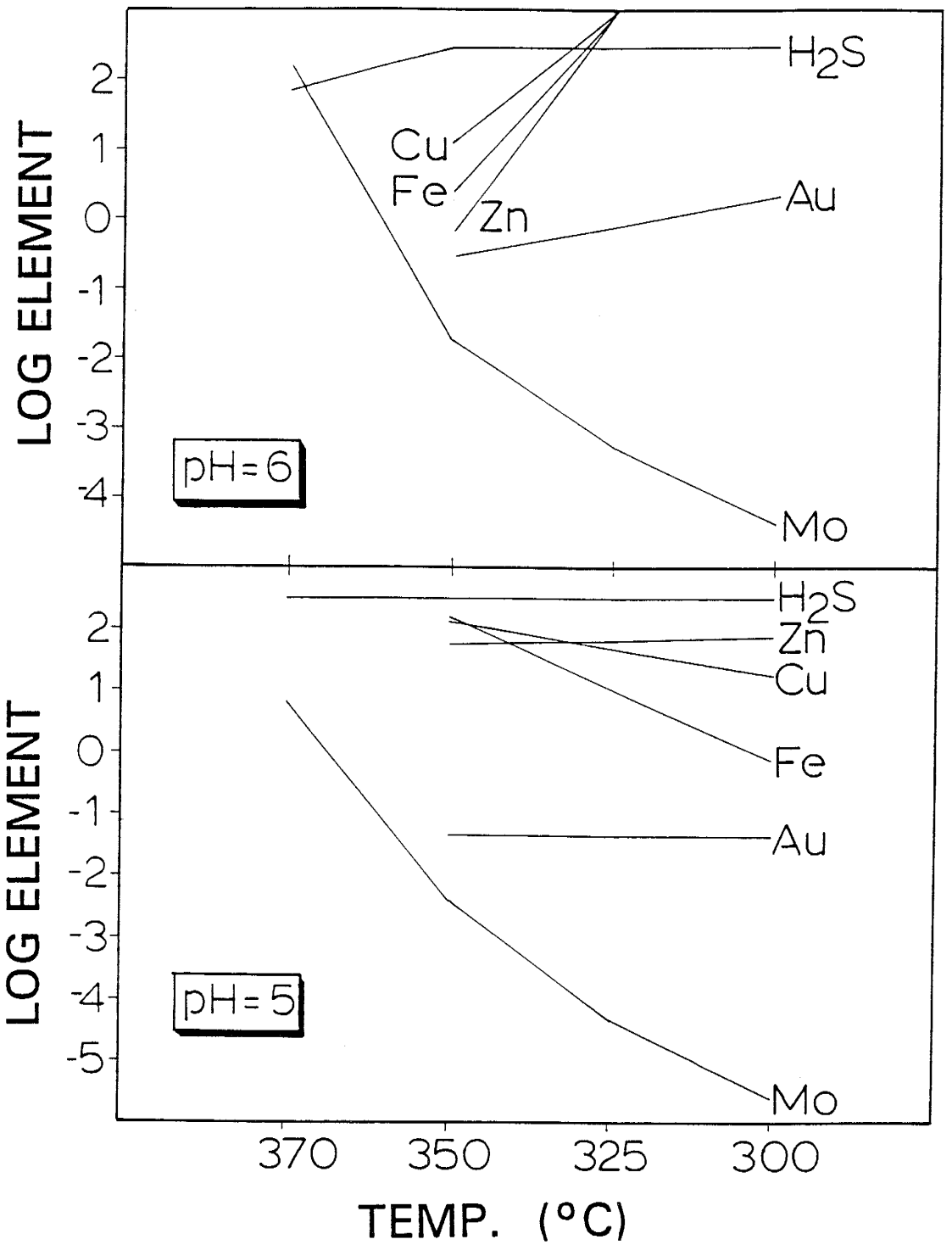
LOG ELEMENT
2
1
0
-1
-2
-3
-4
pH=6
H2S
Cu
Fe
Zn
Au
Mo
LOG ELEMENT
2
1
0
-1
-2
-3
-4
-5
pH=5
H2S
Zn
Cu
Fe
Au
Mo
370
350
325
300
TEMP. (°C)

temperature range. Only molybdenite precipitates if the pH changes from 6 to 5. The solubilities of all the other minerals considered in these calculations increase, and they also increase with temperature drop from 350°C to 300°C. Molybdenite on the other hand decreases in solubility with this temperature drop at pH=6. Iron, Zn, and Cu is expected to mainly be transported as Cl complexes (Burnham, 1981; Holland, 1972). If MoS_2 and pyrite precipitate, the activity of H_2S will rather decrease than stay constant as will reactions of H_2S with wall rock Fe_3O_4 to form pyrite. This decrease in H_2S activity will again increase the solubility of the other sulfide minerals considered in the calculations. The solubility lines in Fig. 3.18 represent minimum solubility. If the concentration of $H_2S \leq Mo$ as indicated by the analyses, a reduction in H_2S activity following MoS_2 precipitation will result in destabilizing of Au-bisulfide complex, resulting in Au precipitation. As shown in Fig. 3.18a, dropping the temperature from 350°C to 300°C, will precipitate 99% of the dissolved Mo. This results in a 20 wt.% decrease of the H_2S (based on ΣS=0.01m and ΣMo= 100 ppm). To keep the sulfur system in equilibrium some sulfate will react to form H_2S. Therefore, the H_2S activity will not change much, and the calculations (based on not calculating MoS_2 and the other sulfide minerals as two separate systems and keeping the sulfur concentration constant) will not create any significant errors.

A strong positive correlation exists between MoS_2 solubility and pH and negative correlation with temperature (200-370°C) at pH 5.5 to 8 (neutral to strong basic solution) (Fig. 3.19), based on otherwise same conditions as for Fig. 3.18. If the pressure was much higher and constant a temperature decrease will rather increase than decrease the solubility of MoS_2. These calculations are also based upon Smith's (1983) data.

An increase in reduced sulfur, especially H_2S, will extensively reduce the molybdenite solubility (Walder et al., 1987). Such an increase in H_2S is seen in the fluids from the miarolitic quartz to the vein quartz. The effect of a decrease in temperature by about 100°C on molybdenite solubility is enigmatic. Wood et al. (1987) did solubility measurements in a multi-metal sulfide system, where pH and $f(O_2)$ were not buffered, indicating that the solubility of molybdenite is independent of temperature in the range 200°C to 350°C. On the other hand, calculations done by Smith et al. (1980), Smith (1983) and Kudrin (1986) indicate strong temperature dependence for the molybdenite solubility. These two calculation studies are based on much more simple systems than Wood et al.'s (1987) experiments. Smith et al. (1980) found that the solubility of molybdenite, mainly as $HMoO_4^-$ in aqueous solution is extremely temperature dependent, decreasing about 10^6 for a temperature change from 350°C to 300°C. Such a mechanism could explain the MoS_2 mineralization

Fig. 3.19.

MoS_2 solubility in an aqueous at different pH versus temperature for total S=0.01 m, F=0.0001 m, Cl=1.0 m, and with $f(O_2)$ controlled by the hematite-magnetite buffer. The pH range is from 5.5 to 8 in 0.5 increments.

Fig. 3.19

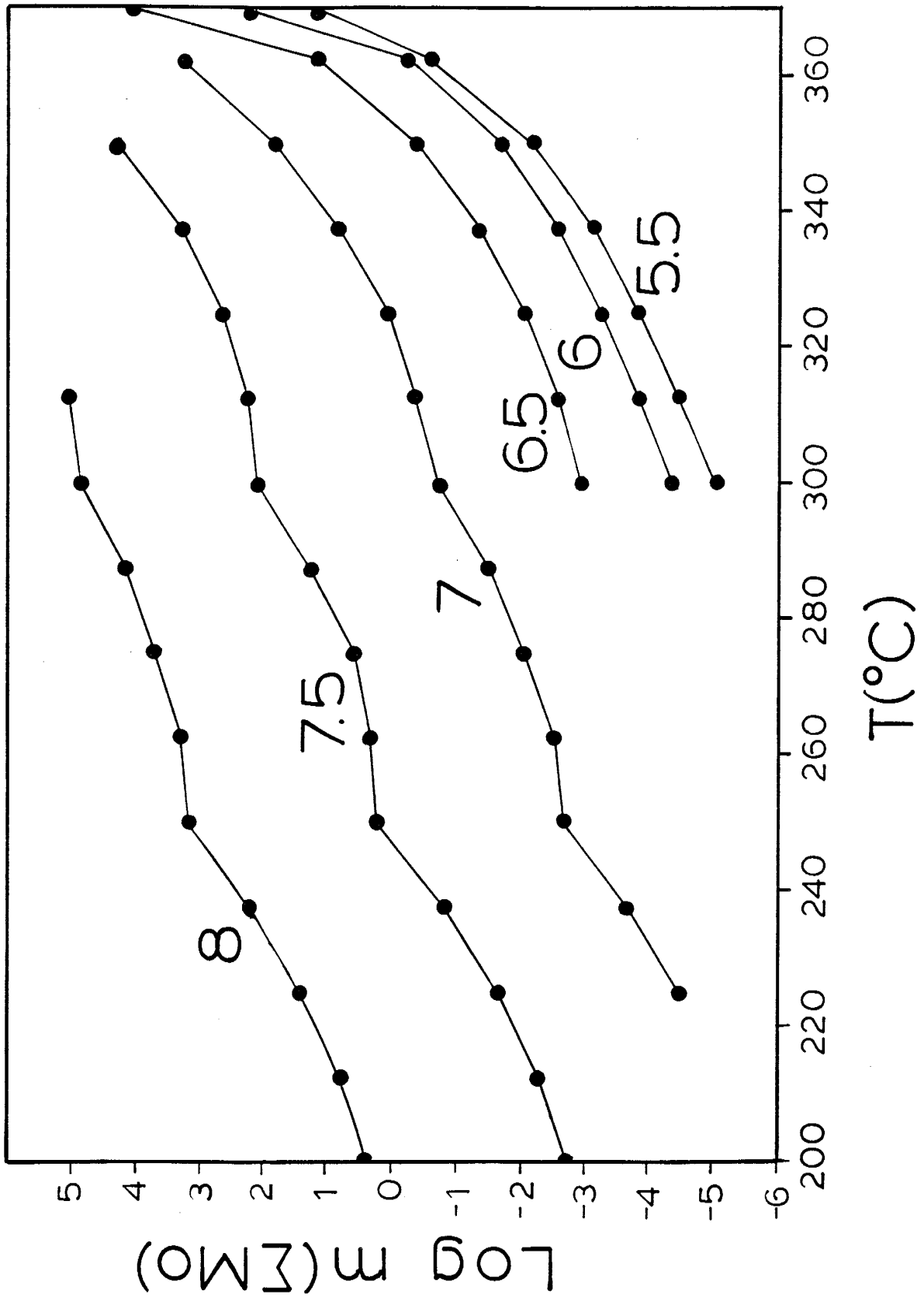
Log m(ΣMo)
T(°C)
8
7.5
7
6.5
6
5.5
5
4
3
2
1
0
-1
-2
-3
-4
-5
-6
200
220
240
260
280
300
320
340
360

in a mono-metallic system like the Drammen granite quartz-molybdenite mineral deposits and also explains the extremly confined cupola-shaped MoS_2 mineralization in porphyry MoS_2 deposits. A pressure decrease from 1 kbar to 0.5 kbar or a pH decrease from 6 to 5, both at 300°C would also decrease the molybdenite solubility in the way that it could cause extensive molybdenite mineralization (Fig. 3.18a,b).

Molybdenite precipitation mechanism

The precipitation of molybdenite may be controlled by the following redox reaction:

$$4HMoO_4^- + 9H_2S + 2H^+ = 4MoS_2 + 12\ H_2O + SO_4^{2-}. \qquad \text{(Eq. 18)}$$

This seems to be the controlling reaction for some of the geothermal waters at Iceland that deposited MoS_2 (Arnorson and Ivarsson, 1985). If such is the case for Drammen granite mineralization this could explain why oxidized sulfur is the main sulfur species. The precipitation may have been fast resulting in non equilibrium among aqueous species, hence giving reduced condition for the CO_2-H_2-CH_4-H_2O and oxidized for the sulfur in the ore forming solutions.

DISCUSSION AND CONCLUSIONS

DISCUSSION

Mineralization

Alteration associated with porphyritic granites in the Drammen batholith is possibly related to fluid release from these intrusive phases, a fluid release which in turn may be related to the Mo mineralization. High Na^+/H^+ ratio (>10,000 at 500°C; Rose and Burt, 1979) for the fluids (100-50,000 for fluids extracted from miarolitic quartz of the Drammen granite) may cause albitic alteration which is widespread in the Drammen granite. High alkali/acid ratio is typically found in some central parts of porphyry Cu and Mo mineralization (Burnham, 1979). The argillic alteration where alkali/acid ratio is lower (and/or lower temperature) than for alkali alteration, is commonly found associated with fractures in the Drammen granite indicating that it is post-magmatic alteration. Fluid evolution from high to low alkali/acid ratio is likely and results in an alteration mineral evolution from alkali feldspar → sericite → kaolinite, pyrophylite, smectite → epidote and chlorite. There is probably more than one episode of fluid release from the crystallizing magma, which has made it difficult to distinguish between alteration zones. The variety of the alteration types indicates a fluid chemistry change.

The Drammen granite batholith is a multiple intrusion,

with at least two major intrusive phases (petrographic types g1, g2, g3, g4, g5; versus g6 and g8). Most of the molybdenite mineralization is associated with the last intrusive phase. The mineralization associated with the g7 granite porphyry (e.g. Sörumsåsen mine) does not fit this evolutionary model because rocks and fluids have seen hydrothermal Rb/Sr exchange and isotopic resetting.

Molybdenum concentrations are higher for the late fluids extracted from the vein quartz relative to the early fluids extracted from the miarolitic quartz. Molybdenum may be enriched as molybdenum silicates ($MoSi_2O_5^+$, $MoSi_2O_6$ and/or $MoSi_2(OH)_3^+$) in the granitic melt during fractionation and crystallization, and the proportion of molybdenum silicates in the melt increases with decreasing temperature (Isuk and Carman, 1981) until the melt becomes saturated with respect to water. Molybdenum is then dissolved in the fluid phase with a distribution coefficient K_D (water/melt) $\approx$ 3 (Candela and Holland, 1984). The chloride content of the fluids does not interfere with the K_D (water/melt) for molybdenum, since Mo is not transported as a chloride complex (Candela and Holland, 1984; Smith, 1983). Second boiling of the granitic melt can cause fracturing of the cap rock (Burnham and Ohmoto, 1980) permitting the necessary permeability for the veins to form. Smith and Norman (1980) have pointed out that the solubility of molybdenite as $HMoO_4^-$ in aqueous solution is extremely temperature dependent, decreasing about 6 orders of magnitude

for a temperature change of 350°C to 300°C.

The granitic melt exsolved granitic fluids through second boiling. The saline and molybdate-carrying silicic magmatic fluids showing magmatic sulfur signature mixed with colder water that had equilibrated with upper crustal rocks; this caused a decrease in $\delta^{18}O$ and an increase in Sr isotope ratio. This mixing caused rapid cooling of the fluid, and decreased the solubility of both molybdenite and silica in the ore-forming fluids, hence resulting in precipitation of molybdenite and quartz veins.

Mineralization relative to granites

Temperature versus $f(O_2)$ (Fig. 4.1) for hydrothermal fluids from the Drammen granite and Mo mineralization are plotted in the diagram of Burnham and Ohmoto (1980). The $f(O_2)$ calculated for the hydrothermal fluids reported in this paper are plotted at 300°C and 500°C. Miarolitic quartz from the Drammen granite and the Grefsen syenite reported by Norman et al. (1979) give fluid inclusion temperatures of formation near 550°C and $f(O_2)$ calculated from fluid inclusion gas analyses to 10^{-22} and 10^{-21}, respectively.

Neumann (1976) has investigated the temperature versus $f(O_2)$ relations in the Oslo Rift plutons mainly based on microprobe analyzed mineral relations. Her results for the Oslo Rift monzonites and for the ekerites (peralkaline

Fig. 4.1.

T(°C) versus log $f(O_2)$ modified from Burnham and Ohmoto (1980) for carbon species and sulfur species with mineral stability fields at 1 Kbar and pH=6. Mineral equilibria represented are: (1) hematite+magnetite, (2) anorthite+K-feldspar+pyrite+muscovite+quartz+anhydrite, (3) fayalite+magnetite+quartz, (4) as 3 with 15 wt.% Mn content; biotite (38 wt.% annite)+K-feldspar+magnetite, (5) total Mo dissolved 1 ppm for total S=0.01 m, Cl=1 m, F=.0000001 m, (5′) as 5 with total S=0.001 m, (5′′) as 5 with total S= 0.0001 m. The dot shaded area represents the condition for which molybdenite precipitated in veins in the Drammen granite.

Fig. 4.1

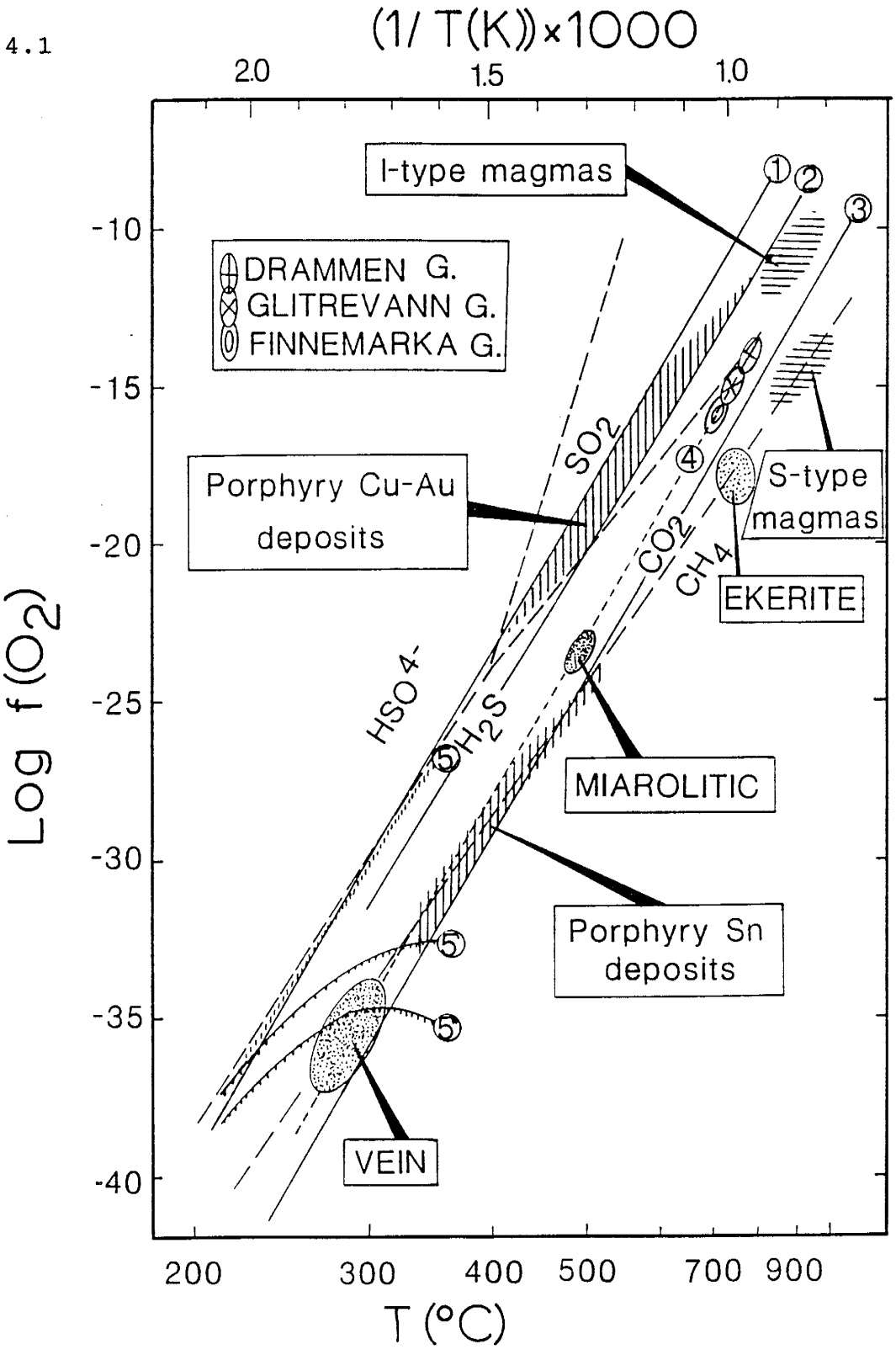
(1/ T(K))×1000
2.0
1.5
1.0
I-type magmas
DRAMMEN G.
GLITREVANN G.
FINNEMARKA G.
Porphyry Cu-Au deposits
S-type magmas
EKERITE
MIAROLITIC
Porphyry Sn deposits
VEIN
SO2
CO2
CH4
HSO4-
H2S
①
②
③
④
⑤
⑤
⑤
-10
-15
-20
-25
-30
-35
-40
Log f(O2)
200
300
400
500
700
900
T (°C)

granites) are outlined in Fig. 4.1.

Mole fraction analyses of annite (Fe^{II} in octahedral position) in biotite in the Finnemarka igneous rock complex gave 0.54 for monzonite, 0.29 for granodiorite, and 0.23 for granite (Czamanske and Wones, 1973). From these data the oxygen fugacity versus temperature for the Finnemarka granite has been recalculated by Segalstad (unpub. data) to approx. 10^{-17} at 680°C.

From fluid inclusion data combined with experimental liquidus temperatures and intrusion mechanics modelling Segalstad (unpub. data) has estimated solidus temperatures for the Drammen (Fig. 4.1, cross) and Glitrevann granite to approximately 780°C and 750°C, respectively. The corresponding log $f(O_2)$ would be approximately -15 and -16, respectively, on the Ni-NiO buffer.

The hydrothermal fluids, the Finnemarka granite, and a large portion of the Oslo Rift monzonites cluster around the Ni-NiO oxygen buffer line. Most Oslo Rift igneous rocks and magmatic fluids seem to follow a slightly more oxidizing $f(O_2)$ vs. temperature path than the QFM (quartz + magnetite → fayalite) buffer, but parallel with it, in the vicinity of the location of the Ni-NiO buffer because of the Mn content (Neumann, 1974, 1976; Norman et al., 1979).

Studies by Ishihara (1981), White et al. (1981), Kamilli (1978), and White and Chappell (1977) indicate that we can expect porphyry molybdenum deposits occurrences in a more

oxidizing environment than porphyry tin deposits, at somewhat lower temperatures than porphyry copper-gold deposits. With high sulfur content it is expected that deposition of molybdenite will occur at temperatures 350°C to 400°C because the level of reduced sulfur greatly effects molybdenite solubility. One order of magnitude increase in reduced sulfur can decrease the molybdenite solubility by several orders of magnitude.

The solubility calculations show that ΣS is also important, where increasing amount of sulfur gives decreasing MoS_2 solubility with everything else constant. MoS_2 precipitation will occur at a higher temperature with high sulfur content. Therefore, deposition of MoS_2 occurred at 300°C because ore fluids indicated to have only 0.01 mole % H_2S. In contrast, H_2S contents of Questa fluids are measured to be 0.1 mole % (Smith, 1983).

Mineral Exploration

The Drammen Granites are a classic example of intrusives that have all the proper indicators for molybdenum mineralization, such as tectonic setting (Sawkins, 1990), rock geochemistry (Mutchler et al. 1981), shallow intrusion, and evolution of a chloride-rich volatile phase (White et al., 1981). However, only a few of the intrusive phases are mineralized, and total mineralization is volumetrically minor. The data presented here indicate that favorable intrusive

phases within a batholith may be identified by analysis of fluid inclusion volatiles because there is a close correlation of molybdenum sulfide mineralization and detectable H_2S in fluid inclusions. Obviously, the concentration of reduced sulfur in ore fluids is just as important as the concentration of metals; it requires both to precipitate sulfide minerals.

Although there is not as yet a good data base on the necessary concentrations of sulfur in ore solutions, the levels of sulfur species measured in most inclusion fluids appears to be low. This suggests that the Drammen batholith was a low-sulfur intrusive, and hence could not generate solutions that would precipitate large amounts of sulfide mineralization. Fluid inclusion volatile analysis may also prove to be of value in mineral exploration by identifying intrusives that generated sulfur-rich metal-bearing solutions.

Genesis models

This study supports Candela and Holland's (1984 and 1986) model where evolution of the granite is the main contributor for making granite-associated Mo mineralization. The molybdenite-bearing phases of the granite show the most evidences for fractional crystallization. The molybdenite-barren phases show only little fractionation and rather extensive assimilation of the surrounding sedimentary rocks. Sr and O isotope ratios and whole-rock trace-element geochemistry indicate that the granite has not been formed

through partial melting of the Precambrian gneisses, but rather evolved from a mantle source. This precludes Burnham's (1979 and 1980) model where partial melting of a Mo-enriched crust is assumed to be a necessary precondition for forming porphyry Mo deposits.

CONCLUSIONS

Only fluids from the late granite intrusions were transporting significant Mo amounts - inspite of the fact that non of the granite phases contained any H_2S. This suggest that the late intrusive phases alone produced fluids, by whatever means, that could form MoS_2 mineralization.

The early exsolved fluids associated with the miarolitic quartz shows high gas contents and low Mo, W, Sm, and Eu concentrations relative to later exsolved fluids trapped in the vein quartz. The gaseous components have high distribution coefficients and will be associated will early exsolved fluids together with volatile elements as As and Cs. Mo and W have low distribution coefficients between melt and aqueous phase and they are incompatible elements. The higher concentration of Mo and W in the vein quartz trapped fluid, therefore, indicates crystallization of the magma and a late aqueous phase exsolution relative to the fluids trapped in the miarolitic quartz.

Factor analysis indicates that four factors control 73% of the data variation. The main control of these factors are inferred to be Cl and F contents and source geochemistry/aqueous phase exsolution timing. The latter factor is suggested to be the factor controlling the differences between liquids from vein quartz and miarolitic and rock-forming quartz from the three granites. This factor is also important for controlling the potential of Mo

mineralization.

The age of the granite is not well constrained because of a resetting/disturbance of Rb-Sr systematics due to hydrothermal alteration. The granite was emplaced somewhere between 235 Ma and 285 Ma, where 235 Ma is Re-Os dating of molybdenite and 285 Ma is an age of basalts of which the granite intruded.

Constituents of quartz-molybdenite veins in the late stage intrusive phases of the Drammen granite were derived from a mix of crustal and magmatic-igneous sources. This mixing is indicated by Sr-isotope analyses of salts extracted from inclusion fluids from vein quartz, oxygen-isotope ratios of the vein quartz, and sulfur-isotope ratios of molybdenite.

Early stage fluids from the Drammen granite and fluids extracted from the Glitrevann granite carried oxidized sulfur, while late stage fluids from some of the mineralized veins of the Drammen granite carried both oxidized and reduced sulfur. The sulfur content was low for all three systems. No sulfur was detected in the Finnemarka granite inclusion fluids.

The calculated log $f(O_2)$ based on the gas analyses of inclusion fluids for Drammen, Glitrevann, and Finnemarka, and Drammen granite vein quartz indicating a reducing environment. The $f(O_2)$ fall along the Ni-NiO buffer line. Log $f(S_2)$ calculated for three vein samples with reduced sulfur ranges from -8.9 to -11.2.

Precipitation of molybdenite did generally not occur throughout the granites, even though Mo was present in the

mineralization.

The age of the granite is not well constrained because of a resetting/disturbance of Rb-Sr systematics due to hydrothermal alteration. The granite was emplaced somewhere between 235 Ma and 285 Ma, where 235 Ma is Re-Os dating of molybdenite and 285 Ma is an age of basalts of which the granite intruded.

Constituents of quartz-molybdenite veins in the late stage intrusive phases of the Drammen granite were derived from a mix of crustal and magmatic-igneous sources. This mixing is indicated by Sr-isotope analyses of salts extracted from inclusion fluids from vein quartz, oxygen-isotope ratios of the vein quartz, and sulfur-isotope ratios of molybdenite.

Early stage fluids from the Drammen granite and fluids extracted from the Glitrevann granite carried oxidized sulfur, while late stage fluids from some of the mineralized veins of the Drammen granite carried both oxidized and reduced sulfur. The sulfur content was low for all three systems. No sulfur was detected in the Finnemarka granite inclusion fluids.

The calculated log $f(O_2)$ based on the gas analyses of inclusion fluids for Drammen, Glitrevann, and Finnemarka, and Drammen granite vein quartz indicating a reducing environment. The $f(O_2)$ fall along the Ni-NiO buffer line. Log $f(S_2)$ calculated for three vein samples with reduced sulfur ranges from -8.9 to -11.2.

Precipitation of molybdenite did generally not occur throughout the granites, even though Mo was present in the

mineralization.

The age of the granite is not well constrained because of a resetting/disturbance of Rb-Sr systematics due to hydrothermal alteration. The granite was emplaced somewhere between 235 Ma and 285 Ma, where 235 Ma is Re-Os dating of molybdenite and 285 Ma is an age of basalts of which the granite intruded.

Constituents of quartz-molybdenite veins in the late stage intrusive phases of the Drammen granite were derived from a mix of crustal and magmatic-igneous sources. This mixing is indicated by Sr-isotope analyses of salts extracted from inclusion fluids from vein quartz, oxygen-isotope ratios of the vein quartz, and sulfur-isotope ratios of molybdenite.

Early stage fluids from the Drammen granite and fluids extracted from the Glitrevann granite carried oxidized sulfur, while late stage fluids from some of the mineralized veins of the Drammen granite carried both oxidized and reduced sulfur. The sulfur content was low for all three systems. No sulfur was detected in the Finnemarka granite inclusion fluids.

The calculated log $f(O_2)$ based on the gas analyses of inclusion fluids for Drammen, Glitrevann, and Finnemarka, and Drammen granite vein quartz indicating a reducing environment. The $f(O_2)$ fall along the Ni-NiO buffer line. Log $f(S_2)$ calculated for three vein samples with reduced sulfur ranges from -8.9 to -11.2.

Precipitation of molybdenite did generally not occur throughout the granites, even though Mo was present in the

geothermal solutions, because sulfur was very low and principally in the oxidized form. In addition, the low sulfur content of geothermal fluids limited molybdenite mineralization. Thermodynamic calculations indicate that low sulfur content also results in low precipitation temperature for molybdenite.

This study suggests that there is no need for partially melting an Mo-enriched crust for producing granite associated Mo deposits. To make the ore-forming fluids enriched in Mo, fractional crystallization with a late aqueous phase exolution is preferable. For producing a molybdenite deposit, it seems to be necessary to have high concentration of sulfur and a transition from oxidized to reduced sulfur.

This study supports the genesis model of Candela and Holland (1984, 1986) for porphyry molybdenum mineralization, in which the chemistry and evolution of the magma greatly influence the mineralization.

REFERENCES

Ague, J.J. and Brimhall, Jr., G.H., 1988: Magmatic arc asymmetry and distribution of anomalous plutonic belt in the batholiths of California: Effects of assimilation, crustal thickness, and depth of crystallization. Geol. Soc. Am. Bull. 100, 912-927.

Analytisk Sporelement Komité Norden, 1975: Reported concentration values for minor and trace elements ASK-1, ASK-2, and ASK-3. Oslo, 10 pp.

Baker, B.H. and McBirney, H.R., 1985: Liquid fractionation. Part III: Geochemistry of zoned magmas and compositional effects of liquid fractionation. Journ. Volc. Geotherm. res. 24, 55-81.

Bandurkin, G.A., 1961: Behavior of the rare earths in fluorine-bearing media. Geochem. Transl. (USSR), 159-167.

Barbarin, B., 1990: Granitoids: main petrogenetic classification in relation to origin and tectonic setting. Geol. Journ. 25, 227-238.

Best, M.G., 1982: Igneous and metamorphic petrology. W.H. Freeman and Company, New York. 630 pp.

Björlykke, K., 1974: Depositional history and geochemical composition of lower Paleozoic epicontinental sediments from the Oslo Region. Norges Geol. Unders., 305, 81 pp.

Black, R., Jacobson, R.R.E., and MacLeod, W.N., 1957: Ring complexes in the Younger Granite province of northern Nigeria. Geol. Soc. London, Pr. no. 1545, 21-28.

Borthwick, J. and Harmon, R.S., 1982: A note regarding ClF_3 as an alternative to BrF_5 for oxygen isotope analysis. Geochim. Cosmochim. Acta 46, 1665-1668.

Bowen, N.L., 1928: The evolution of igneous rocks. Princeton Univ. Press., Princeton, New Jersey, 651 pp.

Brookins, D.G., 1989: Aqueous geochemistry of rare earth elements. In Ribbe, P.H., Geochemistry and mineralogy of rare earth elements. Reviews in Mineralogy. Min. Soc. Am., 21, 201-225.

Brooks, C.K., 1969: On the distribution of zirconium and hafnium in the Skjaergaard intrusion, East Greenland.

Geochim Cosmochim Acta 33, 357-374.

Bugge, A., 1963: Norges molybdenforekomster. Norges Geol. Unders., 259, 65-84.

Burke, K., Dessauvagie, T.F.J., and Whiteman, A.J., 1971: Opening of the gulf of Guinea and geological history of the Benue Depression and Niger delta. Nature Phys. Sci. 238, 51-55.

Burnham, C.W., 1979: Magmas and hydrothermal fluids. In Barnes, H.L., Geochemistry of hydrothermal ore deposits. John Wiley & Sons, New York, 71-136.

Burnham, C.W., 1981 Physicochemical constraints on porphyry mineralization. In Dickinson, W.R. and Payne, W.D., Relations of tectonics to ore deposits in the southern Cordillera. Arizona Geol. Soc. Dig. 14, 71-77.

Burnham, C. W. and Ohmoto, H., 1980: Late-stage processes of felsic magmatism. Mining Geology Special Issue 8, 1-11.

Candela, P.A., 1989a: Magmatic ore-forming fluids: Thermodynamic and mass transfer calculations of metal concentrations. In Whitney, J.A. and Naldrett, A.J., Ore deposition associated with magmas. Review in Econ. Geol. 4, 203-221.

Candela, P.A., 1989b: Felsic magmas, volatiles, and metallogenesis. In Whitney, J.A. and Naldrett, A.J., Ore deposition associated with magmas. Review in Econ. Geol. 4, 223-233.

Candela, P.A., 1991: Physics of aqueous phase evolution in plutonic environments. Am. Mineral. 76, 1081-1091.

Candela, P.A. and Holland, H.D., 1984: The partitioning of copper and molybdenum between silicate melts and aqueous fluids. Geochim. Cosmochim. Acta, 48, 373-380.

Candela, P.A. and Holland, H.D., 1986: A mass transfer model for copper and molybdenum in magmatic systems: the origin of porphyry type ore deposits. Econ. Geol. 81, 1-19.

Cao, X., 1989: Solubility of molybdenite and the transport of molybdenum in hydrothermal solutions. Unpubl. PhD Thesis, Iowa State Univ., 111 pp.

Carmichael, I.S.E, Turner, F.J., and Verhoogen, J., 1974: Igneous petrology. McGraw-Hill Book Co., New York, 739 pp.

Carron, J.P. and LeGache, M., 1980: Etude experimental du fractionnement des elements Rb, Cs, Sr, et Ba entre feldspaths alcalins, solutions hydrothermals et liquids silicates dans le systeme Q.Ab.Or.H_2O a 2K bar entre 700 et 800°C. Bull Mineral. 703, 571-578.

Carpenter, R.H., 1968: geology and ore deposits of Questa molybdenum mine area, Taos County, New Mexico. In Ridge, J.D., Ore deposits of the United States, 1933-1967. Pub. Am. Inst. Mining, Metal. Petrol. Eng. Inc., New York, 1328-1350.

Casadevall, T.J. and Ohmoto, H., 1977: Sunnyside mine, Eureka mining district, San Juan County, Colorado;geochemistry of gold and base metal ore deposition in a volcanic environment. Econ. Geol. 72, 523-537.

Chappell, B.W. and White, A.J.R.,, 1974: Two contrasting granite types. Pacific Geology 8, 173-174.

Chappell, B.W. and White, A.J.R., 1983: Granitoid types and their distribution in the Lachan fold belt, southwestern Australia. Memoir Geol. Soc. Am., 159, 21-34.

Christie, O.H.J., 1975: The trace-element geological materials certified as a result of a co-operative investigation. Talanta, 22, 1048-1050.

Clayton, R.N. and Mayeda, T.K., 1963: The use of bromine pentafluoride in the extraction of oxygen from oxides and silicates for isotopic analysis. Geochim. Cosmochim. Acta 27, 43-52.

Clough, P.W.L. and Field, D., 1980: Chemical variations in metabasites from a Proterozoic amphibolite-granulite transition zone, South Norway. Contr. Miner. Petrol., 73, 277-286.

Collins, W.J., Beams, S.D., White, A.J.R., and Chappell, B.W., 1982: Nature and origin of A-type granites with particular reference to Southeastern Australia. Cont. Mineral. Petrol. 80, 189-200.

Crocket, J.H., 1978: Platinum metals. In Wedephole, K.H., Handbook of geochemistry. II/5, Springer Verlag, 78-1.

Czamanske, G.K., 1965: Petrologic aspects of the Finnmarka igneous complex, Oslo Area, Norway. J. Geol. 73, 293-322.

Czamanske, G.K. and Mihálik, P., 1972: Oxidation during magmatic differentiation, Finnmarka complex, Oslo Area,

Norway: Part I, The opaque oxides. J. Petrol. 13, 493-509.

Czamanske, G.K., Roedder, E., and Burns, F.C., 1963: Neutron activation analysis of fluid inclusions for copper, manganese, and zinc. Science 140, 401-403.

Czamanske, G.K. and Wones, D.R., 1973: Oxidation during magmatic differentiation, Finnemarka complex, Oslo area, Norway: part 2, the mafic silicates. Journ. Petrol. 14, 349-380.

DePaolo, D.J., 1981: Trace element and isotopic effectsof combined wallrock assimilation and fractional crystallization. Earth Planet Sc. Let. 53, 189-202.

DePaolo, D.J. and Wasserburg, G.J., 1976: Inferences about magma sources and mantle structure from variations of $^{143}Nd/^{144}Nd$. Geophys. Res. Lett., 3, 743-746.

Dewey, J.F. and Burke, K.C., 1973: Tibetan, Variscan and Precambrian basement reactivation: products of continental collision. J. Geol. 81, 683-692.

Dingwell, D.B. and Scarfe, C.N., 1983: Major element partitioning in the systemhaplogranite-HF-H_2O: implications for leucogranites and high silica rhyolites. Abstract, Am. Geophys. Union (EOS), 64, p. 342.

Dons, J.A. and Larsen, B.T., 1978 (Eds.): The Oslo Paleorift. A riview and guide to excursions. Norges Geol. Unders. 337, 199 pp.

Drummond, S.E., Jr., 1981: Boiling and mixing of hydrothermal fluids: Chemical effects on the mineral precipitation. PhD Thesis, Pennsylvania State University, 380 pp.

Durasova, N.A., Khramov, D.A., Polosin, A.V., Barsukov, V.L., Ryabchikov, V.S., Urusov, V.S., Kravtsova, R.P., and Ignatenko, K.I., 1985: The solubility, valency, and structural states of tin in magnetite. Geochem. Intern. 23, 48-52.

El-Bouseily, A.M., 1971: Petrography and geochemistry of the Drammen granite, Drammen, Norway. Unpub. paper. Mineralogisk-Geologisk Museum, Oslo, Norway, 54 pp.

Ellis, A.J., 1979: Explored geothermal systems. In Barnes, H.L., Geochemistry of hydrothermal ore deposits. John Wiley & Sons, New York, 632-683.

Evensen, N.M., Hamilton, P.J., and O'Nions, R.K., 1978: Rare-earth abundances in chondritic meteorites. Geochim. Cosmochim. Acta 42, 1199-1212.

Faul, H., Elmore, P.L.D. and Brannock, W.W., 1959: Age of the Fen carbonatite (Norway) and its relations to the intrusives of the Oslo Region. Geochim. Cosmochim. Acta, 17, 153-156.

Faure, G., 1986: Principles of isotope geology. John Wiley & Sons, New York, 589 pp.

Field, D. and Elliott, R.B., 1974: The chemistry of gabbro/amphibolite transitions in South Norway. II. Trace elements. Contr. Mineral. Petrol., 47, 63-76.

Flynn, R.T. and Burnham, C.W., 1978: An experimental determination of rare earth partition coefficients between chloride-containing vapor phase and silicate melt. Geochim. Cosmochim. Acta 42, 685-701.

Fournier, R.O., 1981: Application of water geochemistry to geothermal exploration and reservoir engineering. In Ryback, L. and Muffler, L.J.P., Geothermal systems: Pricipals and case histories. John Wiley & Sons, New York, 109-143.

Fournier, R.O. and Potter, R.W, II, 1982: An equation correlating the solubility of quartz in water from 25°C to 900°C at pressures up to 10,000 bars. Geochim Cosmochim. Acta, 46, 1969-1973.

Furlong, K.P. and Myers, J.P., 1985: Thermal-mechanical modelling of the role of thermal stress and stoping in magma contamination. Journ. Volc. Geotherm. Res. 24, 179-191.

Gaut, A., 1981: Field relations and petrography of the biotite granite of the Oslo Region. Norges Geol. Unders., 367, 39-64.

Gammon, J.B., Borcsic, M, and Holland, H.D., 1969: Potassium-sodium ratio in aqueous solutions and co-existing silicate melts. Science 163, 179-181.

Geyti, A. and Schönwandt, H.K., 1979: Bordvika - a possible porphyry molybdenum occurrence within the Oslo province, Norway. Econ. Geol., 74: 1211-1220.

Giggenbach, W.F., 1981: Geothermal gas equilibria. Geochim. Cosmochim. Acta 44, 2021-2032.

Glyuk, D.S., Trufanova, L.G., and Bazarova, S.B., 1980: Phase relationa in the granite-H_2O-LiF system at 1000 kgf/cm^2. Geochem. Intern. 18, 35-48.

Goldschmidt, W.M., 1911: Die contactmetamorphose im Kristianiagebiet. Skr. Norske Vidensk. Akad., Oslo, Mat. Naturv. kl., No11, 405 pp.

Goldschmidt, V.M., 1954: Geochemistry. Fair Lawn, New York, Oxford Univ. Press, 730 pp.

Goldschmidt, V.M. and Peters, C.L., 1932: Geochemie der edelmetalle. Nachr. Akad. Wiss. Götting. Math.-Physik. Kl IV, 377-412.

Haas, J.L., 1971: The effect of salinity on the maximum thermal gradient of a hydrothermal system at hydrostatic pressures. Econ. Geol. 66, 940-946.

Hall, W.E., Friedman, I., and Nash, J.T., 1965: Fluid inclusion and light stable isotope study of the Climax molybdenum deposits, Colorado. Econ. Geol. 69, 884-901.

Hanson, G.N., 1978: The application of trace elements to the petrogenesis of igneous rocks of granitic composition. Earth Planet. Sci. Lett., 38, 26-43.

Haselton, H.T., Jr., 1986: Tin and tungsten solubilities (500-700°C, 1 kbar) in the presence of synthetic quartz monzonite. Abstract, EOS, 67, 388.

Heier, K.S. and Compston, W., 1969: Rb-Sr isotopic studies of the plutonic rocks of the Oslo Region. Lithos, 2, 133-145.

Heinrich, C.A. and Eadington, P.J., 1986: Thermodynamic prediction of the hydrothermal chemistry of arsenic, and their significance for paragenetic sequence of some cassiterite arsenopyrite-base metal sulfide deposits. Econ. Geol., 81, 511-529.

Helgeson, H.C., 1969: Thermodynamics of hydrothermal systems at elevated temperatures and pressures. American J. Sci. 267, 729-804.

Helgeson, H.C., 1991 Thermodynamic constraints on the geobiochemical evolution of the petroleum in the Earth's crust. Geol. Soc. Am. Annual Meet. Abstrac with prog. p. A25.

Henley, I.A. and McNabb, A., 1978: Magmatic vapor plumes and ground-water interaction in porphyry copper emplacement. Econ. Geol., 73, 1-20.

Henley, R.W., Truesdell, A.H., and Barton, Jr.,P.B., 1984: Fluid-mineral equilibria in hydrothermal systems. Review Econ. Geol., vol. 1, 267 pp.

Higgens, N.C., 1980: Fluid inclusion evidence for the transport of tungsten by carbonate complexes in hydrothermal solutions. Can. J. Earth Sci., 17, 823-830.

Hintze, J.L., 1990: Number cruncher statistical system, version 5.03. Kaysville, Utah.

Hildreth, W., 1981: Gradients in silicic magma chambers: Implications for lithospheric magmatism. Journ. Geophys. Res. 86, b11, 10153-10192.

Hoefs, J., 1987: Stable isotope geochemistry. Springer-Verlag, Berlin. 241 pp.

Holland, H.D., 1972: Granites, solutions, and base metal deposits. Econ. Geol. 67, 281-301.

Ihlen, P.M. and Martinsen, M., 1986: Ore deposits spatially related to the Drammen granite batholith. In: Olerud, S. and Ihlen, P.M., Metallogeny associated with the Oslo Paleorift. Sveriges Geol. Unders., Ser. Ca., 59, 38-42.

Ihlen, P.M., Trönnes, R., and Vokes, F.M., 1982: Mineralization, wall rock alteration and zonation of ore deposits associated with the Drammen granite in the Oslo Region, Norway. In: Evans, A.M., Metallization associated with acid magmatism, John Wiley & Sons, Chichester, 111-136.

Ihlen, P.M. and Vokes, F., 1978: Metallogeny. In Dons, J.A. and Larsen, B.T. (Editors), The Oslo Paleorift. A review and guide to excursions. Norges Geol. Unders., 337: 75-92.

Ineson, P.R., Mitchell, I.G. and Vokes, F.M., 1975: K-Ar dating of epigenetic mineral deposits: an investigation of the Permian metallogenetic province of the Oslo Region, southern Norway. Econ. Geol., 70, 1426-1436.

Ishihara, S., 1981: The granitoid series and mineralization. Economic Geology 75th Anniversary Volume, 458-484.

Isuk, E.E., 1983: Behavior of molybdenum in alkali silicate

melts: Effects of excess SiO_2 and CO_2. Lithos, 16, 17-22

Isuk, E.E. and Carman, J.H., 1981: The system $Na_2Si_2O_5$ - $K_2Si_2O_5$ - MoS_2 - H_2O with implications for molybdenum. Econ. Geol., 76, 2222-2235.

Jackson, K.J. and Helgeson, H.C., 1985: Chemical and thermodynamic constraints on the hydrothermal transport and deposition of tin: I. Calculation of the solubility of cassiterite at high pressures and temperatures. Geochim. Cosmochim. Acta 49, 1-22.

Jacobsen, S.B., 1975: Geochronology, geochemical, and petrological investigations of the Precambrian rocks in the Kongsberg area. Unpubl. thesis, Univ. of Oslo, 269 pp.

Jacobsen, S.B., 1980: Study of crust and mantle differentiation processes from variations in neodymium, strontium and lead isotopes. Unpubl. thesis, Calif. Inst. Tech., 289 pp.

Jacobsen, S.B. and Heier, K.S., 1978: Rb-Sr isotope systematics in metamorphic rocks, Kongsberg Sector, South Norway. Lithos, 11, 157-276.

Jacobsen, S.B. and Wasserburg, G.J., 1978: Nd and Sr isotopic study of the Permian Oslo Rift. U.S. Geol. Surv. Open-File Report, 78-701, 194-196.

James, M., 1985: Classification algorithms. John Wiley & Sons. New York, 262 pp.

Jensen, I.S., 1985: Geochemistry of the central granitic stock in the Glitrevann cauldron within the Oslo Rift, Norway. Nor. Geol. Tidsskr., 65, 201-216.

Kaiser, H.F., 1958: The varimax criterion for analytical rotation in factor analysis. Psychometrica, 23, 187-200.

Kamilli, R.J., 1978: The genesis of stockwork molybdenum deposits: Implication from fluid inclusion studies at the Henderson Mine. (Abstr.) Geol. Soc. Am., Abstr. with Progr. 10, 431.

Khitarov, N.I., Malinin, Lebedev, Ye.B., and Shibayeva, N.P., 1982: The distribution of Zn, Cu, Pb, and Mo between a fluid phase and a silicate melt of granitic composition at high temperatures and pressures. Geochem. Intern., 19, 123-136.

Kilinc, I.A. and Burnham, C.W., 1972: Partitioning of chloride between a silicate melt and coexisting aqueous phase from 2 to 8 kilobars. Econ. Geol., 67, 231-235.

Killeen, P.G. and Heier, K.S., 1975: A uranium and thorium province of the Fennoscandian shield in southern Norway. Geochim. Cosmochim. Acta, 39, 1515-1524.

Koch, P., 1959: Le Precambrien de la frontiere occidentale du Cameroun Central. Bull. Dir. Mines et Geol., Cameroon, No. 3, 160-164 and 211-217.

Koga, A., 1967: Germanium, molybdenum, copper and zinc in New Zealand thermal waters. New Zealand Journ. Sci. 10, 428-446.

Korotev, R.L. and Lindstrom, D.J., 1985: Interference from fission of U-235 in INAA of rocks. Trans. Am. Nucl. Soc., 49, 177-178.

Kosterin, A.V., 1959: The possible modes of transport of the rare earths by hydrothermal solutions. Geochem. Transl. (USSR), 381-387.

Kudrin, A.V., 1986: The solubility of tugarinovite MoO_2 in aqueous solutions at elevated temperatures. Geochem. Intern., 24, 126-138.

Lavorsen, A.I., 1967: Geology and petroleum. W.H. Freeman and C., San Francisco. 724 pp.

Lang, J.R., Guan, Y., and Eastoe, C.J., 1989: Stable isotope studies of sulfates and sulfides in the Mineral Park porphyry Cu-Mo system, Arizona. Econ. Geol., 84: 650-662.

Laughlin, A.W., Rehreig, W.A., and Mayer, R.L., 1969: K-Ar chronology and sulfur and strontium isotope ratios at the Questa Mine, New Mexico. Econ. Geol., 64, 900-909.

Loiselle, M.C. and Wones, D.R., 1979: Characteristics and origin of anorogenic granites. Geol. Soc. Am., Abstr. with Progr., 11, p. 468.

Malinin, S.D. and Khitarov, N.I., 1984: Base-metal and petrogenetic elements in a magma-fluid system. Geochem. Intern., 21, 93-104.

Martin, R.F. and Bonin, B., 1976: Water and magma genesis: the association hypersolvus granite - subsolvus granite. Can. Mineral., 14, 228-237.

Martinsen, M., 1987: Petrografi og geokjemi av Drammens-granitten, Oslofeltet. Unpubl. Dr. Ing. thesis, NTH, Trondheim, Norway, 201 pp.

Mason, B., 1966: Priciples of geochemistry. Third ed. John Wiley and Sons, Inc. New York, 329 pp.

Matsuhisa, Y., Goldsmith, J.R., and Clayton, R.N., 1979: Oxygen isotope fractionation in the system quartz-albite-anorthite-water. Geochim. Cosmochim. Acta, 43: 1131-1140.

McCarthy, T.S., 1976: Chemical interrelationships in a low pressure granulite terrain in Nomaqualand, South Africa, and their bearing on granite genesis and the composition of the lower crust. Geochim. Cosmochim. Acta, 40, 1057-1068.

McLennan, S.M., 1989: Rare earth elements in sedimentary rocks: influence of provenance and sedimentary processes. In Ribbe, P.H., Geochemistry and mineralogy of rare earth elements. Reviews in Mineralogy, 21, 169-200.

Mearns, E.W., 1986: Sm-Nd ages for Norwegian garnet peridotite. Lithos, 19, 269-278.

Michard, A., Albarède, F., Michard, G., Minster, J.F., and Charlou, J.L., 1983: Rare-earth elements and uranium in high-temperature solutions from East Pacific Rise hydrothermal vent field (13°N). Nature, 303, 795-797.

Mineyev, D.A., 1963: Geochemical differentiation of the rare earths. Geochem. Transl. (USSR), 1129-1149.

Mitchell, A.H.G. and Garson, M.S., 1981: Mineral deposits and global tectonic settings. Academic Press, London, 405 pp.

Mutchler, F.E., Wright, E.G., Ludington, S., and Abbot, J.T., 1981: Granite molybdenite systems. Econ. Geol., 76: 874-897.

Nakagawa, R., 1971: Solubility of orpiment (As_2S_3) in Tamagawa Hot Springs, Akita Prefecture. Nippon Kagaku Zasshi, 92, 154-159.

Naumov, G.B., Ryzhenko, B.N., and Khodakovsky, I.L., 1974: handbook of thermodynamic data. U.S. Geol. Surv., 328 pp.

Neumann, E.-R., 1972: The distribution of Mn^{2+} and Fe^{2+} between ilmenites and magnetites in igneous rocks. Am. J. Sci., 274, 1974-1088.

Neumann, E.-R., 1976: Compositional relations among pyroxenes, amphiboles and other mafic phases in the Oslo region plutonic rocks. Lithos, 9, 85-109.

Neumann, E.-R., Brunfeldt, A.O., and Finstad, 1977: Rare earth elements in some igneous rocks in the Oslo Rift, Norway. Lithos, 10, 311-319.

Neumann, E.-R., Tilton, G.R. and Tuen, E., 1988: Sr, Nd, and Pb isotope geochemistry of the Oslo rift. Cont. Mineral. Petrol., 98, 184-193.

Neumann, H., 1960: Apparent ages of Norwegian minerals and rocks. Norsk Geol. Tidsskr., 40, 173-191.

Neumann, H., Mead, J. and Vitaliano, C.J., 1954: Trace element variation during fractional crystallization as calculated from the distribution law. Geochim. Cosmochim. Acta, 6, 90-99.

Noddack, I. and Noddack, W., 1931: Die geochemie des Rhenium. Z. Physik. Chem. 54, 207-

Norman, D.I., 1978: Analysis of Rb, Sr, and Sr isotopes in fluid inclusion waters (Abstr.). In Intern. Assoc. of the Genesis of Ore Dep., 5th Symp., Snowbird, Alta, Utah, Progr. and Abstracts. p 135.

Norman, D.I., Benton, L.D., and Albinson, T.F., 1991: Calculations of $f(O_2)$ and $f(S_2)$ of ore fluids, and depth and pressure of mineralization from fluid inclusion gas analyses for the Fresnillo, Colorada, and Pb-Zn-Ag deposits, Mexico. In Pagel, M. and Leroy, J.L, Source, transport and deposition of metals. Proceed. of the 25th years SGA anniv. Meet. Nancy, 1991. A.A. Balkema, Rotterdam, 209-212.

Norman, D.I., Condie, K.C., and Smith, R.W., 1987: Geochemical and Sr and Nd isotopic constraints on the origin of late Proteozoic volcanics and associated tin-bearing granites from Franklin mountains, West Texas. Can J. Earth Sci., 24, 830-849.

Norman, D.I., Holt, L.E. and Landis, G.P., 1979: Chemistry of post-magmatic fluids associated with alkalic intrusives, Oslo, Norway. Abstract, EOS, 60, 974.

Norman, D.I., Kyle, P.R., and Walder, I.F., 1987: Mobility of trace elements in granite terrains in light of fluid inclusion microanalysis. Abstract vol NATO conf. Mobility of elements in the earth's crust, Bergen, Norway 1987.

Norman, D.I., Kyle, P.R., and Baron, C., 1989: Analysis of trace elements including rare earth elements in fluid inclusion liquids. Econ. Geol., 84, 162-166.

Norman, D.I. and Mearns, E.W., 1986: Sm-Nd isotopic analysis of fluid inclusion waters. Abstract, Geol. Soc. Am. Annual meet., Abstr. Prog., 18, 708.

Norman, D.I. and Sawkins, F.J., 1987: Analysis of volatiles in fluid inclusions by mass spectrometry. Chemical Geol., 61, 1-10.

Norrish, K. and Chappell, B.W., 1967: X-ray fluorescence spectrography. In: Zussman, J., Physical methods in determinative mineralogy, Academic Press, London, 161-214.

Oftedahl, C., 1960: Permian rocks and structures of the Oslo Region. In Holtedahl, O., Geology of Norway. Nor. Geol. Unders., 208, 298-343.

Ohmoto, H., 1985: Stable isotope geochemistry of ore deposits. In Valley, J.W., Taylor, Jr, H.P., and O'Neil, J.R., Stable isotopes in high temperature geological processes. Reviews in Mineralogy, vol. 16, Mineral. Soc. Am., pp. 491-559.

Ohmoto, H. and Rye, R.O., 1979: Isotopes of sulfur and carbon. In Barnes, H.L., Geochemistry of hydrothermal ore deposits. 2nd. ed., John Wiley & Sons, New York, pp. 509-561.

Olmez, I., Finnigan, D.L., and Zoller, W.H., 1986: Iridium emission from Killauea volcano. Journ. Geophys. Res. 91, B1, 653-663.

Olsen, K.I., 1981: Fluid inclusion studies of the Drammen granite and the Glitrevann cauldron molybdenite deposit. Unpubl. report, NTNF, 97 pp.

Olsen, K.I. and Griffin, W.L., 1984a: Fluid inclusion studies of the Drammen granite, Oslo Paleorift, Norway. 1. Microthermometry. Contr. Mineral. Petrol., 87, 1-14.

Olsen, K.I. and Griffin, W.L., 1984b: Fluid inclusion studies of the Drammen granite, Oslo Paleorift, Norway. II. Gas- and leachate analyses of miarolitic quartz. Contr. Mineral. Petrol., 87, 15-23.

Patterson, D. and Ohmoto, H., 1976: Stable isotope and fluid inclusion studies at the Rension Bell cassiterite-sulfide deposits, Western Tasmania. Abstr. Intern. Conf. Stable

Isotope, New Zealand, 52.

Pichavant, M., 1981: An experimental study of the effect of boron on a water saturated haplogranite at 1 kbar vapor pressure. Cont. Mineral. Petrol., 76, 430-439.

Pitcher, W.S., 1983: Granite type and tectonic environment. In Hsu, K.J., Mountain building processes. Academic Press, London, 19-40.

Piperov, N.B., and Penchev, N.P., 1973: A study on gas inclusions in minerals. Analysis of gases from micro-inclusions in allanite. Geochim. Cosmochim. Acta, 37, 2075-2097.

Popova, M.Y., Khodakovski, I.L., and Ozerova, N.A., 1975: Experimental determination of the thermodynamic parameters of antimony at temperatures up to 200°C. Geochem. Intern., 12, 223.

Powell, R, 1984: Inversion of ssimilation and fractional crystallization (AFC) equations: Characterization of contaminants from isotope and trace element relationships in volcanic suites. Journ. Geol. Soc. London, 141, 447-452.

Raade, G., 1969: Cavity minerals from the Permian biotite granite at Nedre Eiker church. Norsk Geol. Tidsskr., 49, 227-239.

Raade, G., 1971: Om druserom i Drammensgranitten. Nytt fra Oslofeltgruppen, 1, 10-13.

Raade, G., 1972: Mineralogy of miarolitic cavities in the plutonic rocks of the Oslo Region, Norway. Mineral. Record, 3, 7-11.

Raade, G., 1973: Distribution of radioactive elements in the plutonic rocks of the Oslo Region. Unpubl. thesis, Univ. of Oslo, 162 pp.

Ramberg, I.B., 1976: Gravety interpretation of the Oslo Graben and associated igneous rocks. Norges Geol. Unders., 325, 193 pp.

Ramberg, I.B. and Larsen, B.T., 1978: Tectonomagmatic evolution. In Dons, J.A. and Larsen, B.T., The Oslo Paleo rift. A review and guide to excursions. Norges Geol. Unders., 337. 55-73.

Razine, L., Khvostov, V. and Novikov, V, 1965: Platinum metals in the essential and accessory minerals in ultramafic

rocks. Geochem. Intern. 2, 118-222

Reed, M.J., Candela, P.A., Cygan, G.L., and Grossman, J.N., 1991: Experimental investigation of rare earth partitioning between aluminosilicate melts and chloride-bearing aqueous fluids. Abstract, Geol. Soc. Am., Ann. Meet., Abstr. with Progr., A291.

Robie, R.A., Hemingway, B.S., and Fisher, J.R., 1979: Thermodynamic properties of minerals and related substances at 298.15 K and 1 Bar (10_5 Pascals) pressure and at higher temperatures. U.S. Geol. Surv. Bull., 1452, 1-456.

Roedder, E., 1967: Fluid inclusions as samples of ore fluids. In Barnes, H.L., Geochemistry of hydrothermal ore deposits. Holt, Reinhardt and Winston, Inc., New York, 515-574.

Roedder, E., 1984: Fluid inclusions. In Ribbe, P.H., Reviews in mineralogy. Mineral. Soc. Am., 12, 644 pp.

Roedder, E., Ingram, B., and Hall, W.E., 1963: Studies of fluid inclusions III: Extractions and quantitative analysis of fluid inclusions in the milligram range. Econ. Geol., 58, 353-374.

Rose, A.W. and Burt, D.M., 1979: Hydrothermal alteration. In Barnes, H.L., Geochemistry of hydrothermal ore deposits. John Wiley & Sons, New York, 173-235.

Ryabikov, I.D., Rekharsky, V.I., and Kudrin, A.V., 1981: Mobilization of molybdenum by magmatic fluids in the process of crystallization of granite melts. Geokhemia, 8: 1243-1246 (In Russian).

Sawkins, F.J., 1990: Metal deposits in relationship to plate tectonics. Springer-Verlag, Berlin, 461 pp.

Schott, J., 1983: Themal diffusion and magmatic differentiation: a new look at an old problem. Bull. Mineral., 106, 247-262.

Schönwandt, H.K., 1986: The volcanic history and molybdenite mineralization of the Glitrevann caldera. Sveriges Geol. Unders. Ser. Ca, 59, 26-30.

Schönwandt, H.K. and Petersen, J.S., 1983: Continental rifting and porphyry-molybdenum occurrences in the Oslo Region, Norway. Tectonophysics, 94, 609-631.

Segalstad, T.V., 1982: Geokjemi av stabile isotoper i Oslo-riften. Geolognytt, 17, 42-43.

Segalstad, T.V. and Johansen, H., 1985: Sölvdannelse i Kongsberg sölvforekomst. In Vokes, F.M., Malmgeol. Symp. Nye malmtyper in Norge. Abstract, Bergforskningen, Trondheim, Norway, p. 100.

Segalstad, T.V. and Ohmoto, H., 1986: Magmatic and crustal waters in hydrothermal solutions associated with ore deposition in the Permian Oslo Rift, Norway. Terra Cognita, 6, 555.

Shand, S.J., 1943: Igneous rocks, their genesis, composition, classification, and their relations to ore-deposits. John Wiley, New York, 444 pp.

Shaw, D.M., 1970: Trace element fractionation during anatexis. Geochim. Cosmochim. Acta, 34, 237-243.

Shock, E.L., 1991: Hydrothermal dehydration. Abstarct, Geol. Soc. Am., Ann. Meet., Abstract with Prog. p. A25.

Sienko, M.J. and Plane, R.A., 1974: Chemical principles and properties. McGraw-Hill, Tokyo, 2nd. ed., 788 pp.

Sillitoe, R.H., 1972: A plate tectonic model for the origin of porphyry copper deposits. Econ. Geol., 67, 184-197.

Silitoe, 1980: Mining Mag., 142, 150-153.

Simpson, P.R., Brown, G.C., Plant, J., and Ostle, D., 1979: Uranium mineralization and granite magmatism in the British Isles. Phil Trans. R. Soc. Lond., 291A, 133-160.

Smalley, P.C. and Field, D., 1985: Geochemical constraints on the evolution of the Proterozoic continental crust in southern Norway (Telemark sector). In: Tobi, A.C. and Touret, J.L.R., The deep Proterozoic crust in the North Atlantic Province. D. Reidel Publ. Co., Dordrecht, 551-578.

Smith, R.W., 1983: Aqueous chemistry of molybdenum at elevated temperatures and pressures with application to porphyry molybdenum deposits. PhD Thesis, New Mexico Institute of Mining and Technology, 309 pp.

Smith, R. W. and Norman, D.I., 1980: Calculated solubility of molybdenite in hydrothermal solutions. Abstract, Geol. Soc. Am., Ann. Meet., Abstr. Prog., 12, 525.

Smith, R.W., Norman D.I., and Poåå, C.J., 1980: Calculated

solubility of molybdenite in hydrothermal solutions. Abstract, Geol. Soc. Am., Ann. Meet., Abstr. Prog., 12, 525.

Streckeisen, A.L., 1976. To each plutonic rock its proper name. Earth Sci. Rev., 12, 1-33.

Stone, W.E., Crocket, J.H., and Fleet, M.E., 1990: Partitioning of palladium, irridium, and gold between sulfide liquid and basalt melt at 1200°C. Geochim. Cosmochim. Acta 54, 2341-2344.

Stumm, W. and Morgan, J.J., 1981: Aquatic chemistry. 2nd ed. John Wiley & Sons, New York, 780 pp.

Sundvoll, B., 1978a: Isotope- and trace-element chemistry, geochronology. In Dons, J.A. and Larsen, B.T., The Oslo Paleorift. A review and guide to excursions. Norges Geol. Unders., 337, 35-40.

Sundvoll, B., 1978b: Rb/Sr-relationship in the Oslo igneous rocks. In Neumann E.-R. and Ramberg, I.B., Petrology and geochemistry of continental rifts. 181-184. D. Reidel Publ. Co., Dordrecht.

Takenouchi, S. and Kennedy, G.C., 1965: The solubility of CO_2 in NaCl solutions at high temperatures and pressures. Am. J. Sci., 263, 445-454.

Taylor, H.P., 1969: The oxygen isotope geochemistry of igneous rocks. Cont. Mineral. Petrol., 19, 1-71.

Taylor, H.P., Jr., 1978: Oxygen and hydrogen isotope studies of plutonic granitic rocks. Earth Planet. Sci. Let., 38, 177-210.

Taylor, H.P., Jr., 1979: Oxygen and hydrogen isotope relationships in hydrothermal mineral deposits. In Barnes, H.L., Geochemistry of hydrothermal ore deposits. 2nd. ed. John Wiley & Sons, New York, 236-277.

Till, R., 1985: Statistical methods for the earth scientist. MacMillan Education Ltd, Houndwill, 154 pp.

Tingle, T.N. and Fenn, P.M., 1984: Transport and concentration of molybdenum in granite molybdenite systems: Effects of fluorine and sulfur. Geology, 12, 156-158.

Touray, J.-C., 1976: Activation analysis for liquid inclusion studies: a brief review. Bull. Soc. Franc. Mineral. Cristallogr., 99, 367-382.

Truesdell, A.H., 1974: Oxygen isotope activities and con centrations in aqueous salt solutions at elevated temperatures: Consequences for isotope geochemistry. Earth Planet Sci. Let., 23: 387-396.

Tuttle, O.F. and Bowen, N.L., 1958: Origin of granite in the light of experimental studies in the system $NaAlSi_3O_8$-$KAlSi_3O_8$-SiO_2-H_2O. Geol. Soc. Am. Mem., 74.

Wager, L.R. and Mitchell, R.L., 1951: The distribution of trace elements during strong fractionation of basic magmas: a further study of the Skjeargaard intrusin, East Geenland. Geochim. Csmochim Acta., 1, 129-209.

Walder, I.F., 1986: Biotitt-granite some kilde for metallavsetninger: molybdenförende lösninger assosiert med Drammensgranitten, Oslofeltet. Abstract, Malmgeol. Symp. Bergforskningen, Trondheim, Norway, 6.

Walder, I.F., Norman, D.I., and Smith, R.W., 1987: Calculations of molybdenite solubility, and its use in explaining the molybdenite mineralization in the Drammen granite, Norway. In Wood, S. A., Experimental investigations of hydrothermal processes: Applications to ore deposit genesis. IREM-MERI Conf. Montreal, Canada, Feb. 1988.

Wallace, S.R., MacKenzie, W.B., Blair, R.G., and Muncaster, N.K., 1978: Geology of the Urad and Henderson molybdenite deposits. Clear Creek county, Colorado. 2. A comparison of these deposits with those at Climax, Colorado. Econ. Geol., 73, 325-368.

Watson, E.B. and Harrison, T.M., 1983: Zircon saturation revisited: temperature and composition effects in a variety of crustal magma types. Earth Planet. Sci. Letters, 64, 295-304.

Webster, J.D., 1987: Experimental studies of a F-, Cl-, and lithophile trace element-enriched vitrophyre from Spor mountain, Utah. PhD Thesis, Arizona State Univ., 208 pp.

Webster, J.D. and Holloway, J.R., 1987: Cl, F, and lithophile trace element partitioning between H_2O and H_2O + CO_2-bearing fluids and high-silica rhyolite magmas. Abstract, Intern. Union. Geodesy Geophys. 14th Gen. Assem., 3-2, p 403.

Webster, J.D., Holloway, J.R., and Hervig, R.L., 1989: Partitioning of lithophile trace elements between H_2O and H_2O+CO_2 fluids and topaz rhyolite melt. Econ. Geol., 84,

116-134.

Westra, G. and Keith, S.B., 1981: Classification and genesis of stockwork molybdenum deposits. Econ. Geol., 76, 844-897.

Whalen, J.B., 1985: Geochemistry of an island-arc plutonic suite: the Uasilau-Yau intrusive complex, New Britain, P.N.G. Journ. Petrol., 26, 603-632.

White, A.J.R., 1979: Sources of granite magmas. Abstract, Geol. Soc. Am., Ann. Meet., Abstr. with Progr., 11, p 539.

White, A.J.R. and Chappell, B.W., 1977: Ultrametamorphism and granitoid genesis. Tectonophysics, 43, 7-22.

White, W.H., Bookstrom, A.A., Kamilli, R.J., Ganster, M.W., Smith, R.P., Ranta, D.E., and Staininger, R.C., 1981: Characteristica and origin of Climax-type molybdenum deposits. Econ. Geol. 75th anniv. vol., 270-316.

Whitney, J.A., 1989: Origin and evolution of silicic magmas. In Whitney, J.A. and Naldrett, A.J., Ore deposition associated with magmas. Review in Econ. Geol., 4, 183-201.

Wood, S.A., Crerar, D.A., and Borcsik, M.P., 1987: Solubility of the assemblage pyrite-pyrrothite-magnetite-galena-gold-stibnite-bismuthinite-argentite-molybdenite in H_2O-NaCl-CO_2 solutions from 200° to 350°C. Econ. Geol., 82, 1864-1887.

Wright, J.B., 1970: Controls of mineralization in the older and younger tin fields of Nigeria. Econ. Geol., 65, 945-951.

Wright, T. and Fleischer, M., 1965: Geochemistry of platinum metals. U.S. Geol. Surv. Bull., 1214-A, A1-A5.

Zoller, W.H., Parrington, J.R., and Kofra, J.M.P., 1983: Iridium enrichment in airborn particles from Kilauea volcano: January 1983. Science, 222, 1118-1121.

APPENDIX A

CALCULATIONS OF PRECISION AND ACCURACY FOR WHOLE ROCK MAJOR AND TRACE ELEMENT ANALYSES.

Each sample was analyzed in duplicate. For the major element analysis two pellets were made for each of the samples; for trace element analysis one pellet per sample were made and analyzed on both sides.

Calculated accuracy is based on "Standard pool deviation" where standard deviation σ (%) is given by:

$$\sigma = \frac{100St^2}{\overline{X}\sqrt{2}}, where \overline{X} = \frac{1}{N}\sum_{i=1}^{N} \overline{X_i},$$

and

$$St^2 = \frac{1}{N}\sum_{i=1}^{N} S_i^2, where$$

$$S_i^2 = (X_i^a - \overline{X_i})^2 + (X_i^b - \overline{X_i})^2$$

X_i^a and X_i^b are the pair analyses and X_i is the mean of each pair. N is the amount of samples used for each σ calculation.

Element	1σ%	N	MEAN ANAL. STD± (N)	ACT CON.	STD
SiO_2	0.31	31			
TiO_2	0.02	31			
Al_2O_3	0.06	31			
FeO_t	0.02	31			
MnO	0.01	31			
CaO	0.35	31			
Na_2O	0.05	31			
K_2O	0.02	31			
P_2O_5	0.01	31			
Rb	2.2	40	169.8 ± 0.85 (12)	169.3	G2
Sr	0.23	40	476.8 ± 0.2 (12)	476.3	G2
Y	0.67	41	28.74 ± 0.44 (12)	29	GSP
Zr	4.1	41	103.0 ± 2.9 (16)	105	W1
Nb	0.97	41	85.9 ± 0.97 (10)	85	GH
Ba		41			

For Ba no data are available for calculation of stadard deviation. Ba was analyzed by Brenda Jensen at Mineralogisk-Geologisk Museum, Oslo, Norway.

APPENDIX B

BULK DISTRIBUTION COEFFICIENT CALCULATIONS AND TRACE ELEMENT MODELLING

1. Bulk distribution coefficients

Initial trace element contents in ppm:

	Rb	Sr	Ba
Assimilating shale[1]:	200	175	800
Precambrian gneiss[2]:	375	40	400
Fractionating magma[3]:	175	40	220

[1] Björlykke, 1974.
[2] Jacobsen and Heier, 1978.
[3] This study and Ihlen et al., 1982.

Mineral assemblage in wt. % X_I:

	Qtz	Plag.	K-feld.	Biotite
Precambrian gneiss:	0	59	40	1
Fractionating magma:	30	45	23	2

$K_{D,i}$ mineral/melt for individual minerals (McCarthy, 1976; Hanson, 1978):

	Qtz	Plag.	K-feld.	Biotite
Rb	0.0	0.04	0.66	3.0
Sr	0.0	2.8	3.6	0.1
Ba	0.0	3.6	6.0	6.0

Bulk distribution coefficient is calculated based on the following equation:

$$K_D = (\Sigma X_I * K_{D,i})/100$$

giving K_D crystal/melt:

	Rb	Sr	Ba
Precambrian gneiss	0.37	2.27	2.94
Fractionating magma:	0.35	1.92	2.17

2. Trace element modelling

Crystal fractionation model for crystal composition:

$$C_S = C_O * K_D * (1-F) EXP(K_D-1)$$

Crystal fractionation model for melt composition
$C_L=C_O*(1-F)EXP(K_D-1)$

Partial melting model:
$C_M=C_O(1/(F+K_D-FK_D))$

Assimilation and fractional crystallization model
$Cs=Co*Df*(1-F)exp(Df-1)$, where
$f=F^{(r-1+KD)/(R-1)}$

C_S - abundance of trace element solid fraction.
C_O - initial trace element abundance in melt.
C_L - abundance of trace element in melt fraction.
C_M - abundance of trace element in melt fraction during partial melting.
F = weight fraction of magma remaining.
r - rate of assimilation to rate of fractionation.
K_D - bulk distribution coefficient for fractionationg assmeblage.

Calculated concentrations of Rb, Sr, and Ba based on the initial compositions given above and the modelling equations:

F	Rb (ppm)	Sr (ppm)	Ba (ppm)
CRYST FRACTIONATION, MINERAL COMPOSITION			
0.05	41.8	79.1	356.9
0.1	43.6	74.5	344.0
0.2	47.8	65.6	317.6
0.3	52.9	56.7	290.0
0.4	59.6	47.9	261.1
0.5	68.6	39.3	230.7
0.6	81.4	30.8	198.2
0.7	101.7	22.5	163.0
0.8	138.9	14.5	123.7
0.9	236.9	6.8	77.2
0.95	404.1	3.2	48.2
CRYSTAL FRACTIONATION, MELT COMPOSITION			
1	175	40	220
0.95	182	38	212
0.9	190	36	205
0.8	208	31	189
0.7	230	27	173
0.6	259	23	155
0.5	298	19	137
0.4	354	15	118
0.3	442	11	97
0.2	604	7	74
0.1	1031	3	46
0.05	1758	2	29

PARTIAL MELTING

0.05	123.3	84.0	2485.3
0.1	127.8	76.7	2305.1
0.2	137.9	65.4	2013.1
0.3	149.8	57.0	1786.9
0.4	163.8	50.5	1606.3
0.5	180.8	45.3	1458.9
0.6	201.7	41.1	
0.7	228.0	37.6	1232.6
0.8	262.3	34.7	1143.9
0.9	308.7	32.2	1067.1
0.95	338.6	31.1	1032.5

ASSIMILATION & FRACTIONAL CRYSTALIZATION r=0.8

1	175	40	220
0.95	215	38	211
0.90	256	39	217
0.85	299	43	231
0.80	345	47	251
0.75	393	52	274
0.70	444	56	298
0.65	498	60	321
0.60	556	64	342
0.55	618	66	361
0.50	685	69	378
0.45	758	70	392
0.40	838	72	404
0.35	927	73	413
0.30	1028	73	420
0.25	1144	74	425
0.20	1282	74	429
0.15	1454	74	431
0.10	1683	74	432
0.05	2045	74	432

MIXING BETWEEN SHALE AND INITIAL MELT

0	175	40	220
0.1	178	54	278
0.2	180	67	336
0.3	183	81	394
0.4	185	94	452
0.5	188	108	510
0.6	190	121	568
0.7	193	135	626
0.8	195	148	684
0.9	198	162	742
1	200	175	800

APPENDIX C

ANALYTICAL METHOD FOR GAS ANALYSES

Cleaned quartz samples were loaded in a clean sample holder made of quartz glass and connected to a vacuum line as showed in Fig. A1. Two samples are connected to the line, and valves are opened to the vacuum pump. The samples are preheated to about 100°C for 4 hours. The quadropol mass spectrometer is kept closed from the vacuum line at valve 1. Pumping is done until the pressure reaches about 1 to 3 times 10^{-6} torr. and then the vacuum pump is disconnected from the glass line.

Each sample is heated to about 500-525°C and dry ice + alcohol (-76°C) coolant is used as the first trap (A; glass balls inside) and liquid nitrogen (-196°C) at the second trap (B). The sample is kept at this temperature of -196°C for about 15 minutes, until the decrepitation has stopped (no more pressure increase in the vacuum line). The pressure increase in the line makes us able to calculate the total amount of gas which decrepitated from the samples.

The analytical background for the non-condensable gases is measured by recording the pressure of the leftover gases after vacuum pumping between valve 2 and the analyzer. The gas flow through the analyzer during the background run is kept steady at 1-2 x 10^{-8} torr. Then the non-condensable gases from the sample are analyzed. The gases are moved through the

Fig. A1.

Schematic diagram of the vacuum extraction line used for the gas analysis. See text for explanation. Modified from Norman and Sawkins (1987)

Fig. A1

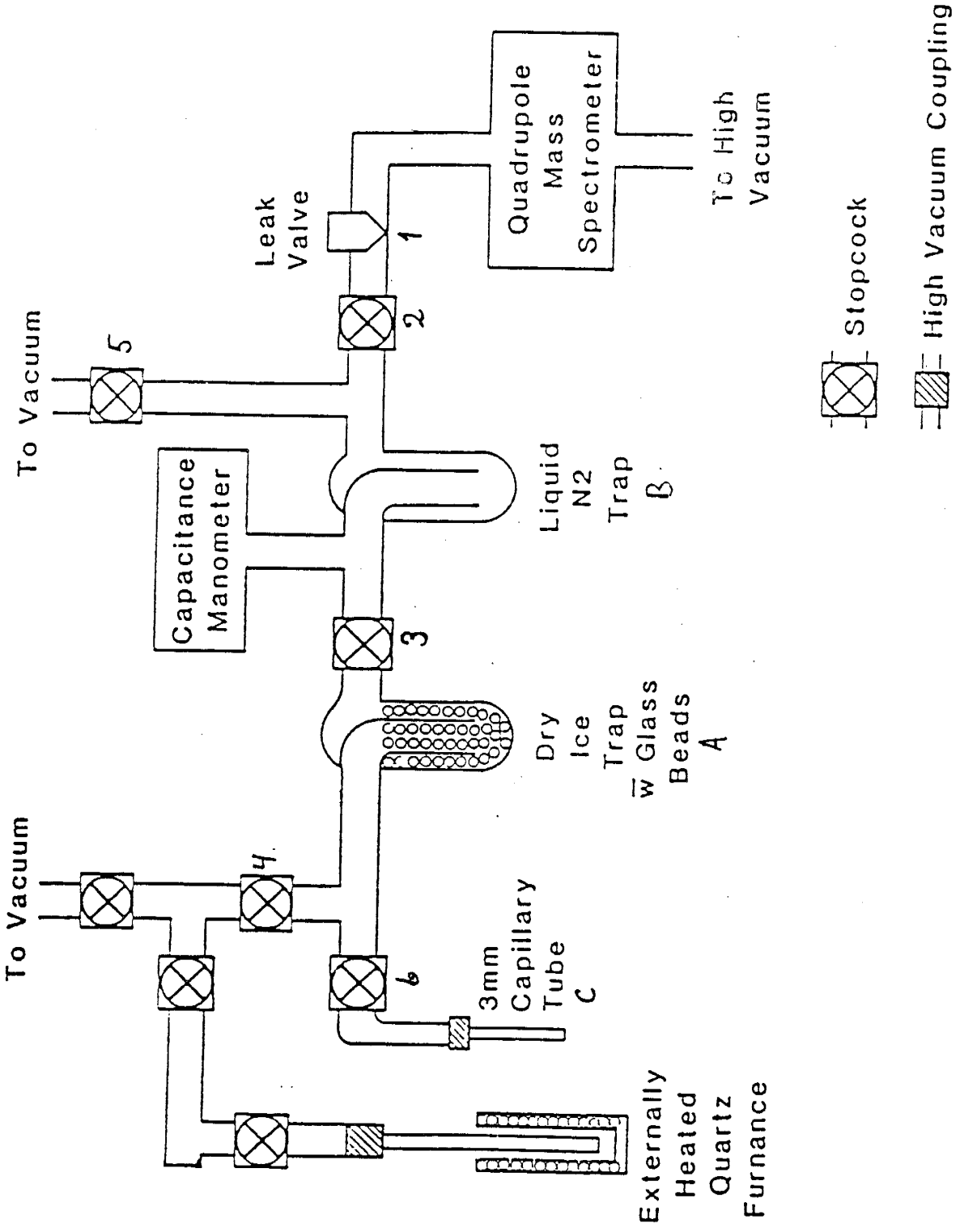
To Vacuum
5
Leak Valve
1
Quadrupole Mass Spectrometer
To High Vacuum
2
Capacitance Manometer
Liquid N2 Trap B
3
Dry Ice Trap w Glass Beads A
To Vacuum
4
6
3mm Capillary Tube C
Externally Heated Quartz Furnance
Stopcock
High Vacuum Coupling

analyzer by a turbo molecular pump connected to the system at the far side of the analyzer. After the run the vacuum line and the mass spectrometer are cleaned by using the vacuum pump, the valves 2 to 5 are closed and valve 6 is opened. The liquid nitrogen trap is moved to trap C, in order to trap the water from the inclusion fluids. The dry ice - alcohol coolant is moved to trap B. Trap A is heated slightly to vaporize the water faster. When the pressure is stable among the lines between valves 2, 3, and 5 the pressure for the condensable gases is recorded.

The analytical background for the condensable gases is measured in the same way as for the non-condensable by using gases between valve 2 and the analyzer. After the background level is established for the condensable gases (for each sample) condensable gases (except H_2O) are analyzed the same way as for non-condensable gases, still with dry ice - alcohol coolant at trap B. After the analysis, the gas line between the valves 2, 3, and 5 is cleaned by vacuum pumping. The valves 2 and 5 are closed, valve 3 is opened and the dry ice - alcohol coolant is removed from trap B. Trap B is heated slightly to vaporize the remaining water faster. When there is no excess gas left in the line the thin glass vial is closed by melting and removed for weighing.

The analyzer is set to scan between atomic mass unit 2 and 50 for the non-condensable gases, and between 2 and 100 for the condensable gases. The electron multiplier is set to

2200 V. The analyzer automatically scans over 10 mass units 8 times before moving to higher masses. The gas flow is kept at a constant level during the whole run.

Before every second sample the analyzer peak-setting is controlled for drift by letting some air pass through the analyzer, controlling the mass peaks for H_2 (2), N_2 (28), and CO_2 (44). The room temperature is always kept at 25°C.

The raw data is calculated for a best fit of gas composition. Each gas species gives a signal width wider than one mass unit, partly because of different isotopes in the gas molecules and partly because of decomposition of the molecules, in known ratios. These ratios are controlled by analyzing a multi-gas standard (Freon-4) after a shut down of the system. When the calculated residual from the raw data is as close as possible to zero, by subtracting the values of the specific gases, we have the best fit for the gas composition. This gas composition is also recalculated to 100 % including the weighed amount of water for each sample. All calculations are done on an HP-85 computer.

After analyzing the condensable gases, the remaining gases are trapped in a glass vial which is closed by melting the glass. The remaining gas is dominantly CO_2 which can be analyzed for carbon isotopes.

The uncertainty for the measurement of the major gaseous species is less than ± 10 %, and for the minor species it is less than ± 20 % (Norman and Sawkins, 1987).

APPENDIX D

CALCULATIONS OF GAS FUGACITIES

$$\triangle G_R = \Sigma\triangle G_{fp} - \Sigma\triangle G_{fr} \qquad \text{(Eq. 17)}$$

$\triangle G_R$ - Gibb's free energy for reaction

$\Sigma\triangle G_{fp}$- Gibb's free energy of formation for products

$\Sigma\triangle G_{fr}$- Gibb's free energy of formation for reactants

$$\triangle G_R = -R*T*\ln K \qquad \text{(Eq. 18)}$$

R - gas constant = 0.008314 $J*mol^{-1}*deg^{-1}$

T - absolute temperature (Kelvin)

K - equilibrium constant for a chemical reaction

Equilibrium constants are calculated from rearging Eqs. 17 and 18 giving:

$$\log K = -\triangle G_R/(0.0191*T) \qquad \text{(Eq. 19)}$$

Gibb's free energy of formation ($\triangle G_f$) in kJ/mol is estimated from Robie et al. (1979) for 300°C and 500°C:

Compound	300°C	500°C

CO_2	-395.086	-395.494
H_2O	-194.97	-204.908
H_2S	- 46.03	- 49.216
H_2	0	0
CH_4	- 25.7	- 5.4
O_2	0	0
CO	-162.062	-180.043
SO_2	-300.27	-301.8

Calculated log K for the following reactions are:

		300°C	500°C
$CH_4 + 2O_2 = CO_2 + 2H_2O$	(Eq. 3)	69.36	54.17
$CH_4 + O_2 = CO_2 + 2H_2$	(Eq. 4)	33.74	26.42
$C + O_2 = CO_2$	(Eq. 5)	36.09	26.78
$H_2 + CO_2 = H_2O + CO$	(Eq. 8)	-3.48	-0.71
$CH_4 + H_2O = CO + 3H_2$	(Eq. 9)	-5.35	-2.05
$H_2S + 2H_2O = SO_2 + 3H_2$	(Eq. 10)	-12.40	-10.65
$H_2S + CO_2 = SO_2 + H_2 + C$	(Eq. 11)	-12.86	-9.68
$H_2S + O_2 = SO_2 + H_2$	(Eq. 12)	-8.66	-6.34
$H^+ + HSO^{4-} + = SO_2 + H_2 + O_2$	(Eq. 13)	-52.31	
$4SO_4^{2-} + CH_4 + 8H^+ = 4SO_2 + CO_2 + 6H_2O$	(Eq. 14)	-115.56	
$2H_2S + O_2 = S_2(g) + 2H_2O$	(Eq. 15)	27.21	
$SO_4^{2-} + H^+ = \frac{1}{2}S_2 + H_2O + 3/2O_2$	(Eq. 16)	-34.34	

Fugacity of individual gases (f(i)) is at 300°C given by:

$f(i) = K_H * X(i)$ (Eq. 20)

K_H - Henry's law constant

X(i) - mole fraction of gas i

where activity of H_2O is 1.

At 500°C the fugacity is given by:

$f(i) = ¥ * X(i) * P_{tot}$ (Eq. 21)

¥ - fugacity coefficient

P_{tot} - total pressure

where $f(H_2O)$ is calculated the same way.

Log K_H (Henley et al., 1984) and log ¥ (Naumov et al., 1973; at 1.5 kbars) used in fugacity calculations:

	log K_H	log ¥
CO_2	3.573	0.16
H_2O		-0.39

H_2S	3.201	0.05
H_2	4.109	0.18
CH_4	4.019	0.27
CO	4.284	0.3 (as N_2)
SO_2	≈3.2	0.05 (as H_2S)

APPENDIX E

BASIC MOLYBDENUM SOLUBILITY PROGRAM

This program is made in basic for running with DOS 3.2 on COMPAQ computers.

```
10   REM THIS PROGRAM "MOSOL" WILL CALCULATE AMOUNT OF THE
DIFFERENT MOLYBDENUM AND SULFUR SPECIES IN THE SOLUTION GIVEN
pH, I, LOG f(O2), t (°C), AND TOTAL SULFUR IN EQUILIBRIUM WITH
MoS2. THERMODYMNAMIC DATA ARE FROM SMITH, 1983, NAUMOV ET AL.,
1976, AND ROBIE ET AL. 1979. USER OF THE PROGRAM IS RESPONIBLE
FOR KNOWING THE BACKGROUND FOR THE CALCULATIONS.
20   RESET
30   DIM H1$(10), H2$(10)
40   CLS
50   DIM A$(30), B(30), C(30), D(30), E(30), F(30), G(10),
G2(10), AM(30), BM(30), CM(30), DM(30),LGK(40),M(30), W(20),
U(20), V(20)
60   FOR I=1 TO 14
70   READ A$(I)
80   READ C(I)
90   READ E(I)
100  NEXT I
110  DATA  Na+,  22.9898,4,  K+,39.089,3,  Li+,6.941,6,
Rb+,85.4678,3,  Cs+,132.9,3,  Mg++,24.305,8,  Ca++,40.08,6,
```

```
Mn++,54.938,5, Fe++,55.847,5, Cl-,35.43,3.5, F-,18.998,3.5,
Br-,79.9,3, HCO3-,61.0159,4.5, SO4--,96.056,4
120  REM DATA FOR ION CHARGE
130  FOR I=1 TO 14
140  READ H(I)
150  NEXT I
160  DATA 1,1,1,1,1,2,2,2,2,-1,-1,-1,-1,-2
170  CLS
180  INPUT " ENTER IONIC STRENGTH -I-";IS
190  ALOG=2.303
200  INPUT " ENTER TEMPERATURE";T
210  INPUT " ENTER PRESSURE IN KBAR (0,.5,1,1.5,2) ";P
220  TK=T+273.15
230  INPUT " ENTER pH ";PH
240  INPUT " ENTER LOG FO2";LO2
250  INPUT " ENTER TOTAL SULFUR (MOLAL) ";S
260  INPUT " ENTER TOTAL FLUORINE (MOLAL)";F
280  INPUT " ENTER TOTAL CHLORINE (MOLAL)";CL
290  REM ************************************
300  REM CALCULATING LOG GAMMA
310  FOR N=1 TO 10
320  NEXT N
330  DATA 2.5,3,3.5,4,4.5,6,7,8,9
340  FOR N=1 TO 10
350  Z=1
360  AZ=G(N)
```

```
370  A=.4914844 + 3.65317E-04*T + 1.55023E-05T^2 - 1.650365E-
07*T^3 + 1.142142E-9*T^4 - 3.704296E-12*T^5 + 4.754928E-15*T^6
380  B=.3240423 + 1.85311E-04*T - 1.17617E-07*^2 + 1.057105E-
09*T^3
390  LOGM = A*Z^2*IS^.5/(1+AZ*B*IS^.5) + .03*IS
400  G1(N)=-LOGM
410  Z=2
420  A=.4914844 + 3.65317E-04*T + 1.55023E-05T^2 - 1.650365E-
07*T^3 + 1.142142E-9*T^4 - 3.704296E-12*T^5 + 4.754928E-15*T^6
430  B=.3240423 + 1.85311E-04*T - 1.17617E-07*^2 + 1.057105E-
09*T^3
440  LOGM = A*Z^2*IS^.5/(1+AZ*B*IS^.5) + .03*IS
450  G2(N)=-LOGM
460  IF P=0 THEN TE=TK
470  IF P=0 THEN GOTO 550
480  REM ****************************************
490  REM CALCULATION OF THE TE AT ELEVATED PRESSURS
500  TE1=171.55+2.3819*T-.0055229*T^2+7.04E-06*T^3
510  TE2=(248.041-3.3388*T+.01285*T^2-1.728E-05*T^3)*P
520  TE3=(-207.26+2.6455*T-.0103*T^2+1.3067E-05*T^3)*P^2
530  TE4=(51.0964-.64058*T+.0024335*T^2-3.07556E-6*T^3)*P^3
540  TE=TE1+TE2+TE3+TE4
550  LCL=LOG(CL)/ALOG
560  LF=LOG(F)/ALOG
570  G2(N)=-LOGM
580  NEXT N
```

```
590  CLS
600  PRINT USING" LOG GAMMA CL-                ##.###";G1(3)
610  PRINT USING" LOG GAMMA HSO4-, HS-         ##.###";G1(4)
620  PRINT USING" LOG GAMMA S--, SO4--         ##.###";G2(4)
630  PRINT USING" LOG G HMoO4-, MoO2+          ##.###";G1(6)
640  PRINT USING" LOG G MoO4--, MoO2S2--       ##.###";G2(6)
650  LGHSO4=G1(4)
660  LGHS=LGHSO4
670  LGS=G2(4)
680  LGSO4=LGS
690  LGHMOO4=G1(6)
700  LGMOO2=LGHMOO4 : LGMOO2CL=LGHMOO4 : LGMOO2CL3=LGHMOO4
710  LGMOO4=G1(6)
720  LGMOO2S2=LGMOO4
730  LGCL-G1(3)
740  PRINT "
750  INPUT "HIT ENTER TO CONTINUE, 1 START AGAIN, 2 GOTO MAIN
MENU ";C
760  IF C=1 THEN GOTO 30:IF C+2 THEN CHAIN"C:\FLUID\MENU
770  REM CALCULATING EQ. CONST.
780  REM K1=HSO4- K2=H2S K3=HS- K4=S2 K5S--
790  K1=-13.59+4324.08/TK
800  REM ******************************************
810  REM CALCULATION OF LOG K FOR H2S - HS- AT SAT
820    K2=-(6.646  +  1.261906e-04*T  -  1.085714E-05*T^2  +
8.666667E-08*T^3)
```

```
830  K3=-31.75+49975.5/TK
840  K4=-9.99+21287.7/TK
850  K5=11.183+2629/TK
860  REM ***********************************************
870  REM CALCULATION OF LOG K FOR DIFFERENT Mo REACTIONS
880       AH=.01875:BH=-12.741:CH=.000784:OH=219:WH=1.00322:
R=1.987: TR=298.15: BT=0
890 DSR1=-5.8:DSR2=-27.3: DSR3=-49.7: DSR4=-32.2: DSR5=-22.2:
DSR6=-11.7:  DSR7=-14.9:  DSR8=-18.1:  DSR9=-26.8:  DSR10=-21:
DSR11=-48.8
900  DSE1=-14.98: DSE2=-15: DSE3=-12.94: DSE4=-10.43: DSE5=-
16.8: DSE6=-21.2: DSE7=-24.4: DSE8=-27.6:DSE9=-15.82: DSE10=-
21: DSE11=-26.21
910   DH1=8735:  DH2=1712:  DH3=-6386:  DH4=-3897:  DH5=22273:
DH6=6564:   DH7=4928:   DH8=1395:   DH9=-8916:   DH10=-10627:
DH11=2256
920   AL1=-40.12:  AL2=-31.62:  AL3=-52.2:  AL4=-38.81:  AL5=-
107.73: AL6=-40.1: AL7=-40.1: AL8=-40.1: AL9:-53.57: AL10=0:
AL11=-39.41
930  REM CALC. LOG K FOR MoO2++ = MoO4--
940  RESTA1=DH1/(2.303*R*TK)
950  RESTB1=DSR1/(2.303*R)
960  RESTC1=(AL1/(2.303*R))*(LOG(TK/TR)-1+TR/TK)
970  RESTD1=(BT*(TK-TR)^2)/(4.606*R*TK)
980   LOGK1=((DSE1/(2.303*R*TK))*(TR  -  TE  -  ((OH/WH)*(1  -
EXP((EXP(BH+AH*TK))  -  CH  +  (TE-TR)/OH))))) - RESTA1 + RESTB1
```

```
+ RESTC1 + RESTD1
990  REM CALC LOG K FOR MoO2(OH)+ = MoO4--
1000 RESTA2=DH2/(2.303*R*TK)
1010 RESTB2=DSR2/(2.303*R)
1020 RESTC2=(AL2/(2.303*R))*(LOG(TK/TR)-1+TR/TK)
1030 RESTD2=(BT*(TK-TR)^2)/(4.606*R*TK)
1040  LOGK2=((DSE2/(2.303*R*TK))*(TR  -  TE  -  ((OH/WH)*(1  -
EXP((EXP(BH+AH*TK)) - CH + (TE-TR)/OH))))) - RESTA2 + RESTB2
+ RESTC2 + RESTD2
1050 REM CALC LOG K FOR H2MoO4 = MoO4--
1060 RESTA3=DH3/(2.303*R*TK)
1070 RESTB3=DSR3/(2.303*R)
1080 RESTC3=(AL3/(2.303*R))*(LOG(TK/TR)-1+TR/TK)
1090 RESTD3=(BT*(TK-TR)^2)/(4.606*R*TK)
1100  LOGK3=((DSE3/(2.303*R*TK))*(TR  -  TE  -  ((OH/WH)*(1  -
EXP((EXP(BH+AH*TK)) - CH + (TE-TR)/OH))))) - RESTA3 + RESTB3
+ RESTC3 + RESTD3
1110 REM CALC. LOG K FOR HMoO4- = MoO4--
1120 RESTA4=DH4/(2.303*R*TK)
1130 RESTB4=DSR4/(2.303*R)
1140 RESTC4=(AL4/(2.303*R))*(LOG(TK/TR)-1+TR/TK)
1150 RESTD4=(BT*(TK-TR)^2)/(4.606*R*TK)
1160  LOGK4=((DSE4/(2.303*R*TK))*(TR  -  TE  -  ((OH/WH)*(1  -
EXP((EXP(BH+AH*TK)) - CH + (TE-TR)/OH))))) - RESTA4 + RESTB4
+ RESTC4 + RESTD4
1170 REM CALC LOG K FOR MoO2S2-- = MoO4--
```

```
1180 RESTA5=DH5/(2.303*R*TK)
1190 RESTB5=DSR5/(2.303*R)
1200 RESTC5=(AL5/(2.303*R))*(LOG(TK/TR)-1+TR/TK)
1210 RESTD5=(BT*(TK-TR)^2)/(4.606*R*TK)
1220  LOGK5=((DSE5/(2.303*R*TK))*(TR  -  TE  -  ((OH/WH)*(1  -
EXP((EXP(BH+AH*TK)) - CH + (TE-TR)/OH))))) - RESTA5 + RESTB5
+ RESTC5 + RESTD5
1230 REM CALC LOG K FOR MoO2CL+ = MoO4--
1240 RESTA6=DH6/(2.303*R*TK)
1250 RESTB6=DSR6/(2.303*R)
1260 RESTC6=(AL6/(2.303*R))*(LOG(TK/TR)-1+TR/TK)
1270 RESTD6=(BT*(TK-TR)^2)/(4.606*R*TK)
1280  LOGK6=((DSE6/(2.303*R*TK))*(TR  -  TE  -  ((OH/WH)*(1  -
EXP((EXP(BH+AH*TK)) - CH + (TE-TR)/OH))))) - RESTA6 + RESTB6
+ RESTC6 + RESTD6
1290 REM CALC LOG K FOR MoO2CL2 = MoO4--
1300 RESTA7=DH7/(2.303*R*TK)
1310 RESTB7=DSR7/(2.303*R)
1320 RESTC7=(AL7/(2.303*R))*(LOG(TK/TR)-1+TR/TK)
1330 RESTD7=(BT*(TK-TR)^2)/(4.606*R*TK)
1340  LOGK7=((DSE7/(2.303*R*TK))*(TR  -  TE  -  ((OH/WH)*(1  -
EXP((EXP(BH+AH*TK)) - CH + (TE-TR)/OH))))) - RESTA7 + RESTB7
+ RESTC7 + RESTD7
1350 REM CALC LOG K FOR MoO2CL3- = MoO4--
1360 RESTA8=DH8/(2.303*R*TK)
1370 RESTB8=DSR8/(2.303*R)
```

```
1380 RESTC8=(AL8/(2.303*R))*(LOG(TK/TR)-1+TR/TK)
1390 RESTD8=(BT*(TK-TR)^2)/(4.606*R*TK)
1400  LOGK8=((DSE8/(2.303*R*TK))*(TR  -  TE  -  ((OH/WH)*(1  -
EXP((EXP(BH+AH*TK))  -  CH  +  (TE-TR)/OH)))))  -  RESTA8  +  RESTB8
+ RESTC8 + RESTD8
1410 REM CALC. LOG K FOR MoO2+ = MoO4--
1420 RESTA9=DH9/(2.303*R*TK)
1430 RESTB9=DSR9/(2.303*R)
1440 RESTC9=(AL9/(2.303*R))*(LOG(TK/TR)-1+TR/TK)
1450 RESTD9=(BT*(TK-TR)^2)/(4.606*R*TK)
1460  LOGK9=((DSE9/(2.303*R*TK))*(TR  -  TE  -  ((OH/WH)*(1  -
EXP((EXP(BH+AH*TK))  -  CH  +  (TE-TR)/OH)))))  -  RESTA9  +  RESTB9
+ RESTC9 + RESTD9
1470 REM CALC LOG K FOR MoOCL3 = MoO2+
1480 RESTA10=DH10/(2.303*R*TK)
1490 RESTB10=DSR10/(2.303*R)
1500 RESTC10=(AL10/(2.303*R))*(LOG(TK/TR)-1+TR/TK)
1510 RESTD10=(BT*(TK-TR)^2)/(4.606*R*TK)
1520  LOGK10=((DSE10/(2.303*R*TK))*(TR  -  TE  -  ((OH/WH)*(1  -
EXP((EXP(BH+AH*TK))  -  CH  +  (TE-TR)/OH)))))  -  RESTA105  +
RESTB10 + RESTC10 + RESTD10
1530 REM CALC LOG K FOR MoO3F- = MoO4--
1540 RESTA11=DH11/(2.303*R*TK)
1550 RESTB11=DSR11/(2.303*R)
1560 RESTC11=(AL11/(2.303*R))*(LOG(TK/TR)-1+TR/TK)
1570 RESTD11=(BT*(TK-TR)^2)/(4.606*R*TK)
```

```
1580 LOGK11=((DSE11/(2.303*R*TK))*(TR - TE - ((OH/WH)*(1 -
EXP((EXP(BH+AH*TK)) - CH + (TE-TR)/OH))))) - RESTA11 + RESTB11
+ RESTC11 + RESTD11
1590 REM CALC. LOG K FOR Mo-SPECIES  = HMoO4-
1600 K7=LGK4
1610 K8=LGK3 - LGK4
1620 K9=LGK9 - LGK4
1630 K10=LGK5 - LGK4
1640 K12=LGK6 - LGK4
1650 K13=LGK7 - LGK4
1660 K14=LGK8 - LGK4
1670 K15=LGK10 + LGK9 - LGK4
1680 K16=LGK2 - LGK4
1690 K17=LGK1 - LGK4
1700 K18=LGK11 - LGK4
1710 REM ***********************************************
1720 REM CALCULATION OF LOG K FOR MoS2 - MoO42- + S2(g) AT
ELEVATED PRESSURS
1730 I=0
1740 FOR I=1 TO 16
1750 READ W(I)
1760 NEXT I
1770 DATA 48.91476, -.09850868, -.07794283, -.01236438, -
.1946929, .01366639, -.003930251, .000406925, .0004181988, -
.00009808221, .00002936216, -.000002880954, -.4753087E-6,
.2083920E-6, -.606408E-7, .574518E-8
```

```
1780 W1=W(1)+W(5)*T+W(9)*T^2+W(13)*T^3
1790 W2=W(2)+W(6)*T+W(10)*T^2+W(14)*T^3*P
1800 W3=W(31)+W(7)*T+W(11)*T^2+W(15)*T^3*P^2
1810 W4=W(4)+W(8)*T+W(12)*T^2+W(16)*T^3*P^3
1820 K20=W1+W2+W3+W4
1830 REM ************************************************
1840 REM CALCULATION OF LOG K FOR MoS2 - MoO42- + S2(g) AT SAT
1850  K21=49.0779-.2018628*T + 4.88334E-04*T^2 - 6.679737E-
07*T^3
1860 REM ************************************************
1870 REM CALCULATION OF LOG K FOR HS- - S2 (g) AT SAT
1880  K22= -(-39.58 + .1204667*T - .000268*T^2 + 2.133333E-
07*T^3)
1890 REM ************************************************
1900  REM CALCULATION OF LOG K FOR HS- - S2 (g) AT ELEVATED
PRESSURES
1910 I=0
1920 FOR I=1 TO 16
1930 READ V(I)
1940 NEXT I
1950 DATA 38.64486,-.9983148, .51425, -.0607963, -09084195, -
.003626616, -.6180157E-3, .1342034E-3, .4525463E-4,.1396883E-
3,  -.4493452E-4,  .463448E-5,  .2241821E-6,  -.4127335E-6,
.1457778E-6, -.1555967E-7
1960 V1=V(1)+V(5)*T+V(9)*T^2+V(13)*T^3
1970 V2=V(2)+V(6)*T+V(10)*T^2+V(14)*T^3*P
```

```
1980 V3=V(31)+V(7)*T+V(11)*T^2+V(15)*T^3*P^2
1990 V4=V(4)+V(8)*T+V(12)*T^2+V(16)*T^3*P^3
2000 K23=V1+V2+V3+V4
2010 REM ************************************************
2020 REM CALCULATION OF LOG K FOR H2S - HS- AT ELEVATED
PRESSURES
2030 I=0
2040 FOR I=1 TO 16
2050 READ U(I)
2060 NEXT I
2070 DATA .6948253, 11.4506, -4.390311, .4918914, .1247772, -
.1913109, .07512501, -.008422204, -.0006048114, .000939222, -
.0003692636,.4132039E-4, .9253438E-6, -.1396963E-5, .5456954E-
6, -.6082483E-7
2080 U1=U(1)+U(5)*T+U(9)*T^2+U(13)*T^3
2090 U2=U(2)+U(6)*T+U(10)*T^2+U(14)*T^3*P
2100 U3=U(31)+U(7)*T+U(11)*T^2+U(15)*T^3*P^2
2110 V4=U(4)+U(8)*T+U(12)*T^2+U(16)*T^3*P^3
2120 K24=U1+U2+U3+U4
2130 REM ************************************************
2140 REM CALCULATE LOG K FOR MoS2 - H2S
2150 K11=K21 - 2*K2 - K7 -2*K22
2160 IF P>0 THEN K11=K20 - 2*K23 - K7 - 2*K24
2170 GOSUB 2520
2180 CLS
2190   PRINT   "*********************************************-
```

```
**********************************
2200 PRINT " SULFUR SPECIATATION AND MOLYBDENITE SOLUBILITY
WITH SPECIATION
2210 PRINT USING " FLUID CONDITIONS: LOG FO2=###.#   pH=##.#
mS=#.####       mCl=#.###       mF=#.#######  T=###°C  I=#.##
";LO2,PH,S,CL,F,T,IS
2220 PRINT USING " HSO4-       =###.########## m  ###.### LOG
m"; MHSO4, LMHSO4
2230 PRINT USING " H2S         =###.########## m  ###.### LOG
m"; MH2S, LMH2S
2240 PRINT USING " HS-         =###.########## m  ###.### LOG
m"; MHS, LMHS
2250 PRINT USING " S--         =###.########## m  ###.### LOG
m"; MS, LMS
2260 PRINT USING " SO4--       =###.########## m  ###.### LOG
m"; MSO4, LMSO4
2270 PRINT "
2280 GOSUB 2700
2290 PRINT USING " TOT Mo      =###.########## m  ###.### LOG
m  #####.####### ppm";TOTMO,LTOTMO,PPMMO
2300 PRINT USING " H2MoO4      =###.########## m  ###.### LOG
m";MH2MOO4,LH2MOO4
2310 PRINT USING " HMoO4-      =###.########## m  ###.### LOG
m";MHMOO4,LHMOO4
2320 PRINT USING " MoO4--      =###.########## m  ###.### LOG
m";MHMOO4,LHMOO4
```

```
2330 PRINT USING " MoO2+       =###.########## m  ###.### LOG
m";MMOO2,LMOO2
2340 PRINT USING " MoO2++      =###.########## m  ###.### LOG
m";MMOO22,LMOO22
2350 PRINT USING " MoO2S2--    =###.########## m  ###.### LOG
m";MMOO2S2,LMOO2S2
2360 PRINT USING " MoO2Cl+     =###.########## m  ###.### LOG
m";MMOO2CL,LMOO2CL
2370 PRINT USING " MoO2Cl2     =###.########## m  ###.### LOG
m";MMOO2CL2,LMOO2CL2
2380 PRINT USING " MoO2Cl3-    =###.########## m  ###.### LOG
m";MMOOCL3,LMOOCL3
2390 PRINT USING " MoOCl3      =###.########## m  ###.### LOG
m";MMOOCL3,LMOOCL3
2400 PRINT USING " MoO3F-      =###.########## m  ###.### LOG
m";MMOO3F,LMOO3F
2410 PRINT "************************************************-
**********************************
2420 INPUT " ANOTHER CALCULATION (IF YES PRESS [Y}, [ENTER],
AND [F2]) ";K$
2430 RESET
2440 IF K$="Y" OR K$="y" THEN GOTO 10
2450 CHAIN"C:\FLUID\MENU
2460 STOP
2470 REM SUBROUTINE TO CALCULATE ACTIVITY COEFFICIENTS
2480 A=.4914844 + 3.65317E-04*T + 1.55023E-05*T^2 + 1.650365E-
```

```
07*T^3 + 1.142142E-09*T^4 - 3.704296E-12*T^5 + 4.754928E-
15*T^6
2490 B=.3240432 + 1.85311E-04*T - 1.17617E-7*T^2 + 1.057105E-
09*T^3
2500 LOGM=A*Z^2IS^.5/(1+AZ*B*IS^0.5) + .0.3*IS
2510 RETURN
2520 REM SUBROUTINE TO CALCULATE MOLAL SO4-- IN THE SOLUTION
2530 LM1=-LGSO4+2*PH+2*LO2+K3+K4
2540 LM2=PH+2LO2+K3+K2-K1-LGHSO4
2550 LM3=PH-K5-LGHS
2560 LM4=PH-K5-LGS
2570 M1=10^LM1:M2=10^LM2:LM3=10^LM3:M4=10^LM4
2580 Z=1+M1+M2+M3+M4
2590 MH2S=S/Z
2600 MSO4=M1*MH2S
2610 MHSO4=M2*MH2S
2620 MHS=M3*MH2S
2630 MS=M4*MH2S
2640 LMH2S=LOG(MH2S)/ALOG
2650 LMSO4/LOG(MSO4)/ALOG
2660 LMHS=LOG(MHS)/ALOG
2670 LMHSO4=LOG(MHSO4)/ALOG
2680 LMS=LOG(MS)/ALOG
2690 RETURN
2700 REM SUBROUTINE TO CALCULATE Mo SPECIES
2710 LMHMOO4=-LGHMOO4-2*LOG(MH2S)/ALOG+PH+.5LO2+K11
```

```
2720 BB=LMHMOO4+LGHMOO4
2730 MHMOO4=10^LMHMOO4
2740 LMMOO4=PH+K7-LGMOO4+BB
2750 MMOO4=10^LMHMOO4
2760 LMH2MOO4=-PH+BB+K8
2770 MH2MOO4=10^LMH2MOO4
2780 LMMOO2=-LGMOO2-.25*LO2-2*PH+BB+K9
2790 MMOO2=10^LMMOO2
2800 LMMOO2S2=-LGMOO2S2+BB-PH+2*LGHS+2*LOG(MHS)/ALOG-K10
2810 MMOO2S2=1-^LMMOO2S2
2820 CC=LGCL+LOG(CL)/ALOG
2830 LMMOO2CL=-K12+BB-3*PH+CC-LGMOOSCL
2840 MMOO2CL=10^LMMOO2CL
2850 LMMOO2CL2=-K13+BB-3*PH+2*CC
2860 MMOO2CL2=10^LMMOO2CL2
2870 LMMOO2CL3=-K14+BB-3*PH+3*CC-LGMOO2CL3
2880 MMOO2CL3=10^LMMOO2CL3
2890 LMMOOCL3=-K15+BB--4*PH+3*CC-LO2/4
2900 MMOOCL3=10^LMMOOCL3
2910 LMMOO3F=-K18-PH-LGHMOO4+BB+LGCL+LF
2920 MMOO3F=10^LMMOO3F
2930 LMMOO22=-K17-LGMOO4-3*PH+BB
2940 MMOO22=10^LMMOO22
2950  TOTMO=MHMOO4 + MMOO4 + MH2MOO4 + MMOO2 + MMOO2S2 +
MMOO2CL + MMOO2CL2 + MMOO2CL3 + MMOOCL3 + MMOO3F + MMOO22
2960 PPMMO=TOTMO*1000*95.94
```

```
2970 LTOTMO=LOG(TOTMO)/ALOG
2980 RETURN
```

APPENDIX F

pH CALCULATION VIA CO_2-CARBONATE SYSTEM AND SO_2-SULFATE-H_2S-SULFIDE SYSTEM

To calculate pH via CO_2-carbonate system and SO_2-sulafate H_2S-sulfide system we assume that:

$CO_2 = H_2CO_3$, $SO_2 = SO_4^{2-}$, and H_2S (g) = H_2S (aq).

The following equations can than be used for the pH calculation with equilibrium constants (log K) at 300°C; () is used for activity, [] for concentration, α is activity coefficient, and K_H is Henry's law constant:

I $H_2O = H^+ + OH^-$ $K_1 = (H^+)(OH^-)/(H_2O)$ = 11.03

II $H_2S = HS^- + H^+$ $K_2 = (HS^-)(H^+)/(H_2S)$ = 8.05

III $H_2CO_3 = H^+ + HCO_3^-$ $K_3 = (H^+)(HCO_{3-})/(H_2CO_3)$ = 8.29

IV $HCO_3^- = CO_3^{2-} + H^+$ $K_4 = (CO_3^{2-})(H^+)/(HCO_3^-)$ = 11.89

V $HSO_4^- = SO_4^{2-} + H^+$ $K_5 = (SO_4^{2-})(H^+)/(HSO_4^-)$ = 6.13

VI $\Sigma S = SO_4^{2-} + HSO_4^- + H_2S + HS^- = SO_2 + H_2S'$

VII $\Sigma C = H_2CO_3 + HCO_3^- + CO_3^{2-} = CO_2$

VIII $0 = 2*(SO_4^{2-}) + (HSO_4^-) + (HS^-) + (HCO_3^-) + 2*(CO_3^{2-}) + (OH^-) - (H^+)$

Where H_2S' is detected amounts of H_2S.

Rearranging eqs. I to V giving eqs. IX to XIII:

I → IX $[OH^-] = K_1/(H^+)\alpha_{OH-}$

II → X $[HS^-] = K_2[H_2S]K_{H,H2S}/(H^+)\alpha_{HS-}$

III → XI $(H_2CO_3) = (H^+)[HCO_3^-]\alpha_{HCO3-}/K_3$

IV → XII $[CO_3^{2-}] = K_4[HCO_3^-]\alpha_{HCO3-}/(H^+)\alpha_{CO32-}$

V → XIII $[HSO_4^-] = [SO_4^{2-}](H^+)\alpha_{SO42-}/K_5\alpha_{HSO4-}$

Inserting XI and XII into VII:

$$IX: CO_2 = \frac{(H^+)\,[HCO_3^-]\,\gamma_{HCO3-}}{K_3} + HCO_3^- + \frac{K_4\,[HCO_3^-]\,\gamma_{HCO3-}}{\gamma_{CO32-}(H^+)}$$

Rearranging XIV giving:

$$XV: HCO_3^- = \frac{CO_2}{\frac{(H^+)\,\gamma_{HCO3-}}{K_3} - \frac{K_4\gamma_{HCO3-}}{\gamma_{CO32-}(H^+)} - 1}$$

and

$$XVI: CO_3^{2-} = \frac{K_4\gamma_{HCO3-}}{(H^+)\,\gamma_{CO32-}} * \frac{CO_2}{\frac{(H^+)\,\gamma_{HCO3-}}{K_3} - \frac{K_4\gamma_{HCO3-}}{\gamma_{CO32-}(H^+)} - 1}$$

The total carbonate charge will then be:

$$XVII: A = (1 + 2\frac{K_4 \gamma_{HCO3-}}{(H^+)\gamma_{CO32-}}) * \frac{CO_2}{\frac{(H^+)\gamma_{HCO3-}}{K_3} - \frac{K_4 \gamma_{HCO3-}}{\gamma_{CO32-}(H^+)} - 1}$$

Inserting X and XIII into VI:

$$XVIII: HSO_4^- = \frac{SO_2 + H_2S' - H_2S - \frac{K_2 [H_2S] K_{H,H2S}}{(H^+)\gamma_{HS-}}}{K_5 \gamma_{HSO4-}} (H^+)\gamma_{SO42-}$$

where

$$XIX: SO_4^{2-} = (SO_2 + H_2S' - H_2S - \frac{K_{H,H2S} K_2 [H_2S]}{(H^+)\gamma_{HS-}})$$

The total sulfur charge will then be:

$$XX: B = \frac{SO_2 + H_2S' - H_2S - \frac{K_2 [H_2S] K_{H,H2S}}{(H^+)\gamma_{HS-}}}{K_5 \gamma_{HSO4-}} (H^+)\gamma_{SO42-} + 2 * (SO_2 + H_2S' - H_2S - \frac{K_{H,H2S}}{(H^+}$$

Inserting IX, XVII for carbonate charge, and XX for sulfur

charge into VIII gives:

$$0 = A + B + \frac{K_1}{(H^+)\,\gamma_{OH^-}} - (H^+)$$

pH can be calculated from Eq. XXI where gammas and Henry's law constants are calculated at 300°C for solution with ionic strength I=1 (Giggenbach, 1981).

APPENDIX G

GAS DISTRIBUTION IN A BOILING SYSTEM

Based on an adiabatic process where no heat is gained or lost to the surroundings, that the fluid expands irreversibly, and that changes in potential and kinetic energy is negligible the steam fraction, y, can be calculated from following equation (Henley et al., 1984):

$$y = (H_{l,e} - H_{l,s}) / (H_{l,e} - H_{v,e}) \qquad \text{(Eq. 21)}$$

$H_{l,e}$ - specific enthalpy for liquid water at end temperature.

$H_{l,s}$ - specific enthalpy for liquid water at start temperature.

$H_{v,e}$ - specific enthalpy for vapor at ending temperature.

The change in gas concentration in boiling fluid from 365°C to 300°C has been calculated based on the following reaction (Henley et al., 1984):

$$C_l/C_o = 1/(1 + y*(B - 1)) \qquad \text{(Eq. 22)}$$

C_l - Concentration in liquid after steam fractionation.

C_o - Concentration in steam befor any boiling.

B - Gas distribution coefficent.

B for CO_2, N_2, and H_2 are given by the following equations (Giggenbach, 1980):

$B_{CO2} = 4.0547 - 0.01092*t$

$B_{N2} = 6.4426 - 0.01416*t$

$B_{H2} = 6.2283 - 0.01403*t$

where t is the temperature in degree Celcius. The equations are most accurate between 100 and 340°C.

T	H_l	H_v	y	B_{CO2}	B_{N2}	B_{H2}
365	1816	2421				
360	1761	2481	0.0763	6.73	22.13	15.05
355	1713	2527	0.135	7.63	26.05	17.69
350	1671	2564	0.182	8.66	30.66	29.79
345	1631	2595	0.224	9.82	36.09	24.43
340	1594	2622	0.260	11.13	42.48	28.71
335	1559	2645	0.292	12.62	50.00	33.75
330	1525	2666	0.322	14.31	58.86	39.66
325	1493	2684	0.349	16.23	69.28	46.62
320	1461	2700	0.375	18.40	81.55	54.79
315	1431	2714	0.398	20.87	95.98	64.40
310	1401	2727	0.421	23.67	113.0	75.68
305	1372	2739	0.442	26.84	133.0	88.95
300	1344	2749	0.462	30.43	156.5	104.5

	FRACTION REMAINING IN LIQUID			AMOUNT REMAINING IN LIQUID		
T	C_l/C_o CO_2	C_l/C_o N_2	C_l/C_o H_2	CO_2	H_2	N_2
365	1.000	1.000	1.000	7.00	0.2000	0.500
360	0.696	0.383	0.483	4.87	0.0965	0.191
355	0.527	0.228	0.307	3.69	0.0614	0.114
350	0.417	0.156	0.217	2.92	0.0434	0.078
345	0.336	0.113	0.160	2.35	0.0303	0.057
340	0.275	0.085	0.122	1.93	0.0244	0.043
335	0.228	0.065	0.095	1.59	0.0189	0.033
330	0.189	0.051	0.071	1.32	0.0149	0.026
325	0.158	0.040	0.059	1.11	0.0118	0.020
320	0.133	0.032	0.047	0.93	0.0095	0.016
315	0.122	0.026	0.038	0.79	0.0076	0.013

310	0.095	0.021	0.031	0.66	0.0062	0.010
305	0.081	0.017	0.025	0.56	0.0050	0.008
300	0.069	0.020	0.014	0.48	0.0041	0.007

APPENDIX H

NORMALIZED SALT DATA AND LEACHED AND DECREPITATED QUARTZ DATA

Normalisation: (ELEMENT X/Na)/(X AVG. GRANITE/Na GRANITE).
ER for element X=0.

Extracted salt.

Spml.#	OG-2	OG-9	OG-12A	OG-12B	18A-DG	18C-DG
Na	0.000	0.000	0.000	0.000	0.000	0.000
K	ER	ER	ER	ER	ER	ER
Sc	-1.248	-1.422	-1.470	-1.485	-0.295	-0.846
Cr	-0.613	-0.176	-1.636	-1.218	-0.974	-1.415
Fe	-1.222	-1.057	-0.880	-0.926	-0.611	-0.953
Co	0.216	0.122	-0.306	-0.212	-1.222	-1.462
Zn	1.140	1.958	0.909	0.941	0.839	0.450
As	1.969	2.021	1.848	1.780	2.092	1.713
Br	1.132	ER	0.842	0.895	1.142	0.571
Rb	-0.114	-0.627	0.001	-0.020	0.059	-0.195
Sr	ER	ER	ER	ER	ER	ER
Mo	ER	ER	ER	ER	0.347	ER
Ag	ER	ER	0.773	0.624	ER	ER
Cd	ER	ER	ER	ER	ER	ER
Sb	0.525	0.356	0.811	0.775	0.556	0.720
Cs	2.053	2.076	2.157	2.164	1.993	1.836
Ba	-1.460	-0.564	-1.248	-1.133	ER	-2.557
La	-1.361	-0.717	-1.134	-0.971	-0.877	-0.029
Ce	-1.599	-0.939	-1.313	-1.164	-0.946	0.107
Nd	-1.512	-0.417	-1.414	-0.950	-0.789	0.357
Sm	-2.114	ER	-1.480	-1.200	-0.636	0.419
Eu	-1.595	-1.519	-1.323	-1.376	-1.368	-0.610
Tb	-0.938	-1.083	-1.511	-1.351	-0.196	0.791
Yb	-0.528	-0.087	-1.169	-1.200	0.624	1.969
Lu	-0.134	0.167	-0.503	-0.531	0.873	2.204
Hf	ER	ER	ER	ER	ER	-1.342
Ta	1.010	-0.070	0.067	0.073	-1.313	ER
W	ER	ER	ER	ER	-0.012	1.551
Ir	ER	ER	ER	ER	0.091	0.865
Au	ER	ER	ER	ER	ER	ER
Hg	ER	ER	ER	ER	ER	ER
Th	-1.316	-1.855	-1.708	-1.615	-1.157	-0.777
U	0.086	1.429	-1.017	-0.555	0.272	0.103

Extracted salt, cont.

Smpl.#	18D-DG	21B-DG	21B-DG	23B-DG	DG-23C	27A-DG
Na	0.000	0.000	0.000	0.000	0.000	0.000
K	ER	ER	ER	ER	-0.627	ER
Sc	-0.264	-1.053	-1.305	-0.733	-0.077	0.339
Cr	0.172	ER	ER	-0.054	0.085	-0.304
Fe	-0.385	-0.679	-0.784	-0.833	-0.331	-0.578
Co	-0.866	-0.580	-1.040	0.613	0.016	0.752
Zn	0.738	0.891	0.683	0.640	0.868	ER
As	1.895	2.096	1.958	1.977	1.656	2.339
Br	0.635	1.053	1.135	1.506	1.832	1.801
Rb	0.201	-0.407	-0.612	-0.503	-0.404	-0.081
Sr	ER	ER	ER	ER	ER	ER
Mo	1.067	0.418	0.213	1.106	1.413	1.145
Ag	ER	0.939	ER	ER	1.480	ER
Cd	ER	ER	ER	ER	ER	ER
Sb	0.661	0.588	0.530	0.334	0.665	0.865
Cs	1.997	1.900	1.761	1.728	1.563	2.226
Ba	-0.792	ER	ER	-1.653	-0.853	-0.329
La	-0.079	-0.865	-1.130	-1.483	-0.024	0.259
Ce	-0.038	-1.011	-1.276	-1.572	-0.332	0.247
Nd	0.034	-1.037	-1.178	-1.473	0.181	-0.106
Sm	0.122	-1.588	-1.956	-1.428	0.156	ER
Eu	0.325	-1.501	-1.614	-1.280	0.220	-0.639
Tb	0.672	-1.011	-1.053	-0.720	0.444	-0.078
Yb	1.532	0.207	0.068	0.102	1.521	1.094
Lu	1.721	0.444	0.350	0.358	1.756	1.391
Hf	0.742	-0.847	-0.734	ER	0.341	-0.043
Ta	ER	-0.449	-0.227	-0.674	ER	0.740
W	1.444	0.755	0.623	ER	1.253	1.388
Ir	ER	-0.075	-0.278	ER	ER	ER
Au	0.293	ER	ER	ER	ER	0.060
Hg	ER	ER	ER	ER	ER	ER
Th	0.088	-0.636	-0.750	-1.340	-0.148	0.418
U	1.412	0.613	0.475	0.149	0.895	1.685

Extrated salt, cont.

Smpl.#	27A-DG2	27A-DG3
Na	0.000	0.000
K	ER	ER
Sc	0.147	0.172
Cr	0.009	-0.416
Fe	-0.787	-0.603
Co	0.907	0.419
Zn	0.240	0.349
As	2.055	2.112
Br	1.166	1.103
Rb	-0.408	-0.392
Sr	ER	ER
Mo	1.224	1.228
Ag	ER	ER
Cd	ER	ER
Sb	0.618	0.626
Cs	1.954	2.110
Ba	-0.602	-0.559
La	0.042	0.114
Ce	0.021	0.151
Nd	-0.288	-0.039
Sm	ER	ER
Eu	-0.743	-0.783
Tb	-0.207	-0.073
Yb	0.898	1.013
Lu	1.179	1.285
Hf	-0.045	-0.409
Ta	0.398	-0.131
W	0.749	0.927
Ir	0.087	ER
Au	ER	ER
Hg	ER	ER
Th	0.236	0.368
U	1.490	1.597

Extracted salt, cont.

Smpl. #	32-DG	36-DG	41B-DG	41D-DG	42-DG	43A-DG
Na	0.000	0.000	0.000	0.000	0.000	0.000
K	ER	ER	ER	ER	ER	ER
Sc	-0.137	-0.431	0.123	-0.297	-0.879	-0.795
Cr	ER	-1.715	0.183	ER	-1.068	-1.704
Fe	-1.242	0.665	-0.399	-0.758	-1.419	-1.461
Co	-1.350	0.486	-0.739	ER	-2.252	-0.993
Zn	1.698	0.755	1.255	1.491	0.864	1.286
As	1.024	1.005	1.587	2.023	1.374	1.520
Br	0.493	-0.248	1.055	1.364	-0.108	1.170
Rb	-0.475	-0.398	-0.210	-0.206	-0.278	-0.411
Sr	ER	ER	ER	ER	ER	ER
Mo	ER	0.955	0.466	0.315	-0.115	ER
Ag	ER	ER	ER	0.964	0.907	1.327
Cd	ER	ER	ER	ER	ER	ER
Sb	0.323	-0.338	0.239	0.675	0.174	0.316
Cs	1.086	0.857	1.596	1.703	1.611	1.568
Ba	ER	-1.097	-1.225	-1.184	-2.009	-1.544
La	-0.328	-0.325	-0.317	-0.619	-1.452	-1.155
Ce	-0.666	-0.242	-0.365	-0.781	-1.615	-1.288
Nd	-0.625	0.026	-0.169	-0.476	-1.612	-0.911
Sm	-0.832	0.069	-0.206	-0.518	-1.333	-1.038
Eu	-0.644	-0.169	-0.074	-0.133	-1.116	-0.830
Tb	-0.873	0.262	-0.029	-0.103	-0.909	-0.846
Yb	0.247	0.677	1.136	0.905	0.145	-0.144
Lu	0.606	0.829	1.396	1.169	0.446	-0.157
Hf	-2.548	-1.210	-3.048	-0.126	-2.019	-2.232
Ta	ER	ER	-0.357	ER	ER	-1.565
W	0.499	ER	0.296	1.461	0.319	0.996
Ir	ER	ER	ER	0.265	-0.419	ER
Au	ER	ER	ER	ER	ER	ER
Hg	ER	ER	ER	ER	ER	ER
Th	-0.540	-0.650	-0.207	-0.306	-0.719	-1.662
U	0.376	0.298	0.521	0.664	-0.323	-0.411

Extracted salt, cont.

Smpl. #	50-DG	51A-DG	52A-DG	54A-DG	54D-DG	58A-DG
Na	0.000	0.000	0.000	0.000	0.000	0.000
K	-1.020	-0.969	-0.646	-0.666	-0.616	-0.270
Sc	0.071	-0.757	-0.096	-0.294	-0.055	-0.083
Cr	-0.265	-1.167	-0.702	-0.047	0.506	0.170
Fe	-0.537	-0.848	-0.716	-0.740	-0.406	-0.629
Co	0.599	0.296	-0.358	0.134	0.315	-0.030
Zn	0.645	0.892	0.944	1.115	1.286	1.059
As	1.484	1.532	1.743	1.472	1.424	1.228
Br	1.349	1.282	1.872	2.005	1.596	1.390
Rb	-0.856	-1.172	-1.025	-0.236	-0.383	0.228
Sr	ER	-0.551	-0.390	ER	ER	-0.128
Mo	1.470	1.233	1.761	2.018	1.566	1.361
Ag	ER	ER	ER	1.756	2.084	ER
Cd	1.958	ER	ER	ER	ER	ER
Sb	ER	0.761	0.635	ER	0.424	0.255
Cs	0.896	1.926	1.845	1.808	1.776	1.793
Ba	-2.563	-1.524	-0.073	ER	-0.650	ER
La	0.377	-1.039	-0.580	-0.022	0.310	0.889
Ce	0.245	-0.879	-0.701	-0.039	0.417	0.971
Nd	0.478	-0.794	-0.362	0.110	0.763	1.331
Sm	0.200	-0.787	-0.509	2.172	0.854	1.433
Eu	0.147	-0.708	-0.370	1.970	0.482	0.459
Tb	-0.027	-0.676	-0.466	0.670	1.204	1.752
Yb	0.373	0.357	0.272	1.701	2.176	2.822
Lu	0.689	0.621	0.575	1.928	2.392	3.072
Hf	ER	ER	ER	-0.324	-0.389	-1.136
Ta	ER	ER	-0.307	ER	ER	0.362
W	3.089	0.527	2.054	2.258	1.216	1.580
Ir	ER	-0.188	-0.284	0.373	ER	0.729
Au	ER	ER	ER	0.142	1.306	ER
Hg	ER	-0.263	ER	ER	ER	0.529
Th	-1.904	-2.638	-1.775	-0.862	-0.514	-0.867
U	ER	0.603	-0.140	0.784	0.884	0.204

Extracted salt, cont.

Smpl. #	59A-DG	59B-DG	66A-DG	66B-DG	68A-DG	71-DG
Na	0.000	0.000	0.000	0.000	0.000	0.000
K	ER	-0.428	-1.257	-0.844	-0.528	-0.735
Sc	-0.099	0.520	-0.276	-0.498	0.008	-0.274
Cr	-0.286	0.152	-0.447	-0.916	-0.187	-0.182
Fe	-0.690	-0.487	-0.906	-0.854	-0.484	-0.846
Co	-0.523	-0.280	-0.473	-0.602	-0.304	-0.211
Zn	1.187	1.249	1.014	1.011	0.974	1.050
As	1.574	1.448	1.110	1.152	1.312	1.263
Br	0.982	1.294	1.525	ER	1.344	1.604
Rb	ER	0.019	-0.229	-0.087	-1.878	-0.126
Sr	ER	ER	ER	ER	ER	ER
Mo	1.887	2.237	1.390	1.480	1.709	1.148
Ag	1.290	ER	1.286	1.301	ER	ER
Cd	ER	ER	ER	ER	ER	ER
Sb	0.582	0.312	0.155	0.192	0.802	0.540
Cs	1.919	1.817	1.633	1.696	1.839	1.756
Ba	ER	ER	ER	ER	-0.904	ER
La	0.938	1.451	-0.224	-0.497	-0.508	-0.414
Ce	ER	1.530	-0.095	-0.509	-0.615	-0.607
Nd	1.332	1.744	0.206	-0.439	-0.664	-0.161
Sm	1.348	1.726	0.381	-0.356	ER	0.710
Eu	0.372	0.738	-0.215	-0.526	-0.361	-0.998
Tb	1.614	1.950	0.793	0.073	0.000	0.131
Yb	2.749	3.064	1.900	1.163	1.230	1.248
Lu	3.001	3.325	2.161	1.425	1.508	1.507
Hf	-0.938	0.305	-0.793	-0.308	0.101	ER
Ta	0.640	0.754	-0.118	-0.111	0.528	-0.725
W	1.660	1.835	1.151	0.957	1.463	ER
Ir	1.097	0.805	0.332	0.113	0.718	0.281
Au	ER	ER	ER	ER	ER	ER
Hg	0.623	ER	ER	ER	1.559	0.615
Th	ER	0.131	-0.737	-0.179	-0.350	-0.853
U	0.210	1.138	0.014	0.642	1.361	0.407

Decrepitated and leached quartz samples.

Smpl.Q#	18A	Q-18C	Q-18D	Q-21B	Q-21B	Q-23
Na	0.000	0.000	0.000	0.000	0.000	0.000
K	ER	ER	ER	ER	ER	ER
Sc	-0.559	-1.055	-1.728	-0.786	-0.330	-1.356
Cr	ER	ER	ER	-0.952	-0.006	-1.730
Fe	-0.805	-1.388	-1.726	-0.680	-0.663	ER
Co	-0.126	-0.853	-1.673	0.010	0.068	-1.327
Zn	-0.036	-0.193	-1.667	-0.087	-0.070	-0.234
As	0.714	0.177	-0.651	1.272	1.310	ER
Br	0.889	0.389	ER	1.344	1.674	ER
Rb	0.229	-0.087	-0.067	0.127	-0.041	-0.644
Sr	ER	ER	ER	ER	ER	-2.507
Mo	ER	ER	ER	ER	ER	ER
Ag	ER	ER	ER	ER	ER	ER
Cd	ER	ER	ER	ER	ER	ER
Sb	-0.462	-0.180	-0.383	ER	0.782	0.390
Cs	1.052	0.631	0.247	1.261	1.315	0.194
Ba	-0.992	ER	-1.902	-0.997	-1.680	ER
La	-1.577	-0.411	-1.623	-1.528	-1.631	-0.932
Ce	-1.142	-0.329	-1.822	-0.741	-0.665	-1.075
Nd	ER	-0.088	-2.334	ER	ER	-0.834
Sm	-1.901	0.026	-2.313	ER	ER	-1.940
Eu	-0.559	-0.920	-0.970	-0.212	-0.292	0.402
Tb	-0.503	0.429	-1.273	0.048	0.295	-1.262
Yb	-0.383	1.593	-0.544	-0.133	0.611	-0.231
Lu	-0.161	1.823	-0.389	1.131	1.310	-0.041
Hf	-0.673	-0.873	-0.772	-0.284	0.324	-0.615
Ta	0.050	-0.031	-0.477	2.245	1.222	0.432
W	0.900	1.024	-0.417	1.487	1.650	ER
Ir	ER	ER	ER	ER	ER	ER
Au	ER	ER	ER	ER	ER	ER
Hg	ER	ER	ER	ER	ER	1.164
Th	-1.701	-1.529	-2.370	-1.036	-0.707	-1.993
U	-0.826	-0.932	-1.166	0.026	-0.015	-0.521

Decrepitated and leached quartz samples, cont.

Smpl. #	Q-23B	Q-32	Q-41B	Q-41D	Q-42
Na	0.000	0.000	0.000	0.000	0.000
K	ER	ER	ER	ER	ER
Sc	0.153	-0.576	-0.875	-0.556	0.117
Cr	0.412	-1.157	-0.971	-2.045	-0.827
Fe	0.128	-1.321	-1.222	-0.994	-0.856
Co	0.772	-1.154	-0.847	-0.605	-0.489
Zn	1.278	-1.389	-0.365	-0.276	0.105
As	ER	-0.174	ER	0.428	0.595
Br	2.545	-0.037	0.258	0.682	0.999
Rb	ER	-0.257	-0.358	-0.095	-0.128
Sr	ER	ER	ER	ER	ER
Mo	ER	ER	ER	ER	ER
Ag	ER	ER	ER	ER	ER
Cd	ER	ER	ER	ER	ER
Sb	1.471	-0.439	-0.386	-0.158	0.372
Cs	1.332	0.034	-0.045	0.306	0.807
Ba	-0.934	-2.123	-1.460	-1.487	-1.298
La	-1.148	-1.569	-1.816	-1.249	-1.635
Ce	-0.540	-1.729	-1.969	-1.177	-1.302
Nd	ER	-1.902	ER	-1.212	ER
Sm	ER	-2.312	-1.348	-1.539	-1.584
Eu	0.630	-0.794	-0.398	-0.423	0.827
Tb	ER	-1.379	-0.825	-1.045	-0.174
Yb	-0.325	-0.345	0.342	0.161	1.136
Lu	ER	0.115	0.683	0.528	1.526
Hf	-0.041	-0.174	0.662	0.414	1.590
Ta	0.471	0.038	0.373	0.775	1.031
W	2.250	0.323	0.945	0.474	1.836
Ir	ER	ER	ER	ER	ER
Au	ER	ER	ER	ER	ER
Hg	ER	ER	ER	ER	ER
Th	-0.927	-1.567	-1.119	-1.275	-0.426
U	-0.416	-0.591	-0.481	0.099	-0.313

Decrepitated and leached quartz samples, cont.

Smpl. #	Q-50	Q-51A	Q-52A	Q-59A	Q-59B	Q-66A
Na	0.000	0.000	0.000	0.000	0.000	0.000
K	-0.455	ER	-1.643	0.034	0.319	-0.723
Sc	1.369	0.652	0.021	1.108	0.839	0.539
Cr	ER	-0.228	-0.698	ER	0.210	-0.331
Fe	0.352	0.106	-0.570	-0.202	-0.005	-0.042
Co	0.769	0.273	-0.424	ER	-0.226	0.053
Zn	1.270	0.949	0.360	1.642	0.836	1.244
As	2.764	1.953	1.000	1.674	ER	ER
Br	2.113	1.931	0.942	ER	ER	1.840
Rb	0.038	0.184	-0.698	ER	0.693	0.213
Sr	ER	ER	ER	ER	ER	ER
Mo	2.903	2.559	1.113	ER	1.436	2.398
Ag	ER	ER	ER	ER	ER	3.465
Cd	ER	2.551	1.879	ER	3.021	3.323
Sb	ER	2.213	1.292	ER	ER	1.925
Cs	1.767	1.768	0.764	1.547	1.310	1.527
Ba	ER	ER	ER	0.898	ER	ER
La	1.280	0.303	-0.267	2.044	1.345	0.922
Ce	1.228	0.230	-0.262	2.122	1.380	0.880
Nd	1.392	0.467	-0.076	2.451	1.615	1.050
Sm	0.876	0.039	-1.217	2.505	1.592	0.172
Eu	0.769	-0.163	-1.023	2.855	1.908	0.425
Tb	0.561	0.125	-0.964	2.814	1.867	0.384
Yb	0.923	0.622	-0.389	3.928	3.005	1.228
Lu	1.149	1.073	0.092	4.178	3.261	1.674
Hf	ER	0.436	-0.353	0.111	0.419	0.261
Ta	ER	0.625	-0.465	0.896	1.305	1.614
W	4.491	2.513	1.806	2.601	1.950	2.213
Ir	ER	ER	ER	ER	ER	ER
Au	ER	ER	ER	ER	ER	1.845
Hg	ER	ER	ER	ER	1.866	ER
Th	-0.472	-0.300	-1.841	0.461	0.461	0.362
U	ER	0.204	ER	ER	0.546	0.532

Decrepitated and leached quartz samples, cont.

Smpl. #	Q-66B	Q-68B	Q-71	AVG.GRANITE ppm
Na	0.000	0.000	0.000	24600
K	-1.372	ER	ER	45100
Sc	-0.673	-0.170	-0.233	3
Cr	ER	-0.972	-0.911	22
Fe	-1.292	-1.074	-0.861	13700
Co	-1.561	-1.375	-1.130	2.4
Zn	-0.680	-0.729	-0.212	45
As	ER	ER	ER	0.8
Br	ER	ER	ER	0.5
Rb	-0.887	0.662	0.209	220
Sr	ER	ER	ER	250
Mo	-0.031	0.320	ER	7
Ag	ER	ER	ER	0.04
Cd	ER	ER	1.487	0.06
Sb	ER	ER	0.465	0.4
Cs	-0.126	0.793	0.749	1.5
Ba	ER	ER	ER	1220
La	-0.899	-0.863	-1.067	120
Ce	-0.916	-1.020	-1.233	230
Nd	-0.973	-0.889	-0.974	55
Sm	-1.181	ER	-2.253	11
Eu	-0.891	-0.775	-1.081	1
Tb	-0.932	ER	ER	1.1
Yb	0.265	0.257	-0.293	1
Lu	0.553	0.720	-0.050	0.1
Hf	-0.310	-1.075	-0.348	5.2
Ta	0.322	1.160	0.407	1.6
W	0.676	0.986	0.663	0.4
Ir	ER	ER	ER	0.006
Au	ER	ER	ER	0.002
Hg	-0.239	1.612	ER	0.2
Th	-0.987	-1.150	-1.928	52
U	-0.610	0.209	-0.391	3.7

APPENDIX I

FLUID INCLUSION MICROTHERMOMETRY DATA

The following table gives a list of homogenization temperature (Fig. A2) and solid/liquid melting point for fluid inclusions from two vein quartz. Wt. % NaCl eq. has been calculated based on freezing point depression free of CO_2. This assumption may not always be valid because clathrates were observed in some of these inclusion. Some of the melting points were observed to be higher than 0°C. Most of the inclusions are probably pseudo-secondary, where cracks are formed during growth filled with fluid and annealed. A few inclusions have been destiguished to be primary (P) or secondary (S). Calculation of trapping temperature based on that these fluid inclusions were trapped under 1.5 kbars pressure (Olsen and Griffin, 1984a) gives temperature range of 300-600°C.

HOMOGENIZATION TEMPERATURE	wt. %NaCl EQ.	P/S
Sample 53-DG		
128		
141		
240		
191		
162		
245		
151		
190		
236		
345		
185		
155		

158				
157				
306				
Sample 55c-DG				
215				
227				
195				
188				
188				
187		-1.8	3.0	
280				
244				
215				
Sample 58a-DG				
185.6	-1.0		1.7	P
190.1	+1.4			P?
164.8				S
164.8				S
184.3	+1.4			P?
211.3	+1.7			P?
159.6				
		-1.7	2.9	
167.9	-1.6		2.7	
131.0				
		-1.0	1.7	
174.1	-2.0		3.4	
184.3	-1.3		2.2	
205.7	+1.4			
178.2	-1.2		2.1	
322.4	+1.7			
294.6				
316.3				
198.0	+7.8			
257.0	-1.5		2.6	
173.2				
270.0	-0.9		1.5	
217.5	-1.5		2.6	
231.5				
176.1				
291.6				
286.9				
286.2				
316.4				
Sample 66b-DG				
174				
120				
355				
262				

230					
163					
308					
335					
342					
315					
261					
255					
155					
260					
Sample 68a-DG					
172.7	-4.4		7.0		
200.8	-5.9		9.1		
249.6	-4.4		7.0		
238.4					
200.8					
200.5	-4.6		7.3		
241.4	-4.6		7.3		
235.1					
296.0	-5.7		8.8		
		-5.5		8.5	
251.8					
		-5.5		8.5	
222.0	-4.8		7.6		
		-4.9		7.7	
		-4.8		7.6	
144		-1.4		2.4	P
140		-2.9		4.8	
		-3.7		6.0	S
142		-1.5		2.6	P

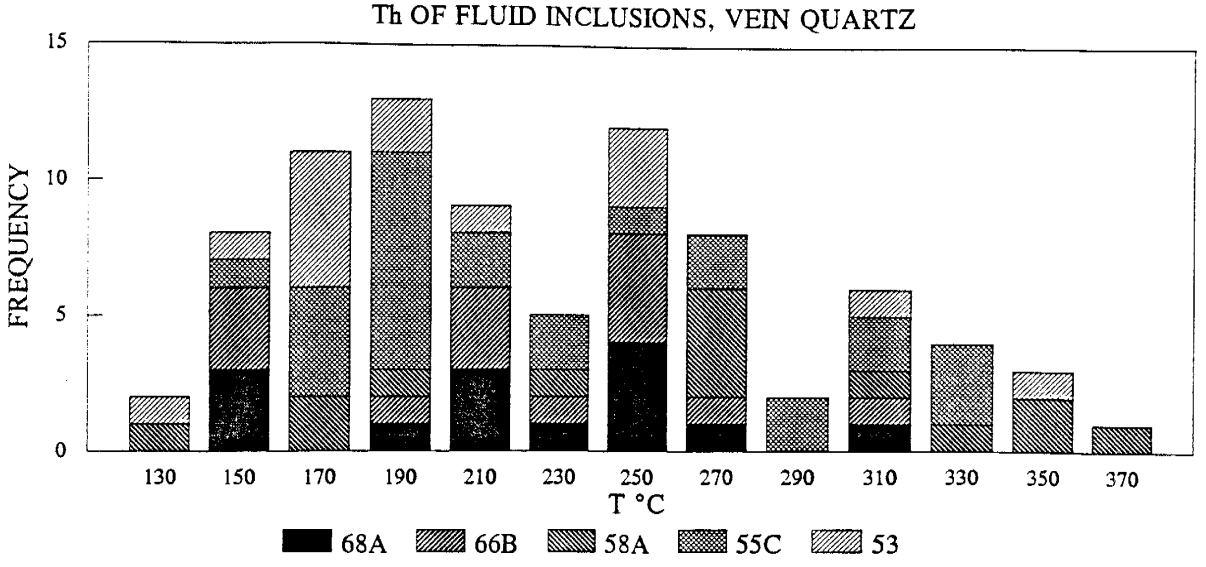

Fig. A2.

Frequency of homogenization temperatures (Th in °C) for the five analyzed vien-quartz samples.

This dissertation is accepted on behalf of the faculty of the Institute by the following committee:

David L. Nunn
Adviser

Philip R. Kyle

Andrew Campbell

William X. Chavez, Jr.

December 31, 1992
Date